Photochimie de molécules organiques photofonctionnelles étudiées par spectroscopie d'absorption ultrarapide et calculs ab-initio

Stéphane Aloïse

▶ **To cite this version:**

Stéphane Aloïse. Photochimie de molécules organiques photofonctionnelles étudiées par spectroscopie d'absorption ultrarapide et calculs ab-initio. Chimie théorique et/ou physique. Université Lille1 - Sciences et Technologies, 2016. ⟨tel-01581788⟩

HAL Id: tel-01581788

https://hal.science/tel-01581788v1

Submitted on 5 Sep 2017

HAL is a multi-disciplinary open access archive for the deposit and dissemination of scientific research documents, whether they are published or not. The documents may come from teaching and research institutions in France or abroad, or from public or private research centers.

L'archive ouverte pluridisciplinaire **HAL**, est destinée au dépôt et à la diffusion de documents scientifiques de niveau recherche, publiés ou non, émanant des établissements d'enseignement et de recherche français ou étrangers, des laboratoires publics ou privés.

Copyright - All rights reserved

Université de Lille 1 SCIENCES ET TECHNOLOGIES

Année : 2016 **n°ordre : 42176**

Habilitation à Diriger des Recherches

Présentée par

Dr. Stéphane Aloïse

Laboratoire de Spectrochimie Infrarouge et Raman (UMR 8516)

Photochimie de Molécules Organiques Photofonctionnelles Etudiées par Spectroscopie d'Absorption Ultrarapide et Calculs Ab-Initio

Soutenance le **28 octobre 2016** devant le jury composé de :

Alexandre Legris, Professeur, Université Lille 1, Sciences et Technologies, Président du Jury.

Isabelle Lampre, Professeur, Université de Paris-Sud, Rapporteur.

Rémi Métivier, Chargé de Recherche, E.N.S de Cachan, Rapporteur.

Pascal Plaza, Directeur de Recherche, E.N.S d'Ulm, Rapporteur.

Bernard Bourguignon, Directeur de Recherche, Université de Paris-Sud, Examinateur.

Guy Buntinx, *Directeur de Recherche, Université Lille 1, Sciences et Technologies, Garant.*

© 2016 Tous droits réservés.

© 2016 Tous droits réservés.

doc.univ-lille1.fr

A la mémoire de l'homme qui m'a fait comprendre la valeur du travail,
mon père.

© 2016 Tous droits réservés.

doc.univ-lille1.fr

© 2016 Tous droits réservés.

doc.univ-lille1.fr

Remerciements

En premier lieu, je tiens à remercier l'ensemble de mon Jury pour avoir accepté d'évaluer mon travail de ces dernières années. L'H.D.R est une étape importante (et difficile) pour les chercheurs français, il est donc appréciable de trouver des collègues ayant déjà franchi cette étape et qui souhaitent aider les autres à leur tour. Ainsi, je remercie Alexandre Legris (Université Lille 1) d'avoir accepté la présidence de ce jury. Je suis sincèrement honoré qu'Isabelle Lampre (Université Paris-Sud), Rémi Métivier (E.N.S de Cachan), et Pascal Plaza (E.N.S d'Ulm) aient accepté d'évaluer mon manuscrit. Je remercie également Bernard Bourguignon, (Université Paris-Sud) de tenir le rôle d'examinateur le jour de ma soutenance. Enfin, je remercie très sincèrement Guy Buntinx (Université Lille 1) d'être mon garant scientifique.

Ce document est le fruit d'un travail qui loin d'être personnel, repose sur de multiples collaborations au sein du LASIR ou venant de l'extérieur. J'aime profondément mon métier d'enseignant-chercheur, métier qui ne connait pas vraiment de quotidien et qui réserve toujours, malgré les tracas, de belles satisfactions. Ceci-dit, la Science est étudiée par des hommes, et les interactions positives et constructives avec les collègues sont d'une importance majeure pour trouver une harmonie sur son lieu de travail. Il est donc important de remercier celles et ceux qui m'ont accompagné tout au long de ces douze dernières années.

Prenons les choses dans un ordre chronologique. Je tiens tout d'abord à rendre hommage à celui qui m'a permis de devenir un scientifique, mon directeur de thèse, Michael Meyer. Dans un environnement aussi stimulant que le monde du Synchrotron, Il m'a appris la rigueur et l'intégrité scientifique et je lui en serai éternellement reconnaissant. Evidemment, j'en profite pour adresser un salut amical à tous le personnel de Paris XI que j'ai côtoyé pendant mon doctorat.

J'ai intégré le LASIR pour la première fois en septembre 2003 en tant qu'ATER pour être titularisé, six mois plus tard, en tant que Maîtres de Conférences. Cette intégration si rapide (je n'avais que 27 ans à l'époque) s'est faite grâce à Olivier Poizat et Guy Buntinx qui ont placé leur confiance en moi. Durant toute ma carrière, Guy et Olivier m'ont soutenu et je tiens à leur exprimer solennellement toute ma gratitude. Mes premières années au LASIR n'ont pas été les plus faciles car il a fallu m'adapter à une discipline que je ne connaissais pas : la photochimie organique. Fort heureusement, j'avais à cette époque mes collègues de choc –Julien Réhault, Baptiste Moine, Christophe Kinowski, Nacer Idrissi, Sylvia Turrell- sur qui j'ai toujours pu compter. Au sein de l'équipe « temps court » j'ai ensuite trouvé des soutiens scientifiques précieux tels que Michel Sliwa qui m'a beaucoup apporté par son savoir, Vincent De Waele pour ses conseils avisés, Julien Dubois pour les réglages laser au quotidien. Au sein de l'équipe « Photophysique, Réactivité et Fonctionnalité » mes interactions avec Stéphanie Delbaere pour la RMN ont toujours été très fructueuses, tout comme ma collaboration avec mes collègues de chimiométrie, Cyril Ruckebusch et Olivier Devos, collaborations qui m'ont permis de valoriser mes données transitoires par le traitement. Finalement au sein du laboratoire, nombres de collègues ont été et sont encore importants pour moi et je me tente à une liste exhaustive : Cyrille (informaticienne de choc), Cécile et Brigitte (merci pour votre travail), Emilie, Myriam, Vivianne, Roger, Pascal, Jean-Pierre, Marie-Josée, Marie, Justine, Matthieu, Emmanuelle, Ophélie, Alberto, Marie-Claire, Alain D'Huysser, Yeny (mi columbiana preferida), Gregory, Karima, François-Alexandre… Une pensée pour les anciens doctorants du LASIR… Une pensée pour Christine et Gaston.

Evidemment, l'enseignement universitaire est une part importante de mon action, raison pour laquelle une place notable lui est consacrée dans ce manuscrit. Je tiens à remercier tout d'abord toutes les secrétaires qui organisent nos enseignements et qui nous rendent le quotidien plus facile (Liliane, Françoise, Julie, Sylvie, Christine, Aude…). Au sein de l'UFR de Chimie, certaines personnes m'ont donné ma chance pour développer des cours centrés sur la Chimie Physique. Sylvain Cristol a été un de ceux qui a cru en moi à de nombreuses reprises, je le remercie. Je tiens également à

© 2016 Tous droits réservés.

doc.univ-lille1.fr

remercier Muriel Bigan (Directrice des Etudes de la licence de Chimie) pour m'avoir permis d'ouvrir l'option « Instrumentation pour la chimie ». Je remercie également mon cher Nacer pour l'aventure « Outils mathématiques pour la chimie » que j'ai fort appréciée même si les étudiants ne sont pas toujours à la hauteur des efforts développés pour eux. Je n'oublierai pas de remercier Alain Rives (Directeur de l'UFR) de m'avoir donné la responsabilité du cours d'atomistique de 1ère année et de m'avoir soutenu dans sa modernisation (TP Balmer, Spartan,…). Je remercie également mes collègues avec qui j'aime collaborer pour l'enseignement : Denis Petitprez, Eric Marceau, Michael Capron, Marie Choël, Yeny Tobon, Marie-Claire Dhamelincourt, Sylvia Turrell, François-Alexandre Miannay, Tony Sanctorum, Eric Therssen, Xavier Mercier, Pierre Suret, Patrice Hubert…etc.

Bien évidemment, j'ai fortement collaboré avec l'extérieur durant ces douze dernières années, collaborations qui ont été capitales pour rendre ma recherche des plus motivantes. Ainsi, il a été agréable de travailler avec le Jovial Vladimir Lokshin à qui je rends hommage. A partir de 2007, collaborer avec l'illustre professeur Jiro Abe a été un honneur pour moi. Je le remercie de m'avoir fourni les bétaïnes pyridinium possédant une photophysique si intéressante et qu'il a fallu débusquer au prix de nombreux efforts. A ce titre, les discussions avec Patrice Jacques ont toujours été passionnantes et je le remercie de m'avoir aiguillé dans la bonne direction jusqu'à aboutir à la fameuse méthode « innovative » de traitement des données de solvatochromie. Je tiens également à remercier Isabelle Leray qui, à la suite d'une de mes conférences, m'a proposé un projet passionnant autour du transfert de cations basé sur les bétaïnes pyridinium. Ensemble, nous avons déjà remporté un projet région Nord-Pas de Calais, et j'espère que nous décrocherons prochainement l'ANR. Je remercie aussi l'équipe de Lionel Poisson qui m'a gentiment accueilli au LFP de Saclay.

De tous mes fournisseurs officiels de molécules, le professeur Michinori Takeshita est le plus illustre, le plus haut en couleur. Michi, est un scientifique à la fois sérieux et fort sympathique qui a su, pendant de nombreuses années, se positionner seul sur le créneau des diaryléthènes pontés. Mon très cher Michi, pour toute notre collaboration et nos projets à venir… « どうもありがとうございました ».

L'année 2010, était une année de détachement à l'ITODYS dans l'équipe de François Maurel chez qui j'ai vraiment apprécié mon apprentissage de la chimie quantique. François, je te remercie sincèrement pour ton accueil chaleureux. J'en profite pour saluer mon cher Florent (nos sushis me manquent) et également Mamadou, avec qui je partageais le bureau et qui me régalait de ses histoires maliennes. Un grand merci également à Denis Jacquemin pour tout son savoir.

Je tiens maintenant à remercier, ma collaboratrice la plus proche, « mon binôme de science », Aurélie Perrier, qui est une éminente scientifique de l'IRCP (salutations à Carlo et Ilaria), spécialiste des calculs DFT, qui a su jouer le jeu de la vraie collaboration avec les expérimentateurs. Ensemble, nous avons connu les joies (JACS) comme les galères (ANR loupées) et sommes toujours restés soudés. Aurélie, je t'adresse un énorme merci pour tout le travail accompli. J'espère que nous connaitrons encore de beaux succès lors de nos futurs « explorations » des effets opto-mécaniques… Cette nouvelle thématique est d'ailleurs mon plus gros projet collaboratif au sein de l'université Lille 1 et je remercie mes collègues qui ont accepté de me suivre dans cette aventure comme Moussa Naït-Abdelaziz (LML), Jean-Marc Lefebvre, Patrice Woisel, Aurélie Malfait (UMET), Laurent Bouteiller (Paris 6) sans oublier Sophie Barrau de l'UMET, grande spécialiste des matériaux avec qui je vais avoir l'honneur de co-diriger la thèse de Maroua Louati portant sur les films polymères photo-activables. Avec Sophie, nous nous sommes battus pour que cette thèse voie le jour… Merci Sophie d'avoir cru en moi.

Durant toutes ces années à l'Université, hormis mes cours, j'ai eu l'occasion d'encadrer des étudiants lors de stages en L3, M1 et M2, stages qui se sont en général toujours déroulés dans de très bonnes conditions… Evidemment, il me serait impossible de tous les nommer mais qu'ils sachent qu'eux-aussi m'ont beaucoup apporté et que je leur suis reconnaissant d'avoir travaillé avec moi. J'ai eu l'occasion également d'encadrer deux post-doctorants ; Amit Tiwari qui a passé 6 mois au LASIR, où il a travaillé d'arrache-pied pour s'adapter à la spectroscopie résolue en temps ; et Ruan

© 2016 Tous droits réservés.
doc.univ-lille1.fr

Yibin, très grand scientifique sachant tout faire, vite et bien… Son court passage au LASIR m'a vraiment marqué. Messieurs, je vous remercie tous deux pour avoir travaillé si dur et si sérieusement.

Mais bien évidemment, l'encadrement le plus marquant pour moi reste l'encadrement de thèse. Ainsi, je remercie très sincèrement Zuzanna Pawloswka d'avoir essuyé les plâtres en étant ma toute première doctorante. Zuzanna a accompli un travail de titan sur une thématique qui était nouvelle pour moi. Les trois articles issus de la thèse de Zuzanna sont une preuve de la valeur de son travail… Ma chère Zuzanna, « dziękuję ». Depuis 2013, j'ai la chance d'encadrer Ismail Hamdi, étudiant de l'Université de Tunis, dans un travail doctoral portant sur le photochromisme. Ismail, est un acharné de travail, un étudiant sérieux, sympathique, qui a une forte motivation… Je n'ai pas voulu dévoiler la primeur des résultats de sa thèse dans ce manuscrit mais je puis vous dire que certains sont à la hauteur de l'entrain qu'il a mis au travail ! Mon cher Ismail, des mois difficiles nous attendent mais j'ai foi en toi… Pour finir, juste laisse-moi te dire une chose : « بك فخور أنا ».

Je finirais ces remerciements par un hommage à tous ceux qui me sont chers, ma famille, mes amis, mes soutiens. Tout d'abord, je remercie mes amis de Lyon avec une pensée spéciale pour « mes camarades de seconde », mes amies de toujours Béné, ma Sonia (je suis si fière de toi) et la Phanagavette (l'unique, la seule, dont aucun scientifique ne percera jamais le mystère), qui étaient toutes trois des grandes adoratrices des sciences physiques (Mme Coste, une pensée pour vous). Une pensée à celui qui a été mon tout premier élève, « ma richouille » ; sans oublier la bande de joyeux lurons (Oualid, Virg, Sab, Raldon, et tous les autres…) ainsi que mes acolytes de la fac Keltoum et Ayoh; Je pense également à mes amis de Paris…Willy, Pauline, Medhi, Fabien, Cedric, Nico, Shalla, Mourad, toute la clique de ma Josy… je ne peux tous vous citer mais j'espère que nous ne cesserons jamais d'être « pour ou pour ». Une spéciale dédicace également pour mon équipe de volley-ball, les « basta bello », avec qui je perds beaucoup de match mais qui me fait tant rire (Giuseppe, Farid, Dominique, Piero, Antoine…je vous adore). Je pense à ceux qui sont loin de moi…Eddy à Tahiti, mon frère québécois Eric, mes chouchous italiens Julien et Elsa. Sylvie, tu le sais, malgré les kilomètres qui désormais nous séparent, je serai toujours là pour toi (the flame …never forget it).

J'embrasse ma famille de Calabre qui est formidable (avec une pensée pour ma cousine Emilia) ainsi que toute ma famille de Lyon que j'aime tant ; ma sœur Virginie et les trois « bolos », Laurine, Carla et Nolan… Hey vous trois ! Suivez les conseils de tonton : « restez libre, restez vous-même, et travaillez sans relâche pour devenir quelqu'un de bien ».

J'embrasse très tendrement ma mère qui m'a toujours soutenu et que j'aime profondément, et mon père bien sûr à qui je dédicace ce manuscrit.

Mes derniers mots seront pour toi. Difficile de décrire l'indicible, le bonheur apporté, le soutien indéfectible, l'harmonie parfaite… Arthur Rimbaud disait « l'Amour est à réinventer ». Tu lui as donné raison.

© 2016 Tous droits réservés.

doc.univ-lille1.fr

© 2016 Tous droits réservés.

doc.univ-lille1.fr

AVANT PROPOS

Si on se reporte à l'arrêté originel de l'habilitation à diriger des recherches, on peut y lire ceci : « *L'habilitation à diriger des recherches sanctionne la reconnaissance du haut niveau scientifique du candidat, du caractère original de sa démarche dans un domaine de la science, de son aptitude à maîtriser une stratégie de recherche dans un domaine scientifique ou technologique suffisamment large et de sa capacité à encadrer de jeunes chercheurs. Elle permet notamment d'être candidat à l'accès au corps des professeurs des universités.* ». Si la volonté de répondre à ces expectatives a guidé mes choix dans la rédaction de ce document, je pense avoir aussi pris quelques libertés par rapport à l'exercice de style quelque peu formel qu'une HDR requiert. Par exemple, j'ai fait le choix d'un document avec un ton plutôt libre à l'image de qui je suis dans mon quotidien en tant que Chercheur et Enseignant (formel ne doit pas forcément dire froid). De même, j'ai fait le choix d'une présentation pédagogique qui s'adresse aussi à un public plus large que la communauté des photochimistes, mon idée étant que ce document puisse me servir à l'avenir auprès de mes futurs collaborateurs, étudiants de M1, M2 ou futurs doctorants.

Ce manuscrit est le fruit de douze années de travail au sein du LASIR, (laboratoire de Spectrochimie Infrarouge et Raman, UMR8516) qui se trouve sur le campus de l'Université Lille 1, Sciences et Technologies. Après un doctorat de l'Université Lyon 1 soutenu en décembre 2002, doctorat en Physique atomique et moléculaire effectué à Paris 11 au LURE (l'ancêtre de SOLEIL) puis un ATER à Paris 11, j'ai été recruté au LASIR en février 2004 (après 6 mois d'ATER). Mon cahier de route, édicté par Guy Buntinx et Olivier Poizat (DR CNRS) était de travailler sur des molécules photofonctionnelles organiques en utilisant la spectroscopie résolue en temps. Dans ce manuscrit, Il m'est apparu important de présenter « un domaine de la science » bien précis, raison pour laquelle je me suis restreint aux travaux centrés sur la photochimie organique faite au LASIR. Ceci-dit, mon bagage doctoral résolument ancré dans la science fondamentale, dans la confrontation entre expérience et théorie quantique, n'a eu de cesse d'alimenter mes choix pour donner « un caractère original » à ma recherche.

Ce document se décompose en cinq chapitres portant sur mes activités de recherche et d'enseignement. Le Chapitre 1 est tout simplement un CV détaillé permettant à mes confrères de juger d'un éventuel « haut niveau scientifique » ; une liste exhaustive de mes publications y est incluse. Le Chapitre 2 est une initiative personnelle puisque j'y traite de mes considérations autour de l'enseignement de la Chimie Physique et de la photochimie. Dans la définition donnée plus haut, nulles traces de l'enseignement hormis une mention sur le cadrage des jeunes chercheurs. Or, il m'est apparu tout bonnement impossible d'écrire un bilan de ma carrière en omettant quasiment la moitié de mon activité. En effet, la formation universitaire et la recherche scientifique sont étroitement liées et il m'a semblé opportun de le coucher par écrit. Le chapitre 3 renvoie (je l'espère) à mon « aptitude à maîtriser une stratégie de recherche » puisque je décris le fameux triptyque qui est la colonne vertébrale de mon travail : spectroscopie résolue en temps, calculs TDDFT et traitement de données MCR-ALS. Enfin, les chapitres 4 et 5 décrivent mes résultats les plus marquants sur les deux types de molécules photofonctionnelles que j'ai étudiées, à savoir les molécules photochromes et les molécules à transfert de charge. Pour chacune de ces deux thématiques, je donnerai en fin de chapitre les perspectives pour les années à venir.

© 2016 Tous droits réservés.

doc.univ-lille1.fr

© 2016 Tous droits réservés.

doc.univ-lille1.fr

TABLE DES MATIERES

© 2016 Tous droits réservés.

doc.univ-lille1.fr

© 2016 Tous droits réservés.

doc.univ-lille1.fr

Chapitre 1

Curriculum détaillé

Stéphane ALOÏSE
54 rue Philippe de Girard
75018 Paris
06 15 94 45 64
stephane.aloise@univ-lille1.fr

Né le 9 octobre 1976 à Lyon 9e (40 ans)
Nationalité française
Pacsé, sans enfant

1. Résumé

Fonction actuelle	**MCF (section 31), Université Lille 1, Sciences et Technologies**
Activités de recherche	***Molécules photofonctionnelles étudiées par spectroscopie d'absorption ultrarapide*** Photochimie organique. Spectroscopie d'absorption ultrarapide. Calculs TDDFT.
Laboratoire	**LASIR** (Laboratoire de Spectrochimie Infrarouge et Raman) UMR8516 Bât. C5, Université Lille 1, Sciences et Technologies 59655 Villeneuve d'Ascq, France Tél. : 03 20 43 40 85 / Fax : 03 20 33 63 54 Mèl : stephane.aloïse@univ-lille1.fr
Communications scientifiques	•**Articles : 31** •**Conférences / Séminaires : 12** •**Posters : 12**
Formation	• Thèse de doctorat *« Processus d'ionisation en couche externe d'atomes de gaz rares étudiés par combinaison d'un rayonnement synchrotron et d'un laser »* Paris 11, 2002. • DEA de Physique fondamentale. Lyon I, 1998-99 (AB). • Maîtrise de Chimie Physique. Univ. McGill (Canada), 1997-98 (AB).
Enseignements	• Chimie générale ; atomistique et liaison chimique • Photochimie organique. Spectroscopie électronique, de vibration, de rotation. • Chimie quantique. Théorie des groupes. • Mathématiques pour les sciences physiques. • Niveau : Licence, Master, Master européen (cours en anglais).
Encadrement	2 thèses, 2 Post-Doc, 3 M2, 6 M1, 5 S6.

© 2016 Tous droits réservés.

2. Formation Académique

- **Depuis février 2004, Maître de Conférences à l'Université Lille 1.** « Molécules photofonctionnelles étudiées par spectroscopie d'absorption ultrarapide ».

- **Septembre 2003-février 2004, Poste complet d'ATER à l'Université Lille 1,** LASIR. « *Étude photochimique de photochromes organiques dérivés de la spirooxazine par spectroscopie d'absorption ultrarapide ».*

- **2002-2003, Poste complet d'ATER à l'Université Paris 6.** DIAM.* « *Double photoionisation des atomes et petites molécules étudiés au moyen du rayonnement synchrotron (coïncidences ions-électrons) ».* Responsables : P. Lablanquie et F. Penent.

- **1999-2002 : Doctorat de l'Université Lyon 1 effectué au LURE† de Paris 11.** *« Processus d'ionisation en couche externe d'atomes de gaz rares étudiés par combinaison d'un rayonnement synchrotron et d'un laser », sous la co-direction de* A. Lahmam-Bennani et M. Meyer. *Soutenance le 18 décembre 2002. Très honorable avec félicitations du jury.*

- **1998-1999 : DEA de Physique fondamentale « Constituants élémentaires de la matière ». Université Lyon 1.** Mention Assez Bien.

- **1997-1998 : Maîtrise de Chimie Physique en échange universitaire à l'Université McGill (Montréal, Canada).** Mention Assez Bien.

- **1994-1997 : Licence de Chimie Physique. Université Lyon 1.** Mention Assez Bien.

3. Formation continue

- **Détachement CNRS Septembre 2010-Septembre 2011 à l'ITODYS, Paris 7 (F. Maurel).**
  Le but de ce détachement était d'apprendre les méthodes TDDFT notamment appliquées aux calculs d'états excités afin de renforcer la synergie calculs-spectroscopie résolue en temps. Depuis cette année de détachement, je suis capable de lancer moi-même ou de superviser des calculs sur Gaussian.

- **École thématique du CNRS 2008 : Modélisation des propriétés chimico-physiques de molécules : maîtrise de l'outil quantique.**
  Cette école d'été pilotée par Carlo Adamo m'a permis de devenir familier avec les outils de la chimie computationnelle. Après un rappel théorique très ciblé, de nombreuses sessions de calculs sur ordinateur ont permis de rapidement nous familiariser avec les calculs de base : optimisation de géométrie, calculs de fréquence, scan sur une coordonnée réactionnelle choisie…

- **École d'été CNRS 2004: Réaction Ultrarapide en Solution.**
  Cette école d'été organisée par Thomas Gustassvson et Mohran Mostafavi a vraiment été un tremplin pour faire le lien entre la communauté de la physique atomique dont je suis issu (phase gaz) et le monde de la photochimie organique (phase condensée).

* Dynamique des Ions, Atomes et Molécules ; Ce laboratoire n'existe plus.

† Le Laboratoire pour L'Utilisation du Rayonnement Electromagnétique, fermé en 2003, est l'ancêtre de SOLEIL, centre synchrotron de l'Ile-de-France.

© 2016 Tous droits réservés.

doc.univ-lille1.fr

4. Activités en matière d'enseignement

Ces dernières années, j'ai enseigné dans de nombreux domaines de la Chimie Physique. Mes premiers enseignements portaient plus sur la chimie générale au sens large : chimie analytique, thermodynamique, cinétique chimique, cristallographie. Depuis quelques années, j'ai regroupé mes enseignements autour de la spectroscopie et de la photochimie.

Chimie Physique (responsable de module) Atomistique, liaison chimique, cristallographie	Licence (S1)	Cours-TD TP	50 h. 10 h.
Outils pour la chimie (mathématique appliquée, traitement du signal)	Licence (S4)	TD	12 h.
Chimie quantique	Licence (S5)	TD	26 h.
Spectroscopies électroniques et de vibration	Licence (S6)	TP	32 h.
Vibrational and Rotational spectroscopy **Advanced Spectroscopy for Chemistry (anglais)**	Master M1	TP	12h.
Organic Photochemistry (anglais)	Master M2	Cours-TD	16 h.
Photophysique - Photochimie	Prépa. agrégation	Cours-TD	10h.

- **Innovation en TP:**
  - TP de fluorescence du pyrène en milieu micellaire (M1)
  - 4 TP **en anglais** pour le Master ASC
    - Vibrational spectra of Methanol assigned by isotopic substitution method
    - Normal mode of vibration of Trans 1,2-dichloroethylene: Semi-empirical calculation, Raman and IR spectroscopy .
    - Rotational analysis of FTIR spectra from cigarette smoke
    - The Electronic absorption spectrum of molecular iodine
  - TP de découverte de la Mécanique Moléculaire (L3)
  - 3 TP d'instrumentation optique pour la spectroscopie (L2)
  - TP sur les groupes de symétrie. (L2)
  - TP utilisation d'Excel pour la chimie (L2)
  - TP de détermination des raies Balmer
  - 2 TP de liaison chimique avec le logiciel Spartan.

- **Responsabilité en enseignement :**

Depuis 2012, j'ai pris la responsabilité du cours de première année (1er semestre) S_1 intitulé « Atomistique et liaison chimique ». Ce cours est obligatoire pour l'ensemble des étudiants des parcours de sciences exactes et sciences de l'ingénieur : 750 étudiants soit 25 groupes, dont 2 groupes où l'enseignement est dispensé en anglais. Sous ma mandature, j'ai réussi (non sans mal) à :

- Unifier les documents de cours et fiches TD entre la vingtaine de collègue.
- Instaurer des TP de modélisations (VSEPR, OM des molécules diatomiques…) avec le logiciel accessible et pédagogique SPARTAN.
- Monter des TP de visualisation des raies de Balmer en utilisant un goniomètre en collaboration avec l'UFR de Physique.

© 2016 Tous droits réservés.

doc.univ-lille1.fr

5. Encadrement

- **Thèse de Doctorat Lille 1:**
  - Ismaïl Hamdi. *Photochimie d'un diaryléthène fonctionnalisé pour l'assemblage supramoléculaire : de la solution jusqu'au film élastomère opto-activable. Thèse en cours depuis le 1er décembre 2013.*

  - Zuzanna Pawłowska. *The Photophysics Of Pyridinium Betaines Studied By Ultrafast Transient Absorption Spectroscopy: Focus On The Photoinduced Intramolecular Charge Transfer Process. Soutenance 18 Janvier 2011.*

- **Post-doctorant :**
  - Ruan Yibin du 01/01 au 15/06/2013. Financement de la CFCSA (Fédération Franco-chinoise pour le science et ses applications). *Etude de translocations à l'état excité de nouveaux fluoroionophores par spectroscopie résolue en temps.*

  - Amit Kumar Tiwari 01/06/2014 au 30/05/2015. **Financement projet émergeant 2013 de la Région Nord-Pas de Calais**. *Photocomplexation de cations polluants pour l'environnement par des nouveaux fluoroionophores : complémentarité entre la spectroscopie résolue en temps et la chimiométrie*.

- **Stage de M2 :**
  - Fariza Si-Ahmed du 01/03 au 27/07/2013 financé par les **Relations Internationales de Lille 1** (Bourse forfaitaire de 2800 €). *Diaryléthènes photochromiques étudiés par spectroscopie UV/Vis et fluorescence.*
  - Ismail Hamdi en collaboration avec le laboratoire ITODYS (Aurélie Perrier, Paris 7). Du 01/12/2012 au 15/05/2013. *Diaryléthènes photochromiques étudiés par calculs TDDFT.*
  - *Yvan Mfunya, Etude par diffusion Raman de Résonance d'une molécule à transfert de charge de la famille des bétaïnes pyridinium*, mars–juin 2009.

- **Stage de M1 :**
  - I. Gulter. A. Tesch. *Molécules organiques à transfert de charge : rendement de triplet par spectroscopie photolyse-éclair,* septembre-novembre 2011.
  - N. Yataghene, R. Deprick. *Solvatochromisme de molécules organiques étudié par spectroscopie d'absorption et théorie de Marcus, septembre-novembre 2010.*
  - A. Lietard. *Etude par RMN et calculs DFT de betaines pyridinium.* Septembre-Novembre 2009.
  - M. Dorchain, M. Prevost. *Mesures des paramètres de photocoloration de molécules photochromes,* février-mai 2008.
  - T. Catteau, N. Djerane, J. Harbonnier. *Étude du retour thermique d'une solution photochromique obtenue à partir du carbinol de vert de malachite,* février-mai 2007.
  - M. Deoffre, V. Freville. *Détermination du nombre d'agrégation micellaire par fluorimétrie*, février-mai 2006.

- **Stage Licence S6 :**
  - V. Prudent. *Etude de l'assemblage supramoléculaire d'une Diaryléthène par suivi spectroscopique*, janvier-mars 2015.
  - D. Ednah Simangoye Ngobissi. *Etude en solution et sous forme de film d'un diaryléthène photochromique*, janvier-mars 2014.
  - L. Elyoussoufi. *Etude théorique de la complexation d'une bétaïne-pyridinium avec Ca^{2+} dans l'acétonitrile et l'eau*, janvier-mars 2013.

- **Stage Classe Préparatoire ENSC (École Nationale Supérieure de Chimie) :**
  - G. Fournet. *Découverte de la recherche en spectrochimie,* juin-juillet 2008.
  - L. Souillart. *Découverte d'un laboratoire de recherche,* juin-juillet 2006.

© 2016 Tous droits réservés.

doc.univ-lille1.fr

6. Activités en matière de recherche

6.1. Activités de recherche au LASIR

voir chapitres 3-5.

6.2. Projet et Financement

- Lauréat de l'appel à Projet, **Projet Emergeant 2013 de la Région Nord-Pas de Calais (Porteur)** *« Photocomplexation de cations polluants pour l'environnement par des nouveaux fluoroionophores : complémentarité entre la spectroscopie résolue en temps et la chimiométrie ».(24 mois).....74 000 €*
- ***2014** : Financement de 6 mois de Post-Doc par la CFCAS.....12 000 €*
- ***2013** : Financement d'un Master M2 étranger (RI Lille 1).....2 800€*
- **2011, 2012 :** Projet retenu par le Laboratoire Francis Perrin du CEA de Saclay pour accéder à la Plateforme de Photoélectron Femtoseconde.
- **2009 : Participation à l'ANR HETEROCOP (porteur : Pr. F. Odebel)**
- **2004 : BQR Lille 1 « Nouvel entrant »**

Etudes de molécules organiques pour la photonique par fluorescence et absorption infrarouge femtoseconde.....50 000 €

6.3. Publications

1. Hamdi, I.; Buntinx, G.; Perrier, A.; Devos, O.; Jaidane, N.; Delbaere, S.; Tiwari, A. K.; Dubois, J.; Takeshita, M.; Wada, Y.; Aloise, S., New insights into the photoswitching mechanisms of normal dithienylethenes. Physical Chemistry Chemical Physics, DOI: 10.1039/C6CP03471C, 2016.
2. Aloise, S.; Ruan, Y.; Hamdi, I.; Tiwari, A. K.; Buntinx, G.; Azarias, C.; Perrier, A.; Leray, I., Can betaine pyridinium derivatives be used to control the photoejection of cation? Physical Chemistry Chemical Physics 2016, 18 (22), 15384-15393.
3. Nair, M. N.; Hobeika, N.; Calard, F.; Malval, J. P.; Aloise, S.; Spangenberg, A.; Simon, L.; Cranney, M.; Vonau, F.; Aubel, D.; Serein-Spirau, F.; Lere-Porte, J. P.; Lacour, M. A.; Jarrosson, T., One- and two-photon absorption and emission properties of an oligo(phenylenethienylene)s series. Physical Chemistry Chemical Physics 2014, 16 (25), 12826-12837.
4. Lietard, A.; Piani, G.; Poisson, L.; Soep, B.; Mestdagh, J. M.; Aloise, S.; Perrier, A.; Jacquemin, D.; Takeshita, M., Competitive direct vs. indirect photochromism dynamics of constrained inverse dithienylethene molecules. Physical Chemistry Chemical Physics 2014, 16 (40), 22262-22272.
5. Aloise, S.; Ruan, Y. B.; Hamdi, I.; Buntinx, G.; Perrier, A.; Maurel, F.; Jacquemin, D.; Takeshita, M., The photochemistry of inverse dithienylethene switches understood. Physical Chemistry Chemical Physics 2014, 16 (48), 26762-26768.
6. Aloise, S.; Pawlowska, Z.; Poizat, O.; Buntinx, G.; Perrier, A.; Maurel, F.; Ohkawa, K.; Kimoto, A.; Abe, J., Excited-state dynamics of thiophene substituted betaine pyridinium compounds. Physical Chemistry Chemical Physics 2014, 16 (4), 1460-1468.
7. Perrier, A.; Aloise, S.; Olivucci, M.; Jacquemin, D., Inverse versus Normal Dithienylethenes: Computational Investigation of the Photocyclization Reaction. Journal of Physical Chemistry Letters 2013, 4 (13), 2190-2196.
8. Aloise, S.; Sliwa, M.; Buntinx, G.; Delbaere, S.; Perrier, A.; Maurel, F.; Jacquemin, D.; Takeshita, M., Do inverse dithienylethenes behave as normal ones? A joint spectroscopic and theoretical investigation. Physical Chemistry Chemical Physics 2013, 15 (17), 6226-6234.
9. Achelle, S.; Malval, J. P.; Aloise, S.; Barsella, A.; Spangenberg, A.; Mager, L.; Akdas-Kilig, H.; Fillaut, J. L.; Caro, B.; Robin-le Guen, F., Synthesis, Photophysics and Nonlinear Optical Properties of Stilbenoid Pyrimidine-Based Dyes Bearing Methylenepyran Donor Groups. Chemphyschem 2013, 14 (12), 2725-2736.
10. Aloise, S.; Pawlowska, Z.; Ruckebusch, C.; Sliwa, M.; Dubois, J.; Poizat, O.; Buntinx, G.; Perrier, A.; Maurel, F.; Jacques, P.; Malval, J. P.; Poisson, L.; Piani, G.; Abe, J., A two-step ICT process for solvatochromic betaine pyridinium revealed by ultrafast spectroscopy, multivariate curve resolution, and TDDFT calculations. Physical Chemistry Chemical Physics 2012, 14 (6), 1945-1956.

© 2016 Tous droits réservés.

11. Poizat, O.; Sliwa, M.; Ruckebusch, C.; Aloise, S.; Buntinx, G., Real-time capture of ultrafast chemical events. Actualite Chimique 2011, (348-49), 21-24.

12. Perrier, A.; Aloise, S.; Pawlowska, Z.; Sliwa, M.; Maurel, F.; Abe, J., Photoinduced intramolecular charge transfer process of betaine pyridinium: A theoretical spectroscopic study. Chemical Physics Letters 2011, 515 (1-3), 42-48.

13. Pawlowska, Z.; Lietard, A.; Aloise, S.; Sliwa, M.; Idrissi, A.; Poizat, O.; Buntinx, G.; Delbaere, S.; Perrier, A.; Maurel, F.; Jacques, P.; Abe, J., The excited state dipole moments of betaine pyridinium investigated by an innovative solvatochromic analysis and TDDFT calculations. Physical Chemistry Chemical Physics 2011, 13 (29), 13185-13195.

14. Buntinx, G.; Poizat, O.; Foley, S.; Sliwa, M.; Aloise, S.; Lokshin, V.; Samat, A., Sub-picosecond transient absorption spectroscopy of substituted photochromic spironaphthoxazine compounds. Dyes and Pigments 2011, 89 (3), 305-312.

15. Sliwa, M.; Mouton, N.; Ruckebusch, C.; Poisson, L.; Idrissi, A.; Aloise, S.; Potier, L.; Dubois, J.; Poizata, O.; Buntinx, G., Investigation of ultrafast photoinduced processes for salicylidene aniline in solution and gas phase: toward a general photo-dynamical scheme. Photochemical & Photobiological Sciences 2010, 9 (5), 661-669.

16. Aloise, S.; Sliwa, M.; Pawlowska, Z.; Rehault, J.; Dubois, J.; Poizat, O.; Buntinx, G.; Perrier, A.; Maurel, F.; Yamaguchi, S.; Takeshita, M., Bridged Photochromic Diarylethenes Investigated by Ultrafast Absorption Spectroscopy: Evidence for Two Distinct Photocyclization Pathways. Journal of the American Chemical Society 2010, 132 (21), 7379-7390.

17. Sliwa, M.; Mouton, N.; Ruckebusch, C.; Aloise, S.; Poizat, O.; Buntinx, G.; Metivier, R.; Nakatani, K.; Masuhara, H.; Asahi, T., Comparative Investigation of Ultrafast Photoinduced Processes in Salicylidene-Aminopyridine in Solution and Solid State. Journal of Physical Chemistry C 2009, 113 (27), 11959-11968.

18. Poizat, O.; Aloise, S.; Sliwa, M.; Buntinx, G.; Shilova, E.; Moustrou, C., Transient absorption studies of the photochromic behavior of 3H-naphtho 2,1-b pyran linked to a p-nitroaniline group. New Journal of Chemistry 2009, 33 (6), 1427-1432.

19. Ruckebusch, C.; Aloise, S.; Blanchet, L.; Huvenne, J. P.; Buntinx, G., Reliable multivariate curve resolution of femtosecond transient absorption spectra. Chemometrics and Intelligent Laboratory Systems 2008, 91 (1), 17-27.

20. Moine, B.; Rehault, J.; Aloise, S.; Micheau, J. C.; Moustrou, C.; Samat, A.; Poizat, O.; Buntinx, G., Transient absorption studies of the photochromic behavior of 3H-naphtho 2,1-b pyrans linked to thiophene oligomers via an acetylenic junction. Journal of Physical Chemistry A 2008, 112 (21), 4719-4726.

21. Moine, B.; Aloise, S.; Buntinx, G.; Poizat, O.; Lokshin, V.; Moustrou, C.; Samat, A., Photoreactivity of organic photochromes in solution. Experimental investigation by femto-picosecond absorption spectroscopy. Actualite Chimique 2008, (320-21), 20-26.

22. Aloise, S.; Ruckebusch, C.; Blanchet, L.; Rehault, J.; Buntinx, G.; Huvenne, J. P., The benzophenone S-1(n,pi*) -> T-1(n,pi*) states intersystem crossing reinvestigated by ultrafast absorption spectroscopy and multivariate curve resolution. Journal of Physical Chemistry A 2008, 112 (2), 224-231.

23. Aloise, S.; Rehault, J.; Moine, B.; Poizat, O.; Buntinx, G.; Lokshin, V.; Vales, M.; Samat, A., Photochromism of photoenolizable ketones in quinoline and 1,8-naphthyridine series studied by time-resolved absorption spectroscopy. Journal of Physical Chemistry A 2007, 111 (10), 1737-1745.

24. Petrov, I. D.; Peters, T.; Halfmann, T.; Aloise, S.; O'Keefe, P.; Meyer, M.; Sukhorukov, V. L.; Hotop, H., Lineshapes of the even mp(1/2)(5)n(p '/f ') autoionizing resonances of Ar, Kr and Xe. European Physical Journal D 2006, 40 (2), 181-193.

25. Aloise, S.; O'Keeffe, P.; Cubaynes, D.; Meyer, M.; Grum-Grzhimailo, A. N., Photoionization of synchrotron-radiation-excited atoms: Separating partial cross sections by full polarization control. Physical Review Letters 2005, 94 (22).

26. O'Keeffe, P.; Aloise, S.; Fritzsche, S.; Lohmann, B.; Kleiman, U.; Meyer, M.; Grum-Grzhimailo, A. N., Resonant Auger decay of Xe(*) 4d(5/2)(-1)6p: A contribution to the complete experiment from fluorescence polarization studies. Physical Review A 2004, 70 (1).

27. Penent, F.; Lambourne, J. G.; Lablanquie, P.; Hall, R. I.; Aloise, S.; Zitnik, M.; Bucar, K.; Hammond, P., Fluorescence of helium doubly excited states. In Correlation and Polarization in Photonic, Electronic, and Atomic Collisions, Hanne, G. F.; Malegat, L.; SchmidtBocking, H., Eds. Amer Inst Physics: Melville, 2003; Vol. 697, pp 151-157.

© 2016 Tous droits réservés.

doc.univ-lille1.fr

28. O'Keeffe, P.; Aloise, S.; Meyer, M.; Grum-Grzhimailo, A. N., Circular polarization of ion fluorescence completing the analysis of resonant Xe*4d(5/2)(-1)6p Auger decay. Physical Review Letters 2003, 90 (2).

29. Meyer, M.; Aloise, S.; O'Keeffe, P.; Grum-Grzhimailo, A. N., Polarization effects in the photoionization of VUV-excited atoms. In Correlation and Polarization in Photonic, Electronic, and Atomic Collisions, Hanne, G. F.; Malegat, L.; SchmidtBocking, H., Eds. Amer Inst Physics: Melville, 2003; Vol. 697, pp 42-47.

30. Johansson, A.; Raarup, M. K.; Li, Z. S.; Lokhnygin, V.; Descamps, D.; Lynga, C.; Mevel, E.; Larsson, J.; Wahlstrom, C. G.; Aloise, S.; Gisselbrecht, M.; Meyer, M.; L'Huillier, A., Two-color pump-probe experiments in helium using high-order harmonics. European Physical Journal D 2003, 22 (1), 3-11.

31. Meyer, M.; Aloise, S.; Grum-Grzhimailo, A. N., Strong, polarized Balmer-alpha fluorescence after resonant core excitation of HCl. Physical Review Letters 2002, 88 (22).

6.4. Séminaires et conférences

CONFERENCES INVITEES:

- **JCTC 10,** X^{èmes} Journées de Chimie Théorique et Computationnelle, 18-20 novembre 2012, ORAN, ALGERIE. Communication orale (30 min): S.Aloïse, *Photochemical pathway of Photofonctional Organic Molecules: complementarity between time-resolved spectroscopy and TDDFT calculations.*

COMMUNICATIONS ORALES :

- **ICP 2015, 27th International Conference on Photochemistry** in Jeju Island, Korea, 28 juin-3 juillet 2015 **:** *Towards Novel Photodriven Actuators?... Photochemical Investigations on original Photochromic Diarylethene/Elastomer*.
- **GDRI PHENICS 2014,** 18-19 juillet 2014, Bordeaux (communication orale 20 min) : *The photochemistry of inverse dithienylethene switches understood*.
- **GFP 2013, Groupement Français de Photochimie**, 12-13 Novembre 2013, Orsay. Communication orale (20 min) : *Complexation of cation by betaine pyridinium derivatives: toward excited states translocation?*
- **IUPAC 2012, International Union of Pure and Applied Chemistry,** 15-20 juillet 2012**,** COIMBRA, PORTUGAL. Communication orale (25 min) : *Diarylethenes photocyclization: Torsionnal modes signature revealed by ultrafast spectroscopies and TDDFT calculations.*
- **GFP 2012, Groupement Français de Photochimie**, 31 mai-1er juin 2012, Bordeaux. Communication orale (20 min) : *Photochimie de bétaïne pyridinium solvatochromes étudiée par spectroscopies ultrarapides et calculs TDDFT.*
- **Seminaire ITODYS Avril 2011.** Communication orale (45 min) : Molécules organiques photofonctionnelles étudiées par spectroscopie ultrarapide et calculs TDDFT.
- **FISPHOTON 2009,** France-Italy symposium on Photosciences, 7-10 décembre 2009, Marseille. Une présentation orale (20 min.) : *Bridged Photochromic diarylethenes investigated by ultrafast absorption spectroscopy: evidences for two distinct photocyclization pathways.*
- **Journées de Printemps 2008 du Groupe Français de la Photochimie.** 21-23 mai 2008, Télécom Bretagne, Brest. Communication orale (20 min.) : *Photochimie de molécules photochromes et molécules modèles étudiées par spectroscopie d'absorption ultrarapide et résolution de données multivariées.*

© 2016 Tous droits réservés.

- **École thématique du CNRS 2008 : Modélisation des propriétés chimico-physiques de molécules : maîtrise de l'outil quantique.** 2-6 juin 2008, Montpellier, France. Une présentation orale (5 min.) : *Photophysique de molécules photoconductrices étudiées par spectroscopie d'absorption femtoseconde.*
- **JFJSP 2008. New Horizons of Photochromism – From design of molecules to applications.** 12-15 octobre 2008, Arras. Communication orale (15 min.) : *Investigation of 1,2-dicyano[2,n]metacyclophan-1-enes photochromism by time-resolved absorption spectroscopy.*
- **CERC 2007 Young Chemists' Workshop: « Time-resolved methods for studies of chemical reactions ».** 26-27 avril 2007, Göttingen, Allemagne. Communication orale (30 min.) : *Photochromism of photoenolizable ketones in quinoline and 1,8-naphthyridine series studied by time-resolved absorption spectroscopy*.
- **POM3,** 19-20 mai 2005, Marseille, France. Communication orale (30 min.) : *Photochromes hétérocycles étudiés par spectroscopie d'absorption ultrarapide résolue en temps*.
- **Séminaire Jeunes Chercheurs du LURE**. 13 juin 2002, Orsay, France. Communication orale (15 min.) : *Effets de polarisation dans la photoionisation du xénon.*
- **Séminaire Jeunes Chercheurs du SPAM**. Juillet 2002, Centre CEA de Saclay, France. Communication orale (45 min.) : *Expériences RS + laser appliquées à l'étude d'espèces atomiques*.

COMMUNICATIONS PAR AFFICHES:

- **France-Japan Symposium On Molecular Technology,** 9 mars 2015, Paris, France, poster : *Advanced molecular technology: toward photodriven actuators based on bistable photochromic diarylethene.*
- **IUPAC 2014,** 13-18 juillet 2014, Bordeaux, France, Poster : *Complexation of cation by betaine pyridinium derivatives: toward excited states translocation?*
- **ISOP 2013, International Symposium On Photochromism**, 23-26 Septembre 2013, Berlin, ALLEMAGNE. Poster : *Ultrafast relaxation dynamics of isolated photochromic molecules.*
- **ISOP 2010, International Symposium On Photochromism**, 17-21 Octobre 2010, YOKOHAMA, JAPON. Poster : *Bridged Photochromic diarylethenes investigated by ultrafast absorption spectroscopy: evidences for two distinct photocyclization pathways.*
- **ICP 2009 – International Conference on Photochemistry.** 19-24 juin 2009, Toledo, Espagne. Un poster *Intramolecular Charge Transfer Of Pyridinium Betainederivatives Based On Stationary And Ultrafast Absorption Spectroscopies.*
- **Russian - French Bilateral Seminar on Molecular Switching.** 22-25 octobre 2007, Saissac, France. Un poster.
- **JPU 2005 - Journée des Processus Ultrarapides.** 5-7 décembre 2005, Villeneuve d'Ascq, France. Un poster. Membre du comité d'organisation.
- **POM3,** 14-15 décembre 2004, Villeneuve d'Ascq, France. Un poster.
- **COMES** (Commutation Moléculaire à l'État Solide) et **POM3**, 8-11 octobre 2003, Collonges la Rouge, France. Un poster.
- **PAMO 2002**, Physique Atomique, Moléculaire et Optique. 1-7 juillet 2002, Bourges, France. Un poster.
- **International Workshop on Photoionization**. 5-9 octobre 2000, Carry Le Rouet, France. Un poster.

© 2016 Tous droits réservés.

doc.univ-lille1.fr

ORGANISATION d'événements :

- **FEMTO 2012, Ecole Thématiques du CNRS "Sources femtoseconde : Technologies et Applications"**, 25-29 juin, St Valery-Sur-Somme, (Comité d'organisation). Choix des intervenants oraux ; aide sur l'intendance (Hôtel); Elaboration des badges, remplissage des sacoches.
- **EMLG/JMLG (European/Japanese Molecular Liquids Group) annual meeting 2013** 09-13 septembre 2013 à Villeneuve d'Ascq, (Comité d'organisation). Accueil des participants (réception des impayés, remise des badges et sacoches)
- **JPU 2005 - Journée des Processus Ultrarapides.** 5-7 décembre 2005, Villeneuve d'Ascq, France. Un poster. (Comité d'organisation). Elaboration des badges, remplissage des sacoches.

© 2016 Tous droits réservés.

doc.univ-lille1.fr

© 2016 Tous droits réservés.

doc.univ-lille1.fr

Chapitre 2

Enseigner la Chimie Physique à l'Université : une gageure ?

Il est peut être inhabituel de détailler sur plusieurs pages ses activités d'enseignements mais je pense que le sens même du diplôme universitaire « Habilitation à Diriger des Recherches » passe par un apprentissage de la pédagogie, de la transmission du savoir, les fameuses « bases scientifiques ». Il va de soi que sans Licence (que beaucoup déprécient), sans Master…point de Doctorat et donc point de Recherche. Le titre de cette partie (délibérément provocateur) reflète, à mon humble avis, un état d'esprit généralisé des enseignants de France qui ne savent plus comment faire pour bien enseigner les sciences en général, la Chimie Physique en particulier. Cette sous-discipline de la chimie est probablement plus difficile à enseigner car outre les concepts de la chimie, elle s'appuie sur deux disciplines redoutées des néo-bacheliers, à savoir la physique (pour l'instrumentation) et les mathématiques (pour le formalisme).

Depuis mon arrivée à l'Université de Lille 1 en septembre 2003 (en tant qu'ATER), hormis les cours de Chimie Générale (très bien cadré d'ailleurs) dispensé aux élèves de Licence des filières de Biologie jusqu'en 2008 (loi d'équilibre, pH-mètrie, oxydo-réduction, thermodynamique…), j'ai rapidement pu recentrer mes enseignements autour de la Chimie Physique, de la spectroscopie et de la photochimie, depuis la Licence jusqu'au Master. Une liste un peu près exhaustive des enseignements que j'ai dispensés se trouve en page 15 de ce document.

Dans la suite de ce chapitre, après quelques considérations sur l'enseignement des sciences en Terminale S, je vais expliciter mon action pédagogique en Licence via deux cours dont je suis responsable, « atomistique et liaison chimique » en L1 et « instrumentation optique pour la chimie » en L2. Je parlerai ensuite de ma participation au Master Européen « Advanced Spectroscopy for Chemistry » qui m'a permis d'enseigner la photochimie organique à un public intéressé. Enfin, je parlerai d'un projet d'enseignement qui me tient à cœur : la mise en place d'une Licence internationale.

1. Les Néo-Bacheliers de terminale S : une réforme contre-productive ?

Pour commencer, j'aimerai vous exposer ici quelques extraits du chapeau de la nouvelle Terminale S publiés au Journal officiel du Bulletin officiel spécial n°8 du 13 octobre 2011. Je me permets de mettre en gras les passages les plus truculents.

« Dans une société où des informations de tous ordres arrivent dans l'immédiateté et de toutes parts, la priorité est donnée à la formation des esprits **pour transformer cette information en une connaissance**. L'enseignant doit être un accompagnateur de chaque élève dans l'acquisition de compétences qui ne peuvent être opérationnelles sans connaissances, qui sont à la fois la base et l'objectif de la didactique, notamment scientifique. Formation des esprits et acquisition de connaissances sont deux facettes indissociables de l'activité éducative…

…Deux compétences occupent une place centrale en terminale: «extraire» et «exploiter» des informations; elles seront mises en œuvre fréquemment, notamment dans les situations identifiées dans la colonne de droite du programme, en respectant l'esprit de la démarche scientifique. Les activités proposées aux élèves au sujet de **la compétence «extraire » et leurs connaissances acquises doivent les conduire à s'interroger de manière critique sur la valeur scientifique des informations, sur la pertinence de leur prise en compte, et à choisir de façon argumentée ce qui est à retenir dans des ensembles où l'information est souvent surabondante et parfois erronée, où la connaissance objective et rationnelle doit être distinguée de l'opinion et de la croyance**. Les supports d'informations proposés aux élèves seront multiples et diversifiés: textes de vulgarisation et textes scientifiques en français et éventuellement en langue étrangère, tableaux de données, constructions graphiques, vidéos, signaux délivrés par des capteurs, spectres, modèles moléculaires, expériences réalisées ou simulées, etc.

© 2016 Tous droits réservés.

doc.univ-lille1.fr

L'exploitation sera conduite en passant par l'étape d'identification des grandeurs physiques ou chimiques pertinentes et par celle de modélisation. Cette formalisation pourra conduire à l'établissement des équations du modèle puis à leur traitement mathématique, numérique ou graphique. L'élève est ainsi amené à raisonner avec méthode et à mettre en œuvre avec rigueur l'ensemble des étapes qui lui permettent de trouver la ou les solution(s) au problème posé. **Le professeur aura cependant à l'esprit que le recours à des outils mathématiques n'est pas le but premier de la formation de l'élève en physique-chimie, même si cela peut être parfois nécessaire pour conduire une étude à son terme**. Dans certains cas, le professeur utilisera des méthodes de résolutions graphique ou numérique, pratiques de plus en plus fréquentes en raison de la complexité des systèmes étudiés. Ce sera aussi l'occasion de souligner que les travaux de recherche sont souvent conduits par des équipes pluridisciplinaires.

Le professeur fera aussi appel à des exploitations qualitatives conduites avec rigueur. L'emploi de celles-ci s'avère particulièrement opportun dans le cas où elles permettent de dégager directement le sens de l'étude que pourrait masquer un développement calculatoire. Ainsi, l'analyse dimensionnelle, l'examen préalable des différents phénomènes en cause, la comparaison d'ordres de grandeur peuvent permettre une simplification efficace du cadre conceptuel de la situation et fournir une résolution élégante, rapide, à un problème a priori complexe.

Familiariser ainsi l'élève à pratiquer des raisonnements qualitatifs, à savoir faire de la physique et de la chimie «avec les mains», c'est aussi l'habituer à savoir communiquer en tant que scientifique avec des non-scientifiques…etc »

A la lecture de ce texte, on comprend à quel point « la science 2.0 » faite « avec les mains » de Terminale S, nous draine une foule de néo-bacheliers sans plus aucune base scientifique. Le formalisme mathématique, meilleur allié d'une science rigoureuse est proscrit et la moindre équation devient un problème. Dans le cadre de la L1, certains collègues réclament le retrait des calculs de moment dipolaire moléculaire (additions de vecteurs) faute de compréhension des étudiants. Même la culture scientifique, la plus basique soit elle, est perdue, noyée dans des chapitres absolument trop complexes pour des Terminales S (Stéréochimie, Spectroscopie Infrarouge, RMN, Physique quantique et Relativité générale !) Certains défenseurs des dernières réformes pédagogiques lycéennes réfuteront que le niveau est en chute libre en fustigeant les partisans du « c'était mieux avant ». Après tout, les statistiques parlent pour eux puisque le taux de réussite au BAC S en 2015 était de 92% … un tel chiffre pousse forcement au questionnement. Concrètement, à l'Université de Lille 1, nous évaluons le niveau scientifique des étudiants grâce à un test d'évaluation de pré-rentrée en mathématique, physique et chimie. Evidemment, pour les étudiants hors mention TB, les résultats sont alarmants. Je me permets juste de soumettre au lecteur cette question de chimie générale (capture d'écran du test) :

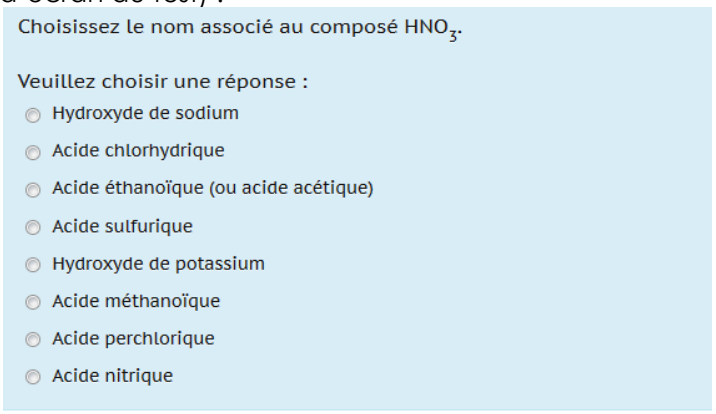

Le taux de bonnes réponses des 450 étudiants présents au test était de 38 % (cqfd). Clairement, il est important de préciser que notre tâche d'enseigner à l'université est de plus en plus difficile par rapport à un public de plus en plus fragile.

Pour ma part, un début de solution pour les nouveaux entrants à l'université serait de leur donner goût à la science avec un discours de vérité (l'exact contraire du texte plus haut) tout en essayant de trouver des solutions aux problèmes suivants :

- manque de vraie culture scientifique ;
- bases mathématiques hésitantes ;
- crainte du formalisme ;
- fragilité des méthodes de travail (pas de fiche de cours, non-analyse de l'énoncé…).
- capacités horaires de travail trop faible

A ces difficultés générales, s'ajoutent les difficultés spécifiques de l'enseignement de la Chimie Physique qui ne sont pas des moindres : i) recours à la physique (instrumentation) et aux

© 2016 Tous droits réservés.
doc.univ-lille1.fr

mathématiques (formalisme) ; ii) mauvaises considérations des étudiants et de certains collègues qui ne considèrent pas la Chimie Physique comme de la « vraie chimie ». Je pense que ces deux problèmes sont assez récurrents dans beaucoup d'Universités. Dans la suite de ce document, en prenant en considération la spécificité de ce public de néo-bacheliers, je vais décrire trois cours de Chimie Physique (ou apparenté) de L1, L2 et Master afin de partager quelques pistes pédagogiques pour essayer de renforcer l'enseignement de cette discipline.

2. Un enseignement innovant de la Chimie Physique en L1 ?

Un cours très important pour n'importe quel scientifique est le « cours d'atomistique et liaison chimique » dispensé aux étudiants de L1. Son contenu est tout à fait classique : depuis la description de l'atome, son arrangement en molécule diatomique jusqu'aux molécules polyatomiques et les interactions faibles entre elles (voir l'Annexe 1 pour plus de détail)

J'ai pris la responsabilité de ce cours en septembre 2012 et à l'époque il n'y avait que 7 groupes de Cours-TD (CTD) à gérer (cours dispensé au S2). Depuis septembre 2014, ce cours a été replacé au S1 où il est dispensé **en tronc commun** pour l'ensemble des étudiants du S1 (la spécialisation intervient ensuite au S2 avec un choix de bi-mention). Outre les difficultés majeures exposées plus haut, il m'a fallu faire des choix pédagogiques importants afin de trouver le bon équilibre entre l'exigence de la discipline et l'attrait des étudiants. Il est à préciser que 750 étudiants sont en général inscrits en L1 et que ces derniers sont répartis selon 20 groupes de SESI (Science Exacte et Science de l'Ingénieur) et 5 groupes PEIP (Parcours Elèves Ingénieurs Polytech). Ces derniers sont sélectionnés sur APB (Admission PostBAc) et ont pour la plupart une mention B ou TB au BAC S.

Le Format du Cours. L'ensemble de l'équipe pédagogique a fait le choix d'un Cours-TD (CTD) dispensé en 48h plutôt que d'un Cours Magistral (CM) accompagné de Travaux Dirigés (TD). Ce choix permet d'accueillir l'étudiant en faisant une transition douce entre le lycée et l'université. De plus, il est plus aisé de repérer les difficultés des étudiants. Il est vrai que le CM oblige l'étudiant à une auto-responsabilisation rapide, mais cela peut se faire progressivement en privilégiant les CM au S2 voire au L2.‡

Le contenu. Au vue du constat alarmant de terminal S, faut-il alléger les contenus ? Faut-il vraiment insister sur l'atome de Bohr ? Les fameuses orbitales moléculaires… doit-on en parler ? Doit-on s'excuser de leur présenter l'équation de Schrödinger ? Ma position est assez ferme sur ce point. Il faut cesser de répéter les mêmes erreurs qu'au lycée en montrant une image falsifiée des sciences. Si un concept repose sur une équation ou des notions déstabilisantes (ex : probabilité de présence), il ne faut pas éliminer le problème mais trouver des leviers pédagogiques pour leur faire comprendre, voir apprécier, le concept en question. J'ai donc refusé tout allègement de la partie atomistique.

Les innovations. Ainsi, depuis ma prise de responsabilité, j'ai essayé d'apporter une cohérence auprès de l'équipe pédagogique (typiquement 18 permanents, 2 non-permanents pour 25 groupes de CTD) autour d'un document commun de cours que chacun retranscrit à sa manière auprès des étudiants. De même, nous avons créé un document commun d'exercices corrigés qui est la base des TD. Les DS sont conçus dans un esprit d'équité avec graduation croissante de la difficulté au fil des questions.

Mais en fait, les innovations principales concernent l'introduction de TP pour illustrer des notions parfois trop théoriques. Ainsi, j'ai mis au point en collaboration avec P. Hubert (Moniteur) et T. Sanctorum (Préparateur TP de l'UFR de physique) un TP de visualisation des raies de Balmer à l'aide d'un goniomètre. De même, j'ai élaboré 2 TP de chimie computationnelle basés sur le software SPARTAN Student qui est très maniable et simple d'utilisation (à la différence de Gaussian). Par exemple, les étudiants calculent l'énergie de deux atomes d'hydrogène à une distance choisie et il retrace sur papier millimétré la courbe d'énergie potentielle : c'est donc un moyen très

‡ Au moment d'écrire ces lignes, j'apprends que pour des raisons budgétaires, nous allons devoir repasser en CM+TD. Tout notre travail tombe à l'eau et il va falloir repenser des CM modernes et pédagogiques pour ne pas perdre un public immature, fragile et volatil.

© 2016 Tous droits réservés.

doc.univ-lille1.fr

pédagogique de leur inculquer la notion de stabilité d'une liaison chimique. L'apport de ces trois TP a permis aux étudiants de mieux appréhender des notions difficiles du cours.

Plateforme pédagogique Moodle. Nous avons la chance à l'Université de Lille 1 d'avoir un service informatique très performant et tourné vers une pédagogie moderne. Le SEMM (Service Enseignement et Multi-Média) est un allié précieux pour une interactivité moderne avec les étudiants. Ainsi, avec l'assistance de Téodorina Tibar, j'ai installé mon cours sur Moodle§ ce qui permet d'interagir rapidement avec les étudiants (messages importants, transmission de documents, sondages…etc).

Les cours en Anglais. Depuis 2014, sous l'impulsion de M. M'Zari (Directeur des études de la L1), plusieurs cours peuvent être déclinés en anglais pour deux groupes de SESI ce qui représente une soixantaine d'étudiants. Précisons que ces étudiants sont sélectionnés sur APB selon leurs notes en sciences (mention B) et en anglais : Bien évidemment, la chimie a joué le jeu en proposant à la fois, un CTD et des TP en anglais. Je reviendrai sur l'enseignement en anglais plus tard.

Les résultats. Sur les 750 étudiants inscrits en S1, tous ayant la même épreuve, le taux de réussite est fortement dépendant du public concerné. Pour les 5 groupes PEIP, le taux de réussite oscille entre 80 et 90% ce qui dépasse de loin nos espérances. Il faut savoir que ces étudiants visent à intégrer l'école d'ingénieur universitaire PolyTech'Lille et ils savent qu'ils doivent valider leur module absolument. Il existe donc des étudiants « bons en science » mais ils sont en désamour avec les filières universitaires classiques. De la même manière, les deux groupes SESI des filières bilingues s'en sortent très bien avec des taux de réussite autour des 70%. A l'inverse, pour les 20 groupes SESI, les résultats sont alarmants puisqu'ils oscillent entre 15 et 55%. Cette mise en exergue interroge sur le système éducatif français avec une élite d'ingénieurs bien formés et des étudiants universitaires fragiles. Ceci étant dit, nous avons été capable via les sections bilingues de créer des filières universitaires avec un bon niveau et avec une réelle motivation (enseignement des sciences en anglais).

3. Consolider les bases de la Chimie Physique en L2 ?

A l'Université Lille 1, au second semestre de la première année, les étudiants tentés par la chimie ont le choix entre 7 bi-mentions au gré de leur envie : Chimie Physique, chimie-méca, chimie-EEA, chimie-génie civil, chimie-informatique…. Cette aberration pédagogique a entrainé un problème majeur : hormis ceux ayant choisis la bi-mention Chimie Physique, les autres étudiants (la moitié de la L2 chimie) n'ont pas suivi de cours d'optique en première année. De plus, sous l'impulsion « des vrais chimistes » la L2 et la L3 ont été purgées de l'ensemble des cours de mathématique et de physique. Ainsi, nous nous retrouvions avec des étudiants de L3 qui ne savaient pas ce qu'était une interférence lumineuse. Ainsi, j'ai proposé d'ouvrir une option au S3, intitulée « Instrumentation pour la Chimie » centrée sur l'optique ondulatoire et les détecteurs (voir fiche de cours sur l'Annexe 1).

Il est vrai que les parties théoriques ont du mal à passer mais il est impératif de faire comprendre aux étudiants que la science et leur vie professionnelle future ne sera pas forcement simple, avenante, presse-bouton. Par contre, la réaction des étudiants face aux TP a été assez réjouissante puisqu'ils ont fait le lien entre ces TP d'instrumentation et les autres matières de la chimie. Par exemple, il leur a été proposé d'enregistrer le spectre d'une lampe Hg avec soit un monochromateur soit un polychromateur. Ainsi, ils ont pu, par eux-mêmes, dégager les points forts et points faibles de chacun des deux instruments. Dans un autre TP, les étudiants commençaient par manipuler un interféromètre de Michelson pour ensuite enregistrer des spectres IRTF de films polymère sur un instrument commercial leur permettant de comprendre le rôle clef de l'interférogramme pour de telles mesures.

§ Moodle est une plate-forme d'apprentissage en ligne (en anglais : Learning Management System ou LMS) sous licence libre servant à créer des communautés s'instruisant autour de contenus et d'activités pédagogiques. Le mot « Moodle » est l'abréviation de Modular Object-Oriented Dynamic Learning Environment : « Environnement orienté objet d'apprentissage dynamique modulaire ».

© 2016 Tous droits réservés.

doc.univ-lille1.fr

4. Donner le goût de la photochimie en Master

A l'Université Lille 1, il n'est pas évident d'imposer la photochimie organique dans le cursus classique du Master de Chimie centré sur l'applicatif (chimie de l'eau, formulation…). Une notable exception concerne le Master « Métiers de l'enseignement et de la formation », mention chimie (J. F. Paul) dans lequel je dispense 8h de CTD sur la photochimie organique aux étudiants préparant l'agrégation. Il est à noter que la photochimie est une matière de plus en plus posée à l'épreuve d'agrégation de chimie (2010, 2015, 2016).

A l'inverse, Le Master européen ERASMUS-MUNDUS (S. Cristol) intitulé « Advanced Spectroscopy for Chemistry » (ASC) est un outil formidable pour l'essor de la Chimie Physique en général et la photochimie organique en particulier. Tous les étudiants suivent le M1 à Lille puis ont le choix entre 5 M2 différents (Lille, Cracovie, Bologne, Helsinki, Leipzig). Le niveau des étudiants de ce Master est très élevé ce qui permet de ne pas se restreindre. J'interviens à la fois en M1 où je donne un cours introductif sur la photochimie organique (diagramme de Jablonski, règle du miroir, notion de rendement quantique…). En M2, je pousse beaucoup plus loin les notions de photochimie (théorie de Marcus, photochromisme…) et j'aborde les montages de la plateforme de spectroscopie ultrarapide du LASIR (F. A. Mianney se charge de la partie fluorescence résolue en temps). Clairement, ce cours de M2 est la charnière parfaite entre la formation universitaire et nos activités de recherche ; il constitue donc un vivier de recrutement des futurs doctorants. Ceci-dit, si les effectifs du M1 sont toujours compris entre 10 et 20 étudiants (ce qui est très bien pour un Master de Chimie Physique), nous peinons à avoir plus de trois étudiants en M2. A titre de comparaison, le parcours M2 du Master de chimie « Chimie et Ingénierie de la Formulation » rassemble chaque année plus de 30 étudiants.

5. Projet d'enseignement : une licence internationale à Lille 1

Après une dizaine d'année d'enseignement et l'expérience de S1 bilingue (voir ci-dessus), un constat clair m'est apparu pour essayer de revigorer les effectifs des Masters de Chimie Physique de Lille 1 qui sont essentiellement en anglais (le MASTER ASC, Atmospheric Environnent (D. Petitprez), Bioraffinery (M. Capron)) : créer une Licence de Sciences de Physique/Chimie entièrement en anglais. Quels sont les intérêts d'une telle filière ? Tout d'abord, cela permettra de créer une filière d'excellence universitaire ce qui va attirer les bons étudiants (c'est ce qui arrive actuellement au S1 bilingue). Est-ce que les étudiants français seront effrayés par cette offre ? Nous avons lancé des sondages auprès des étudiants de l'an dernier et plus de 75 % d'entre eux voulaient l'intégralité de leurs cours en anglais. De plus, il sera possible de lancer massivement des programmes Erasmus avec des pays autres que ceux de la francophonie. Il faut savoir que le Nord-Pas de Calais possède des relations privilégiées avec les Etats-Unis via les programmes FullBright et il serait intéressant de pouvoir établir un partenariat avec des universités américaines.

Dans les faits, nous allons nous adosser à la Licence de Physique/Chimie (O. Houde) supportée par les UFR de Chimie et de Physique, pour attirer un maximum d'étudiants. En ouvrant ce nouveau parcours « international bachelor » sur la L2 et la L3, avec la totalité des cours en anglais, on pourra ainsi constituer un vivier d'étudiants qualifiés et motivés qui auront eu toutes les bases (physiques, mathématique) pour devenir des physico-chimistes performants.

Bien évidemment, ce projet que je porte avec mon collègue F.A. Mianney, commence à peine à voir le jour et il est donc difficile d'en dire plus pour l'instant mais je tenais à en parler dans mon manuscrit d'HDR car ce projet est en fait une élégante synthèse de toutes mes considérations sur l'enseignement de la Chimie Physique. J'ai bien conscience que le projet est très risqué mais j'ai besoin d'essayer de le mettre en œuvre : c'est un devoir moral en quelque sorte.

© 2016 Tous droits réservés.

doc.univ-lille1.fr

© 2016 Tous droits réservés.

doc.univ-lille1.fr

Chapitre 3

Stratégie de recherche : approches expérimentales et théoriques pour étudier les molécules photofonctionnelles

Dès mon arrivée au LASIR en septembre 2003 en tant qu'ATER, il m'a été demandé par Guy Buntinx et Olivier Poizat de travailler sur une thématique nouvelle et prometteuse : « les molécules organiques photofonctionnelles » termes que je ne connaissais pas à l'époque. Il est bon de rappeler qu'à l'issue de ma thèse effectuée à Paris 11 et de mon premier ATER à Paris 6, la plus grosse molécule que j'avais étudiée était le dimère du Xénon. Je tiens cependant à redire encore une fois, combien la formation rigoureuse que j'ai reçue en physique Atomique et Moléculaire m'a permis d'aborder cette thématique avec un regard nouveau. Durant ma thèse,[**] j'ai employé la combinaison d'un rayonnement synchrotron et d'un laser pour pouvoir sonder indépendamment différents mécanismes de photoionisation des atomes de gaz rare. La section efficace expérimentale pouvait ensuite être comparées à la théorie de la matrice densité afin de déduire les différentes voies correspondant à un nombre quantique définit. A cet époque, mon environnement (mes directeurs de thèse, mes collègues) ne se souciaient guère des applications puisque le but de cette science était l'innovation technique (combinaison rayonnement synchrotron et laser) et le perfectionnement des théories quantiques de l'atome via une comparaison avec les spectres expérimentaux.

Le but de mon préambule est de faire comprendre au lecteur que ma formation doctorale a profondément guidé mes choix, mes angles d'attaque pour appréhender la problématique des molécules photofonctionnelles. Je pense que ce bagage de « scientifique du fondamental » ne m'a jamais quitté et probablement ne me quittera jamais même si, après plusieurs années de résistance, je fais maintenant des efforts pour m'ouvrir à l'applicatif en y prenant un certain plaisir.

Dans la suite de ce chapitre, je vais présenter « les moyens » utilisés pour mener à bien ma recherche au sein du LASIR, depuis les techniques expérimentales et théoriques jusqu'à mes choix stratégiques et collaboratifs. Ceci mettra en lumière les chapitres suivants qui seront purement scientifiques. Tout d'abord, je vais présenter l'équipe scientifique au sein de laquelle je travaille au LASIR puis mes collaborations. Bien évidemment, je vais présenter la spectroscopie résolue en temps en me focalisant sur la spectroscopie d'absorption ultrarapide car c'est la technique que j'ai le plus utilisée. Je donnerai dans ce chapitre une place particulière au traitement de données, car je suis le premier « time-resolved » spectroscopiste à avoir proposé un traitement basé sur la chimiométrie. Enfin, je donnerai des détails sur les apports des calculs *ab inito* DFT et sa version TDDFT pour lesquels j'ai quelques connaissances puisque j'ai suivi l'école d'été de Carlo Adamo et que j'ai passé une année de détachement CNRS à l'ITODYS en compagnie de F. Maurel et A. Perrier, ma collaboratrice de toujours.

[**] Je fais un choix délibéré de ne pas parler de mes résultats de thèse pour garder une unité autour de la photochimie organique. Ceci-dit, j'ai adoré ma thèse au LURE, ses nuits entières au cœur de Super-ACO, cette effervescence autour du synchrotron…

© 2016 Tous droits réservés.

doc.univ-lille1.fr

1. Etudier des réactions chimiques photoinduites

BUT de ma recherche

Le but de ma recherche au sein du LASIR est en premier lieu de comprendre des réactions chimiques photoinduites, $A + h\nu \rightarrow B$, via une détermination des mécanismes élémentaires en identifiant les états excités intermédiaires à courte durée de vie ainsi que leurs évolutions cinétiques. En particulier, il s'agit de mettre en relation les propriétés photofonctionnelles macroscopiques d'intérêt avec les mécanismes élémentaires photoinduits ou les voies compétitives. Pareillement, au sein d'une famille de molécules, il s'agira d'établir la relation réactivité–structure qui peut être un point déterminant s'il existe un vrai dialogue (feedback) entre les photochimistes et les chimistes de la synthèse. J'expliciterai ce point dans les chapitres suivants.

Stratégie de travail au sein du LASIR

Tout d'abord, il est important de préciser que durant ma carrière, j'ai beaucoup étudié les molécules photofonctionnelles organiques en solution même si ces dernières années je m'intéresse à la photoréactivité sous forme de matériaux. J'ai également entrepris des études en phases gaz. Un des objectifs majeurs de ma recherche n'est autre que la compréhension de mécanismes élémentaires photoinduits. Il va de soi qu'une combinaison adéquate de techniques tant expérimentales que théoriques est nécessaire. On distinguera les techniques spectroscopiques stationnaires des techniques « résolues en temps ». Une illustration de l'ensemble de ces techniques nécessaires (liste non-exhaustive) se trouve sur la Figure 1 ; l'ensemble de mes collaborations passées ou actuelles sont illustrées sur la Figure 2. J'ai clairement distingué mes collaborations au sein du LASIR de mes collaborations externes.

Bien choisir ses objets d'études. En premier lieu, pour des raisons de compétitivité évidente, il est important d'étudier des molécules aux propriétés originales voire des molécules avec une forte potentialité d'application. Ainsi, les collaborations avec des chimistes de synthèse deviennent d'une importance majeure puisqu'ils sont les seuls à pouvoir modifier les objets moléculaires si l'étude photochimique le nécessite. Durant ma carrière au LASIR, j'ai étudié deux grands types de composés auxquelles sont reliées des collaborations distinctes :

- les bétaïnes pyridinium (molécules à transfert de charge)
- les molécules photochromes (changement conformationel photoinduit).

Ces collaborations ont vu le jour grâce à mon intégration au sein des divers GDR « photochromes » de ces dernières années : GDR POM3[††] (Pr. R. Guglielmetti et Pr A. Samat.), GDRI PHENICS[‡‡] (Pr. J.C Micheau et Pr. K. Nakatani). Jusqu'en 2008, j'ai collaboré avec l'équipe d'André Samat et Vladimir Lokshin sur l'étude de composés à transfert d'hydrogène. A partir de 2008, j'ai focalisé mes efforts sur l'étude de diaryléthènes synthétisés par le Pr. Takeshita de l'Université de Saga (Japon). Cette collaboration est encore à l'heure actuelle, ma collaboration la plus importante, avec un projet phare sur les effets optomécaniques (voir chapitre 4). En parallèle, j'ai collaboré avec le Pr. J. Abe (actuellement à l'Université d'Aoyama Gakuin, Japon) qui me demandait d'étudier une bétaïne pyridinium qui semblait, de prime abord, une molécule à la photophysique « triviale ». Nous avons découvert que les propriétés de cette molécule sont assez uniques (Chapitre 5), ce qui ne tarda pas d'éveiller l'intérêt du Pr. Isabelle Leray de l'ENS Cachan qui me proposa un projet basé sur cette molécule.

Caractériser les espèces à l'état fondamental. Bien évidemment, avant toute mise en œuvre de campagnes de mesures « avancées », les réactions photoinduites nécessitent une détermination propre de leur état initial A et final B par rapport à l'existence éventuelle de plusieurs conformères (ayant chacun leur propre réactivité), ou de produits de photodégradation.

[††] Photochromes organiques : molécules, matériaux, modélisation.
[‡‡] Photo-switchableE orgaNIC molecular systems & deviceS

© 2016 Tous droits réservés.
doc.univ-lille1.fr

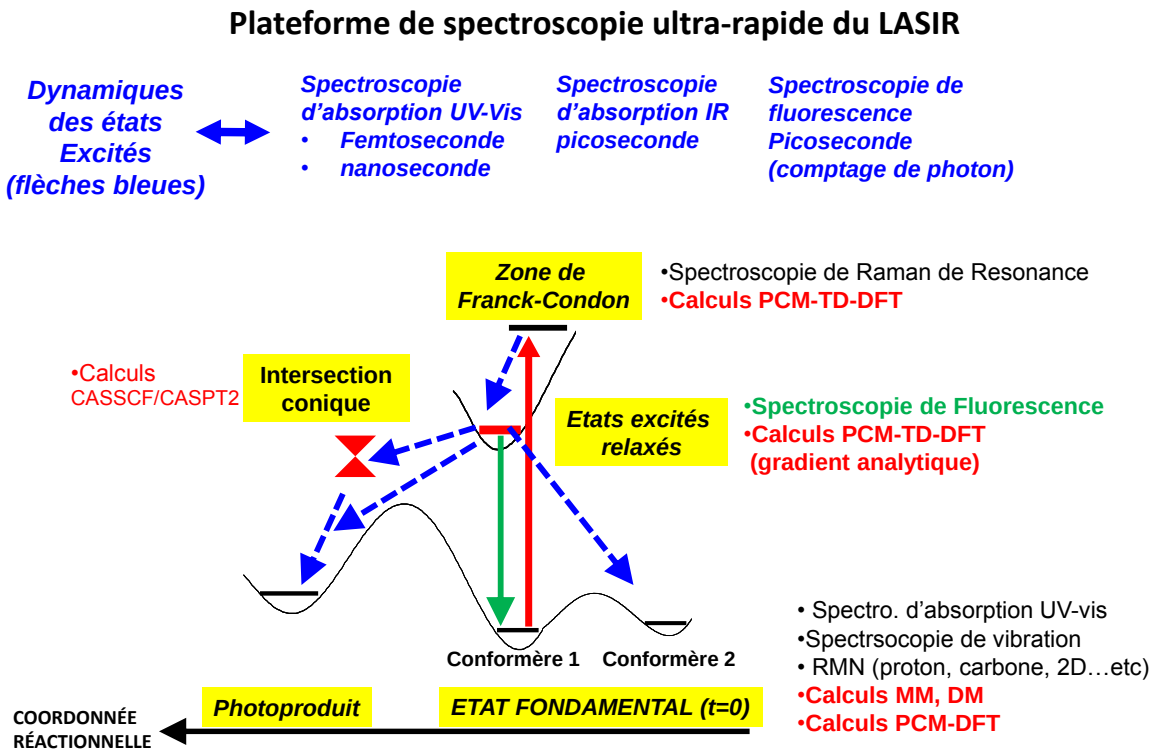

Figure 1 : Techniques expérimentales et théoriques pour étudier les différents points clefs d'une réaction chimique photoinduite.

Pour cela, les techniques standard de laboratoire dont nous avons besoin se trouvent toutes au LASIR (Absorption, Fluorescence, Spectroscopie Raman, IR…). Concernant la RMN, technique de choix pour caractériser des structures moléculaires, en particulier lorsqu'une molécule existe sous plusieurs conformations, je collabore étroitement au sein de l'équipe "Photophysique, Réactivité et Fonctionnalité" avec le Pr. Stéphanie Delbaere, spécialiste de l'étude du comportement par RMN des composés (photo)commutables. L'originalité de son montage réside dans le couplage de spectromètres RMN (1 et 2D, multinoyaux) à des systèmes d'irradiation externes ou *in situ*. Les réactions photochimiques sont induites grâce à l'utilisation d'un banc externe équipé d'une lampe 1000W et de filtres interférentiels. Pour les réactions que l'on souhaite suivre *on line*, l'irradiation est réalisée directement dans le spectromètre RMN, par l'intermédiaire d'une fibre optique couplée à un laser YAG ou à une lampe 100W+filtres, et insérée dans le tube RMN.

Caractériser les dynamiques à l'état excité. Tout d'abord, il faut pouvoir rendre compte des différents points topologiques qui caractérisent les chemins réactionnels entre états excités (figure 1) :

- zone de Franck-Condon (FC)
- états excités relaxés singulet ou triplet, S_n(rel) ou S_n(opt)
- états de transitions (Transition States, TS)
- intersections coniques.

Outre les spectroscopies de Résonance Raman (état FC) et de fluorescence (état relaxé émissif), disponibles au LASIR, l'apport des calculs *ab initio* est bien sûr essentiel et parfois est l'unique moyen d'obtenir des informations sur la molécule (distribution de charges, état TS…).

Dans le passé, J'ai collaboré avec François Maurel (ITODYS) et Denis Jacquemin (CEISAM) mais l'immense majorité de mon travail collaboratif, au niveau computationnel, s'est faite avec le Dr. Aurélie Perrier (IRCP) qui a effectué différents types de calculs en fonction de la problématique, en adéquation avec les expériences.

© 2016 Tous droits réservés.

doc.univ-lille1.fr

Figure 2 : Mise en œuvre de ma recherche via mes choix collaboratifs.

Ayant caractérisé au mieux ces points topologiques depuis A jusqu'à B, **le cœur de ma recherche est ensuite de caractériser les processus cinétiques qui les relient, dans des gammes de temps allant de la femtoseconde à la milliseconde ; ce qui nécessite un recours aux techniques de spectroscopie résolue en temps**. Au LASIR, nous possédons une plateforme unique en France, de spectroscopie transitoire couvrant une large gamme d'énergie d'excitation (UV-IR), une large gamme de fenêtre temporelle (de la femtoseconde à la milliseconde), ainsi qu'un large choix de techniques (absorption UV ou IR transitoire, Raman transitoire, fluorescence transitoire).

Enfin, dans un cadre d'une étude photochimique ou photophysique, les photo-réactions peuvent être variées, le nombre d'intermédiaires réactionnels peut être plus important que prévu ou le signal d'intérêt peut être masqué par un signal d'une réaction compétitive moins intéressante. Dès mon arrivée au LASIR, la question du traitement des données de spectroscopies résolues en temps m'a semblé cruciale et c'est pourquoi je me suis tourné rapidement vers l'équipe de chimiométrie du LASIR afin de tirer un maximum d'information de ces signaux parfois complexes.

En résumé, c'est le triptyque « Calculs-Spectroscopie transitoire-Traitement des données » qui est la colonne vertébrale de ma recherche et que je vais présenter par la suite.

© 2016 Tous droits réservés.

2. Calculs théoriques

Rappels et définitions.

Méthodes HF et post-HF. Tout d'abord, il est bon de rappeler que les méthodes de calcul *ab initio* sont des méthodes de chimie numérique basées sur la chimie quantique. La méthode *ab initio* la plus simple est la méthode Hartree-Fock (HF), dans laquelle la répulsion coulombienne électron-électron n'est pas spécifiquement prise en compte et seul son effet moyen est inclus dans le calcul. En fonction de la problématique traitée, il peut être nécessaire de prendre en compte la corrélation électronique à l'aide des calculs dits « Post Hartree Fock ». La théorie de la perturbation de type Møller-Plesset (MPn) et la méthode « Coupled cluster » sont des exemples de ces méthodes Post-Hartree-Fock. Dans certains cas, particulièrement pour les processus de ruptures de liaisons ou pour la description des états excités, la méthode Hartree-Fock est inadéquate car la fonction d'onde est décrite par un seul déterminant. Il est alors nécessaire d'utiliser des approches « Post Hartee Fock » multi-déterminantales telles que les calculs CASSCF ou CASPT2.

Méthodes Semi-empiriques. Ces calculs sont de type HF où une partie des éléments de matrice à calculer est directement paramétrée numériquement pour reproduire un jeu de donnée expérimentales (souvent thermodynamique). Le gain sur le temps de calcul est considérable au détriment de la description de certaines propriétés électroniques.

DFT. La théorie de la fonctionnelle de la densité (Density Functional Theory, DFT) est une méthode de calcul quantique permettant l'étude de la structure électronique de l'état fondamental, en principe de manière exacte. L'objectif principal de la DFT est de remplacer la fonction d'onde multiélectronique (méthode HF) par la densité électronique en tant que quantité de base pour les calculs. Alors que la fonction d'onde multiélectronique dépend de 3N variables (où N est le nombre total de particules du système), la densité est seulement fonction de trois variables (les 3 variables d'espace x, y, z); il s'agit donc d'une quantité plus facile à traiter tant mathématiquement que conceptuellement. L'idée centrale de la DFT est que la seule densité électronique de l'état fondamental du système détermine entièrement les valeurs moyennes des observables, comme l'énergie qui mathématiquement devient une fonctionnelle de la densité. Un point délicat réside dans le fait que l'expression analytique exacte de la fonctionnelle de la densité n'existe pas et qu'il faut choisir une fonctionnelle d'échange-corrélation qui reproduise au mieux les résultats expérimentaux.

TDDFT. La théorie de la fonctionnelle densité dépendant du temps (TDDFT) se base sur l'équation de Schrödinger dépendante du temps permettant d'étudier les propriétés et la dynamique des systèmes à plusieurs corps en présence de potentiels dépendant du temps, tels que les champs électriques ou magnétiques. L'effet de ces champs peut être étudié par une approche perturbative pour extraire des propriétés telles que les énergies d'excitation, des propriétés de réponse dépendant de la fréquence, et les spectres d'absorption. Les calculs TDDFT permettent d'atteindre une précision remarquable quant aux calculs de spectres d'absorption (transitions verticales vers la zone de FC) des molécules organiques, eu égard, au bon choix de fonctionnelle. Depuis ces dernières années, les calculs TDDFT peuvent aussi être appliqués aux états excités relaxés.

Spécificités pour le calcul des états excités.

A la différence d'un état fondamental, les calculs d'états excités nécessitent de décrire les configurations électroniques ouvertes et cela peut nécessiter des calculs multi-configurationnels. Sachant que le temps de calcul, selon le niveau de théorie, peut être proportionnel à N^4 ou N^7 (où N est le nombre de fonctions de base) on comprend aisément pourquoi ces calculs ont constitué pendant longtemps un vrai challenge pour la chimie quantique. Par le passé, afin de contourner les limitations imposées par le matériel informatique (capacité des processeurs), des méthodes multi-déterminantales reposant sur des niveaux de calculs semi-empiriques ont été mises en œuvre (un exemple d'un tel calcul, CIS-AM1 est donné au chapitre suivant).

© 2016 Tous droits réservés.

doc.univ-lille1.fr

Calcul CASSCF/CASPT2. La première méthode de choix pour les calculs d'états excités, est sans nul doute la méthode « Complete Active Space Self Consistent Field » qui est une méthode post-HF robuste qui réduit la taille du déterminant en fonction du système à étudier. Typiquement, pour les molécules organiques conjuguées, on réduit l'espace actif aux électrons π et aux OM π et π^*, généralement suffisantes pour tenir compte de la délocalisation. L'optimisation de la géométrie de l'état excité en question se fait selon ce niveau de calcul. Ensuite, pour corriger le problème de troncature de l'espace actif et le manque de corrélation dynamique afférent, un calcul perturbatif est réalisé selon le niveau de théorie CASPT2. Ces calculs donnent des résultats très satisfaisants mais nécessitent des temps de calculs très longs.

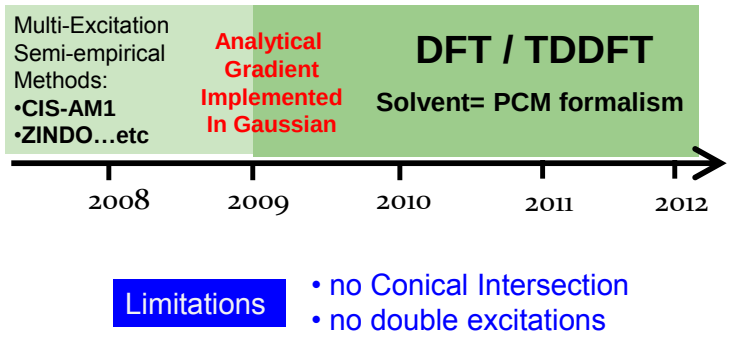

Figure 3 : Possibilité de Calcul selon GAUSSIAN.

L'apport des calculs TDDFT. 2009 est une année charnière pour les utilisateurs de logiciels commerciaux tels GAUSSIAN. En effet, grâce à l'implémentation des gradients analytiques dans ce logiciel, il est devenu possible d'optimiser la géométrie d'un état excité, en partant de l'état FC. Parmi les différentes approches *ab initio* pour traiter des molécules organiques photofonctionnelles, les méthodes TDDFT ont l'avantage considérable de pouvoir traiter des tailles moléculaires considérables bien au-delà des limites de quelques dizaines d'atomes rencontrées pour les méthodes CASSCF/CASPT2. Le choix des méthodes TDDFT se justifie d'autant plus que : i) les fonctionnelles sont de plus en plus optimales ; ii) le solvant peut être inclus explicitement par des approches PCM (Polarisable Continuum Model) réalistes. Un des désavantages de ces calculs mono-excitation, relève de leur incapacité à prédire des points topologiques complexes tels que les Intersections Coniques (IC).

Stratégie Computationnelle.

L'objectif est toujours le même : essayer de caractériser au mieux les chemins réactionnels d'intérêts ou les chemins de désactivation compétitifs en calculant un maximum de points topologiques clefs : états fondamentaux, états de transitions, états excités de FC et relaxés.

La méthode est détaillée sur la Figure 4. En premier lieu, on optimise la géométrie de l'état fondamental par DFT, le choix optimum du niveau de calcul (fonctionnelle et base de calcul) étant fait par comparaison avec la structure RX expérimentale de la molécule étudiée. L'ensemble des espèces à l'état fondamental est ensuite calculé, prenant en compte une possible distribution de conformères. En dernière étape, les états de transitions notés TS (Transition State) entre ces différentes espèces sont calculées. Dans un second temps, on s'intéresse aux états excités. Une fonctionnelle pour les états excités est alors choisie de telle manière que le spectre d'absorption expérimental de la molécule soit reproduit pour le mieux. Ceci est réalisé grâce aux calculs des transitions verticales par TDDFT pour un nombre d'états FC suffisant (typiquement entre 5 et 10). Il est à noter que la sphère de solvatation est introduite via une approche PCM (continuum électrostatique). Le niveau de théorie étant fixé, et une fois les états FC obtenus (ex : S_2(FC)), on lance des procédures d'optimisation d'états excités afin d'obtenir des états excités relaxés notés S_n(Rel) ou S_n(opt). Comme déjà mentionné, ceci est rendu possible depuis 2009 avec l'avènement des gradients analytiques implémentés dans GAUSSIAN. Ces calculs sont non-triviaux car ils doivent

© 2016 Tous droits réservés.

doc.univ-lille1.fr

se faire en plusieurs étapes pour tenir compte du réarrangement de la sphère de solvatation. Il est alors possible de déterminer les transitions émissives théoriques par un calcul TDDFT similaires aux précédents. L'ensemble des points calculés par notre stratégie computationnelle sera sondé par spectroscopie transitoire par ailleurs ; l'une et l'autre des deux « approches » seront mutuellement enrichies par cette comparaison.

Qui calcule Quoi ?

Il faut savoir que la personne clefs pour les calculs (TD)DFT est ma collaboratrice Aurélie Perrier (IRCP) qui a élaboré notre stratégie computationnelle et qui lance les calculs ou les supervise. Aurélie est une théoricienne éminemment efficace et pragmatique qui joue le jeu de la collaboration avec l'expérimentateur et nombre des succès par rapport à la théorie lui incombent. Notre duo a également collaboré par le passé avec Denis Jacquemin (CEISAM), François Maurel (ITODYS), Nacer Idrissi pour la Dynamique Moléculaire (LASIR), Massimo Olivucci pour les calculs CASSCF d'intersection conique (Université de Siene, Italie) et Carlo Adamo (IRCP). Je tiens cependant à préciser que notre collaboration est très fructueuse de par le fait que je comprends parfaitement la faisabilité et les difficultés de certaines approches car je me suis formé aux calculs en suivant l'école d'été de Carlo Adamo (Montpellier, 2008) puis lors d'une année de détachement CNRS à l'ITODYS sous la supervision de François Maurel. Même si mon cœur de métier reste la spectroscopie expérimentale, je pense que mes connaissances de chimie computationnelle m'ont permis de tirer le meilleur profit de mes interactions avec les théoriciens.

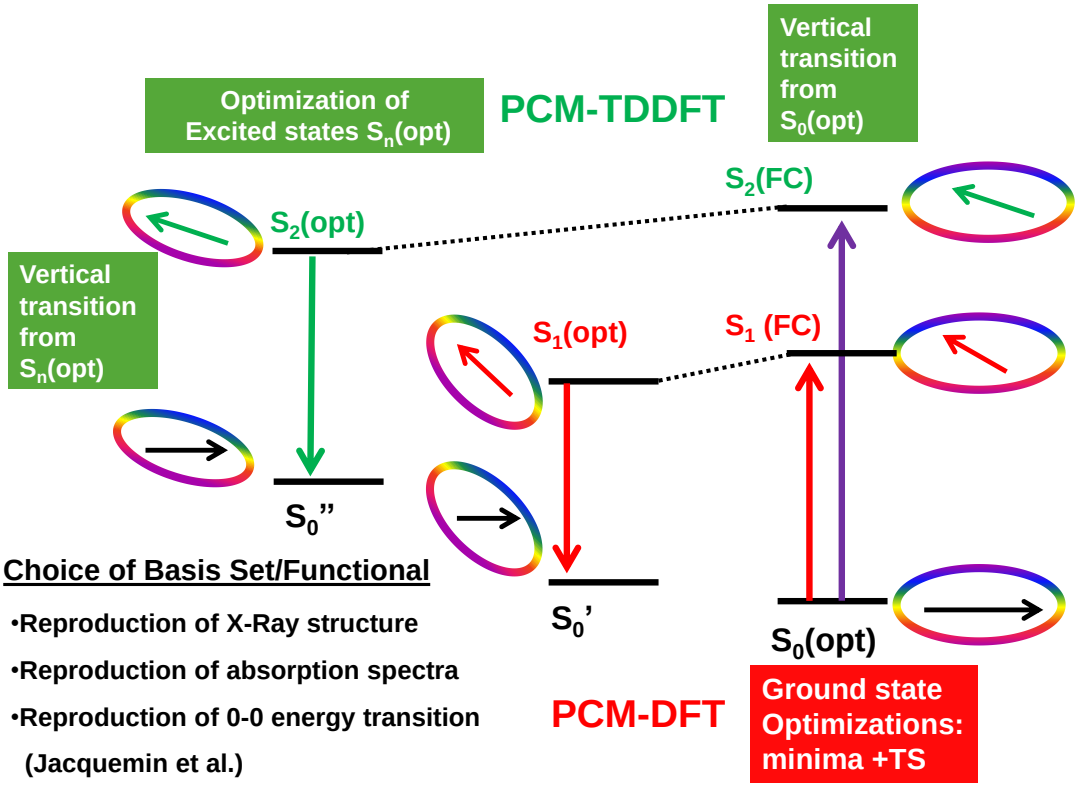

Figure 4 : Stratégie de calcul des points topologiques importants pour les molécules organiques.

© 2016 Tous droits réservés.

doc.univ-lille1.fr

3. Spectroscopie ultrarapide au LASIR

Le cœur de mon métier de chercheur repose sur l'utilisation de montages de spectroscopie transitoire au sein de la plateforme « temps court » du LASIR. Je vais rappeler les principes généraux de la spectroscopie transitoire ultrarapide, utilisant notamment les lasers Ti :Sa femtoseconde, puis je présenterai brièvement l'ensemble des techniques présentes au laboratoire pour me focaliser sur le montage de spectroscopie d'absorption femtoseconde que j'ai utilisé ces dix dernières années.

Principes généraux.

La spectroscopie résolue en temps ou spectroscopie transitoire a pour but de sonder la dynamique des états excités ou des espèces réactives. Hormis les techniques basées sur le comptage de photon, nombre de montages expérimentaux reposent sur une configuration « pompe-sonde » présentée sur la Figure 5a. Un premier rayonnement de pompe monochromatique prépare un état excité bien défini tandis qu'un second rayonnement sonde la population de l'état excité via l'absorption d'un continuum de lumière blanche. On accède à la dynamique des états excités en faisant soit varier le temps d'arrivée des impulsions de pompe et de sonde (via une ligne à retard optique) soit en analysant temporellement le signal d'absorption de la sonde (oscilloscope déclenché par la pompe) ;

En spectroscopie d'absorption transitoire, n'étant intéressé que par la dynamique des états excités (en incluant le processus de repeuplement de l'état fondamental), on s'affranchit de l'absorption de la sonde par les espèces à l'état fondamental selon :

$$\Delta A(\lambda, \Delta t) = A(\lambda, \Delta t)_{pompe+\,sonde} - A(\lambda, \Delta t)_{sonde} \qquad \textbf{(1)}$$

Ainsi, on accède à la dynamique des états excités (variation temporelle des populations) via l'absorption entre états excités (Excited States Absorption, ESA) comme le montre la Figure 5b. Sur cet exemple, on voit que l'ESA $S_2 \rightarrow S_m$ au temps Δt_1, diminue au profit de la nouvelle ESA $S_1 \rightarrow S_n$ au temps Δt_2.

Le signal d'absorption transitoire peut être négatif pour deux raisons. Premièrement, au niveau de la région de la bande d'absorption de l'état fondamental, lors de la soustraction requise selon l'équation (1), si l'ESA est plus faible que l'absorbance de la sonde seule, on obtient une bande négative que l'on appelle bande de dépeuplement ou de blanchiment. L'autre processus provoquant des bandes négatives n'est autre que l'émission stimulée (Stimulated Emission SE) $S_1 \rightarrow S_0$ induite par la sonde. Précisons, qu'on peut s'attendre à un effet miroir entre la bande transitoire de blanchiment/SE et le spectre d'absorption/fluorescence stationnaire à l'unique condition qu'un signal d'ESA trop important ne vienne pas masquer l'effet. Loin d'être un artefact, ces bandes négatives sont très pratiques pour l'assignation des bandes transitoires.

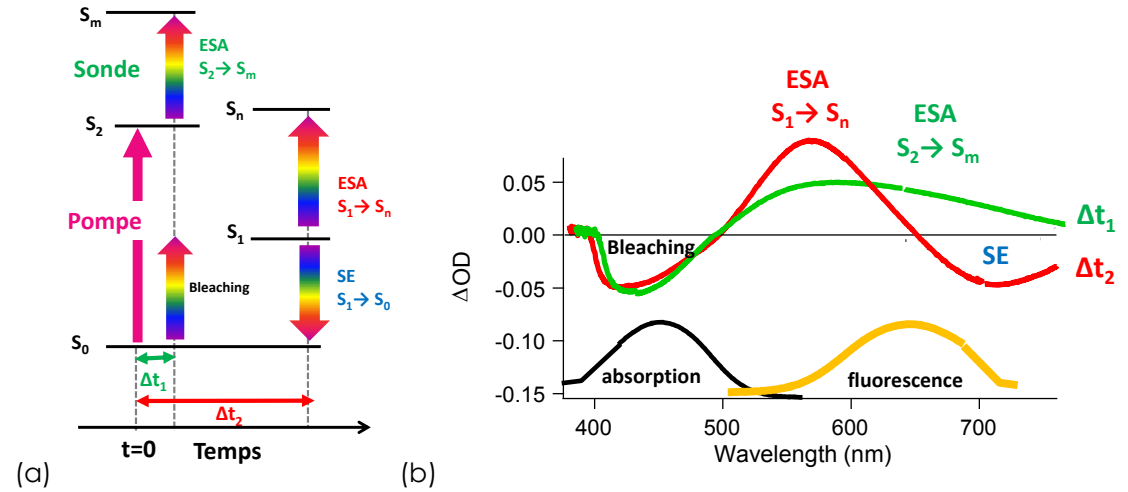

Figure 5 : (a) principe des expériences pompe-sonde ; (b) exemples de signaux transitoires avec des parties positives, relatives à des absorptions $S_n \rightarrow S_m$ avec m>n (ESA band) ou négatives, qui peuvent être dues soit au dépeuplement de l'état fondamental (blanchiment) soit au à de l'émission stimulée produite par le continuum de lumière blanche.

© 2016 Tous droits réservés.

Impulsion femtoseconde

Une impulsion femtoseconde est une oscillation sinusoïdale propagative du champ électromagnétique, modulée en amplitude par une enveloppe dont la durée caractéristique est petite (<< 1 ps). Il est important de se rappeler qu'une impulsion femtoseconde possède nécessairement un spectre large, conséquence direct de la transformée de Fourier.

Laser Titane : Saphir

Les lasers Titane : Saphir sont des lasers accordables qui émettent une radiation électromagnétique rouge et proche-infrarouge de 650 à 1 100 nm. Ces lasers sont principalement utilisés en recherche scientifique grâce à leur accordabilité et leur capacité à générer des impulsions courtes (largeur de la bande de gain importante). Outre un spectre large, la production d'impulsions femtoseconde par un oscillateur Ti : Sa (technique la plus répandue) nécessite le blocage en phase des modes de la cavité (mode-locking). Ils délivrent des impulsions ultracourtes mais de trop faible énergie (nJ) pour être utilisables. Il convient alors de les amplifier. Pendant longtemps, ce fut un challenge technique car l'augmentation des puissances crêtes durant l'amplification entrainait des effets non-linéaires (autofocalisation, automodulation de phase…) et des endommagements des matériaux optiques. Une solution à ces limitations consiste à mettre en œuvre la technique « d'amplification à dérive de fréquence » ou CPA (Chirped Pulse Amplification) qui est illustrée sur la Figure 6. L'idée est de diminuer l'intensité crête en augmentant la durée de l'impulsion (étirer l'impulsion temporellement) issue de l'oscillateur au moyen d'un étireur. La durée de l'impulsion devient alors beaucoup plus importante d'un facteur 10^5 typiquement. Après l'amplification de cette impulsion « longue » celle-ci est ramenée à une durée proche de sa durée initiale au moyen d'un compresseur.

Au sein du LASIR, nous n'avons pas moins de 3 lasers Ti : Sa sur la plateforme « temps court ».

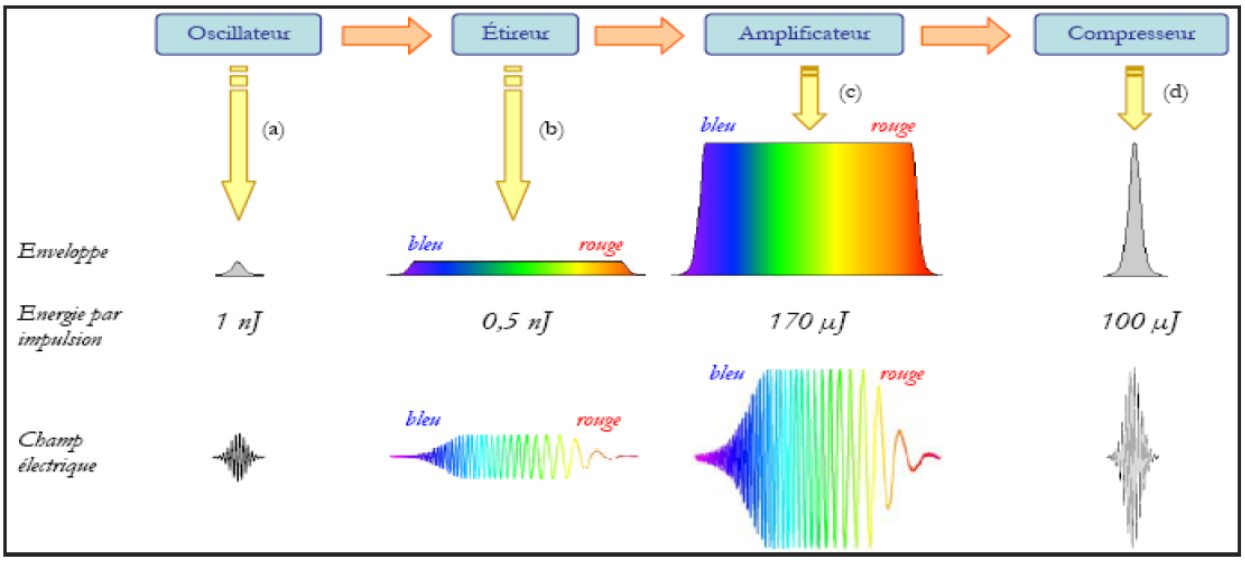

Figure 6 : Illustration du principe de l'amplification à dérive de fréquence : enveloppe et allure du champ électrique en fonction du temps, et ordres de grandeur des énergies par impulsion après chaque composant. L'oscillateur produit des impulsions courtes de faible énergie (a), l'étireur allonge la durée de ces impulsions en séparant temporellement leurs composantes spectrales de sorte que le rouge soit en avance sur le bleu (b), l'amplificateur augmente l'énergie des impulsions (c), et le compresseur restitue leur durée initiale (d)

La plateforme « Temps Court » du LASIR.

Cette plateforme du LASIR rassemble un ensemble d'équipements et de compétences dans le domaine des spectroscopies transitoires. Elle est dédiée à l'étude de la réactivité photoinduite en phase condensée. Elle met en œuvre des sources lasers impulsionnelles (femtoseconde, picoseconde et nanoseconde) émettant sur une large gamme spectrale (de l'ultraviolet jusqu'à l'infrarouge) ainsi que différentes techniques de spectroscopie électroniques (absorption/réflexion

© 2016 Tous droits réservés.

doc.univ-lille1.fr

UV-Vis) et vibrationnelles (Infrarouge et Raman) transitoires. Grâce à la complémentarité de ces spectroscopies et à l'étendue du domaine temporel couvert par les dispositifs (10^{-13}s – 1s), la plateforme est capable de répondre aux besoins des chimistes et physico-chimistes désireux d'appréhender la problématique de la réactivité chimique photoinduite sous des angles allant de l'étude des processus élémentaires à l'optimisation et la fonctionnalisation d'édifices moléculaires complexes.

A ma connaissance, le LASIR est le laboratoire français de chimie avec le plus grand regroupement de montages de spectroscopie transitoire. Cette plateforme est gérée au quotidien par notre ingénieur Laser J. Dubois et mes collègues CNRS M. Sliwa et V. Dewaele. Je fais ici le choix d'en faire une présentation synthétique (Tableau 1).

Tableau 1 : Les différents montages de spectroscopie transitoire répartis dans quatre salles du LASIR.

Montages (#)	**Sources Excitatrices**		**Détecteur**	**Excitation**	**Intervalle temporel**	**Résolution Temporelle**
	Pompe	**sonde**				
(1) Absorption nano/microseconde (Photolyse éclair)	**Laser Nd:YAG** 10 Hz, 5ns Doublé (532 nm) Triplé (355 nm) **+ OPO**[a]	Lampe Xe pulsée	Spectromètre + détection monocanale par PM couplé à un oscilloscope numérique (500 MHz) **[300-900 nm]**	**200 - 2300 nm**	**50 ns - qq ms**	**10 ns**
(2) Absorption UV-Vis femto/picoseconde	**Chaîne laser Ti : Sa amplifiée** (1 W, 1 kHz, ~90 fs) **+ OPA**[b]	Génération de continuum de lumière blanche femtoseconde UV/visible/ proche IR	Spectromètre et détection par caméra CCD **[300-1100 nm]**	**260 - 2000 nm**	**qq fs - 3 ns**	**200 fs**
(3) Diffusion Raman de résonance picoseconde	**Idem que (3)** Mais en régime picoseconde (1 W, 1 kHz, ~100 fs) + doublage (400 nm) + triplage (266 nm)	pompe + OPG[c]/OPA[b]	Spectromètre et détection par caméra CCD **[300-1100 nm]**	**280 - 675 nm** **sonde Raman**	**qq ps - 3 ns**	**3 ps**
(4) Absorption IR femtoseconde	**Chaîne laser Ti : Sa amplifiée** (4 W, 1 kHz, ~100 fs), + 2 OPAs accordabilité indépendante de la pompe et de la sonde		Spectromètre IR + détecteur IR à double barrette de 2 x 32 détecteurs de type MCT	**240 nm - 10 µm**	**qq fs - 2 ns**	**400 fs**
(5) Fluorescence picoseconde (comptage de photon)	**Laser Ti : Sa** **680-1080 nm** (3,8 W, 80 MHz, 200 fs) +sélecteur d'impulsion (4 MHz) +SHG/THG = 270-500 nm + OPO = 500-700 nm		Spectromètre + MCP-PMT + carte de comptage de photon unique			**30 ps**

© 2016 Tous droits réservés.

Le montage de spectroscopie d'absorption UV-Vis femtoseconde.

Une grande partie des résultats de ce manuscrit a été obtenue grâce à ce montage laser, présenté sur la Figure 7.

Le laser femtoseconde. Les impulsions de pompe et de sonde sont générées par un système laser commercial de type Titane-Saphir amplifié, décrit sur la Figure 7 L'oscillateur (Coherent, Mira 900 D), est pompé à 532 nm par un laser Nd-YVO_4 (Spectra Physics, Millenia Vs) délivrant une puissance continue de 5W. Les impulsions femtoseconde issues du MIRA sont accordées à 800 nm. A sa sortie, les impulsions possèdent une durée d'environ 100 fs (FWHM pour « Full Width Half-Maximum ») et un taux de répétition de 76 MHz. Ces dernières étant faiblement énergétiques (10 nJ), elles sont amplifiées à l'aide d'un amplificateur régénératif à dérive de fréquence. Il est composé d'un étireur, d'un compresseur et d'un amplificateur régénératif dont le milieu actif est un cristal de Saphir dopé Titane. Ce dernier est pompé par un laser Nd : YLF déclenché et doublé en fréquence délivrant 12 W à 527 nm, pour un taux de répétition de 1 kHz (Coherent, Evolution 15). L'impulsion ainsi amplifiée est caractérisée par une énergie de 1 mJ, une largeur temporelle de 90 fs (FWHM mesurée par autocorrélation) et un taux de répétition de 1 kHz.

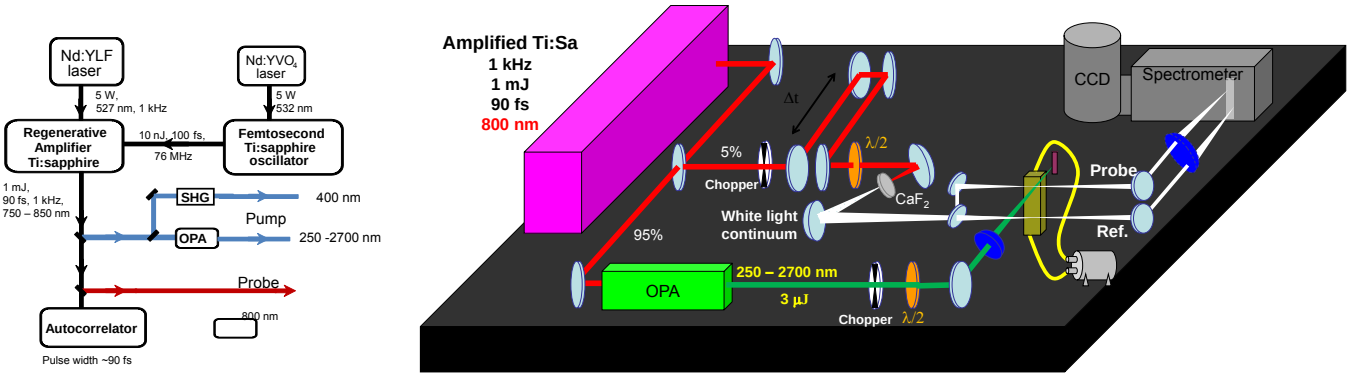

Figure 7 : Détail du Laser femtoseconde et montage d'absorption transitoire femtoseconde.

Génération des impulsions femtoseconde (pompe et sonde). À la sortie de l'amplificateur régénératif, le faisceau est séparé en deux pour obtenir un faisceau de pompe et de sonde. Concernant le faisceau de pompe, il est envoyé à l'intérieur d'un OPA (Quantronix, Palitra) qui permet d'obtenir un faisceau accordable sur la gamme 250-2700 nm. Alternativement, le faisceau de pompe peut être doublé en fréquence dans un cristal de BBO de 0,5 mm d'épaisseur mais seule la longueur d'onde de 400 nm peut être obtenue. L'autre faisceau, véhiculant le reste de l'énergie initiale (quelques microjoules), est focalisé dans une lame de CaF_2 de 1 mm d'épaisseur et génère ainsi un supercontinuum de lumière blanche. Ce phénomène est rendu possible par différents processus non-linéaires dont l'automodulation de phase. C'est ce continuum, caractérisé par un spectre large (nous l'exploitons dans notre expérience sur la bande 300-750 nm), et une durée voisine de celle de l'impulsion laser générative, qui va servir d'impulsion de sonde.

Acquisition des données. Outre la génération et la mise en forme des impulsions femtoseconde, le système se compose d'une ligne à retard (Microcontrôle, précision ± 0.1 µm) permettant un contrôle précis du délai Δt entre la pompe et la sonde. Ce délai peut être fixé sur une plage de temps située entre 0 et 3 ns. Un déplacement de 1 µm de la ligne à retard (un trajet optique effectif aller/retour de 2 µm) correspond à un retard de ~6,66 fs entre les impulsions de pompe et de sonde. En amont de l'échantillon, la sonde est divisée en deux faisceaux à l'aide d'une lame semi-réfléchissante (50-50 %) pour générer respectivement un signal de référence I^{Ref} et un signal de mesure I^{Sonde} (principe du spectromètre à double faisceau). Le recouvrement pompe-sonde est optimisé de sorte à maximiser l'interaction entre les deux faisceaux sur la totalité de l'épaisseur de l'échantillon (faisceaux quasi-colinéaires). La polarisation entre ces deux faisceaux est ajustée à « l'angle magique » (54.7°) à l'aide d'une lame demi-onde positionnée sur la pompe afin

© 2016 Tous droits réservés.

doc.univ-lille1.fr

de s'affranchir de la diffusion rotationnelle des molécules étudiées. L'échantillon est placé dans une cellule à circulation de 2 mm de trajet optique équipée de fenêtres en CaF_2 d'épaisseur 0,2 mm (face avant) et 1 mm (face arrière). La circulation, assurée par une micro-pompe, permet d'éviter la dégradation de l'échantillon mais également de garantir que la fraction du volume pompée soit toujours dans l'état fondamental (volume de solution renouvelé entre chacune des impulsions de pompe).

La chaîne de détection se compose d'un spectromètre, couplé à un détecteur multicanal de type CCD refroidit à l'azote liquide (Princeton Instrument, LN/CCD 1340/400 EB/1) permettant l'enregistrement simultané des signaux I^{Ref} et I^{Sonde}. Le capteur CCD possède une matrice de 1340×400 pixels sensibles dans une gamme spectrale allant de 200 à 1075 nm (dynamique de 16 bits soit 65635 coups, rendement > 50 % entre 350 et 750 nm). Dans le cas présent, la matrice est divisée électroniquement en deux matrices de 1340×200 pixels dédiées à l'enregistrement des signaux I^{Ref}et I^{Sonde} respectivement. La détermination de la variation d'absorbance observée au cours du temps et en fonction de la longueur d'onde s'exprime initialement selon la relation (1). Evidemment, chaque mesure de signal transitoire nécessite la détermination des intensités transmises ($A=\log(I_0/I)$) tout en retranchant la lumière parasite et la fluorescence. En utilisant l'indice *sp* qui indique que l'intensité a été mesurée en l'absence du signal de pompe (*sp*= « sans pompe »), la relation finale qui donne le signal transitoire est la suivante :

$$\Delta A(\lambda, t) = \log \left(\frac{I_{sp}^{Sonde}(\lambda) - I_{noir}(\lambda)}{I^{Sonde}(\lambda, t) - I_F(\lambda)} \times \frac{I^{Ref}(\lambda) - I_F(\lambda)}{I_{sp}^{Ref}(\lambda) - I_{noir}(\lambda)} \right) \qquad (2)$$

Cette formulation fait intervenir les différents signaux enregistrés au cours de la mesure parmi lesquels :

- I_{sp}^{Sonde} et I_{sp}^{Ref} associés respectivement aux intensités de sonde et de référence en l'absence du faisceau de pompe ;
- I^{Sonde} et I^{Ref} associés respectivement aux intensités de sonde et de référence en présence du faisceau de la pompe.
- I_{Noir} correspond au bruit recueilli par le détecteur en l'absence des faisceaux de pompe et de sonde, minimisé par refroidissement du détecteur à l'azote liquide. Il contient également le signal correspondant à la lumière parasite présente dans la pièce.
- I_F contenant le signal de fluorescence de l'échantillon ainsi que la diffusion de la pompe, ce signal est mesuré en début et en fin de mesure afin de détecter une éventuelle dégradation de l'échantillon (faisceau de pompe en l'absence du faisceau de sonde). Il contient aussi, tout comme dans le cas de I_{Noir}, le signal correspondant à la lumière parasite présente dans la pièce.

Afin de minimiser l'influence des fluctuations lentes du laser sur nos spectres, les signaux I^{Sonde} et I^{Ref} d'une part et I_{sp}^{Sonde} et I_{sp}^{Ref} d'autre part, sont enregistrés de manière alternative tout au long du processus d'acquisition des données. Un hacheur optique (« chopper ») est placé sur le trajet de la sonde afin de cadencer ces derniers à une fréquence de 66 Hz correspondant à la vitesse de lecture de la caméra CCD. Compte tenu du taux de répétition des impulsions femtoseconde, ~8 impulsions sont accumulées pour l'enregistrement de chaque spectre. Un second hacheur optique, situé quant à lui sur le trajet de la pompe (cadencé à 33 Hz) permet l'enregistrement des signaux alternativement avec et sans excitation. Pour améliorer le rapport signal sur bruit, plusieurs cycles de mesures sont ainsi réalisés, un cycle correspond à un balayage de la ligne à retard des temps courts vers les temps longs puis inversement. Pour chaque retard pompe-sonde, environ 750 séquences sont accumulées (avec et sans pompe). Les spectres obtenus selon l'équation (2) sont enregistrés à l'aide d'un logiciel « maison » écrit sous Winspec 32 (*Princeton Instrument*).

© 2016 Tous droits réservés.

doc.univ-lille1.fr

4. Analyse des données transitoires : l'apport des méthodes MCR-ALS

⇒ **Article complet en annexe 3**

Estimer précisément le nombre d'espèces excitées photoinduites à l'origine des spectres d'absorption transitoire de nos expériences peut s'avérer parfois délicat à cause des possibles recouvrements spectraux ou temporels entre les signaux des diverses espèces. De plus, la spécificité des processus ultrarapides en phase condensée, solvatation et/ou relaxation vibrationnelle, peut complexifier encore plus l'analyse. En nous basant sur l'expertise de l'équipe de chimiométrie dans l'utilisation des méthodes avancées de résolution de courbes pour l'analyse des données spectrales, nous avons entrepris d'appliquer ces méthodes aux données transitoires femtoseconde. L'avantage majeur des méthodes multivariées dites de « soft modelling », comme la méthode MCR-ALS (Multivariate Curve Resolution-Alternative Least Square), réside dans le fait qu'aucun modèle cinétique n'est postulé *a priori*, à la différence des approches classiques de « hard fitting » (l'ajustement d'une cinétique $\Delta OD=f(t)$ par une fonction analytique mono ou multiexponentielle en est l'exemple le plus fréquent).

Sachant qu'un ensemble de n spectres d'absorption transitoire contenant m points composent une matrice cinétique **D**, le but est de résoudre le problème inverse qui consiste à décomposer **D** dans l'hypothèse de bilinéarité (spectre constant au cours du temps pour chaque espèce).

$$\mathbf{D = C\,S^T + E} \qquad \textbf{(3)}$$

La matrice $\mathbf{S^T}$ contient les spectres purs de chaque espèce et la matrice **C** contient les évolutions temporelles correspondantes. Les résidus de la décomposition factorielle sont contenus dans **E**, matrice qui a les mêmes dimensions que D. Le principe de calcul est basé sur les moindres carrés alternés et repose sur une estimation initiale du nombre d'espèces et des profils de concentration ou des spectres. L'atout de la méthode réside dans la possibilité d'appliquer des contraintes indépendamment sur les facteurs (C et/ou S) voire individuellement sur les espèces (possibilité de contraindre différemment chaque espèce). Les contraintes (non négativité des concentrations, unimodalité, fermeture…) permettent de réduire l'espace des solutions mathématiquement possibles et ayant un sens « chimique ». Sur la base des décompositions sans *a priori*, l'étape suivante est l'utilisation de méthode hybride dite « Hard-Soft MCR » consistant à implémenter des contraintes cinétiques (selon un modèle cinétique), sur les facteurs de la matrice C, tout en conservant les avantages précédents.

En collaboration avec C. Ruckebusch, nous avons appliqué cette approche MCR-ALS à l'étude de la photophysique de la benzophénone, résultats publiés à l'époque dans J. Phys. Chem. A.[1] Sachant que le croisement intersystème $S_1(n,\pi^*)\rightarrow T_1(n,\pi^*)$ est censé être lent (quelques microsecondes) à cause de la violation des règles de El-Sayed, le temps caractéristique de 10 ps, observé expérimentalement, a été très largement expliqué dans la littérature par la participation d'un intermédiaire $T_2(\pi,\pi^*)$, même si aucune preuve directe de l'existence de cet état n'a jamais été fournie. Nos données de spectroscopie d'absorption transitoire de la **Figure 8** montrent le déclin de $S_1(n,\pi^*)$ (λ_{max}=575 nm) avec l'apparition de $T_1(n,\pi^*)$ (λ_{max}=525 nm) entre 2 et 50 ps. Il est à noter qu'un décalage vers le bleu, semblant accompagner l'apparition du triplet, est souvent interprété comme une relaxation vibrationnelle de $T_1(n,\pi^*)$. La décomposition MCR-ALS de ce jeu de données, présentée sur la **Figure 9**a pour les spectres purs et sur la Figure 9b pour les évolutions temporelles des concentrations (les codes de couleurs sont respectés), permet de mettre en lumière la participation d'une éventuelle espèce intermédiaire, notée IS, sous couvert de la validité de l'hypothèse de bilinéarité. Par analogie, l'étude de la 4-méthoxybenzophénone à la photophysique variable en fonction du solvant a permis de corréler cette espèce statistique IS avec la présence d'un état triplet $T_2(\pi,\pi^*)$ au-dessus de l'état triplet $T_1(n,\pi^*)$.

© 2016 Tous droits réservés.

doc.univ-lille1.fr

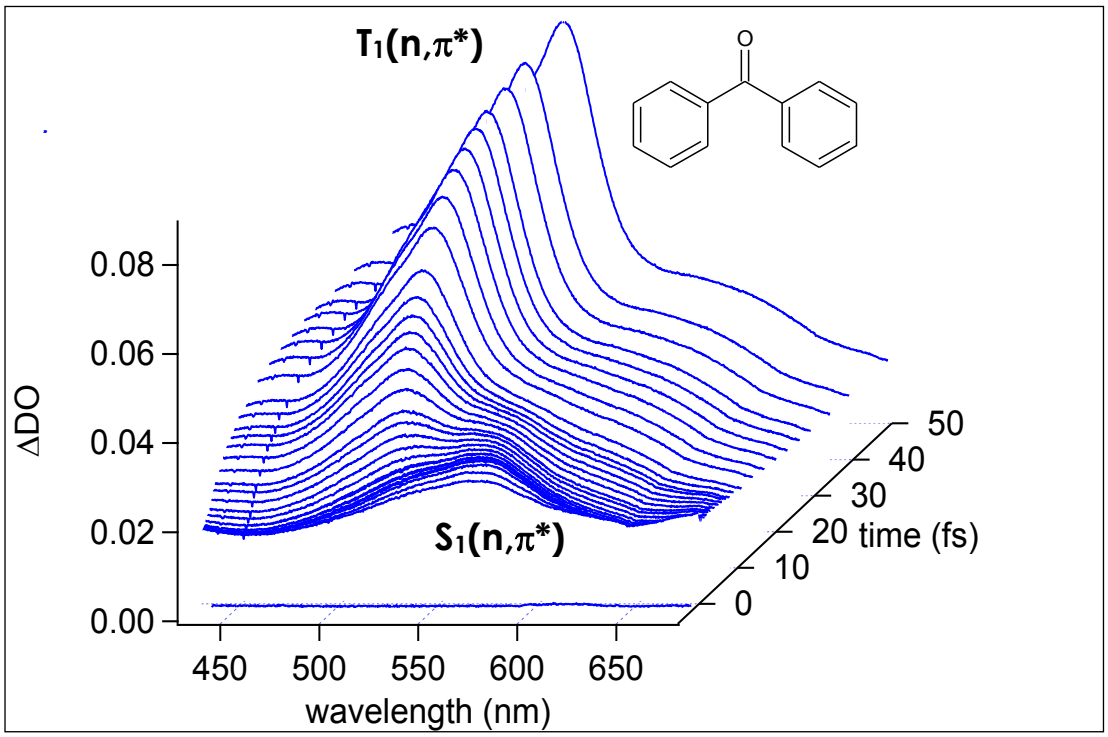

Figure 8 : Spectres d'absorption résolus en temps de la benzophénone dans l'acétonitrile entre 2 et 50 ps, pour une excitation à 267 nm. Résolution temporelle de 200 fs.

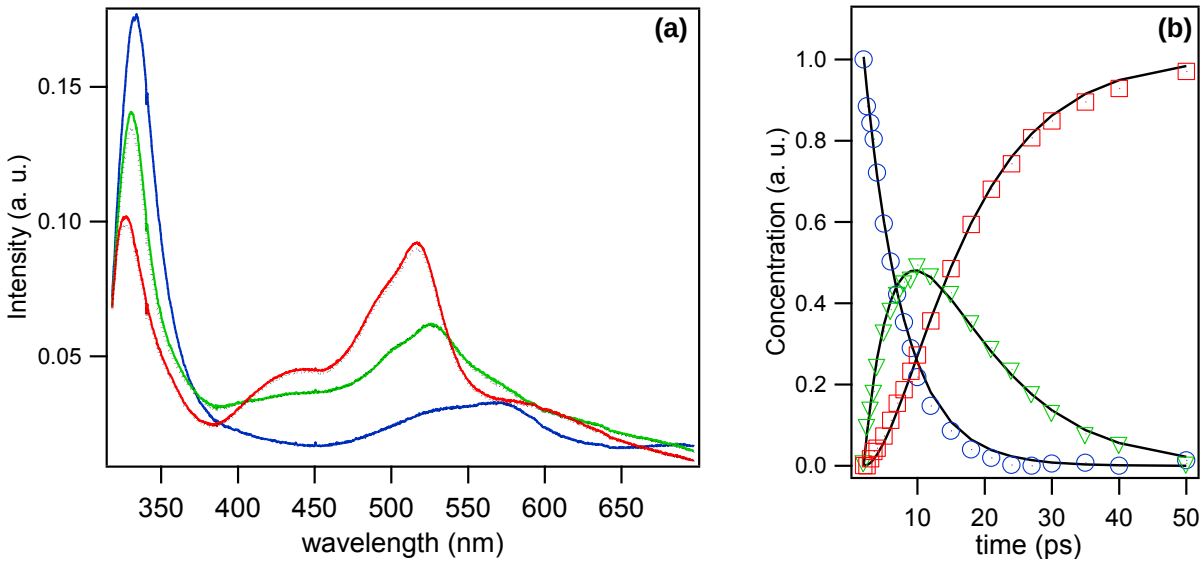

Figure 9 : Spectres purs (a) et profils temporels des concentrations (b) obtenus à partir des données transitoires de la figure 8 après résolution MCR-ALS seule (en couleur) ; après résolution MCR-ALS sous contrainte d'un modèle cinétique type « A→B→C » (en noir). Le code couleur est le suivant : bleu pour le spectre initial (S_1) ; vert pour le spectre intermédiaire IS ; rouge pour le spectre final (T_1).

© 2016 Tous droits réservés.

doc.univ-lille1.fr

Chapitre 4

Vers une compréhension approfondie des mécanismes fondamentaux relatifs aux photochromismes

Dans le chapitre précédent, j'ai détaillé les outils pour mener à bien une recherche, qui je l'espère, soit efficace : spectroscopie transitoire, analyse MCR-ALS et calculs TDDFT. Il est temps de présenter les systèmes chimiques sur lesquelles je me suis penché ces douze dernières années avec en premier lieu : les molécules photochromiques. Si l'exemple grand public des lunettes de soleil photochromiques donne une idée de la nature de ce processus, le lecteur de ce manuscrit aura sans doute compris que je ne traiterai pas des aspects applicatifs du photochromisme mais plutôt de ses fondements au niveau moléculaire : nombre et nature des processus fondamentaux photoinduits, processus compétitifs, influence du milieu extérieur (solvant).

Il est important de préciser que mon immersion dans le monde du photochromisme a pu se faire grâce aux différents Groupement de Recherche du CNRS POM3 puis PHENICS ce qui m'a permis de nouer des collaborations fortes concernant la synthèse (Dr. V. Lokshin, Pr. M. Takeshita, Pr. J. Abe), la RMN (Pr. S. Delbaere), sans oublier les conférences, discussions et conseils fructueux des autres collègues.

Dans la suite de ce chapitre, je vais présenter rapidement la notion de photochromisme, puis faire une présentation chronologique des systèmes que j'ai étudiés ces dernières années : i) le transfert d'hydrogène des quinolones-cétones ; ii) l'électrocyclisation des métacyclophènes ; iii) l'électrocyclisation des diaryléthènes. Je terminerai ce chapitre sur un projet qui me tient à cœur et qui introduit une molécule photochromique au sein d'un élastomère afin de le rendre photo-contrôlable.

1. Généralité sur le photochromisme

1.1 Définitions

Photochromisme. Le photochromisme est la transformation réversible d'une espèce chimique entre deux formes, **A** et **B** possédant chacune un spectre d'absorbance différent, induite dans une ou les deux directions par l'absorption d'un rayonnement électromagnétique. L'interconversion entre les deux états est habituellement accompagné par un changement des propriétés physico-chimiques de l'espèce, telles que l'indice de réfraction, la solubilité, la viscosité, la mouillabilité d'une surface ou les constantes diélectriques…

Comme le montre la Figure 10, la forme stable thermodynamiquement **A** est transformée par irradiation vers la forme moins stable **B**, possédant un spectre d'absorbance différent, laquelle peut être reconvertie en forme **A**, par voie thermique et/ou photochimique. Plus précisément, si **A** et **B** sont thermodynamiquement stables (composés bistables), on parle de photochromes de **Type P** avec une reconversion photoinduite. Si B est thermodynamiquement instable, le photochrome est de **type T** et la reconversion se fait thermiquement.

Habituellement, pour la majorité des composés photochromiques, la forme stable est incolore ou jaune pâle, et se colore lors de l'irradiation (photochromisme positif). Quelques

© 2016 Tous droits réservés.

doc.univ-lille1.fr

composés photochromiques montrent une forme A colorée et une forme B incolore (photochromisme négatif), ou révèle un changement réversible entre différentes couleurs.

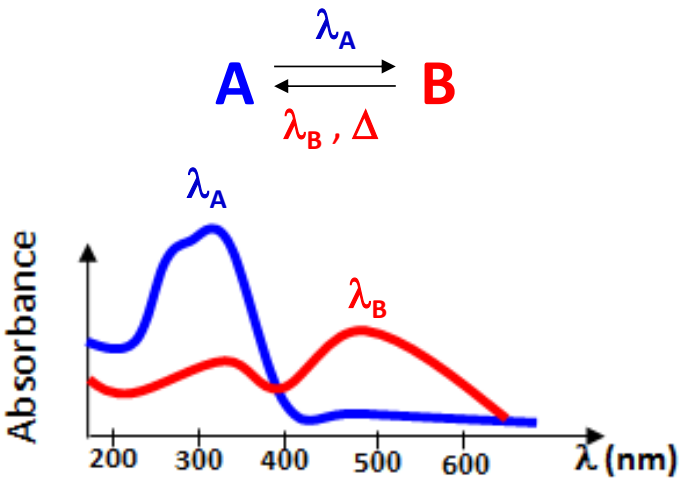

Figure 10 : Concept du photochromisme.

Paramètres photochromiques. Il est important de quantifier l'efficacité des molécules photochromes et évidemment, outre les paramètres photochimiques classiques (λ_A, λ_B) et les coefficients d'extinctions (ε_A, ε_B), il est important de se référer au rendement quantique de formation de B(A) après excitation de A(B) selon :

$$\phi_{A\to B} = \frac{nombre\ de\ molécules\ de\ B\ formées}{nombre\ de\ photons\ absorbés\ par\ A} \quad ou \quad \phi_{B\to A} = \frac{nombre\ de\ molécules\ de\ A\ formées}{nombre\ de\ photons\ absorbés\ par\ B}$$

L'état photostationnaire correspond à l'état d'équilibre thermodynamique de la réaction photochrome, obtenu après irradiation lumineuse durant un temps suffisamment long. Les concentrations en A et B (C_A^∞ *et* C_B^∞) peuvent s'exprimer à l'état photostationnaire selon :

$$\frac{C_A^\infty}{C_B^\infty} = \frac{\varepsilon_B \phi_{B\to A}}{\varepsilon_A \phi_{A\to B}}$$

Dans ces conditions, le taux de conversion (X_B^∞) de A est relié aux rendements quantiques de photoréaction et photoréversion selon :

$$X_B^\infty = \frac{\varepsilon_A \phi_{A\to B}}{\varepsilon_A \phi_{A\to B} + \varepsilon_B \phi_{B\to A}}$$

Il est intéressant de voir que si $\phi_{A\to B}$ tend vers 1 et $\phi_{B\to A}$ tend vers 0 (ce qui est le cas des diaryléthènes que nous étudierons plus loin), le taux de conversion tend vers 100%.

Dans le cas des photochromes de type T, le retour B→A se fait essentiellement par voie thermique. La caractérisation de ce processus implique la détermination de la constante de vitesse $\mathbf{k_\Delta}$ et de l'énergie d'activation $\mathbf{E_A^*}$ (loi d'Arrhenius).

Fatigue des photochromes. Bien que le photochromisme soit un processus pleinement réversible, des réactions secondaires peuvent avoir lieu. Cette photodégradation, même mineure, présente dans le temps ou sous irradiation prolongée est donc responsable de la perte progressive des propriétés photochromiques. Cette perte de performance, souvent provoquée par une oxydation du composé, est qualifiée de fatigue du photochrome. Une manière de quantifier cette fatigue est de déterminer le nombre de cycles, photoréaction/(photo)réversion, A↔B, que le système peut subir sans photodégradation notable de A.

© 2016 Tous droits réservés.

doc.univ-lille1.fr

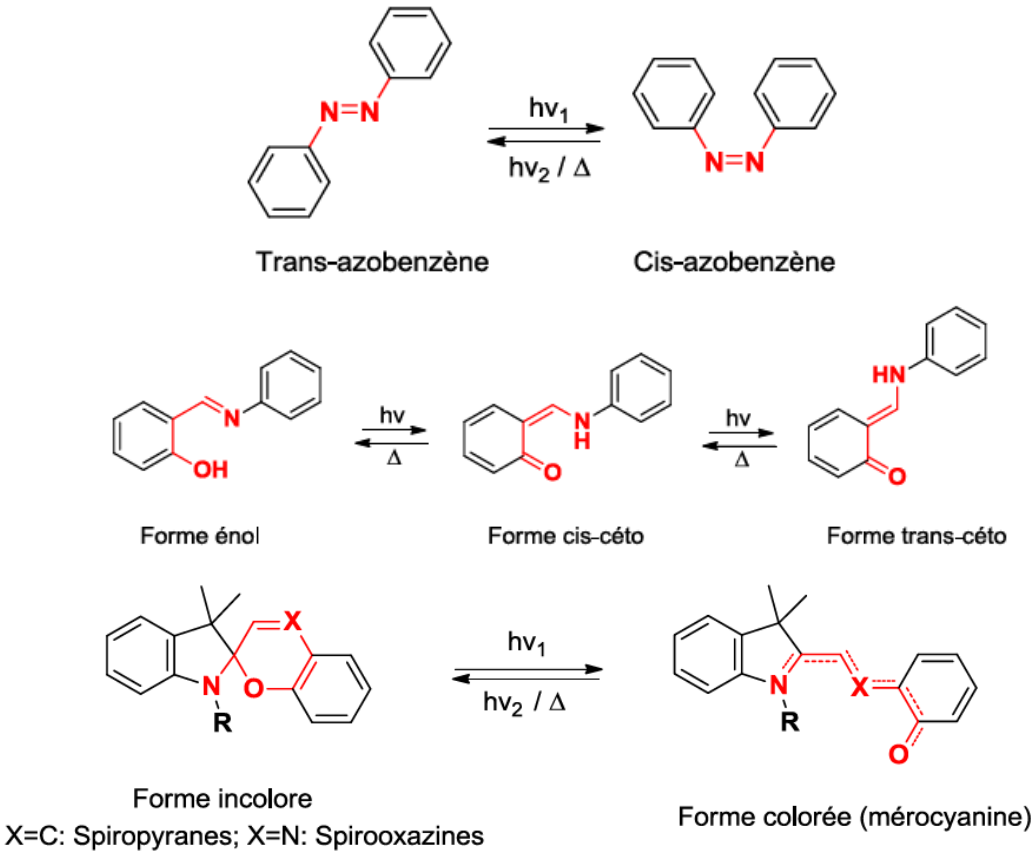

Figure 11 : Différentes familles de photochromes.

1.2 Familles de photochromes

Il n'est pas question ici de donner une liste exhaustive des différentes familles de photochromes. Nous renvoyons le lecteur aux livres[2] et revues complètes.[3] Il me semble judicieux de donner ici quelques exemples de photochromes qui serviront aussi à comprendre quelques points de ce manuscrit. Evidemment, les différentes familles de photochromes peuvent être classées selon le type de réaction chimique à l'origine de la modification structurale et donc spectrale.

Photochromisme par isomérisation cis-trans. Une famille importante de photochromes est basée sur l'isomérisation cis-trans photoinduite des doubles liaisons C=C, pour les stilbènes, ou N=N, pour les azobenzènes,[4] ces derniers étant de loin les plus répandus dans la littérature. Le changement spectral des azobenzènes entre les formes trans et cis, induit par les rayonnements UV, est en général modéré à cause de la similitude concernant la délocalisation des électrons π des deux formes. Par contre, la différence de géométrie étant très forte entre les formes trans et cis, ces molécules sont utilisées pour les applications nécessitant un déplacement de matière (actionneur, Surface Relief Grating...).

Photochromisme par transfert de particule/groupement moléculaire. Pour ces familles de photochromes, généralement de type T, la photoréaction est basée sur le transfert d'un électron (viologènes), d'un proton (anils), dun atome d'hydrogène (quinolone-cétone) ou sur le transfert d'un groupement chimique (quinone)…. Evidemment, ce type de photochromisme est très sensible à l'environnement.

© 2016 Tous droits réservés.

doc.univ-lille1.fr

Photochromisme basé sur une réaction péricyclique.§§ Outre les réactions de cycloaddition (ex : dimérisation de l'anthracène), plusieurs familles importantes de photochromes sont basées sur l'électrocyclisation qui est un réarrangement électronique entraînant la transformation d'une liaison π en liaison σ ou vice-versa. Qu'elles soient concertées ou non, les réactions de photoélectrocyclisation font intervenir dans la majeure partie des cas, 6 électrons π et 6 atomes. Les spiropyranes et spirooxazines (voir Figure 11) sont des photochromes de type T (molécules que j'ai un peu étudiées à mon arrivée au LASIR) tandis que les fulgides, fulgimides et les diaryléthènes sont en général des photochromes de type P. Bien évidemment, je vais détailler plus longuement les principes de cette famille par la suite.

1.3 Les Diaryléthènes

Généralités. Les diaryléthènes sont des dérivés du cis-stilbène construits autour d'une double liaison C=C substituée par deux groupements aryles. La réaction photochrome des diaryléthènes repose sur une réaction d'électrocyclisation [1,6] du motif 1,3,5-hexatriène formé par l'enchaînement Aryle-Ethylène-Aryle comme le montre la Figure 12. Un exemple très courant de diaryléthènes, très étudiés dans la littérature, concerne la famille des dithiényléthènes qui possèdent des noyaux thiophéniques (Y=C ;X=S) et un pont perfluorocyclopentane.

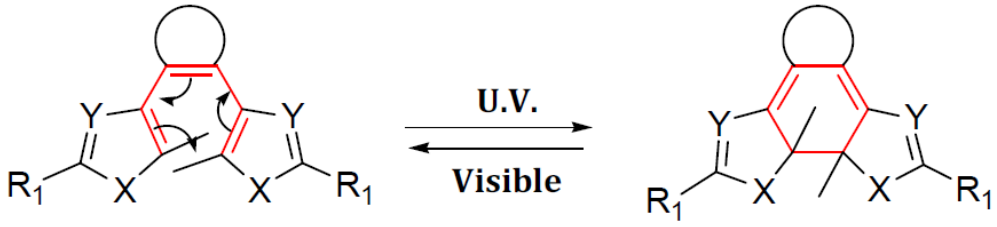

Forme Ouverte (Open Form, OF) incolore **Forme Fermée (Closed Form, CF) colorée**

Figure 12 : L'électrocyclisation des diaryléthènes.

Cette réaction obéit aux règles de sélection de Woodward-Hoffmann, résumées dans le Tableau 2. Ainsi, dans le cas des diaryléthènes, puisque la réaction d'électrocyclisation implique 6 électrons π, elle serait théoriquement possible selon un processus thermique via un mécanisme disrotatoire ou selon un processus photochimique, dit de « photocyclisation » via un mécanisme conrotatoire. Cela étant, les calculs révèlent que la grande barrière énergétique entre le réactif et le produit inhibe la cyclisation par voie thermique et **seule la voie photochimique permet donc d'accéder au produit de cyclisation de manière efficace.**

Tableau 2 : Règles de « sélection » de Woodward-Hoffmann. ($n \in \mathbb{N}$).

Systèmes d'électrons	Processus thermique	Processus photochimique.
4n	conrotatoire	disrotatoire
4n+2	disrotatoire	**conrotatoire**

Les différents conformères. De par la nature même des diaryléthènes, et selon la réaction d'électrocyclisation carbone-carbone, une terminologie précise est employée. En général, la forme thermodynamiquement la plus stable est la **Forme Ouverte (Open Form, OF)** qui est généralement incolore avec un spectre prédominant dans l'UV. Si on excite cette bande d'absorption UV, on induit la photocyclisation et on produit la **Forme Fermée (closed form, CF)** colorée avec une nouvelle bande d'absorption dans le Visible. Si une seule conformation existe pour la CF, l'OF peut

§§En chimie organique, une réaction péricyclique est une réaction dans laquelle une réorganisation concertée des liaisons passe par un ensemble cyclique d'atomes (comprenant souvent six atomes) liés en permanence.

© 2016 Tous droits réservés.

doc.univ-lille1.fr

exister sous la forme de deux conformères par rapport à l'orientation relative des groupements aryles : un conformère parallèle, noté **P**(ou cis) et un autre anti-parallèle, noté **AP** (ou trans) comme le montre la Figure 13.

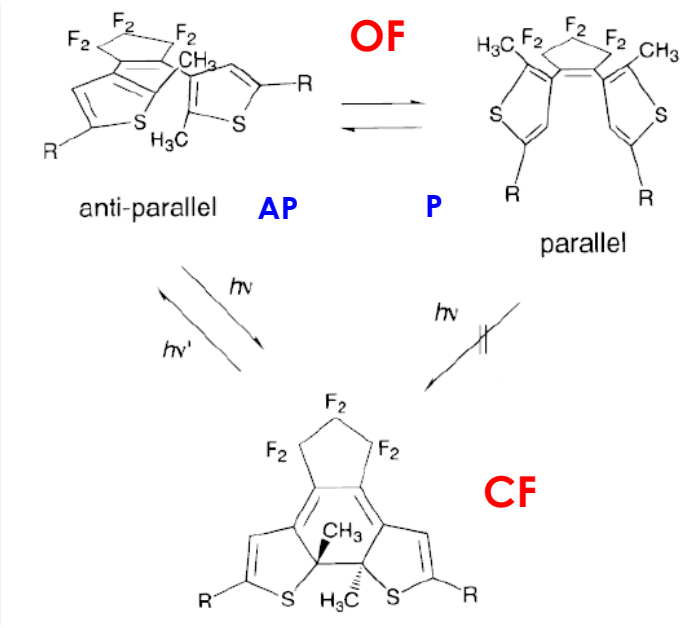

Figure 13 : Conformère AP en équilibre avec le conformère P non photoactif ; forme colorée CF.

Suivant les règles de Woodward-Hoffmann édictées plus haut, la réaction de photocyclisation ne peut se produire qu'à partir de la conformation anti-parallèle. D'une manière générale, la proportion de chacun des conformères en solution est proche de 50%, notamment pour les diaryléthènes faiblement encombrés au niveau des carbones photo-actifs. Le rendement quantique de cyclisation ne pourrait alors théoriquement pas dépasser 0,5. Un des enjeux de beaucoup de chercheurs est de contourner cette limitation conformationnelle pour d'atteindre des rendements avoisinant l'unité.

2. Photochromisme basé sur le transfert d'hydrogène des quinolones-cétones

⇒ **Article complet en annexe 4**

Trouver et comprendre la photochimie de nouvelles familles de photochromes était (et est encore) un challenge fort de l'équipe de l'Université d'Aix-Marseille (Luminy) au sein de laquelle Vladimir Lokshin se spécialisait dans la chimie hétérocyclique. Ainsi, en 2007, il synthétisait des nouvelles quinolone-cétones aux propriétés photochromiques originales : le passage de la forme incolore à la forme colorée se fait par un transfert d'atome d'hydrogène intramoléculaire vers un groupement carbonyle, processus dit de « photoénolisation ». Une des propriétés remarquables de ces composés est la stabilisation de la forme colorée par liaison hydrogène intramoléculaire.

A l'époque, il m'a été proposé d'étudier le mécanisme de photoénolisation pour le composé photochromique **QC18a** et de découvrir pourquoi le composé voisin **QC18b** était lui non-photochrome. Cette étude a été publiée au J. Phys. Chem. A.[5]

© 2016 Tous droits réservés.

doc.univ-lille1.fr

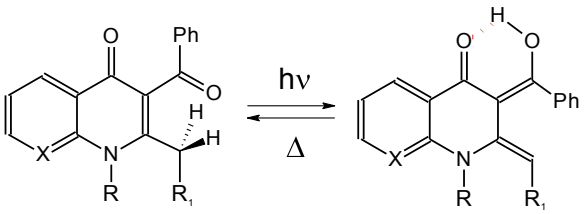

QC18a: X= N R =Bn R_1 =Bn
QC18b: X= N R =Bn R_1 =Me

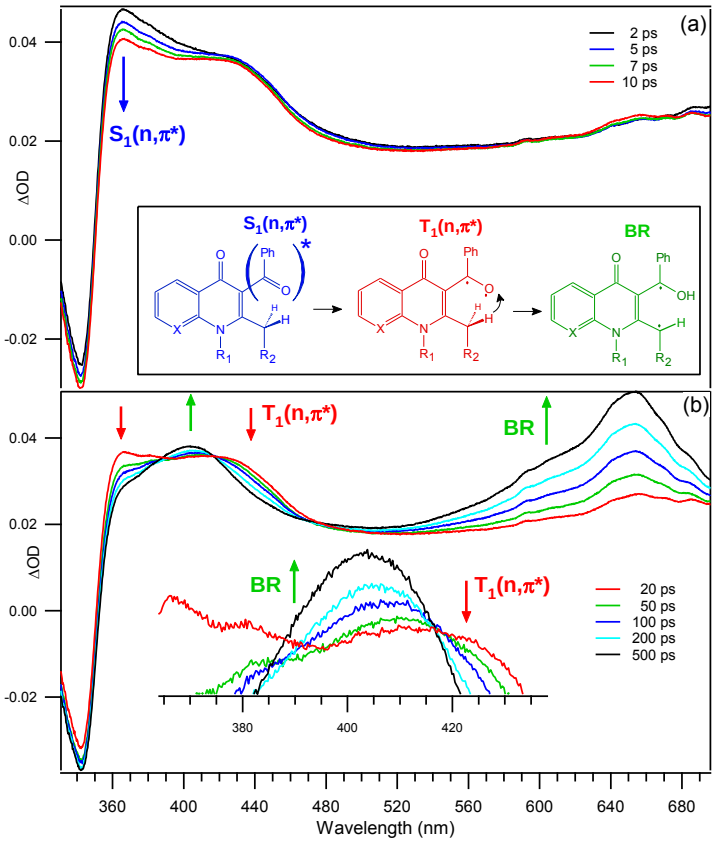

Figure 14 : Spectres d'absorption résolus en temps [267 nm (pompe)/lumière blanche (sonde)] de QC18a /acétonitrile entre 2 et 10 ps (a) ; 20 et 500 ps (b). Résolution temporelle de 200 fs. Les parties négatives sont dues au dépeuplement de l'état fondamental. L'encart donne une représentation structurale des espèces transitoires concernées, l'état singulet (bleu), triplet (rouge) et biradical (vert).

Afin d'accéder aux tout premiers instants de la dynamique des populations excitées, le montage d'absorption transitoire femtoseconde (voir chapitre précédent) a été utilisé. Après une excitation à 267 nm[***], qui équivaut à une excitation n→π* du carbonyle externe, les spectres transitoires résultant, pour les fenêtres temporelles [2-10 ps] et [20-500 ps] sont distinctement présentés sur la Figure 14. Sur la Figure 14a, on peut suivre la désexcitation de **$S_1(n,\pi^*)$** par la décroissance de la bande transitoire dans l'UV (λ_{max} ~360 nm). Par un ajustement mono-exponentiel de la cinétique de décroissance, on obtient un temps caractéristique ~10 ps typique d'une transition de croisement intersystème **$S_1(n,\pi^*)\rightarrow T_1(n,\pi^*)$** comme celui observé pour la benzophénone[1] (se reporter à la **Figure 9**).

Pour des temps plus longs (Figure 14b), l'apparition d'une forte bande d'absorption vers 640 nm et la présence d'un point isosbestique à 417 nm montre que la population de l'état triplet

[***] Triplage de fréquence de l'émission à 800 nm (Ti : Sa) ; A cette époque, l'OPA n'était pas installé.

© 2016 Tous droits réservés.

doc.univ-lille1.fr

évolue vers une autre espèce. Des effets de structure entre **QC18a** et **QC18b** ont permis d'identifier ce processus comme étant un transfert d'atome d'hydrogène intramoléculaire (voir l'encart) : plus la liaison γC-H est fragilisée par le groupement voisin, plus le transfert d'hydrogène est rapide. En toute logique, la nouvelle espèce devrait être une espèce biradicalaire. Or, les temps de vie de ces espèces étant beaucoup plus longs, il convenait d'utiliser le second montage d'absorption transitoire nanoseconde disponible sur la plateforme du LASIR.

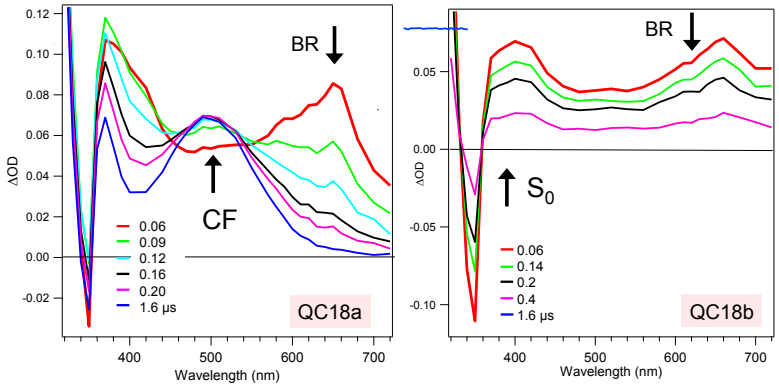

Figure 15 : Spectres d'absorption transitoire nano/microseconde pour QC18a et QC18b (dans l'acétonitrile) suivant une excitation de 267 nm.

Pour une excitation laser toujours à 267 nm, les spectres transitoires en régime nano/microseconde pour les deux molécules sont présentés sur la figure 15. On reconnait dans les deux cas la bande de l'espèce biradicalaire vers 640 nm qui décroit pour donner soit la forme colorée (colored form, CF) dans le cas QC18a, soit le retour à l'état fondamental pour l'analogue non photochrome. Ce résultat tout à fait frappant montre à quel point la spectroscopie transitoire est importante pour expliquer l'observation macroscopique : les chimistes de Marseille supputaient à l'époque que le transfert d'atome d'hydrogène n'avait pas lieu pour QC18b alors que ce n'est pas du tout le cas. Il y a bien photoénolisation pour QC18b mais son biradical n'est pas assez stable pour permettre l'apparition de la forme colorée.

Durant notre étude, nous avons poussé la caractérisation chimique du biradical assez loin. Par des expériences de quenching par l'oxygène et par le cis-1,3-diène, nous avons prouvé que l'espèce en question était un état triplet ; le quenching efficace par le méthylviologène indiquait sa nature biradicalaire. Par ailleurs, une approche quantitative du type Sterm-Volmer a permis de prouver sans ambiguïté que cette espèce transitoire était le précurseur direct, soit de la CF, (molécules photochromes QC18a), soit de l'état fondamental S_0 de la molécule de départ (QC18b). Enfin, des effets de solvants originaux (en comparaison avec des molécules photoénolisables simples) ont été mis à jour, suggérant la présence d'une liaison hydrogène intramoléculaire à l'état fondamental (comme attendu) mais aussi pour l'état précurseur biradicalaire.

L'ensemble des résultats obtenus pour la QC18a et QC18b est résumé sur la Figure 16.

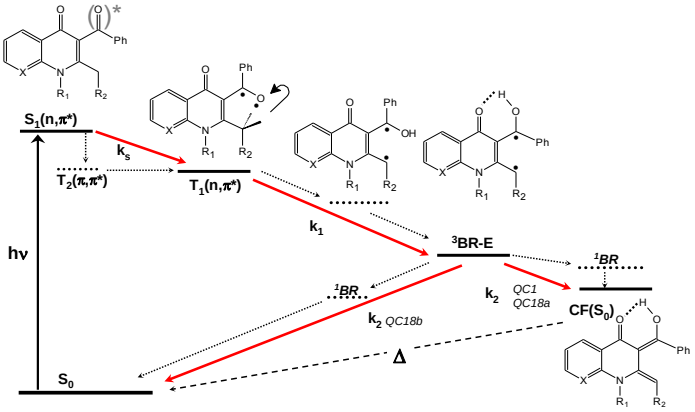

Figure 16 : Mécanismes photoinduits pour QC18a (photochrome) et QC18b (non-photochrome).

© 2016 Tous droits réservés.

3. Photochromisme des diaryléthènes pontés

Ma collaboration avec le professeur Takeshita, de l'Université de Saga au Japon a débuté en 2007. Cet ancien élève du prof. Irié (l'inventeur des diaryléthènes photochromiques), est devenu un spécialiste dans la fonctionnalisation de ces interrupteurs moléculaires. Comme nous l'avons expliqué précédemment, ce principe de photochromisme des diaryléthènes est basé sur l'électrocyclisation carbone-carbone et il faut savoir (ce qui est loin d'être une évidence) que si le rendement de photocyclisation a longtemps été limité à ϕ(cycl)=0.5 celui de photoréversion est de deux ordres grandeurs inférieur ϕ(rev)<0.01.

La faible valeur pour le processus de photoréversion a été expliquée dans la littérature par la présence d'une barrière à l'état excité qu'il faut franchir avant d'atteindre le point topologique permettant la réaction CF*→OF.[6] La valeur limite pour le rendement quantique de photocyclisation s'explique par la présence d'un équilibre plus ou moins stœchiométrique entre les conformères AP et P de la forme ouverte (voir Figure 13) ce qui implique que seuls ~50% de ces conformères sont photoactifs.[7] Ces dix dernières années, un des grands challenges des équipes essentiellement japonaises étaient de synthétiser de nouvelles molécules avec une forme ouverte n'existant que sous la seule conformation AP.[8] Une des spécialités du professeur Takeshita a été de synthétiser des diaryléthènes avec un pont alkyle ou poly-éther liant les deux groupements aryles et bloquant ainsi la molécule dans la configuration AP. Même si l'objectif initial, un rendement de photocyclisation tendant vers 1, n'a pas toujours été atteint, les diaryléthènes pontés avaient le gros avantage de bouleverser plus ou moins fortement la topologie relative des états fondamentaux et excités, une aubaine quand notre objectif est de comprendre les détails mécanistiques reliés à cette topologie.

Il est bon de souligner que la synthèse des diaryléthènes pontés est en général assez lourde, raison pour laquelle seul le professeur Takeshita a longtemps été le seul à réaliser une telle prouesse. Depuis 2008, je me suis penché sur trois types de systèmes illustrés sur la Figure 17 mais je me focaliserai uniquement sur les deux premières familles. La troisième famille est en rapport avec mon projet de recherche autour des effets photomécaniques.

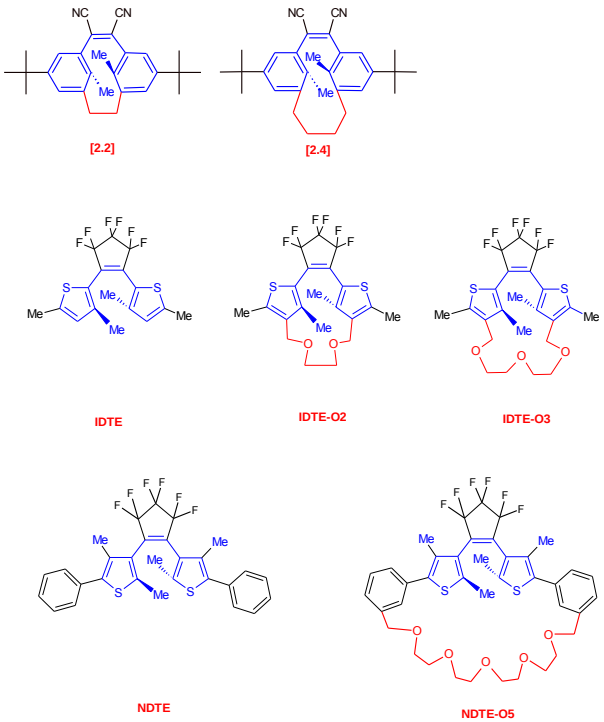

Figure 17 : Familles de diaryléthènes d'intérêt étudiées au LASIR et leurs analogues pontés.

© 2016 Tous droits réservés.

doc.univ-lille1.fr

3.1 Métacyclophan-1-ène

⇒Article complet en annexe 5

Ma première étude portant sur les diaryléthènes pontés concernait deux membres de la famille des 1,2-dicyano-[2.n]métacyclophan-1-ène synthétisés par le professeur Takeshita avec une chaîne alkyle variable n=2 et n=4. En faisant varier l

a longueur de la chaîne alkyle entre les deux noyaux benzéniques, il a été possible de générer soit un photochrome bistable (Type P) pour [2.2] ; soit un photochrome présentant un retour thermique de (type T) pour [2.4].[9] Une simple spectroscopie stationnaire permet de caractériser la photocyclisation de [2.2] (**Figure 18**a) alors que l'emploi de la spectroscopie transitoire nanoseconde devient nécessaire pour détecter la CF de [2.4] (Figure 17b).

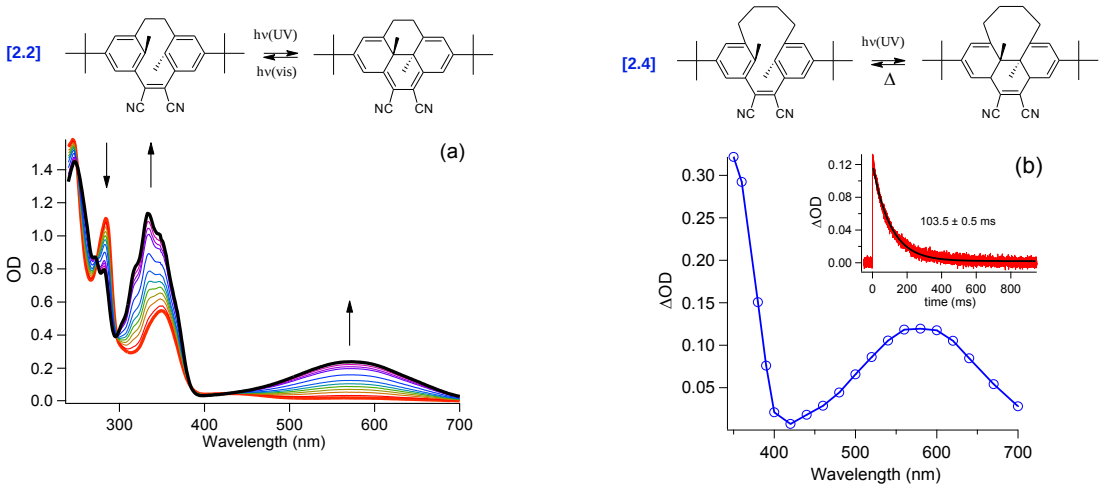

Figure 18 : (a) Spectres d'absorption UV-Vis de [2.2] (dans l'acétonitrile) sous irradiation continue @ 313 nm enregistrés toutes les minutes ; (b) Spectres d'absorption transitoire de [2.4] dans l'acétonitrile 20 µs après l'excitation laser @ 355 nm. L'encart montre la cinétique du déclin @ 595 nm qui caractérise la CF.

Outre la capacité à moduler le type de photochromisme, les chaînes alkyles étaient censées améliorer considérablement le rendement de photocyclisation qui pour l'analogue non-ponté était de ϕ=0,35. Or pour la molécule [2.2], ce rendement s'élevait seulement à ϕ=0,39, bien loin de le la valeur unitaire espérée alors même que le pourcentage de conformère AP était bien de 100%. (Pour la molécule [2.4], qui n'est pas bistable, ce rendement n'avait jamais été mesuré). Ainsi, le but de notre étude était de comprendre pourquoi la chaîne alkyle améliorait si faiblement les performances photochromiques de [2.2].

Pour atteindre notre objectif, nous avons combiné, comme expliqué aux chapitres précédents, les spectroscopies résolues en temps à l'échelle de la nanoseconde notamment pour la molécule [2.4] et le montage d'absorption femtoseconde pour les deux molécules. Du point de vue des calculs, deux niveaux ont été choisis : la (TD)DFT pour les états fondamentaux et les transitions verticales ainsi que des calculs CIS-AM1 pour les états excités (étude pré- 2009, voir chapitre précédent). Outre des effets de solvant sur les propriétés spectroscopiques de ces molécules (caractère de transfert de charge conféré par les groupements cyano) et des effets de structure sur la dynamique post-excitation, le résultat phare de cette étude est sans nul doute un effet de longueur d'onde d'excitation. En 2008-2009, nous n'avions pas d'OPA couplé au laser Ti : Sa et donc la seule alternative était de doubler ou tripler la fréquence des impulsions femtoseconde IR pour obtenir une excitation à 390 nm et 266 nm respectivement. Lorsque l'on enregistrait des spectres d'absorption transitoire à ces deux longueurs d'onde, pour [2.4], aucune différence spectrale majeure n'était obtenue. A l'inverse pour la molécule [2.2], comme indiqué sur la Figure 18a, une excitation à 266 nm donne deux bandes transitoires (maxima à 370 et 640 nm) qui déclinent selon un temps caractéristique de 1,5 ps pour laisser apparaitre le spectre de la CF. A l'inverse, pour une

© 2016 Tous droits réservés.

doc.univ-lille1.fr

excitation à 390 nm, comme indiqué sur la Figure 18b, on observe une forte bande transitoire vers 600 nm qui décline très rapidement tout en se déplaçant vers le rouge pour laisser apparaitre au bout de 10 ps le spectre de la CF. Cet effet a été corroboré par des mesures stationnaires de rendement de photocyclisation à différentes longueurs d'onde entre 266 et 440 nm comme le montre la Figure 18c : on peut voir qu'il existe effectivement un seuil vers 380 nm au-dessus duquel le rendement de photocyclisation tend finalement vers 1 !

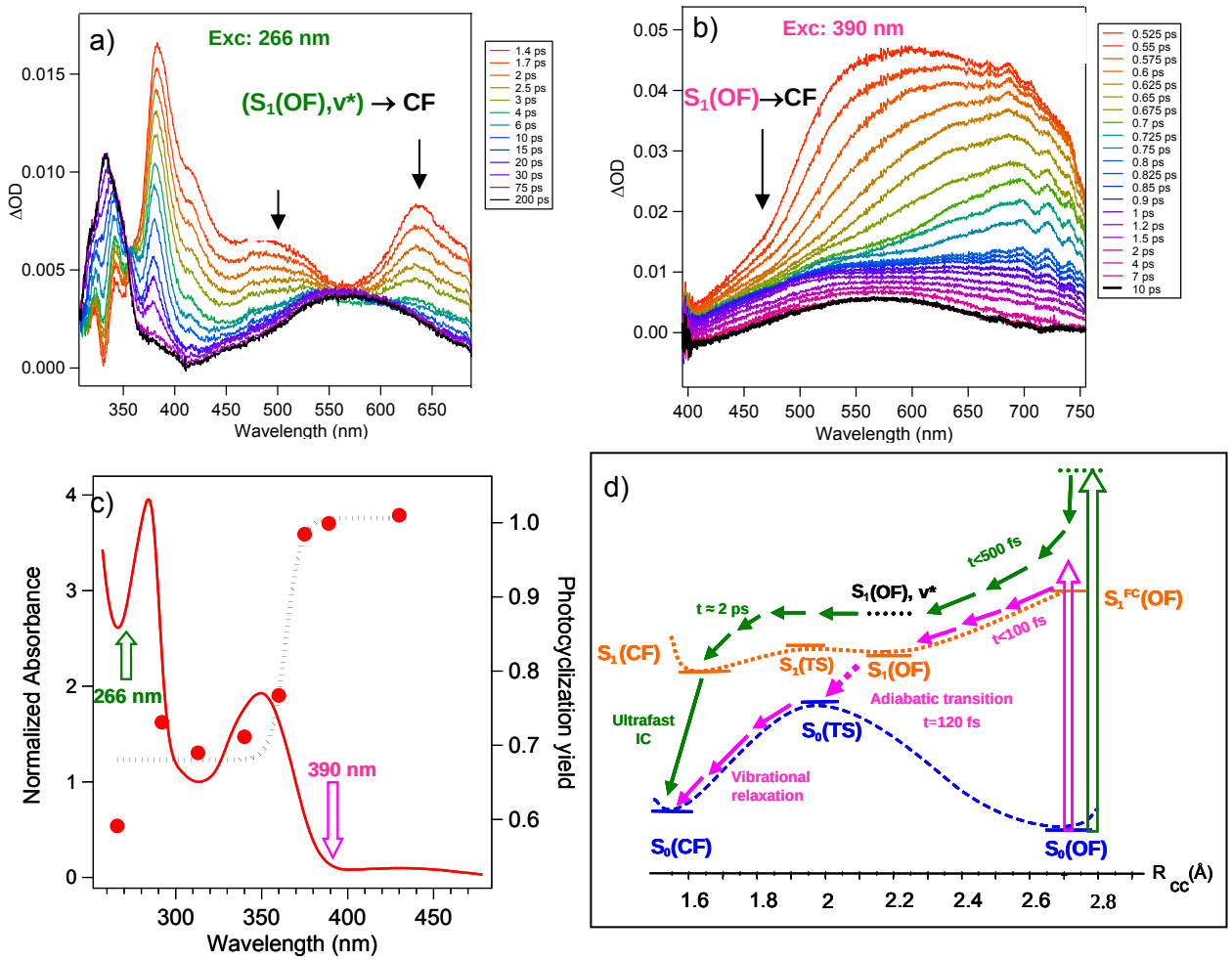

Figure 19 : Spectres d'absorption femtoseconde pour le 1,2-dicyano[2,2]métacyclophan-1-ènes (acétonitrile) pour une excitation à 266 nm, [Δt= 1.4-200 ps] (a) et 390 nm [Δt=0.5-10ps] (b). Rendement de photocyclisation de la forme ouverte dont le spectre stationnaire est inclus (c). Différents états optimisés en CIS-AM1 des formes ouverte (OF) et cyclisée (CF) ; les excitations laser à 266 nm et 390 nm sont reportées ainsi que les mécanismes photochimiques déduits de la spectroscopie femtoseconde (d).

L'explication mécanistique finale a été obtenue grâce aux calculs CIS-AM1, résumés sur la Figure 18d où l'on peut voir les états fondamentaux, excités et états de transition (transition state TS) pour la OF et la CF. Rappelons toutefois qu'il est admis que les mécanismes de photocyclisation se font via des intersections coniques[10] incalculable au niveau CIS-AM1. Sur cette figure, deux voies de photocyclisation selon la longueur d'onde d'excitation sont proposées. Si l'on note les états de Franck-Condon par le symbole FC, le premier mécanisme serait une voie adiabatique du type :

$$S_0(OF) + h\nu \rightarrow S_1^{FC}(OF) \rightarrow S_1(OF) \rightarrow (CI_1) \rightarrow S_0,(CF,v^*) \rightarrow S_0(CF)$$

Depuis l'état excité de FC, une relaxation vers un état excité relaxé $S_1(OF)$ s'opère à des temps inférieurs à 100 fs, et la réaction d'électrocyclisation à proprement dit a lieu à cet instant avec

© 2016 Tous droits réservés.

doc.univ-lille1.fr

un passage par l'intersection conique avec un temps caractéristique de 120 fs. Le mécanisme se termine par une relaxation vibrationnelle dont la signature spectrale consiste en un affinement des spectres transitoires avec une augmentation d'intensité (se reporter à la séquence 1- 10 ps sur la Figure 19b). Le rendement de photocyclisation ϕ=1 s'expliquerait par l'absence de voies photochimiques compétitives et par la proximité de S_1(OF) avec l'intersection conique.

Pour expliquer l'effet de seuil, nous avons proposé le passage par un état vibrationnel excité de S_1(OF) avec une énergie suffisante pour pouvoir franchir la barrière énergétique représentée par S_1(TS) et permettant de peupler l'état singulet de la CF en un temps caractéristique ~2 ps. Le processus final se faisant ensuite, par une conversion interne ultrarapide. Ce mécanisme pourrait se résumer de manière suivante :

$$S_0(OF) \rightarrow S_n(OF) \rightarrow S_1,(OF,v^*) \rightarrow S_1(TS) \rightarrow S_1(CF) \rightarrow S_0(CF)$$

La chute du rendement de photocyclisation s'expliquerait par l'existence d'une voie de relaxation compétitive à savoir la conversion interne $S_1(OF,v^*) \rightarrow S_0(OF)$.

3.2 Dithiényléthène iInverse

3.2.A Etude en solution

⇒Article complet en annexe 6

A partir de 2009, le professeur Takeshita nous a demandé d'étudier une série de dithiényléthènes (DTE) inverses basés sur la molécule IDTE et ses analogues pontés IDTE-O2 et IDTE-O3. Rappelons que les dithiényléthènes sont normaux (N) ou inverses (I) quand les groupements méthyle des carbones réactifs sont en α ou en β du soufre respectivement. A la différence des DTE normaux, la proportion des conformères P et AP des DTE inverses ne peut pas être déterminée directement par RMN. Ceci s'explique par une interconversion AP↔P plus rapide que quelque µs, temps plus court que la largeur des impulsions électromagnétiques utilisées en spectrométrie RMN. En d'autres termes, le signal RMN des protons d'une DTE inverse est une moyenne pondérée par le pourcentage de chaque isomère. Par ailleurs, la mesure des rendements de photocyclisation (méthode stationnaire) donne les résultats suivants :

	IDTE	IDTE-O2	IDTE-O3
ϕ(cycl)	**0.40**	**0.70**	**0.42**
ϕ(fluo)	**0.008**	**0.004**	**0.011**

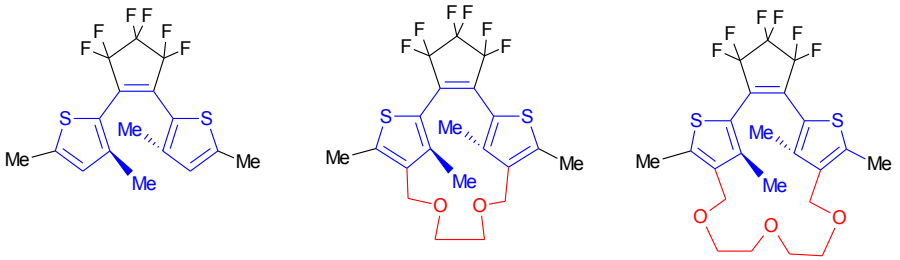

Figure 20 : La série des DTE inverses avec les rendements de photocyclisation et de fluorescence.

Un optimum assez inattendu est obtenu pour IDTE-O2 (ϕ=0.7). De plus, à la différence des DTE de type N, ceux de type I sont connus pour être fluorescents ce qui donne des informations supplémentaires précieuses sur le premier état excité relaxé (noté S_1(opt) ou S_1(rel)). Notre problématique était donc la suivante : déterminer le plus précisément possible les mécanismes liés à la photocyclisation tout en rationalisant les valeurs trouvées pour les rendements quantiques de la Figure 20. Comme à notre habitude, mes collaborateurs et moi-même avons combiné les

© 2016 Tous droits réservés.

doc.univ-lille1.fr

techniques spectroscopiques stationnaires, d'absorption transitoire femtoseconde et les calculs TDDFT incluant les états excités (étude post-2009) pour atteindre ces objectifs.

Dans un premier temps, nous avons dû trouver un moyen d'évaluer la proportion de conformère AP/P à partir des spectres RMN du proton des IDTE. Pour cela, avec S. Delbaere, nous avons développé une approche basée sur l'évolution du système en fonction de la température. En effet, pour IDTE, l'environnement chimique des groupements méthyle externes (vers 2,4 ppm) et des protons (en β du S ; vers 6,5 ppm) est le même quel que soit le conformère considéré et donc aucune dépendance en température n'est attendue. A l'inverse, les groupements méthyle internes ayant un environnement chimique différent pour les deux conformères, une dépendance en température du déplacement chimique est attendue et il est possible de la quantifier. En effet, si on définit la constante d'équilibre K :

$$K = \frac{[P]}{[AP]} \qquad \textbf{(5)}$$

que l'on développe en fonction des données thermodynamique pour faire apparaitre la dépendance en température

$$K(T) = e^{\frac{\Delta S_{AP-P}}{R}} \times e^{-\frac{\Delta H_{AP-P}}{RT}} \qquad \textbf{(6)}$$

la valeur du déplacement chimique des groupements méthyle internes s'écrit :

$$\delta_{app}(T) = \frac{1}{1+K(T)}\delta_{AP} + \frac{K(T)}{1+K(T)}\delta_{P} \qquad \textbf{(7)}$$

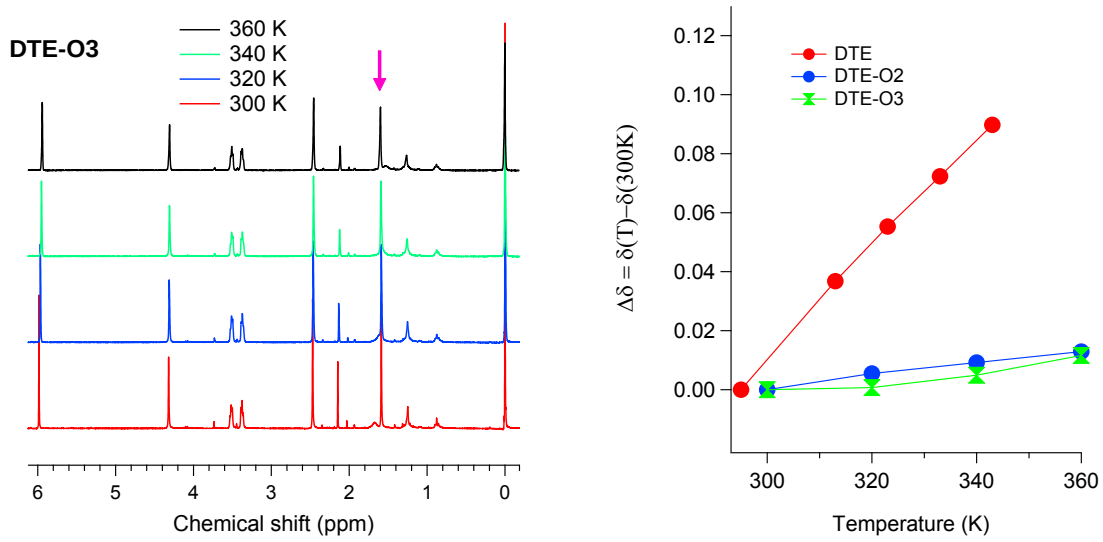

Figure 21 : **(gauche) Spectres RMN du proton pour IDTE dans le chloroforme deutéré entre 27 et 87°C ; (droite) Evolution du déplacement chimique des protons des groupements méthyle internes (~1.6 ppm) en fonction de la température pour IDTE, IDTE-O2 et IDTE-O3.**

En ajustant les données expérimentales pour IDTE, présentées sur la , avec l'équation (7) nous évaluons ΔS_{AP-P} et ΔH_{AP-P} ce qui nous permet de calculer la population de conformères ; par ce biais, nous avons trouvé 75% de AP et 25% de P pour IDTE. Ces valeurs s'éloignent déjà des 50% reportés pour les DTE normaux. Ceci-dit, le résultat le plus probant est sans nul doute la comparaison de la molécule IDTE avec ses deux analogues pontés. Comme on peut le voir sur la Figure 21, la dépendance en température est totalement supprimée, ce qui permet de déduire que la population de AP est d'environ 100%. Ainsi, le pont polyéther a totalement rempli sa fonction première qui était de bloquer la IDTE dans la bonne conformation. Mais, pourquoi IDTE-O2 et IDTEO3, tous deux bloqués dans la conformation AP, ont-ils des rendements de cyclisation si différents ?

© 2016 Tous droits réservés.

doc.univ-lille1.fr

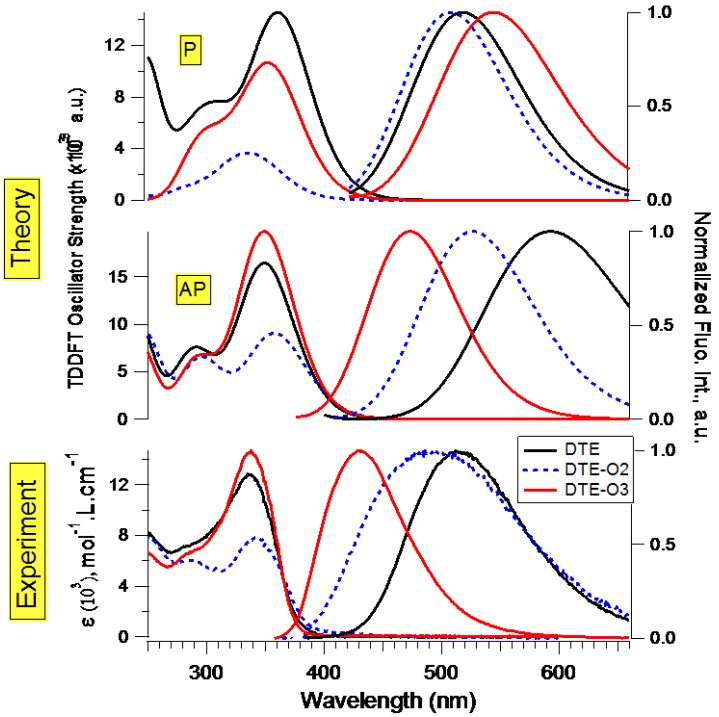

Figure 22 : Spectres d'absorption et d'émission expérimentaux (dans l'hexane) comparés aux spectres calculés par la méthode PCM-TDDFT pour IDTE, IDTE-O2 and IDTE-O3. Les calculs pour les conformères AP et P ont été entrepris.

Une des particularités des DTE de type I est reliée à leur propriété de fluorescence. Dans notre approche conjointe spectroscopie-calculs, cette série revêtait donc un enjeu fondamental, puisque l'on se devait de reproduire au mieux par TDDFT les spectres d'absorption et d'émission expérimentaux. Ainsi, la comparaison expérience-théorie, pour les deux conformères AP et P (il est intéressant de l'inclure tout de même) est présentée sur la Figure 22. Figure 22Comme on peut le voir en premier lieu, tant les spectres d'absorption que l'hyspochromisme des spectres d'émission sont reproduits de manière très satisfaisante pour le conformère AP, ce qui confirme bien la participation minoritaire voire négligeable du conformère P. Il est surtout intéressant de remarquer que pour la série IDTE, IDTE-O2 et IDTE-O3, on a un effet de structure significatif sur la géométrie de l'état relaxé S_1(opt) par rapport à celle de l'état fondamental (Tableau 2). Ainsi, il sera intéressant d'envisager l'étude de cette série par spectroscopie transitoire, en essayant de rationaliser cet effet de structure.

Tableau 3. Distance Carbone-Carbone en Å pour l'état fondamental et l'état singulet relaxé. Temps caractéristiques des bandes transitoires obtenus après « global fitting » des cinétiques à quatre longueurs d'onde d'intérêt.

	Rcc (Å)		**Bandes X/Y Croissance**	**Bande X Déclin**		**Bande Z Déclin**
	Etat Fondamental S_0	**Etat Excite S_1(opt)**	**τ_1 (ps)**	**τ_2 (ps)**	**τ_3 (ps)**	**τ_4 (ps)**
IDTE	3.58	2.85	0.09(2)	0.8(1)		120(5)
IDTE-O2	3.48	3.10	0.140(2)	4.7(6)	36(4)	-
IDTE-O3	3.65	3.45	0.15(2)	15(5)	70(10)	-

© 2016 Tous droits réservés.

doc.univ-lille1.fr

Les spectres transitoires des trois molécules dans l'hexane pour une excitation @ 350 nm, i.e. une excitation de l'état S_1, sont présentés sur la Figure 23. Les bandes transitoires sont nommées X, Y et Z et leurs temps caractéristiques d'apparition et de déclin déduits par « global fitting » sont regroupés dans le Tableau 3. Il est clair que les trois jeux de données sont assez similaires et qu'il est donc opportun de les analyser dans leur ensemble.

Tout d'abord, juste après l'excitation laser, le signal est caractérisé par une montée rapide d'une bande intense X (λ_{max} ~ 610 nm), la position de cette bande étant étonnamment conservée quel que soit le photochrome considéré. En parallèle, avec une cinétique similaire comprise entre τ_1= 90 et 150 fs selon les composés, on remarque la montée de bande Y culminant vers le bleu. Si cela est moins clair pour les IDTE pontés, à cause des bandes d'émission stimulée SE négatives qui viennent se superposer, on voit parfaitement pour IDTE que la bande Y est à la même position que la bande d'absorption CF tout en étant un peu plus large. Nous relions donc cette bande transitoire Y à la CF vibrationnellement excitée et le temps τ_1 représente donc la réaction ultrarapide de photocyclisation.

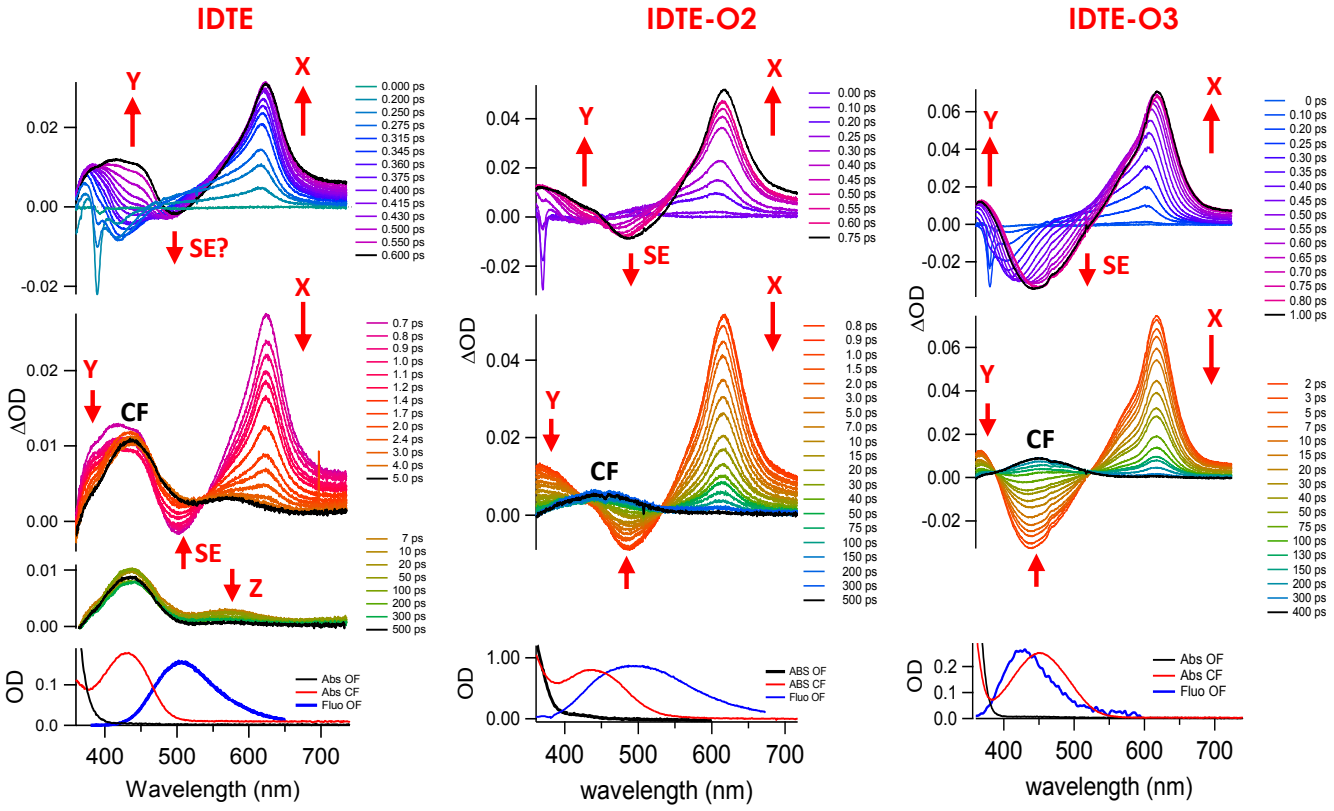

Figure 23 : Spectres d'absorption transitoire femtoseconde (résolution temporelle 200 fs) pour IDTE, IDTEO2 et IDTEO3 dans l'hexane après une excitation laser @ 350 nm. Les données sont corrigées de la GVD. Les données transitoires sont séparées en deux ou trois fenêtres temporelles. Pour aider à l'identification des bandes transitoires (X, Y et Z ; SE=émission stimulée), les spectres d'absorption (OF, CF) et d'émission (OF) sont indiqués en bas.

Ensuite, comme on peut le voir sur les panneaux centraux de la Figure 23, on observe la disparition des bandes X, Y et SE, avec l'apparition claire du spectre des CF pour les trois molécules. En fait, la CF étant déjà formée par photocyclisation, la disparition des bandes transitoires laisse juste apparaître son spectre. L'assignation de la bande X comme étant due à l'état singulet relaxé du conformère AP est plutôt simple si on se base sur les faits suivants : i) les cinétiques des bandes X et SE sont identiques ; ii) la fluorescence (et l'hypsochromisme de la série) a été attribuée à S_1(opt) du

© 2016 Tous droits réservés.

conformère AP. En toute logique, la bande X est donc reliée à S_1(opt). Nous soulignons que le déclin global des bandes X et Y est mono-exponentiel pour IDTE (τ_2 = 0,80 ps) mais bi-exponentielle pour les analogues pontés (τ_2 et τ_3 dans le Tableau 3). Nous proposons que τ_2 soit relié à une relaxation vibrationnelle de CF amplifiée par la présence du pont polyéther tandis que τ_3 serait relié aux mécanismes de relaxation photophysique de S_1(opt) du conformère AP, fluorescence bien sûr mais la conversion interne étant également possible. Il est intéressant de corréler l'effet de structure présenté plus haut avec l'augmentation de τ_3 pour la série. L'ensemble des résultats est résumé sur la Figure 24.

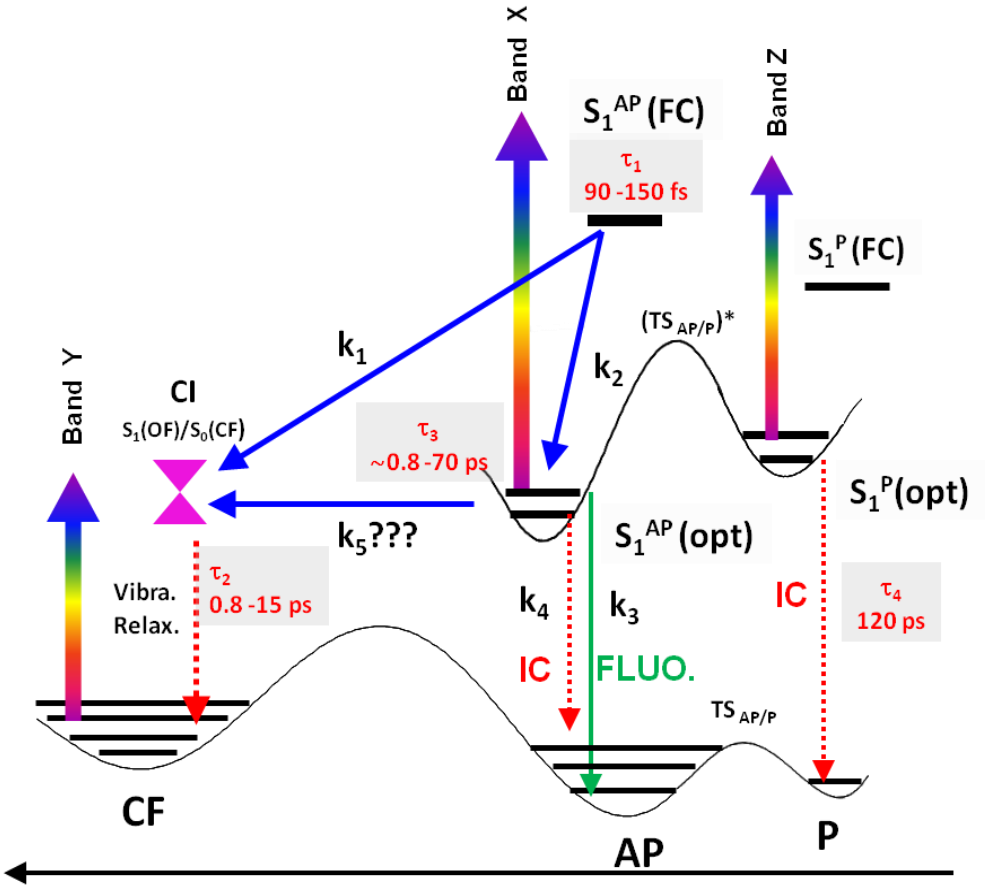

Figure 24 : Proposition de mécanisme photochimique pour la série IDTE. Le conformère P n'est présent que pour la molécule non-pontée.

Une caractéristique supplémentaire, uniquement observable pour IDTE, est la présence de la bande Z transitoire (λ_{max} ~ 570 nm) avec un temps de déclin de τ_4 = 120 ps. Bien évidemment, ceci constitue une élégante signature spectrale du conformère P se désexcitant par conversion interne.

Au final, la description assez poussée de la photocyclisation et des processus compétitifs, incluant les conformères AP et P est donnée par la Figure 22. Depuis la zone de Franck-Condon pour le conformère AP, on observe une photocyclisation directe (k_1) via une intersection conique suivi d'une relaxation vibrationnelle. En parallèle, l'état S_1 se relaxe (k_2) vers un minimum de potentiel, S_1(opt), qui lui se relaxe par fluorescence (k_3) ou par conversion interne (k_4). Une question fondamentale subsiste : l'intersection conique conduisant à la CF est-elle accessible à partir de S_1(opt), i.e. une photocyclisation indirecte (k_5) ?

Plus haut, nous avons vu qu'il y a une relation inverse entre les rendements quantiques de photocyclisation et de fluorescence. Nous avons pu établir une telle relation analytique entre les rendements de cyclisation et de fluorescence mais à l'unique condition de considérer à la fois les mécanismes direct et indirect :

© 2016 Tous droits réservés.

doc.univ-lille1.fr

$$\phi(cycl) \approx 1 - \frac{k4}{k3}\phi(fluo) \quad \textbf{(8)}$$

En effet, en ne considérant que le mécanisme indirect seul, il viendrait :

$$\phi(cycl) = \frac{k5}{k3}\phi(fluo) \quad \textbf{(9)}$$

Cette équation serait incompatible avec nos observations expérimentales.

La conclusion de cette étude est donc que l'approche synthétique consistant à bloquer le conformère AP par un pont inter-cycle pour améliorer l'efficacité des photochromes est intéressante (saut de 0.3 unité pour ϕ(cycl) entre IDTE et IDTE-O2) mais connait des limitations (même valeur entre IDTE et IDTE-O3). Les raisons pour lesquelles on observe une valeur optimum pour IDTE-O2 sont doubles : i) tout comme IDTE-O3, on a 100 % de conformère AP ; ii) grâce à sa chaîne poyéther plus courte, la molécule est d'autant plus contrainte, ce qui doit maintenir la zone de Franck-Condon plus proche de l'intersection conique. Dans le futur, il serait bon d'envisager l'optimisation des photochromes en prenant en compte la géométrie particulière de ces points topologiques complexes.

3.2.B Etude en phase Gaz

⇒Article complet en annexe 7

En collaboration avec L. Poisson du LFP (CEA Saclay), et dans le cadre de la thèse d'Aude Liétard, nous avons étudié la même série que précédemment mais en utilisant le montage de photoélectron résolu en temps avec une résolution temporelle de 50 fs. Ainsi, il nous a été possible de mettre à jour des superbes oscillations quantiques interprétées en termes de voies compétitives de photocyclisation.

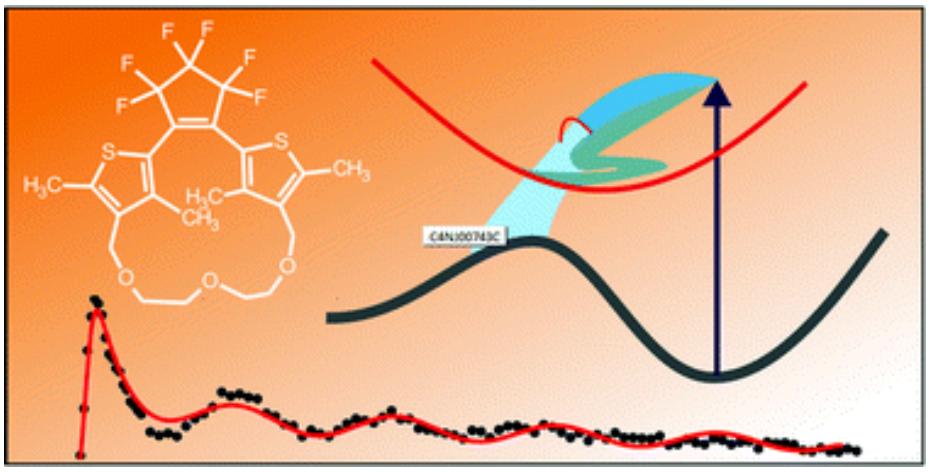

Figure 25 : Illustration de la publication Liétard et al. PCCP, 2014.

© 2016 Tous droits réservés.

doc.univ-lille1.fr

4. Projet : "Multi-Physics investigation of novel photodriven actuators based on bistable photochromic diarylethene."

(En japonais: フォトクロミックジアリールエテンを用いた新規光駆動アクチュエーターの開発と物性)

L'objectif du projet, suivant une stratégie **multi-physiques et multi-échelles**, est de comprendre les **effets optomécaniques** de films minces formés à partir de dithiényléthène A (photoswitch) liés à des élastomères B, tous deux pareillement fonctionnalisés par des groupements ureidopyrimidinone (voir Figure 26) .

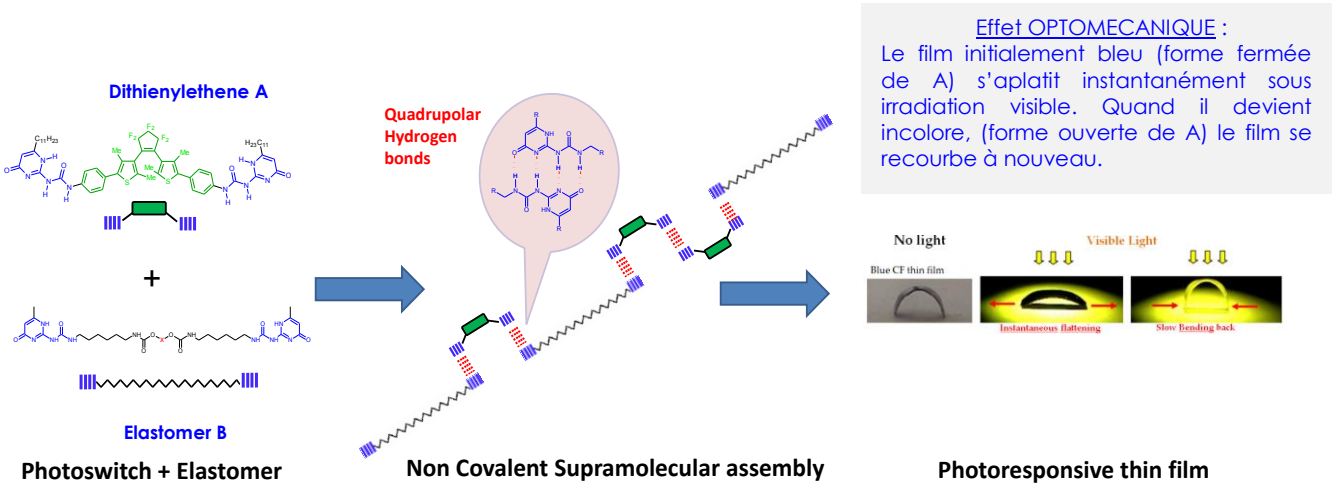

Figure 26 : Présentation des molécules A et B à la base des films « intelligents » photoactivables .

Le projet repose prévoit 4 étapes complémentaires :

(1) Etude des mécanismes de photocommutation de A et du système (A+B) combinant spectroscopies résolues en temps et analyse chimiométrique
(2) Modélisations moléculaires (A. Perrier)
(3) étude structurale des systèmes A et (A+B) via une combinaison de techniques d'analyse des matériaux (Unité Matériaux Et Transformation (UMET), Saga University)
(4) Etude de la réponse photomécanique des films minces (profilométrie laser...) et confrontation avec un modèle micromécanique innovant utilisant comme entrées les paramètres photochimiques/structuraux déterminés en (1)-(3) (UMET et Laboratoire de Mécanique de Lille)

Les étapes (1) et (2) de ce projet ambitieux ont largement été initiées dans le cadre de la thèse de Ismail Hamdi intitulée « Photochimie d'un diaryléthène fonctionnalisé pour l'assemblage supramoléculaire : de la solution jusqu'au film élastomère opto-activable » avec une soutenance prévue en janvier 2017. C'est dans le cadre de cette thèse, que nous avons étudié les molécules NDTE et NDTE-O5 (Figure 17). Des résultats très intéressants ont été obtenus comme :

- des effets cinétiques inattendus lors de l'auto-assemblage supramoléculaire de A seul
- la découverte d'une voie de photocyclisation via les états triplets

Les étapes (3) et (4) de ce projet, quelque peu initiées ces dernières années (stages de L3, M1) vont maintenant être approfondies dans le cadre de la thèse de Maroua Louati qui débute en octobre 2016 ayant pour titre : « Etude multi-échelle de films minces photo-activables basés sur l'assemblage supramoléculaire d'interrupteurs moléculaires et d'unités élastomères ». Cette thèse sera codirigée par S. Barrau de l'UMET et par moi-même.

Je reste persuadé que cette approche pluridisciplinaire sera bénéfique en termes d'avancées scientifiques et de qualité de publications.

© 2016 Tous droits réservés.
doc.univ-lille1.fr

© 2016 Tous droits réservés.

doc.univ-lille1.fr

Chapitre 5

Transfert de charge photoinduit dans les bétaïnes pyridinium

Ce chapitre présente ma deuxième thématique de recherche scientifique qui se concentre sur les propriétés de transfert de charge intramoléculaire d'une molécule de la famille des bétaïnes pyridinium. L'approche est strictement la même qu'au chapitre précédent bien que les mécanismes de désexcitation mis en jeu relèvent davantage de la photophysique.

Par la suite, nous allons présenter l'intérêt de la bétaïne pyridinium, puis traiter de ses propriétés de solvatochromie pour ensuite explorer les différents processus post-excitation et notamment s'intéresser au transfert de charge. Nous terminerons ce chapitre en traitant des propriétés de complexation et de photo-relargage de cations en rapport avec un récent projet soumis à l'ANR.

1. Présentation et enjeux autour de PyB

La definition IUPAC des transitions à transfert de charge est la suivante : "An electronic transition in which a large fraction of an electronic charge is transferred from one region of a molecular entity, called the electron donor D, to another, called the electron acceptor A (intramolecular CT) or from one molecular entity to another (intermolecular CT)."

Dans le cas du transfert de charge intramoléculaire (Intramolecular Charge Transfer, ICT), la réaction photoinduite peut s'écrire entre le donneur et l'accepteur :

$$D{-}A \; + h\upsilon \; \rightarrow \; D^{+|\delta|}{-}A^{-|\delta|}$$

Evidemment, un tel processus entraine un changement de moment dipolaire entre l'état fondamental et l'état excité et par suite un changement d'hyperpolarisabilité, ce qui est intéressant dans le domaine de l'optique non-linéaire par exemple.

Parmi toutes les molécules présentant des propriétés ICT, l'équipe du professeur J. Abe s'est intéressée à la molécule de (1-pyridinio)benzimidazolate ou PyB, qui est caractérisée par un état fondamental avec un certain caractère zwittérionique, les charges négatives et positives étant supposées être localisées sur les parties bétaïne et pyridinium respectivement.[11]

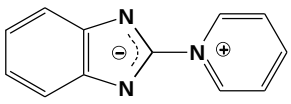

Figure 27. La molécule (1-pyridinio)benzimidazolate ou PyB.

Par le passé, deux études préliminaires ont montré que PyB présentait des propriétés de transfert de charge photoinduites. Premièrement, Boyd *et al.*[12] invoquaient des propriétés ICT de PyB pour expliquer le fort solvatochromisme des spectres d'absorption et suggéraient un important changement du moment dipolaire comme le montre la Figure 28. Fin des années 80, Alcade et *al.*[13] ont mesuré un moment dipolaire pour l'état fondamental de +10.33 D par des méthodes électrotechniques conventionnelles. Finalement, ce n'est qu'en 1997 que notre collaborateur J. Abe et al. [11c] a mis en lumière l'intérêt de PyB pour l'optique non-linéaire en mesurant par diffusion Hyper-Rayleigh une hyperpolarisabilité de $|\beta|=(115\pm25)10^{-30}$ esu, valeur 5 fois supérieure aux standards de l'époque (4-nitroaniline).

© 2016 Tous droits réservés.

doc.univ-lille1.fr

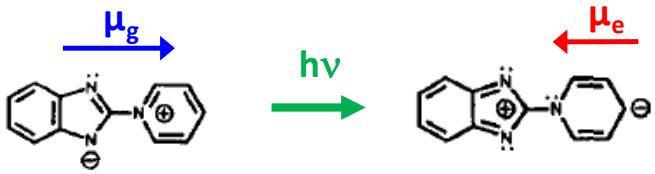

Figure 28 : Inversion photoinduite du moment dipolaire de PyB

Si cette inversion du moment dipolaire semblait avérée, aucune caractérisation des processus photophysiques engagés dans la réaction d'ICT n'avait jamais été réalisée. Nous avons donc entrepris une telle étude à partir de 2008, menée entre autre par Zuzanna Pawłowska dont la thèse avait pour titre : « *The Photophysics Of Pyridinium Betaines Studied By Ultrafast Transient Absorption Spectroscopy: Focus On The Photoinduced Intramolecular Charge Transfer Process.* » *(Soutenance 18 Janvier 2011)*. Cette thèse codirigée par G. Buntinx m'a permis de m'initier à l'encadrement doctoral avec ses temps forts mais aussi certaines erreurs à ne pas reproduire.

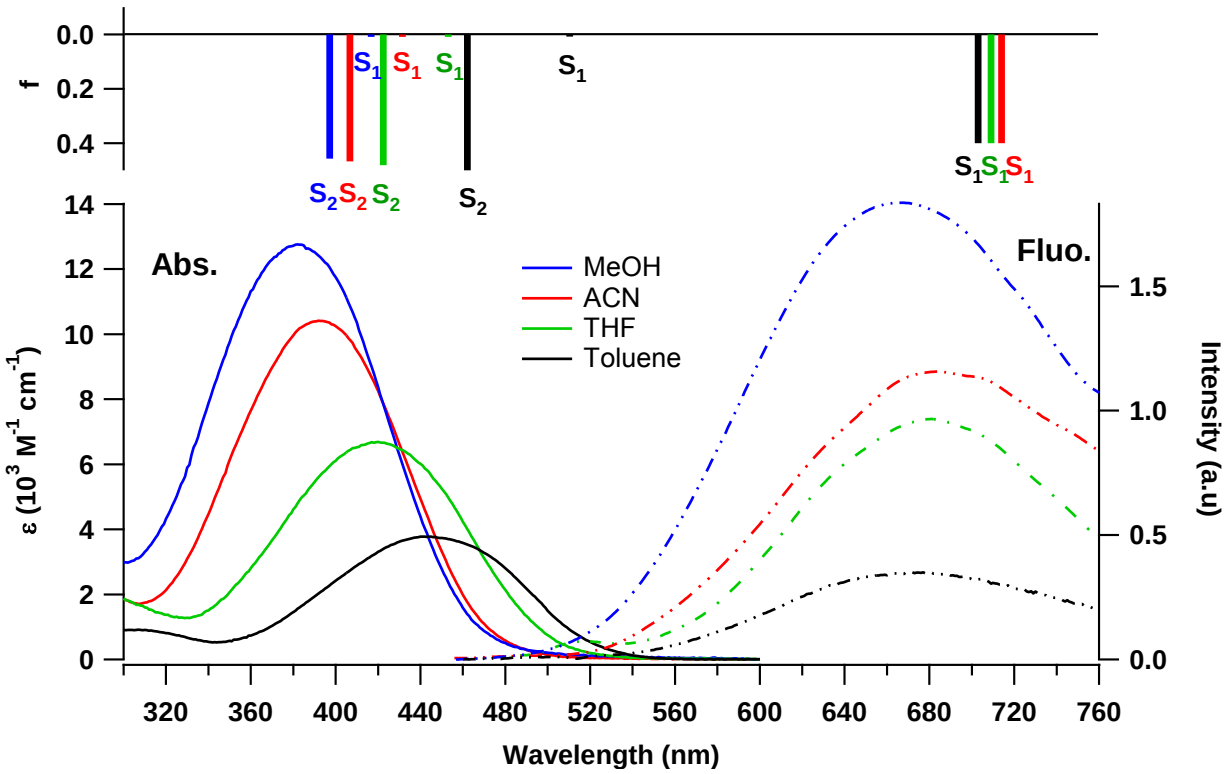

Figure 29 : Spectres d'absorption et de fluorescence de PyB dans quatre solvants différents : méthanol (bleu), ACN (rouge), THF (vert) et toluène (noir) avec les forces d'oscillateur et les longueurs d'onde des transitions verticales de S_0 vers les deux premiers états excités déterminées par TDDFT ainsi que la longueur d'onde (les forces d'oscillateur ne sont pas calculables) de la transition verticale de S_1 (opt) vers S_0 (même code de couleur).

© 2016 Tous droits réservés.

doc.univ-lille1.fr

2. La compréhension du solvatochromisme††† de PyB : états S_2(CT) et S_1(E)

⇒Article complet en annexe 8

Les spectres expérimentaux d'absorption et de fluorescence de PyB dans le Toluène, THF, ACN et MeOH sont présentés sur la Figure 29, ainsi que les résultats de TDDFT (traits respectant le même code couleur). Le niveau de calcul choisi par Aurélie Perrier, **PCM-TD-PBE0/6-311++G(2d,p)//PBE0/6-311G(d)**, l'a été pour reproduire au mieux tant la géométrie de la molécule (comparaison avec la structure obtenue par rayons X) que ses propriétés de solvatochromie.

Tout d'abord, Le solvatochromisme de PyB se caractérise par un très fort déplacement de la bande d'absorption (~60 nm) vers le bleu pour une augmentation de la polarité du solvant. Ce solvatochromisme dit « négatif » résulte des interactions dipôle-dipôle entre la molécule et le solvant, ces dernières entrainant une plus forte stabilisation de l'état fondamental par rapport à l'état excité (Figure 30). En parallèle, on remarque un fort effet hyperchrome de la bande d'absorption probablement relié à l'augmentation de μ_g.

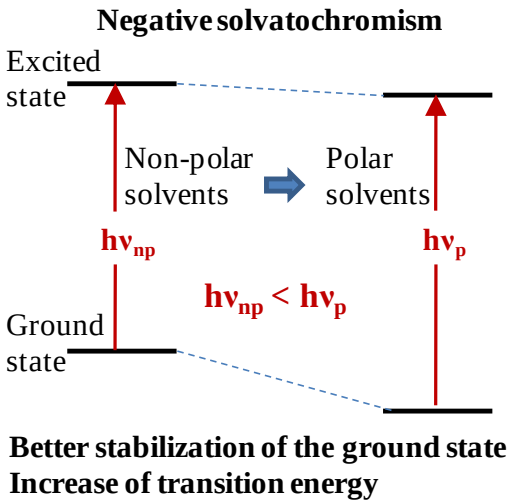

Figure 30 : Solvatochromisme négatif.

Ensuite, il est intéressant d'observer que l'important solvatochromisme négatif de la bande d'absorption contraste avec la quasi-absence d'un tel effet pour la bande d'émission qui présente plutôt un effet inverse, i.e. un solvatochromisme positif plus modéré (λmax 669, 675 et 687 nm pour toluène, le THF, et de l'ACN, respectivement). Il est à noter que ce résultat semble inhabituel puisque c'est la situation inverse (émission solvatochromique/absorption non-solvatochromique) qui est souvent rapportée dans la littérature[14].

Il est clair que la transition émissive n'implique pas le même état excité que la transition d'absorption vers l'état excité à transfert de charge, S_n(CT). De plus, en considérant les règles de Kasha, l'état fluorescent est probablement l'état singulet de plus basse énergie, noté S_1(E). Clairement, la TDDFT devenait cruciale pour identifier ces deux états excités.

Sur la Figure 29, on voit parfaitement que les transitions verticales $S_0 \rightarrow S_1$(FC) ont des forces d'oscillateurs quasi-nulles par rapport aux transitions $S_0 \rightarrow S_2$(FC). Ces dernières, calculées dans les

††† Le solvatochromisme est la propriété d'une molécule à changer de couleur selon la polarité du solvant dans lequel elle est dissoute. On distingue le solvatochromisme négatif correspondant à un déplacement hypsochromique (i.e. vers les longueurs d'onde plus courtes), lors de l'augmentation de la polarité du solvant au solvatochromisme positif, relatif à un déplacement bathochromique (i.e. vers les longueurs d'onde plus longues). Le signe du solvatochromisme dépend du sens de variation du moment dipolaire entre l'état fondamental et l'état excité du chromophore.

© 2016 Tous droits réservés.

doc.univ-lille1.fr

quatre solvants, reproduisent parfaitement le solvatochromisme négatif attendu, ce qui veut dire que l'état ICT solvatochrome n'est pas l'état S_1 mais bien l'état S_2. De surcroît, l'optimisation du premier état excité singulet en TDDFT, S_1(opt), et la transition émissive résultante, S_1(opt)→S'_0 montre qu'il est possible de reproduire le solvatochromisme légèrement positif de la fluorescence. Nous verrons qu'il faut pousser l'analyse plus loin pour définitivement attribuer S_1(opt).

Pour résumer, une première analyse des résultats permet de conclure que :

- La bande d'absorption présentant un solvatochromisme élevé est reliée à la transition S_0 → S_2(FC)
- La bande d'émission présentant un solvatochromisme faible est reliée à un état émissif S_1(E)

Sous l'impulsion du Pr. Patrice Jacques (U.H.A de Mulhouse), l'étude de la solvatochromie quantitative en a été poussée très loin afin de pouvoir déduire des valeurs de moments dipolaires. Nous avons travaillé avec plus d'une quinzaine de solvants et il nous a fallu trouver une nouvelle approche dans la mesure où un traitement du type Lippert-Mataga[15] devenait impossible, l'état de FC et l'état émissif n'étant pas les mêmes. En repartant des équations fondatrices du solvatochromisme, et par une paramétrisation judicieuse, nous sommes arrivés à déterminer la valeur de 4 moments dipolaires μ(S0), μ(S2), μ(S1) et μ(S0'). Nous invitons les lecteurs intéressés à se reporter à l'annexe 8.

3. Analyse des charges électrostatiques : 2 états ICT

⇒Article complet en annexe 9

Le calcul des charges électrostatiques, qui tient compte du solvant, se fait selon une approche Merz-Kollman (MK)[16], et s'applique aux états électroniques pertinents à savoir : S_0 et S_2(FC) ; son homologue relaxé dont la géométrie a été optimisée, S_2(opt) ; et en se fiant aux règles de Kasha, il était enfin primordial d'inclure S_1(opt). L'enjeu est bien sûr de découvrir les états à transfert de charge. Comme le montre la Figure 31, nous avons découvert que la somme partielle des charges MK selon trois parties distinctes de la molécule – cycle benzénique, pont imidazole, cycle pyridinium – était beaucoup plus instructive. Dans le but de mettre l'accent sur le processus photophysique réel, on examine d'abord l'excitation de S_0→S_2(FC) qui induit une diminution drastique du moment dipolaire en raison du transfert d'environ -0,44|e|du benzène vers le cycle pyridinium. Ensuite, de manière inattendue, la relaxation de S_2(FC) vers le minimum le potentiel, S_2(opt), provoque un transfert partiel en sens inverse (environ -0,2|e|) du cycle pyridinium vers le benzène, de telle sorte que la charge globale transférée lors de la transition S_0 → S_2(opt) est tout de même de - 0,24|e|. Ce caractère ICT non négligeable de S_2(opt) nous incite à le renommer S_2(CT) pour la suite. Pareillement, la relaxation S_2(opt) → S_1(opt) est reliée avec un transfert de charge de -0,26|e|depuis le pont imidazole vers le pyridinium, ce qui suggère que S_1(opt) peut être également renommé S_1(CT). En résumé, deux points importants sont à retenir :

- Un transfert de charge total de (-0,44|e| + 0,2|e| -0,26|e|) = -0.5|e| est ainsi prédit lors des processus photophysiques post-excitation conduisant à S_1(CT)
- Une conversion interne entre états excités S_2(CT) → S_1(CT) est donc attendue

Bien évidemment, le recours aux expériences résolues en temps va montrer toute sa complémentarité avec les calculs TDDFT.

© 2016 Tous droits réservés.

doc.univ-lille1.fr

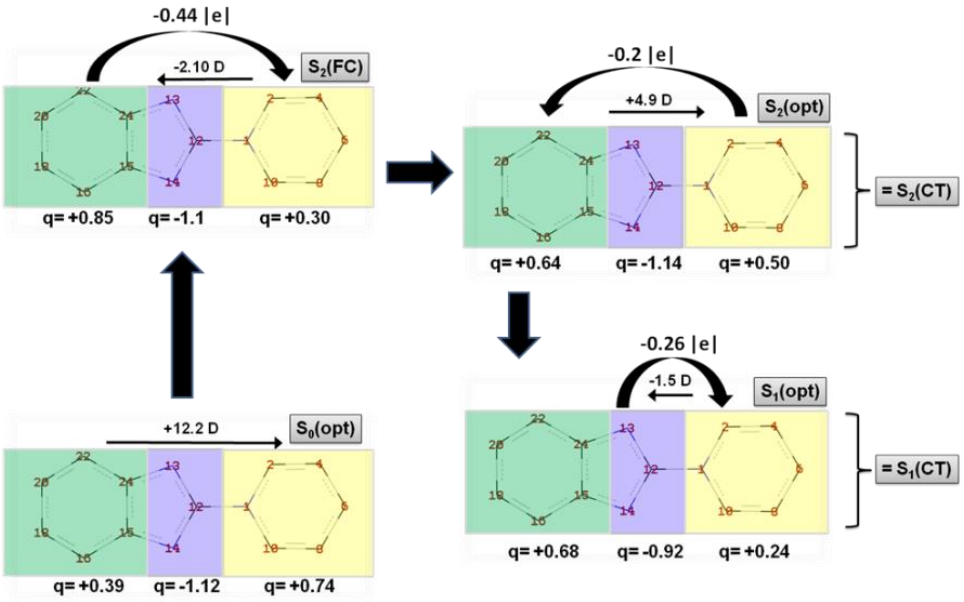

Figure 31 : Charges MK calculées (cas de l'ACN) sommées sur trois parties de PyB (benzène, imidazole et pyridinium) pour les états S_0(opt), S_2(FC), S_2(opt) et S_1(opt). Les moments dipolaires moléculaires de chaque état et les fractions de charge transférées pour chaque transition sont également indiqués.

4. La photophysique sous-jacente au processus ICT

⇒**Article complet en annexe 9**

Les données d'absorption femtoseconde de PyB (dans l'acétonitrile) suivant une excitation @390 nm sont présentées sur Figure 32a-c selon trois fenêtres temporelles distinctes :

- Dynamique Initiale [0-0,6 ps]
- Dynamique ICT [0,65-1,5 ps]
- Dynamique Post-ICT [2-500 ps]

tandis que les cinétiques @415, 485 ,600 et 700 nm sont indiquées sur la Figure 32d-e. Les courbes obtenues par la procédure de « global fitting »sont indiquées. En parallèle, la décomposition MCR-ALS de ce jeu de donnée est indiquée sur la Figure 33a pour les spectres pures (^{T}S) et Figure 33b pour les profils de concentration (C).

Dynamique Initiale. Dans l'acétonitrile, comme vu précédemment, une excitation à 390 nm correspond à la transition S0 → S2(FC) et par conséquent, au temps initial, c'est l'état S_2(FC) qui est peuplé. Comme on peut le voir, sur la Figure 31a, on observe l'apparition d'un signal avec trois types de bande : une bande de dépopulation de l'état fondamental (miroir négatif du spectre d'absorption) ou bande de blanchiment B ; une bande Y_1 de type ESA et une bande d'émission stimulée SE (miroir négatif du signal de fluorescence). Deux points isosbestiques à 450 et 610 nm sont présents et une analyse trop hâtive des données pourrait laisser croire que les bandes évoluent de manière concomitante. Or, lors de la procédure de « global fitting » nous avons inclus une fonction exponentielle croissante, ce qui veut dire qu'une ou des espèces apparaissent pendant l'excitation laser de S_2(FC) avec un temps caractéristique $\tau 1 \sim 100$ fs. De plus, pour être consistant avec les résultats de solvatochromie, (deux états S_1(E) et S_2(CT) bien distincts), nous attendions pour des temps inférieurs à 200 fs (résolution temporelle) une désexcitation parallèle S_2(FC) → S_2(CT) et S_2(FC) → S_1(E). Dans cette hypothèse, les états S_2(CT) et S_1(E) seraient alors reliés aux bandes transitoires Y_1 et SE respectivement. L'analyse MCR-ALS est venue réconforter cette hypothèse puisqu'elle trouve bien deux profils de concentration distincts pour les bandes Y1 et SE comme on peut le voir sur la Figure 32b.

© 2016 Tous droits réservés.

doc.univ-lille1.fr

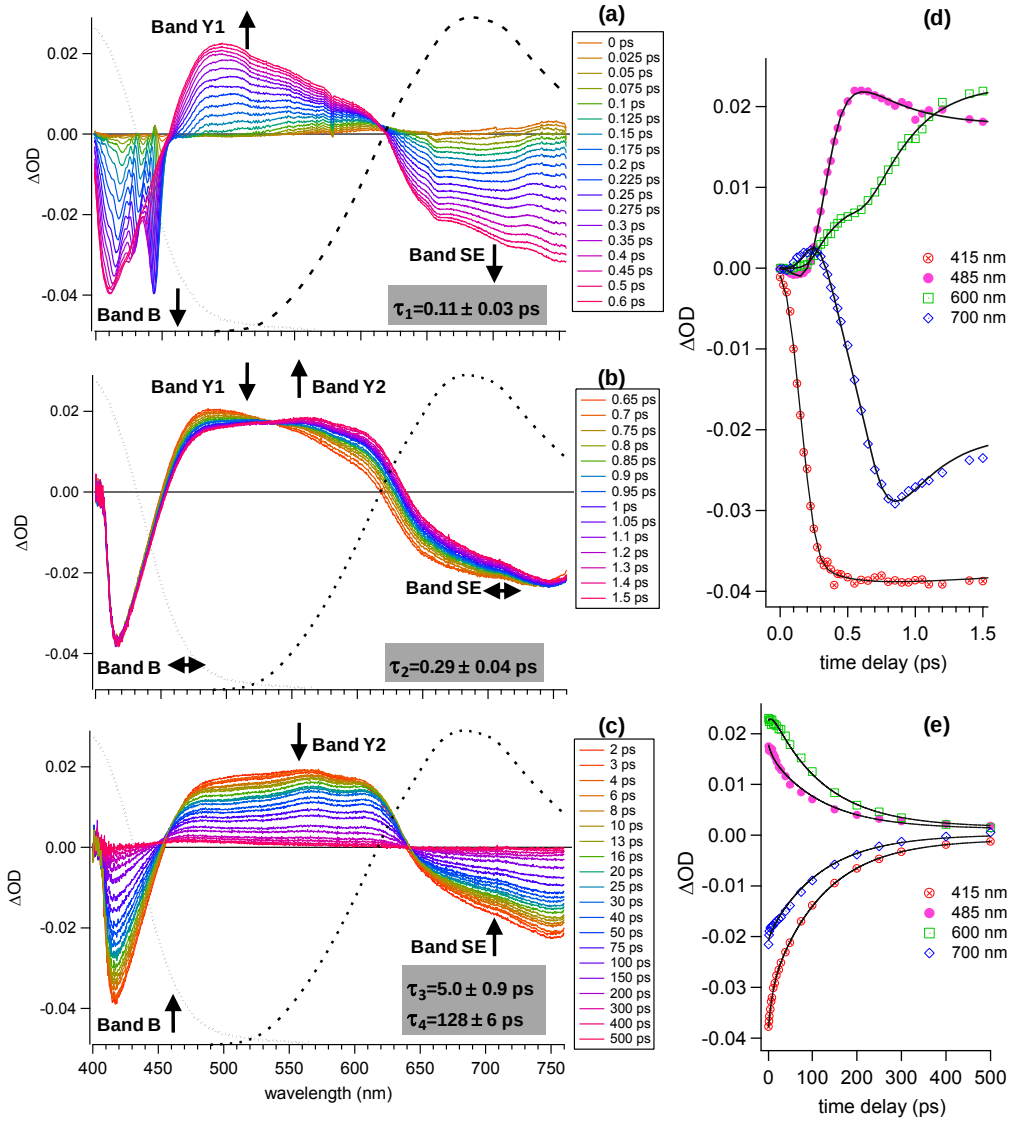

Figure 32 : (Gauche) Spectres transitoires de PyB (excitation à 390 nm) présentés selon trois fenêtres temporelles distinctes (a) 0-0,6 ps, (b) 0.65-1.5 ps et (c) 2-500 ps. (Le pic étroit vers 450 nm est dû au Raman stimulé). (Droite) Cinétiques @ 415 nm (Band B), 485 nm (Band Y1), 600 nm (Band Y2) et 700 nm (Band SE) présentées selon les fenêtres temporelles (d) 0-1.5 ps et (e) 2-500 ps ; les lignes noires correspondent au résultat du « global fitting » utilisant une fonction à 4 exponentielles convoluée avec une gaussienne.

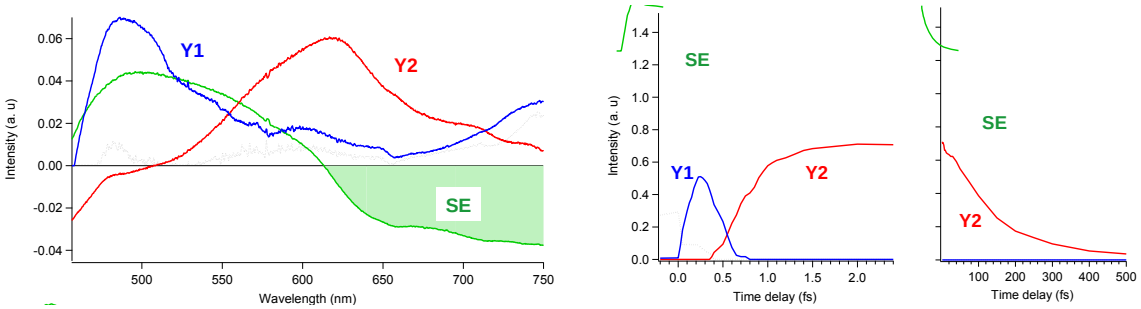

Figure 33 : Décomposition MCR-ALS des données transitoires de la Figure 32 en spectres purs et profils de concentration (même code couleur).

© 2016 Tous droits réservés.

doc.univ-lille1.fr

Dynamique ICT. Ce résultat est probablement le plus important de notre étude. On peut voir la bande Y1 qui disparait pour donner naissance à une nouvelle bande Y2 (de type ESA) avec un temps caractéristique de τ_2= 290 fs ; le point isosbestique à 530 nm attestant d'un processus ultrarapide $Y_1 \rightarrow Y_2$. Or, on voit bien que pendant ce processus, les bandes de blanchiment et d'émission stimulée restent constantes, ce qui signifie que : i) l'état S_1(E) n'est pas impliqué dans le processus ; ii) l'état fondamental n'étant pas repeuplé, il s'agit forcement d'un processus entre états excités. En fait, il s'agit bien sûr du processus ICT que l'on pouvait prédire par les calculs ; la conversion interne S_2(CT) → S_1(CT). Le caractère de transfert de charge de ce processus a été corroboré par une étude poussée en changeant le solvant. Il a été possible de trouver de fortes corrélations entre le temps caractéristique τ_2 et la polarité ou viscosité du solvant. Ce qui implique que la réaction de transfert de charge dépend directement de la dynamique de solvatation de PyB.

Dynamique Post-ICT. On voit clairement sur la Figure 31b le déclin quasi-total des bandes Y2, B et SE pour laisser apparaitre une faible bande vers 450 nm qui s'avère être un état triplet. Le déclin est en fait bi-exponentielle avec des temps caractéristiques τ_3=5 ps et τ_4=128 ps attribués à la relaxation photophysique de S_1(CT) et S_1(E) respectivement. Des effets de solvant ont également été reportés. De même, nous nous sommes intéressés à la possible géométrie « twisté » de l'état excité S_1(CT) en comparant la photophysique de PyB avec un analogue non-plan et avons trouvé des résultats assez similaires. Nous en avons déduit que la torsion de la bétaïne pyridinium n'est pas une coordonnée réactionnelle importante. Nous invitons le lecteur à se reporter à l'article en annexe 10 pour plus d'information.

En résumé, le processus ICT de PyB, responsable de la solvatochromie de la molécule est en fait un processus en deux étapes comme on peut le voir sur la Figure 34 :

- Un premier ICT instantané lors de l'excitation de S_2(CT) qui est localisé depuis le noyau benzénique vers le cycle pyridinium ;
- Après qu'une partie de la charge soit retournée vers le donneur (~ 100 fs) et que l'état émissif S_1(E) soit peuplé, un second ICT se déclenche lors de la conversion interne S_2(CT)→S_1(CT). Cette réaction est elle aussi localisée, depuis le pont imidazole jusqu'au pyridinium, et se déroule avec des temps caractéristiques se situant entre 300 fs et 20 ps selon le solvant. La dynamique de transfert de charge est donc contrôlée par le solvant.
- En régime picoseconde, on observe la relaxation de S_1(E) par fluorescence, conversion interne et croisement intersystème (production d'un état triplet) tandis que l'état S_1(CT) se relaxe par conversion interne.

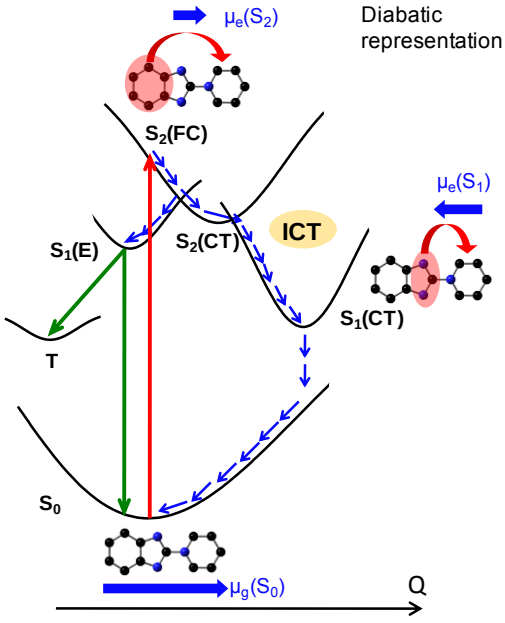

Figure 34 : Mécanismes ICT au sein de PyB.

© 2016 Tous droits réservés.

doc.univ-lille1.fr

5. Projet: "Novel Photoswitch based on Excited State Cation Transfer"

⇒Article complet en annexe 10

Ce projet a débuté en 2012 lorsqu'Isabelle Leray de l'ENS Cachan assistait à ma conférence GFP2P à Bordeaux qui traitait des résultats fondamentaux obtenus sur PyB, intitulée « Photochimie de bétaïnes pyridinium solvatochromes étudiées par spectroscopie ultrarapide et calculs TDDFT ». Son idée de base consistait à coupler un fluorophore de type ICT capable de complexer les cations pour faire de la photo-complexation de cations voire de la translocation de cations photoinduite entre deux sites de complexation. Son doctorant de l'époque, le Dr. Ruan Yibin, a alors synthétisé une molécule PyB fonctionnalisée par une éther-couronne, composé nommé PyB- Aza, avec l'idée que la charge négative serait redistribuée sur l'azote du macrocycle comme le montre la Figure 35. Nous avons donc initié une étude poussée sur les processus photophysiques de PyB et Pyb-Aza (entre autres) en présence de divers cations. Cette étude vient d'être publiée au PCCP (Aloïse et *al* PCCP, 2016, 15384) mais nous nous focaliserons sur les résultats les plus marquants.

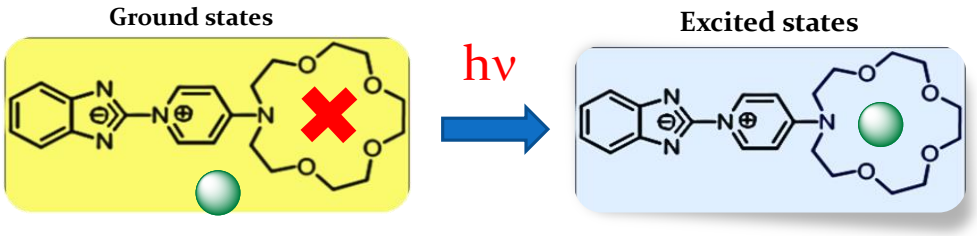

Figure 35 : Principe de la photo-complexation pour la molécule PyB-Aza.

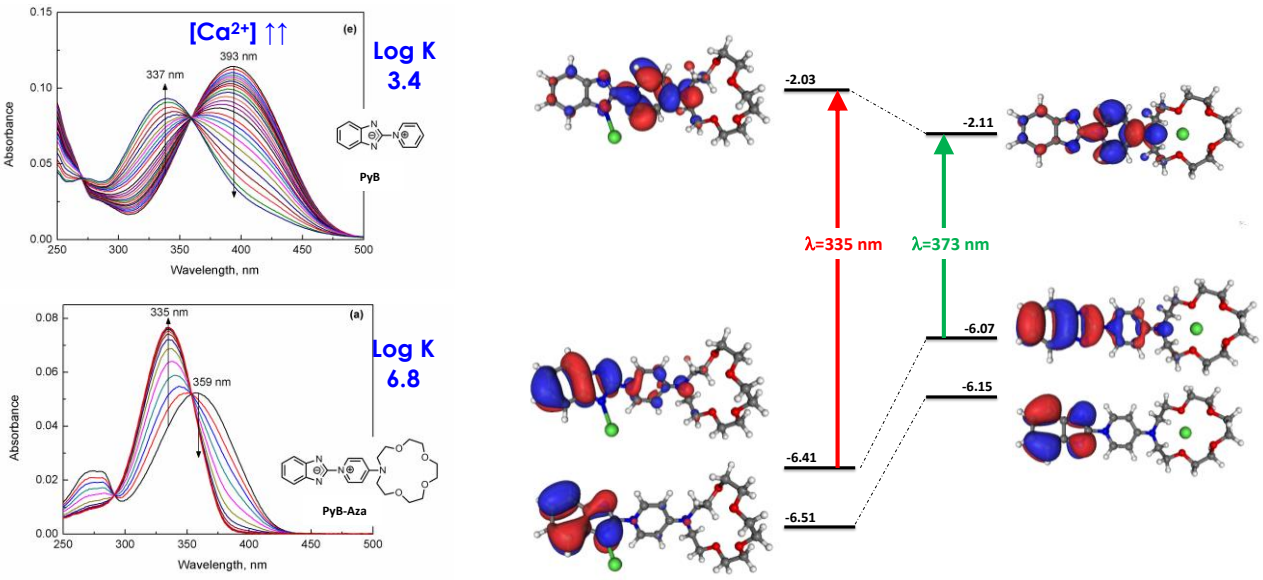

Figure 36 : (gauche) Spectre d'absorption (dans l'acétonitrile) pour PyB et PyB-Aza en présence d'une quantité croissante de Ca^{2+} (droite) Calcul TDDFT des transitions optiques de PyB-Aza en supposant que le cation se trouve soit en position latérale soit au centre de l'éther-couronne.

Tout d'abord, nous avons découvert qu'à l'état fondamental il se forme un complexe entre n'importe quelle molécule analogue de PyB et les cations. En effet, comme on peut le voir sur la Figure 36, les spectres d'absorption initialement bien distinct λ_{max} 393 et 359 nm pour PyB et PyB-Aza respectivement sans Ca^{2+} deviennent similaires avec un excès de Ca^{2+} (λ_{max} 337 et 335 nm). L'interaction des bétaïnes pyridinium et du cation Ca^{2+} est purement électrostatique et se fait de

© 2016 Tous droits réservés.

manière latérale avec le pont imidazole, comme cela est montré de façon probante par les calculs TDDFT. Ceci signifie que, les propriétés chélatantes du macrocycle ne rentrent nullement en compétition avec l'efficacité complexante de l'imidazole. Par contre, il est possible de faire varier la constante de complexation de plusieurs ordres de grandeurs par des effets inductifs appropriés ; par exemple, le logK varie de 3.4 à plus de 6 en rajoutant soit l'éther-couronne soit un azo-diméthyle. Il est important de préciser que les calculs TDDFT ont été capables de reproduire également l'effet d'exaltation du logK.

Nous nous sommes ensuite penchés sur le devenir de ce complexe quand celui-ci est exposé à la lumière. Comme nous pouvons le voir sur les spectres transitoires de la Figure 37, aux tout premiers instants jusqu'à 250 fs, l'émission stimulée SE_2 est celle de l'espèce complexée (miroir négatif de E_2 modulé par de l'ESA). Entre 280 fs et 1.5 ps, nous pouvons suivre la photo-éjection du cation via le glissement bathochrome du signal de SE_2 vers une autre bande négative SE_1 qui n'est autre que l'émission stimulée de l'espèce non-complexée. Ceci implique que le cation ait été éjecté au-delà de la sphère de solvatation. Au-delà de 2 ps, la photophysique du système redevient celle déjà décrite plus haut, incluant, la fluorescence émanant de $S_1(E)$ et le croisement inter système qui donne naissance à un état triplet (signal à1000 ps).

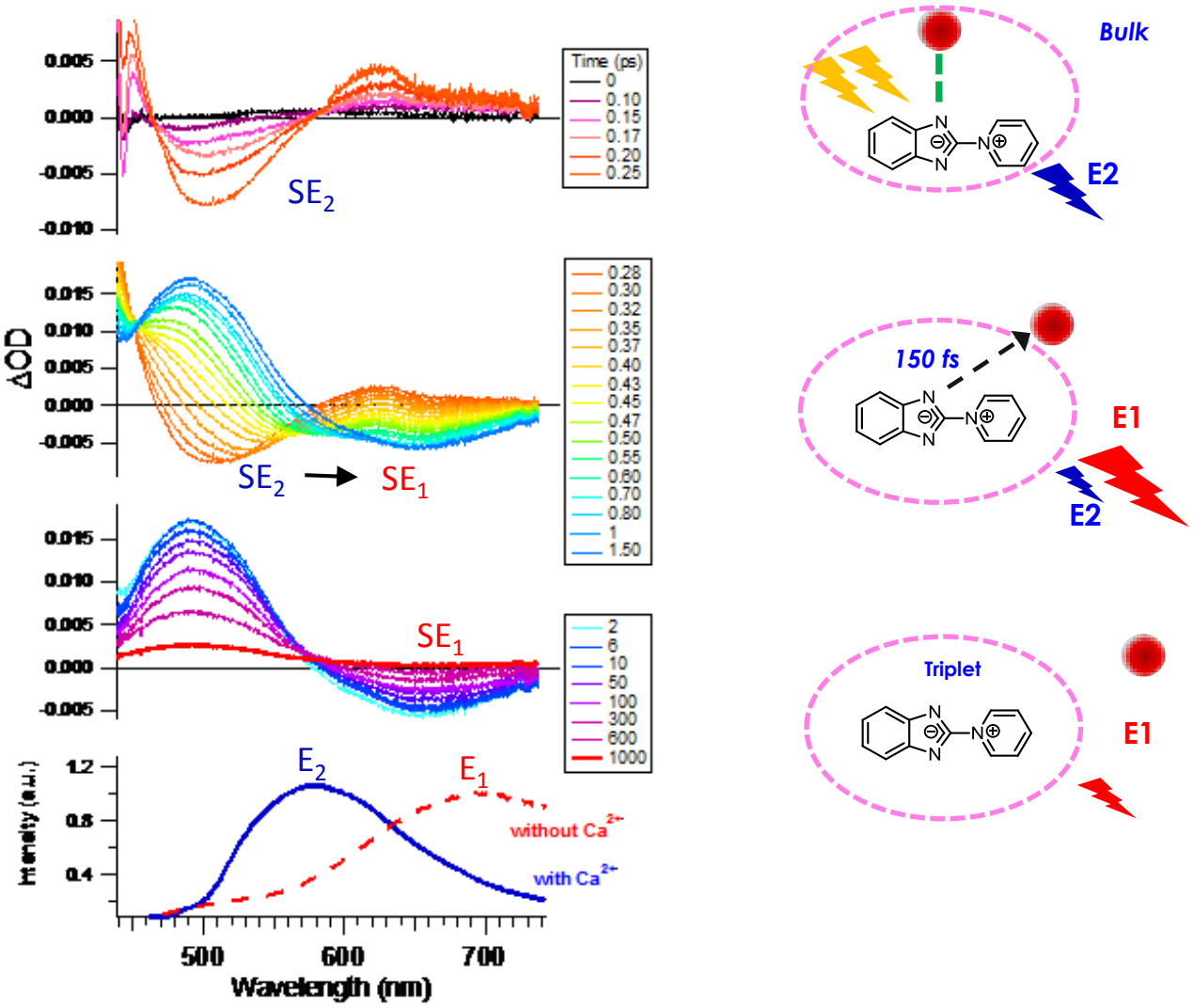

Figure 37 : Spectres d'absorption femtoseconde (excitation laser @ 320 nm) de PyB [50 µM] avec 40 eq. de Ca^{2+} dans l'ACN ; Les spectres de fluorescence stationnaire avec (E_2) et sans Ca^{2+} (E_1) sont également indiqués pour aider à l'attribution des émissions stimulées SE_1 et SE_2.

© 2016 Tous droits réservés.

doc.univ-lille1.fr

Grâce à ces résultats inattendus, nous avons réorienté le projet afin de tirer profit des caractéristiques de PyB. En collaboration avec l'ENS Cachan, nous essayerons d'élaborer une nouvelle famille de photoswitch basée sur le transfert de cation photoinduit (**Excited State Cation Transfer ESCT)** comme le montre la Figure 38. Le cation initialement complexé sur PyB (site #1) ira, en conséquence de la réaction de transfert de charge, se complexer sur une autre partie de la molécule (site #2). Ce projet a été déposé à l'ANR en 2016 (pré-proposition ayant reçu la note de 37/41) mais n'a pas été retenu au final. Nous comptons redéposer ce projet en 2017.

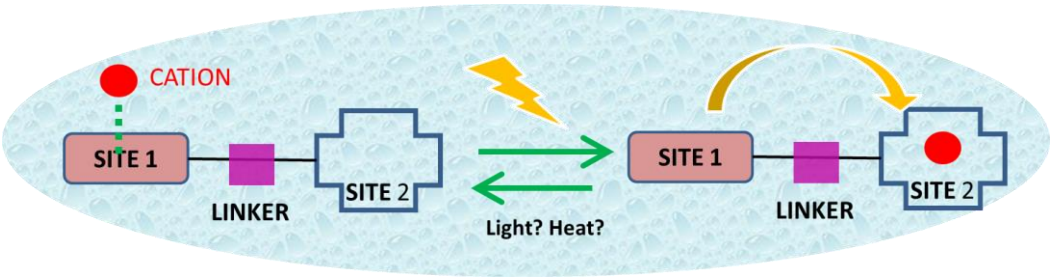

Figure 38. Illustration du projet ESCT-switch.

© 2016 Tous droits réservés.

doc.univ-lille1.fr

Bibliographie

(1) Aloise, S.; Ruckebusch, C.; Blanchet, L.; Rehault, J.; Buntinx, G.; Huvenne, J. P. *Journal of Physical Chemistry A* **2008**, *112*, 224.

(2) (a) Crano, J. C.; Guglielmetti, R. J. *Organic Photochromic and Thermochromic Compounds*; Plenum: New York, 1999(b) Dürr, H.; Bouas-Laurent, H. *Photochromism, Molecules, and Systems*; Elsevier: Amsterdam, 1990.

(3) Bouas-Laurent, H.; Durr, H. *Pure Appl. Chem.* **2001**, *73*, 639.

(4) Rau, H. *Photochemistry and photophysics*; Rabek, J.F. ed.; CRC Press: Boca Raton, 1990.

(5) Aloise, S.; Rehault, J.; Moine, B.; Poizat, O.; Buntinx, G.; Lokshin, V.; Vales, M.; Samat, A. *Journal of Physical Chemistry A* **2007**, *111*, 1737.

(6) (a) Nakamura, S.; Uchida, K.; Hatakeyama, M. *Molecules* **2013**, *18*, 5091(b) Nakamura, S.; Kobayashi, T.; Takata, A.; Uchida, K.; Asano, Y.; Murakami, A.; Goldberg, A.; Guillaumont, D.; Yokojima, S.; Kobatake, S.; Irie, M. *J. Phys. Org. Chem.* **2007**, *20*, 821(c) Ishibashi, Y.; Tani, K.; Miyasaka, H.; Kobatake, S.; Irie, M. *Chemical Physics Letters* **2007**, *437*, 243(d) Dulic, D.; Kudernac, T.; Puzys, A.; Feringa, B. L.; van Wees, B. J. *Advanced Materials* **2007**, *19*, 2898.

(7) (a) Uchida, K.; Tsuchida, E.; Aoi, Y.; Nakamura, S.; Irie, M. *Chem. Lett.* **1999**, 63(b) Irie, M.; Lifka, T.; Kobatake, S.; Kato, N. *J. Am. Chem. Soc.* **2000**, *122*, 4871(c) Morimitsu, K.; Kobatake, S.; Irie, M. *Tetrahedron Lett.* **2004**, *45*, 1155.

(8) (a) Jukes, R. T. F.; Adamo, V.; Hartl, F.; Belser, P.; De Cola, L. *Inorganic Chemistry* **2004**, *43*, 2779(b) Indelli, M. T.; Carli, S.; Ghirotti, M.; Chiorboli, C.; Ravaglia, M.; Garavelli, M.; Scandola, F. *Journal of the American Chemical Society* **2008**, *130*, 7286(c) Fukaminato, T.; Doi, T.; Tanaka, M.; Irie, M. *Journal of Physical Chemistry C* **2009**, *113*, 11623.

(9) Takeshita, M.; Yamato, T. *Tetrahedron Letters* **2001**, *42*, 4345.

(10) (a) Perrier, A.; Aloise, S.; Olivucci, M.; Jacquemin, D. *Journal of Physical Chemistry Letters* **2013**, *4*, 2190(b) Boggio-Pasqua, M.; Bearpark, M. J.; Klene, M.; Robb, M. A. *J. Chem. Phys.* **2004**, *120*, 7849.

(11) (a) Abe, J.; Nemoto, N.; Nagase, Y.; Shirai, Y. *Chem. Phys. Lett.* **1996**, *261*, 18(b) Abe, J.; Shirai, Y. *Journal of American Chemical Society* **1996**, *118*, 4705(c) Abe, J.; Shirai, Y.; Nemoto, N.; Miyata, F.; Nagase, Y. *J. Phys. Chem. B* **1997**, *101*, 576(d) Abe, J.; Shirai, Y.; Nemoto, N.; Nagase, Y. *J. Phys. Chem. B* **1997**, *101*, 1910.

(12) Boyd, G. V. *Tetrahedron Letters* **1966**, *29*, 3369.

(13) Alcalde, E.; Dinares, I.; Elguero, J.; Fayet, J.-P.; Vertut, M.-C.; Miravitlles, C.; Molins, E. *Journal of Organc Chemistry* **1987**, *52*, 5009.

(14) (a) Reichardt, C. *Solvents and Solvent effects in Organic Chemistry*; Wiley-VCH, 2003(b) Reichardt, C. *Chem. Rev.* **1994**, *94*, 2319.

(15) (a) Lippert, E. *Z. Naturforsh* **1955**, *109*, 571(b) Lippert, E. *Ber. Bunsenges* **1957**, *61*, 962(c) Mataga, N.; Kaifu, Y.; Koizumi, M. *Bull. Chem. Soc. Jpn.* **1955**, *28*, 690(d) Mataga, N.; Kaifu, Y.; Koizumi, M. *Bull. Chem. Soc. Jpn.* **1956**, *29*, 465.

(16) Perrier, A.; Maurel, F.; Pawlowska, Z.; Sliwa, M.; Aloise, S.; Abe, J. *Chem. Phys. Lett.* **2011**, *515*, 42.

© 2016 Tous droits réservés.

doc.univ-lille1.fr

© 2016 Tous droits réservés.

doc.univ-lille1.fr

Annexe 1: Fiche descriptive du Cours de Chimie Physique du S1

	Atomistique et Liaison Chimique
	Responsable : Aloïse Stéphane LASIR - Bat C_5
Descriptif des objectifs	***Détails des objectifs*** *. Comprendre l'organisation intime de la matière via ses constituants élémentaires : noyaux, atomes et molécules.* *. Acquérir des notions de spectroscopie atomique (interaction lumière-matière)* *. Connaitre la configuration électronique des éléments, leurs propriétés* *. Comprendre la classification périodique des éléments.* *. Comprendre les notions d'orbitales atomiques et moléculaires* *. Savoir prédire les propriétés structurales (géométrie, isomérie, liaisons hydrogène) et électroniques (moment dipolaire, magnétisme) des molécules et en déduire certaines propriétés macroscopiques de la matière comme la solubilité, la température de fusion...*
Descriptif du Contenu	***Détails des contenus couverts par l'UE – Notions principales*** *L'UE se décompose en 2 séquences complémentaires et d'égales proportions.* ***Partie 1: Composition et propriétés des atomes*** *Chapitre 1 Composition du noyau* *Chapitre 2 Spectre atomique des hydrogénoïdes* *Chapitre 3 Description quantique d'un atome. Notion d'orbitale atomique* *Chapitre 4 Configuration électronique, classification périodique.* *Chapitre 5 Atomes polyélectroniques: Méthode de Slater* *Chapitre 6 Propriétés des éléments* ***Partie 2: Géométrie et propriétés des molécules*** *Chapitre 7 Liaison chimique : description quantique* *Chapitre 8 Géométrie des molécules : théorie VSEPR* *Chapitre 9 Géométrie des molécules polyatomiques. Isomérie.* *Chapitre10 Interactions faibles*
Organisation pédagogique	- ***44h CTD*** - ***9h TP*** - ***1H colles orales (3 x 20 min)***
Connaissances et compétences acquises	***Détails de ce que les étudiants auront acquis par les enseignements de l'UE*** *<u>Connaissances</u> : Le but de cette UE est de fournir les connaissances théoriques indispensables à la compréhension des atomes et des molécules et de faire le lien avec certaines des propriétés macroscopiques de la matière.* *<u>Compétences</u> (1 à n) : par exemple :* *1-capacité à comprendre, manipuler et comparer des théories avancées (Bohr vs Modèle ondulatoire) ; Comparer les résultats expérimentaux et théoriques (Slater).* *2-capacité à savoir analyser un spectre d'absorption et d'émission à partir d'un diagramme d'énergie ; savoir manipuler les unités de la spectroscopie (J, eV, nm, cm^{-1}...)* *3- Comprendre le tableau périodique des éléments (base de la chimie)* *4-savoir prédire des propriétés atomiques ou moléculaires par des raisonnements qualitatifs simples. Savoir prédire la géométrie d'une molécule.* *5- Savoir utiliser un logiciel de modélisation pour visualiser les différentes propriétés des molécules (OM, moment dipolaire, géométrie....)*
Type d'activité auquel cette UE prépare et secteur d'activité	*Connaissances théoriques/pratiques indispensables pour n'importe quel scientifique tourné vers les sciences physiques (chimie, physique, électronique...)*
Modalités d'évaluation	***Détails de la façon dont sont évaluées les compétences*** *SUP ((DS1 + DS2)/2, (DS1+DS2+MoyInterro)/3)*
Pré-requis conseillés	*Mathématiques de Base*
Langue de l'enseignement	*Français*
ECTS	4

© 2016 Tous droits réservés.

doc.univ-lille1.fr

© 2016 Tous droits réservés.

doc.univ-lille1.fr

Annexe 2 : Fiche descriptive du Cours d'Instrumentation pour la Chimie

Nom code UE :	Instrumentations pour la Chimie.
	Responsable : Stéphane Aloïse LASIR Bat C_5
Descriptif des objectifs	***Détails des objectifs*** *Depuis la simple analyse routinière de laboratoire jusqu'à la conception des matériaux intelligent du futur, la maitrise des méthodes optiques de reconnaissance des molécules est indispensable pour le chimiste averti qui se doit de maitriser les instruments qu'il utilise. Ce module vise à donner les bases indispensables aux chimistes concernant les méthodes optiques : optique ondulatoire simplifiée, présentation des éléments dispersifs des monochromateurs, notion de résolution spectrale, détecteurs, laser…*
Descriptif du Contenu	***Détails des contenus couverts par l'UE – Notions principales*** *Une méthode d'analyse physico-chimique repose sur trois éléments : une source de lumière, un élément dispersif (prisme, réseau…etc) et un détecteur. Nous allons passer en revue ces 3 éléments aux travers de 5 grands chapitres : I) Rappel d'optique (simplifié ! Pas beaucoup d'équation) ; II) Eléments dispersifs, monochromateur ; III) Source de Lumière-LASER ; IV) Détecteurs ; V) Méthodes optiques de détection des molécules.*
Organisation pédagogique	• ***30 h de Cours-TD*** *avec un fascicule pédagogique. (S. Aloïse)* • ***20 h de TP (5x4h).*** *(F. Mianney, P. Hubert)* *Les TP se feront en binôme ; Une forte interactivité enseignant/étudiant serait l'idéal.*
Connaissances et compétences acquises	***Détails de ce que les étudiants auront acquis par les enseignements de l'UE*** *Connaissances :* *Nature de la lumière ; Optique géométrique et ondulatoire ; Eléments dispersifs, monochromateur (notion de résolution spectrale); Détecteurs comme le Photomultiplicateur ou la caméra CCD ; Sources lumineuse, LASERS (version simplifiée) ; exemples concrets de méthodes optiques d'analyse des molécules (absorption UV-Vis, spectroscopie IRTF, Raman…etc)* *Compétences :* *1- Posséder les notions d'optiques de base pour être à l'aise au sein des laboratoires modernes de chimie* *2- comprendre et savoir choisir une méthode optique d'analyse moléculaire pour pouvoir travailler de façon autonome* *3- Maitriser et améliorer le « vrai signal » par rapport au bruit : notion de résolution spectrale, rapport signal/bruit…*
Type d'activité auquel cette UE prépare et secteur d'activité	*UE ABSOLUMENT INDISPENSABLE A TOUT CHIMISTE, INGENIEUR, TECHNICIEN SUPERIEUR qui sera forcément amené à utiliser une méthode d'analyse optique.* *Cette UE vous permettra de comprendre nombre d'UE en L3, M1, M2…*
Modalités d'évaluation	***Détails de la façon dont sont évaluées les compétences*** *Note 1= note sur le présentiel (il suffit de ne pas louper les cours !)= 20%* *Note 2= DS final d'évaluation = 50%* *Note 3 = Moyenne des comptes rendus de TP =30%* *Un étudiant sérieux qui aura bien suivi les cours, validera forcement son module.*
Acquis et Pré-requis conseillés	*Connaissances en optique souhaitables mais pas obligatoires*
Langue de l'enseignement	*Français* *(certains documents seront en anglais pour acquérir les termes techniques)*
ECTS	5

© 2016 Tous droits réservés.

doc.univ-lille1.fr

© 2016 Tous droits réservés.

doc.univ-lille1.fr

Annexe 3. Aloïse et al, J. Phys. Chem. A 112, 224, 2008

The Benzophenone $S_1(n,\pi^*) \rightarrow T_1(n,\pi^*)$ States Intersystem Crossing Reinvestigated by Ultrafast Absorption Spectroscopy and Multivariate Curve Resolution

Stéphane Aloïse,* Cyril Ruckebusch, Lionel Blanchet, Julien Réhault, Guy Buntinx, and Jean-Pierre Huvenne

Laboratoire de Spectrochimie Infrarouge et Raman (CNRS UMR 8516), Centre d'études et de recherches Lasers et Applications (CNRS FR 2416), Université des Sciences et Technologies de Lille, Bat C5, 59655 Villeneuve d'Ascq Cedex, France

Received: July 24, 2007; In Final Form: October 19, 2007

The well-known benzophenone intersystem crossing from $S_1(n,\pi^*)$ to $T_1(n,\pi^*)$ states, for which direct transition is forbidden by El-Sayed rules, is reinvestigated by subpicosecond time-resolved absorption spectroscopy and effective data analysis for various excitation wavelengths and solvents. Multivariate curve resolution alternating least-squares analysis is used to perform bilinear decomposition of the time-resolved spectra into pure spectra of overlapping transient species and their associated time-dependent concentrations. The results suggest the implication of an intermediate (IS) in the relaxation process of the S_1 state. Therefore, a two step kinetic model, $S_1 \rightarrow IS \rightarrow T_1$, is successfully implemented as an additional constraint in the soft-modeling algorithm. Although this intermediate, which has a spectrum similar to the one of $T_1(n,\pi^*)$ state, could be artificially induced by vibrational relaxation, it is tentatively assigned to a hot $T_1(n,\pi^*)$ triplet state. Two characteristic times are reported for the transition $S_1 \rightarrow IS$ and $IS \rightarrow T_1$, ~6.5 ps and ~10 ps respectively, without any influence of the solvent. Moreover, an excitation wavelength effect is discovered suggesting the participation of unrelaxed singlet states in the overall process. To go further discussing the spectroscopic relevancy of IS and to rationalize the expected involvement of the $T_2(\pi,\pi^*)$ state, we also investigate 4-methoxybenzophenone. For this neighboring molecule, triplet energy level is tunable through solvent polarity and a clear correlation is established between the intermediate resolved by multivariate data analysis and the presence of a $T_2(\pi,\pi^*)$ above the $T_1(n,\pi^*)$ triplet. It is therefore proposed that the benzophenone intermediate species is a $T_1(n,\pi^*)$ high vibrational level in interaction with $T_2(\pi,\pi^*)$ state.

1. Introduction

The relaxation of the photoexcited $S_1(n,\pi^*)$ state of benzophenone (BP) and other related molecules is one of the most important photophysical processes within the field of organic photochemistry due to its fundamental role in photoreactivity of aromatic ketones. Many time-resolved absorption studies[1−7] have dealt with this subject, and the main results can be summarized as follows: (i) the $S_1(n,\pi^*)$ state decay gives rise to the triplet $T_1(n,\pi^*)$ state through intersystem crossing (ISC) process; (ii) a unique ~10 ps characteristic time describes this dynamic with a quantum yield close to unity and does not depend on the excitation wavelength; (iii) the commonly admitted non-solvent dependency[1−5] of the process has been questioned recently;[6] (iv) the observation of a blue shift[2,5] during the growth of triplet state absorption spectra has been contradicted[3] raising the question of vibrational relaxation engagement in the $S_1 \rightarrow T_1$ transition.

The photophysical issue discussed in this article is related to the fact that the very fast ISC process observed for the BP $S_1(n,\pi^*)$ state is in contradiction with the El-Sayed rules, predicting a slow process for the forbidden n,π^*-n,π^* transition. In fact, controversy still exists regarding the exact photophysical mechanism of the S_1 state relaxation process. On one hand, some explanations rely on the participation of the $T_2(\pi,\pi^*)$ state ensuring $S_1(n,\pi^*) \rightarrow T_2(\pi,\pi^*)$ ISC then followed by an ultrafast $T_2(\pi,\pi^*)-T_1(n,\pi^*)$ internal conversion (IC).[8] Very recently, this photophysical scheme was confirmed by Yabumoto et al. through their observation of the T_1-T_2 absorption band detected by time-resolved infrared absorption experiments.[9] On the other hand, low field Zeeman experiments performed at very low temperatures have totally ruled out the participation of a triplet intermediate during ISC of BP strongly suggesting a direct $S_1(n,\pi^*) \rightarrow T_1(n,\pi^*)$ mechanism.[10] Furthermore, optically detected magnetic resonance (ODMR) and related experiments have given evidence of $(n,\pi^*-\pi,\pi^*)$ configuration mixing for the lowest triplet state, which allows direct ISC to occur.[11] To further discuss the controversy, new subpicosecond time-resolved absorption experiments combined with advanced multivariate curve resolution for data analysis are attempted to investigate the BP photophysics relaxation of the $S_1(n,\pi^*)$ state.

In numerous chemical fields, multivariate curve resolution—alternating least squares (MCR-ALS)[12,13] is becoming the standard chemometric method to resolve multicomponent evolving systems into pure contributions. Some convincing results have been obtained in the field of time-resolved spectroscopy,[14,15] but to our knowledge spectral and temporal characterizations of ultrafast transient species was only attempted very recently.[16] Multivariate curve resolution aims to perform decomposition of kinetic data matrix D (i.e., a set of individual spectra probed at different time delays, $\{\Delta OD(t,\lambda)\}$) into pure spectra of overlapping transient species and their associated time-dependent concentrations, without specifying any phe-

* Corresponding author. E-mail: stephane.aloise@univ-lille1.fr.

10.1021/jp075829f CCC: $40.75 © 2008 American Chemical Society
Published on Web 12/22/2007

© 2016 Tous droits réservés.

doc.univ-lille1.fr

HDR de Stéphane Aloïse, Lille 1, 2016

nomenological model. More precisely, only the assumption of a bilinear decomposition of the data set into additive contributions of concentration and spectra is underlying. The originality with regard to global analysis[17] and target data analysis[18] relying on the same mathematical decomposition is that the proposed method is basically soft-modeling. Indeed, only initial estimation of the concentration profiles or spectra are to be input in MCR-ALS, which thus do require the number of significant contributions to the signal (the rank of *D*) to be estimated using singular value decomposition (SVD).[20] But bilinear decomposition of *D* must be constrained in order to limit rotational ambiguities.[12] Basically, soft-modeling constraints[12,21] are nonparametric information, e.g., non-negativity of the concentration profiles and spectra, that are implemented during the ALS optimization to focus on chemically meaningful data decomposition. Multivariate curve resolution enables one to decompose the phenomena describing the measured data, but the interpretation of the results should be done with caution, as in the other more conventional data analysis.[19] When a kinetic model is suspected, a step forward is the consideration of kinetic constraints[22] implemented on the concentration profiles in the ALS algorithm. An advantage from the photophysical point of view is that the rate constants[22,23] of the model implemented can be obtained as additional information. From the point of view of chemometrics, this so-called hard−soft multivariate curve resolution (HS-MCR) provides solutions with very small ambiguity. In particular, when combined with the application of soft-modeling non-negative constraints to the pure spectra, the slow−fast ambiguity associated with several model fits of successive first-order reactions can be accounted for.

The present paper aims at gaining a better understanding of the $S_1 \rightarrow T_1$ photophysical process for the BP molecule through multivariate curve resolution of subpicosecond time-resolved absorption data for various solvents and excitation wavelengths. The results obtained are compared with similar spectroscopic data acquired for 4-methoxybenzophenone (4-MeOBP). Indeed, for the latter compound, Boscà et al. have demonstrated recently a T_1-T_2 triplet state inversion induced by the solvent polarity,[24] allowing different El-Sayed schemes to be tested including the one for BP.

2. Experimental Methods

2.1. Experimental. The pump−probe subsubpicosecond absorption experiments were carried out using an amplified Ti:sapphire laser (BM Industries) delivering 0.8 mJ and 80 fs pulses tunable between 766 nm and 800 nm with a repetition rate of 1 kHz. The 383 nm pump pulses were obtained by frequency doubling the fundamental at 766 nm while the 267 nm pump pulses were obtained by frequency tripling the fundamental at 800 nm. Energies higher than 20 μJ were provided in both cases. The probe beam was generated by focusing 1 μJ of the fundamental on a 1 mm CaF_2 plate giving a white light continuum with a spectrum covering the UV−vis and near IR range. The probe beam was split into signal and reference beams before crossing the sample, and the resulting beams were recorded on 2 different channels of a multichannel spectrograph equipped with a CCD camera. Transient absorbance was obtained by comparing signal and reference spectra for different time delays. The time delay between the pump and probe was varied up to 1.5 ns (using a micrometric optical delay line), and the temporal resolution of the apparatus was better than 300 fs. Pump and probe beams, with relative linear polarizations set at the magic angle, were focused in a 2 mm flow cell equipped with CaF_2 windows. Typical sample concentrations used were 5×10^{-4} M for 267 nm excitation and 0.2 M for 383 nm excitations. The following Sigma-Aldrich products were used: benzophenone, 4-methoxybenzophenone, acetonitrile (ACN), methanol (MeOH), dichloromethane (CH_2Cl_2) and cyclohexane (CH). All solvents (spectroscopic grade) were used without further purification.

2.2. Data Analysis. The basic mathematical model is a bilinear decomposition of the data matrix **D** according to eq 1, in matrix notation. The matrix **D** (with elements d_{ij}) contains *i*

$$\mathbf{D} = \mathbf{C}\mathbf{S}^{\mathbf{T}} + \mathbf{E} \tag{1}$$

spectra recorded at *i* successive delay times and *j* wavelengths. The matrix **C** (elements c_{jk}) contains the resolved concentration profiles (*i* time points) of the *k* components contributing to **D**. The matrix $\mathbf{S}^{\mathbf{T}}$ (elements s_{kj}) contains the corresponding *k* pure spectra. The matrix **E** (elements e_{ij}) contains the residuals of the decomposition. MCR-ALS can be used to solve the bilinear model eq 1, i.e., to extract **C** and $\mathbf{S}^{\mathbf{T}}$ from **D**. The striking aspects of the methodology (applied to time-resolved spectroscopic data) are given below.

Singular Value Decomposition and Related Methods. In any data analysis strategy,[12,18] the first point is to estimate the number of components (transient species) composing the observable **D**. This is usually performed analyzing the chemical rank of **D** using SVD[25] and determining the number of significant singular values. In practice, different kinds of difficulties may appear. The most common one is to settle correctly the threshold that separates chemical contribution from noise in the SVD. Moreover, strong overlapping of the concentration profiles and high intrinsic collinearity of the spectra may blur the situation. However, when two-way data matrices are studied as in time-resolved spectroscopy, advantage can be taken from evolving factor analysis methods such as the so-called evolving factor analysis (EFA).[26] This procedure, instead of calculating SVD or principal component analysis[20] (PCA) of the full data matrix, performs successive analysis on gradually increasing submatrices in the time direction, adding a row at a time from the top of the matrix to the bottom (forward EFA). The emergence and evolution of the singular values can thus be followed individually with increasing time. The same approach is performed from bottom to top (backward EFA). In this case, the emergence and evolution of the singular values can be followed in reverse sequence, i.e., their disappearance can be observed with increasing time. Under the assumption that the evolving system studied is sequential, i.e., the first compound to appear is also the first to disappear, estimation of the profiles **C** can be provided combining the forward and backward traces. It can then be input as initial solution in the MCR-ALS procedure.

Multivariate Curve Resolution−Alternating Least Squares. An alternating least squares (ALS) algorithm is used to fit iteratively the **C** and $\mathbf{S}^{\mathbf{T}}$ matrices to the experimental data **D**. The residuals are obtained computing the difference between the data **D** and the reproduced data $\mathbf{CS}^{\mathbf{T}}$. At each iterative cycle of the optimization, matrices **C** and $\mathbf{S}^{\mathbf{T}}$ are calculated under constraints minimizing the reproduction error, **E**. The lack of fit (eq 2) can be used as global estimator of the fitting error of the experimental data.

© 2016 Tous droits réservés.

doc.univ-lille1.fr

HDR de Stéphane Aloïse, Lille 1, 2016

$$\text{lof}\,(\%) = 100\sqrt{\frac{\sum_{i,j} e_{i,j}}{\sum_{i,j} d_{i,j}}} \qquad (2)$$

The full MCR-ALS procedure can be cast as follows: (1) determination of the number of components contributing to **D**; (2) construction of initial estimates of concentration profiles **C** using chemical insight or chemometric methods such as EFA; (3) given **D** and **C**, least-squares calculation of $\mathbf{S^T}$ under suitable constraints; (4) given **D** and $\mathbf{S^T}$, least-squares calculation of **C** under suitable constraints; (5) reproduction of **D** using **C** and $\mathbf{S^T}$. Check if the convergence criterion is fulfilled. If not, go back to step 3.

As there is no phenomenological (kinetic) model imposed in the decomposition, multivariate curve resolution is affected by rotational ambiguities, i.e., the possibilities to reproduce the original data sets with the same precision using **C** and $\mathbf{S^T}$ matrices that contain linear combinations of the signals of the pure components. The set of possible solutions can be restricted through the implementation of soft-modeling constraints[12,21] (steps 3 and 4), such as non-negativity, unimodality (single peak) or closure (mass balance). Additionally, such constraints ensure that the computed solutions are chemically meaningful.

Hard−Soft Multivariate Curve Resolution−Alternating Least Squares. Hard−soft Multivariate Curve Resolution (HS-MCR) is an evolution of soft-modeling MCR-ALS including hard-modeling constraint[22,23] that can be very useful in the analysis of time-resolved spectroscopy data sets. The optimization starts with the profiles obtained from a soft-modeling MCR-ALS resolution. These profiles are used as input of the HS-MCR algorithm. Then, a kinetic model can be incorporated by means of a hard-modeling kinetic constraint which is applied on the matrix of concentration profiles (step 4 of the MCR-ALS algorithm presented above). Inside each loop of the ALS procedure, the columns of **C** are fitted to the model and the resulting profiles are used to calculate the spectra $\mathbf{S^T}$, deriving advantage from soft-modeling resolution as well. The reliability of the soft modeling solutions[27] can then be discussed, and time constants can be estimated. The confidence intervals calculated with the standard deviations of the fitted parameters are given for information only as they can be seriously underestimated (due to cross-correlations between the parameters).[28] More generally, with regard to classical hard-modeling, HS-MCR has been shown to be much more flexible[22,23] as the columns of **C** can be constrained one independently of the others making it possible to handle interferents for example.

All the calculations have been performed using MATLAB 6.5 and 7.0 (R14) (The Matworks Ltd, Massachusetts). The interface of MCR-ALS is freely available at www.ub.es/gesq/mcr/mcr.htm.

3. Results and Discussion

In the following, subpicosecond time-resolved absorption data of BP obtained for various solvents and excitation wavelengths will be presented. The time-resolved spectra are first analyzed in a conventional way, fitting kinetic traces by monoexponential function at chosen wavelengths (section 3.1). The multivariate curve resolution analyses of the experimental data sets are then performed. The results obtained from both MCR-ALS and HS-MCR are discussed (section 3.2). In order to obtain a chemical validation of the results obtained for BP, a similar approach is applied to 4-MeOBP. Indeed, the neighboring photophysics of this compound is solvent-dependent and can thus be controlled. Finally, the S_1 state photophysics of BP is discussed in light of the new results obtained (section 3.3).

3.1. Conventional Interpretation of Time-Resolved Spectra. The raw (no smoothing applied) transient absorption spectra of BP compound in acetonitrile (0.2 M) at 383 nm excitation recorded in the 420−680 nm spectral range and in the 0.8−100 ps time window are shown in Figure 1. The first short delay times spectrum characterizes the $S_1(n,\pi^*)$ visible spectrum of BP peaking at $\lambda_{max} = 570$ nm (see 0.8 ps trace), as reported elsewhere.[4] It then decreases while the well-known $T_1(n,\pi^*)$ absorption spectrum peaking at $\lambda_{max} = 525$ nm increases. On one hand, the $S_1(n,\pi^*)$ characteristic time can be estimated (monoexponential fitting) at 570 nm to (17 ± 1) ps (see inset). On the other hand, fitting the kinetic growth at 525 nm returns the value (9.4 ± 0.3) ps, in agreement with other studies,[7] but it gives no evidence of a direct S_1-T_1 transition. When the experiment is repeated changing the solvent, the $T_1(n,\pi^*)$ state characteristic growing time is estimated at 525 nm to be (11.6 ± 0.3) ps for MeOH and (11.8 ± 0.3) ps for CH_2Cl_2. This confirms that the apparent ISC process is neither very sensitive to hydrogen bonding ability nor to solvent polarity, as previously reported.[1−5]

The transient absorption spectra of BP obtained for 267 nm excitation in the case of acetonitrile (5×10^{-4} M) are displayed in Figure 2 for a wider spectral range (320−680 nm). The 0.8−1.7 ps time delay (see inset) shows the fast growth of the $S_1(n,\pi^*)$ spectra at 570 nm following the $S_2(n,\pi^*) \rightarrow S_1(n,\pi^*)$ IC process in accordance with the S_2 lifetime of 0.53 ps[7] measured by Shah et al. (in the following, only time delays greater than 2 ps will be considered in order to get rid of the S_2 state contribution). Besides the appearance of the triplet spectra with a characteristic time of (10.9 ± 0.3) ps, the blue band of $S_1(n,\pi^*)$ spectra peaking at 330 nm is observed to be decreasing with a decay time of (10.2 ± 0.5) ps. So, if one considers only these two bands at 330 and 525 nm wavelengths, and ignores the observations just made above, a direct $S_1 \rightarrow T_1$ transition can be assumed for the 267 nm excitation case.

Another important issue concerns the blue shift during the growth of the triplet absorption band around 525 nm. Unlike Hamanoue et al.,[3] a slight shift is observed for 383 nm excitation which is clearly more pronounced for 267 nm excitation. This spectral effect has been previously interpreted in terms of vibrational relaxation of the triplet state.[2] More recently, it has been proposed that the decay of the singlet (band at 570 nm) and the growth of the triplet appear as a blue shift in the observed spectra.[4] One of the advantages using MCR-ALS is to improve the rationalization of such a weak spectral effect.

3.2. Multivariate Curve Resolution of Time-Resolved Spectra. Multivariate curve resolution of the data matrix corresponding to BP transient absorption spectra at 267 nm excitation is presented first. SVD and EFA are performed to estimate the number of significant contributions to consider for the description of the S_1 state relaxation mechanism. The EFA results are displayed in Figure 3. The plot represents the PCA eigenvalues (in log units) as a function of the position of the considered row in the data matrix (row number), which corresponds to time direction. As an example four eigenvalues are calculated at 4 ps since a 4-row submatrix is considered (see forward EFA full-lines). Moreover, if row number 21 is considered (conversely, row number 2 in backward analysis, see dotted lines) the calculated values correspond to PCA or SVD (it is reminded here that eigenvalues are scarred singular

© 2016 Tous droits réservés.

doc.univ-lille1.fr

HDR de Stéphane Aloïse, Lille 1, 2016

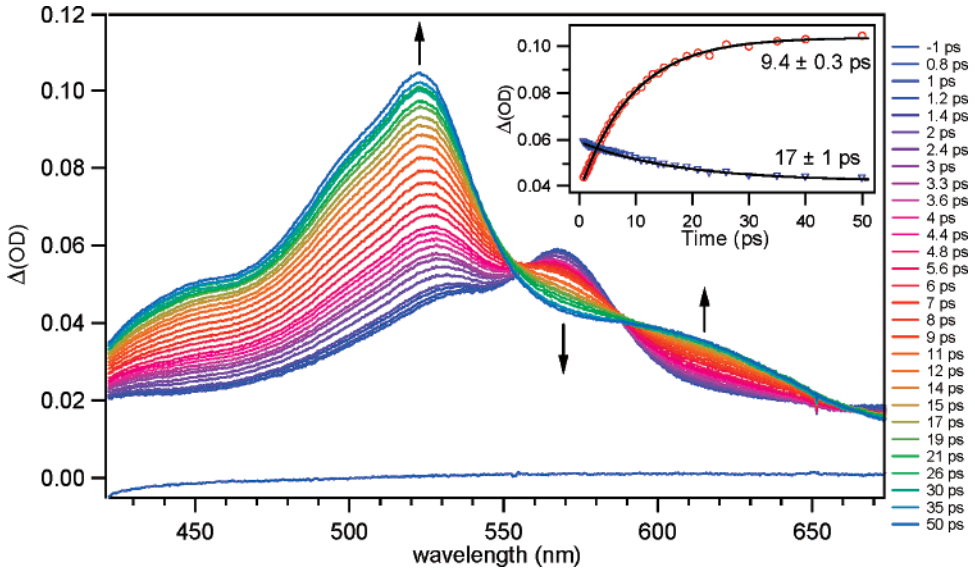

Figure 1. Subpicosecond time-resolved absorption spectra of BP in ACN for 383 nm excitation in the 0.8−50 ps temporal window. The time evolution is shown by arrows. The inset displays the kinetic traces and monoexponential fit at 525 nm (red circles) and 570 nm (blue inverted triangles).

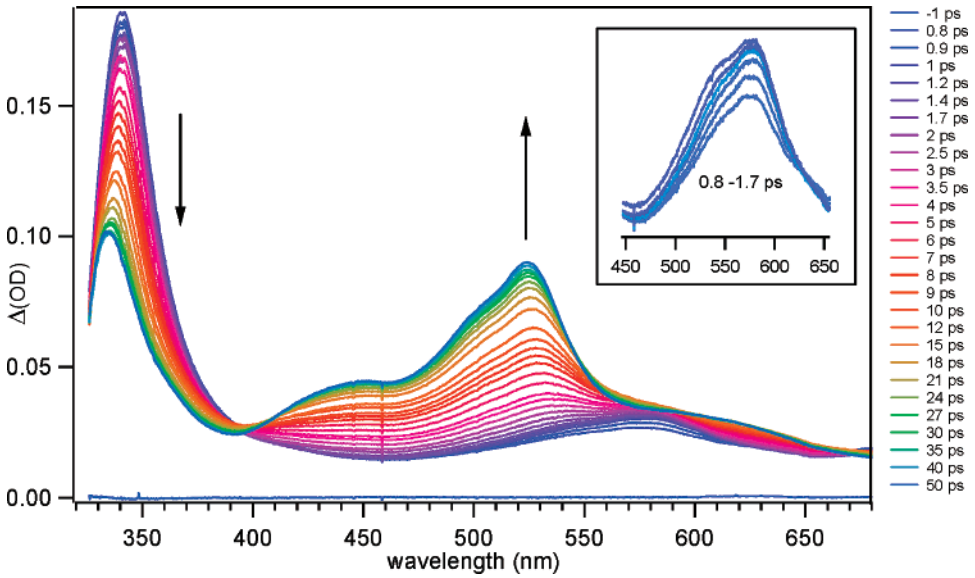

Figure 2. Subpicosecond time-resolved absorption spectra of BP in ACN for 267 nm excitation in the 0.8−50 ps temporal window. The time evolution is shown by arrows. The inset is a zoom of the 450−650 nm regions for the indicated time window.

values) of the full data matrix. A threshold separating minor contributions can be set at ∼−3.4 (in log units), and three contributions are thus found significant. Besides, EFA provides more information as it takes into account the intrinsic temporal evolution of the data matrix. In forward direction, it can then be observed that the second contribution emerges very quickly (<2.5 ps) whereas as the third is significant after ∼10 ps. This third forward trace is a reasonable initial estimate of the kinetic profile of the third contribution involved in the process analyzed. In backward direction, the same analysis returns, for example, the third profile is significantly present only before ∼12 ps and it provides an initial estimate of the profile corresponding to the first contribution (i.e., its disappearance). Finally, combining the second forward and backward traces, an initial estimate of the evolution of an intermediate contribution is observed.

The results of soft-modeling MCR-ALS analysis based on initial estimate from EFA are now discussed. The constraints implemented during the ALS optimization are non-negativity of the concentration profiles and spectra and unimodality of the concentration profiles. The results obtained for BP spectra at 267 nm excitation are given in Figure 4a and 4b for the pure spectra ($\mathbf{S}^T$) and the corresponding time-dependent concentration ($\mathbf{C}$), respectively. First, the initial $S_1(n,\pi^*)$ spectra (in blue; λ_{max}∼330 and ∼570 nm) and the final $T_1(n,\pi^*)$ spectra (in red; λ_{max}∼325 and ∼525 nm) are unambiguously recognized. Meanwhile, the corresponding concentration profiles are found relevant since the disappearance of $S_1(n,\pi^*)$ (blue circles) is concomitant with the appearance of $T_1(n,\pi^*)$ (red squares). Apart from these two species, an intermediate contribution is resolved, which is denoted by IS in the following. The corresponding spectrum (in green in Figure 4a) peaks in the visible region at higher wavelength compared to $T_1(n,\pi^*)$, i.e., $\Delta\lambda_{max}(IS-T_1) = 13$ nm. Similar comparison with the $S_1(n,\pi^*)$ spectrum gives $\Delta\lambda_{max}(S_1-IS) = 41$ nm. Both the values are reported in Table 1. The corresponding time-dependent concentration profile (green triangles in Figure 4b) is found to be in agreement with the EFA results. This resolution introduces the implication of a direct intermediate species in the $S_1(n,\pi^*)$

© 2016 Tous droits réservés.

doc.univ-lille1.fr

HDR de Stéphane Aloïse, Lille 1, 2016

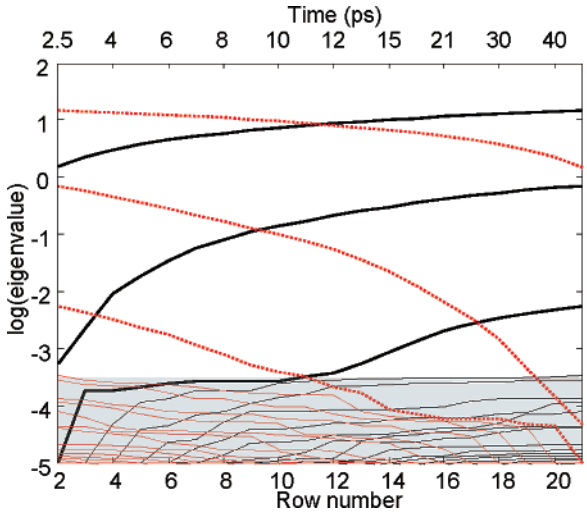

Figure 3. Evolving factor analysis (EFA) for subpicosecond time-resolved absorption data of BP (267 nm excitation; see Figure 2); results of forward (solid lines) and backward (dashed lines) EFA; eigenvalues (in log units) are plotted as a function of the row number of the data matrix and corresponding time (the shadowed region is set to figure out significant contributions).

$\rightarrow$ $T_1(n,\pi^*)$ transition. To support this result, the HS-MCR procedure is then performed. In addition to the non-negativity constraints applied to the pure spectra as mentioned previously, a kinetic constraint which describes the sequential two step kinetic model proposed in eq 3 is considered. The results are

$$S_1(n,\pi^*) \rightarrow IS \rightarrow T_1(n,\pi^*) \quad (3)$$

plotted in Figure 4a,b (black lines) for spectral and time-dependent concentration profiles, respectively. Excellent agreement is found with previous MCR-ALS results. The reliability of the two step kinetic scheme implemented is demonstrated for BP time-resolved absorption spectra (267 nm excitation), at least from a mathematical point of view. The rate constants for the $S_1 \rightarrow$ IS process, denoted by k_1, is (0.154 ± 0.002) ps^{-1} and for the IS $\rightarrow$ T_1 process, denoted by k_2, is (0.093 ± 0.001) ps^{-1}. These values (reported in Table 1) will be discussed in section 3.3. It should be noticed that the application of soft-modeling non-negativity constraint to the spectra enables one to avoid the slow−fast ambiguity (also known as flip-flop phenomenon, such an effect is observed when the rate constants describing a multistep reaction scheme can be interchanged giving an equivalent solution for the fitting). Indeed, this can be verified by checking that the solution obtained is maintained when the model is refit with the constraint turned off.[29]

The same procedure is repeated for BP at 383 nm excitation, and the results are displayed in Figure 4c,d for $\mathbf{S^T}$ and $\mathbf{C}$, respectively. First, comparing the $\Delta\lambda_{max}$ calculated with the previous ones (see Table 1), a comparable value for S_1-IS (40 nm) is obtained while a factor of about 2 is noticed for $IS-T_1$ (5 vs 13 nm). On the other hand, the concentration profiles obtained from soft-modeling MCR-ALS and from HS-MCR under the constraint eq 3 are found consistent despite slight differences (the resolution is more challenging as the wavelength domain is narrowed). Finally, the values obtained for k_1, (0.133 ± 0.002) ps^{-1}, and k_2, (0.099 ± 0.001) ps^{-1} (Table 1), are in good agreement with the previous case.

3.3. The Benzophenone $S_1 \rightarrow T_1$ ISC Process. At this point, whether the intermediate species (IS) is a true spectroscopic state or not has to be discussed. What is its chemical relevance, and to what extent might vibrational relaxation of S_1 or T_1 states contribute[2−6] to the MCR-ALS spectra of IS? Before beginning such a discussion, it is important to remember that IS is recovered under the assumption of a bilinear decomposition of the data (see eq 1). It means that significant collective processes such as pure vibrational effect or excited-state solvation (inducing spectral band shift, see for example ref 30) can hardly be included in a 3 component resolution. In any case, among these two types of processes, the solvation effects have never been reported for BP.

The first striking aspect of IS is that its full spectrum is very similar but broader compared to the T_1 state spectrum. In light of this argument, there are two possible explanations concerning the chemical relevancy of IS: (i) IS is a mathematical artifact induced by pure vibrational relaxation during a direct ISC from S_1 to T_1 states (one electronic transition); (ii) the IS species is related to one or several vibrational states in the $T_1(n,\pi^*)$ manifold, i.e., IS is a hot triplet state that is involved in a two step mechanism (two electronic transition). We do not believe that we can give a final answer to this dilemma, but we want to insist on the good agreement between the soft-modeling results (without any model prerequisites) and the ones constrained to follow a two step sequential model. In our opinion, such an agreement would not be obtained in case the blue shift observed during growth of T_1 was due to pure vibrational effect alone.[2,5]

Furthermore, another meaningful result is the discovery of an excitation wavelength effect (see Table 1): $\Delta\lambda_{max}(IS-T_1)$ is more than two times larger comparing the 383 nm and 267 nm excitation cases (for ACN solvent). This difference stands for the fact that the S_1 state is populated near the $\upsilon = 0$ threshold for 383 nm excitation while numerous vibrational states can be populated by 267 nm excitation through the S_2-S_1 IC process. In terms of vibronic coupling, one explanation would be that some high vibrational levels in the S_1 manifold are in effective interaction with the triplet state vibrational levels. It is to be noted that the proposition of ISC that occurs for unrelaxed singlets has been already proposed by Sun et al. in the past.[31]

Let us assume now that the characterized intermediate species is chemically relevant. Can it be related to the $T_2(\pi,\pi^*)$ state, as already proposed in the litterature?[8,9] Among unsuccessful experimental attempts to locate directly the $T_2(\pi,\pi^*)$ state,[32] the dual phosphorescence of BP in polar solvent is one of the most striking pieces of evidence of the simultaneous population of both (n,π^*) and (π,π^*) triplet states[33] allowing one to presume about some participation of the $T_2(\pi,\pi^*)$ state in the photophysics of singlet states. As we will see, the study of 4-MeOBP in CH, ACN and ACN/water (1:3) solvent by ultrafast absorption spectroscopy coupled with multivariate curve resolution analysis will help to bring some insights about this issue. Indeed, as Boscà et al.[24] demonstrated recently (with laser flash photolysis and phosphorescence measurements), the 4-MeOBP possesses the property to get the $T_2(\pi,\pi^*)-T_1(n,\pi^*)$ relative position varying with solvent polarity allowing different El-Sayed scheme to be probed. More precisely, for CH solvent, the (π,π^*) triplet state is well higher than the (n,π^*) triplet state, while for ACN, the gap between the two states is less than 8 $kJ\cdot mol^{-1}$ allowing vibronic coupling to occur. For solvents with the higher polarity, the triplet ordering is switched to the opposite situation and the lowest triplet state possesses then (π,π^*) character.[24] The subpicosecond absorption spectra obtained for 4-MeOBP in the three solvents and the corresponding MCR-ALS decompositions are presented all together in Figure 5. Note that HS-MCR analysis has not been performed because additional charge-transfer deactivation of the S_1 singlet excited state prevents the application of a simple kinetic mechanism.[34]

© 2016 Tous droits réservés.

doc.univ-lille1.fr

HDR de Stéphane Aloïse, Lille 1, 2016

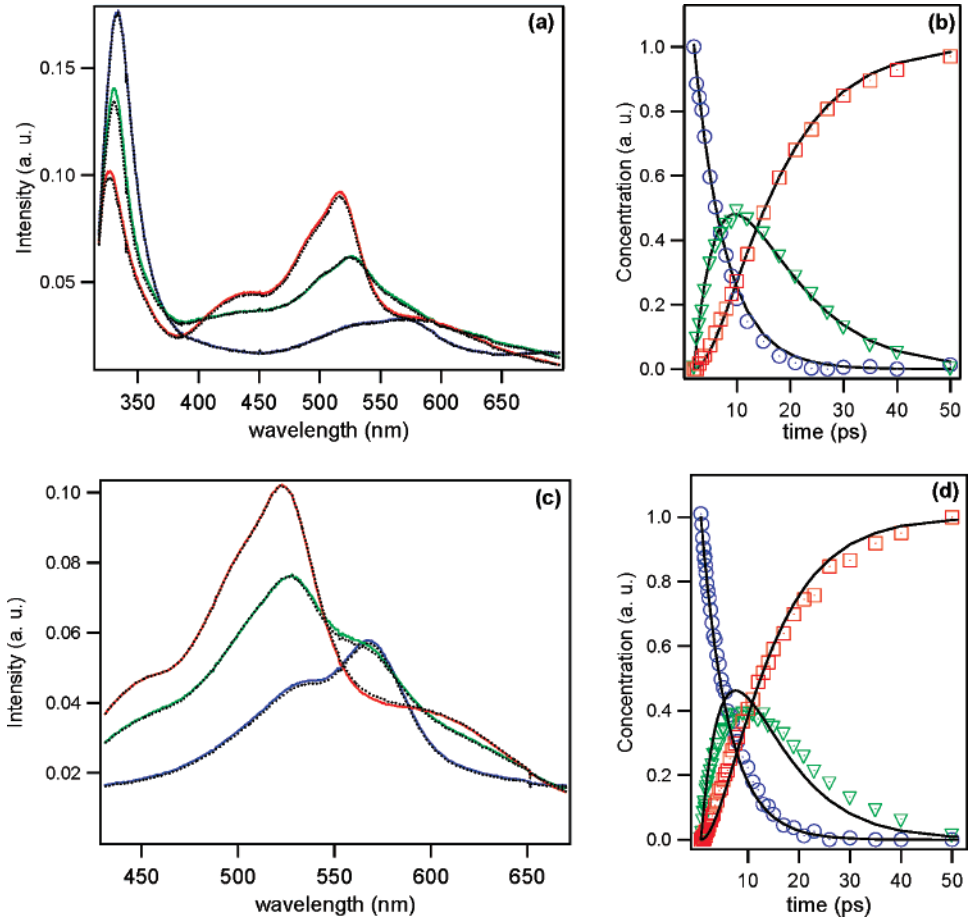

Figure 4. Spectra and time-dependent concentrations obtained from MCR-ALS (colored lines and markers, respectively) and from HS-MCR (black lines in both cases) analysis of subpicosecond time-resolved absorption data of BP excited at 267 nm, (a) and (b); and 383 nm, (c) and (d) in ACN. The color code is the following: blue for S_1; green for IS; red for T_1.

TABLE 1: Spectrokinetic Properties Obtained from HS-MCR Analysis of Subpicosecond Time-Resolved Spectra of BP for Different Solvents and Excitation Wavelengths

		$\Delta\lambda_{max}$ (nm)				
solvent	λ_{exc} (nm)	S_1-IS	$IS-T_1$	$S_1 \rightarrow IS$ k_1 (ps^{-1})[a]	$IS \rightarrow T_1$ k_2 (ps^{-1})[a]	lof (%)
ACN	267	41	13	0.154(2)	0.093(1)	0.59
ACN	383	40	5	0.133(2)	0.099(1)	0.92
MeOH	383	42	3	0.167(4)	0.117(3)	1.21
CH_2Cl_2	383	41	4	0.146(3)	0.103(3)	0.70

[a] Uncertainty estimations are given in parentheses (see ref 28 for more details).

For CH solvent, one observes the growth of the $T_1(n,\pi^*)$ triplet spectrum around 525 nm (Figure 5a) concomitant with the S_1-(n,π^*) spectrum disappearance at 340 nm. For ACN (Figure 5b), an additional shoulder peaking near 440 nm is clearly observed while for ACN:water (1:3) only the $T_1(\pi,\pi^*)$ triplet growth peaking at 440 nm is observed. All these results are in good agreement with the laser-flash photolysis spectra of Boscà et al. (see Figure 3 of ref 24). The inspection of the spectra and time-dependent concentration profiles obtained from multivariate curve resolution are proposed in Figure 5d−f. For the two cases where the (π,π^*) triplet is the highest state, three transient species are extracted (Figure 5d and 5e) with meaningful kinetics (see the insets). On the contrary, when the (π,π^*) triplet is the lower one, opening the possibility of a direct $S_1(n,\pi^*) \rightarrow T_1$-$(\pi,\pi^*)$ ISC process allowed by El-Sayed rules, only two species are found significant in the EFA procedure and the corresponding MCR-ALS resolution is given in Figure 5f. This solution is very reliable, and attempts to force a 3-species resolution lead to meaningless results. So, on one hand, a clear correlation between the intermediate and the higher T_2 triplet state relative to T_1 can be established for 4-MeOBP. On the other hand, the similitude between the two IS spectra for BP (whatever the solvent) and 4-MeOBP in CH are particularly striking knowing that these two compounds have a quite similar energy ordering of the S_1, T_2 and T_1 states.[8,24] This last point makes an analogy between the two molecules reasonable, allowing one to assume that for BP the probable intermediate species during the ISC of $S_1(n,\pi^*)$ is also correlated with the presence of the $T_2(\pi,\pi^*)$ state above the final $T_1(n,\pi^*)$ triplet.

In fact, the two attempts performed in this section in order to assign IS are not exclusive: IS could be a hot $T_1(n,\pi^*)$ triplet state in strong vibronic interaction with the $T_2(\pi,\pi^*)$ state. The more pronounced (π,π^*) character for the high vibrational levels of T_1 states, by comparison with the ones near the vibrational threshold, would be conferred through the proximity of the two triplet states. This point is important in order to make the El-Sayed rules respected.

Within the indirect mechanism hypothesis for the S_1 state photophysics, i.e., IS is chemically relevant and attributed to be a mixture between hot $T_1(n,\pi^*)$ and $T_2(\pi,\pi^*)$ state, it becomes instructive to analyze the characteristic times (ignoring minor competitive processes, $\tau \approx 1/k$) given by the HS-MCR procedure. The S_1-IS and $IS-T_1$ transitions are characterized by mean times of ~6.5 ps and ~10 ps, respectively, irrespective of the solvent or excitation wavelength (see Table 1). The former time can be easily assigned to an ISC from $S_1(n,\pi^*)$ to IS which

© 2016 Tous droits réservés.

doc.univ-lille1.fr

HDR de Stéphane Aloïse, Lille 1, 2016

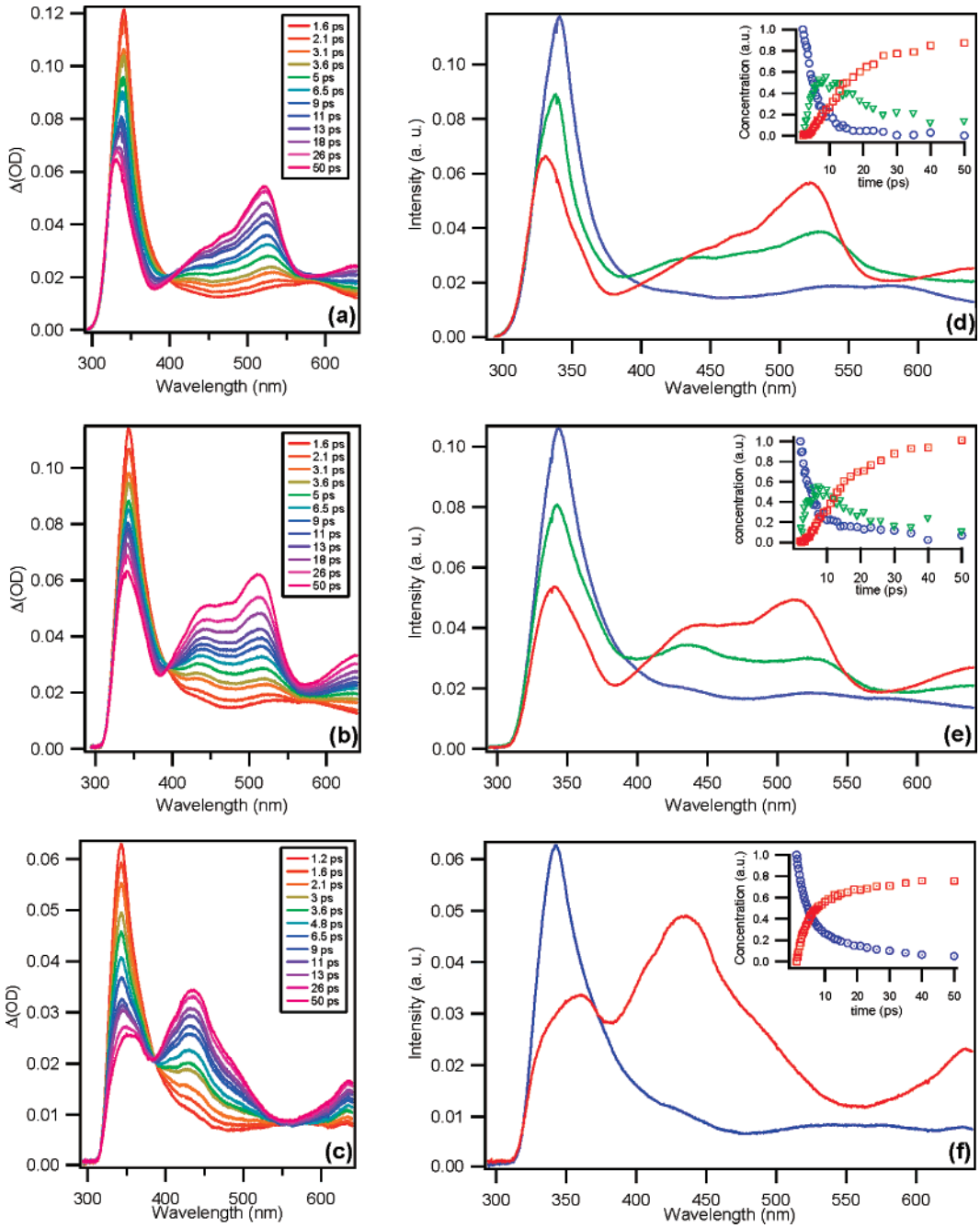

Figure 5. Subpicosecond time-resolved absorption data of 4-MeOBP excited at: 267 nm in CH (a), in ACN (b) and ACN/water 1:3 (c); respective spectra, (d), (e) and (f), obtained by MCR-ALS. The insets contain the time-dependent concentrations (same color code as for Figure 4).

is in the triplet manifold in all the considered situations. Considering the second transition like an IC from IS to the fully relaxed $T_1(n,\pi^*)$, much care has to be taken because of few published values in the literature for $T_2 \rightarrow T_1$ transition.[8] Due to the small gap between T_1 and T_2 states, $\sim$2000 cm^{-1} as recently measured,[9] a 10 ps lifetime of the IS state appears overestimated.

In conclusion, the exact interaction of the $T_2(\pi,\pi^*)$ state with both the $T_1(n,\pi^*)$ triplet and the $S_1(n,\pi^*)$ singlet on the full relaxation mechanism of the latter is probably one of the key points to answer the controversy studied in this paper. In this sense, a recent advanced CASSCF calculation on carbonyl compounds has revealed the existence of a $S_1/T_1/T_2$ surface intersection that may play a crucial role in the relaxation dynamics upon photoexcitation,[35] but it is not clear whether this can possibly be related to a detectable intermediate species during the relaxation mechanism of the S_1 state of BP or not. New experimental and theoretical efforts are required to definitively answer this question and some of those raised in this paper.

Acknowledgment. The authors acknowledge Prof. A. de Juan from the Department of Analytical Chemistry of the Universitat de Barcelona for making available the modification of the MATLAB code for the implementation of hard-modeling constraint in MCR-ALS. The authors are grateful to B. N. Shivakiran Bhaktha for help with the revision of the English version. L.B. acknowledges a PhD scholarship from the Ministère délégué à l'Enseignement supérieur et à la Recherche, France. The authors thank the Groupement de Recherche GDR 2466 from CNRS and the Centre d'études et de Recherches Lasers et Applications (CERLA) for their help in the development of this work. CERLA is supported by the Ministère chargé

© 2016 Tous droits réservés.

doc.univ-lille1.fr

HDR de Stéphane Aloïse, Lille 1, 2016

de la Recherche, Région Nord/Pas de Calais, and the Fonds Européen de Développement Economique des Régions.

References and Notes

(1) (a) Hochstrasser, R. M.; Lutz, H.; Scott, G. W. *Chem. Phys. Lett.* **1974**, *24*, 162. (b) Anderson, R. W.; Hochstrasser, R. M.; Scott, G. W. *Chem. Phys. Lett.* **1974**, *28*, 153. (c) Damschen, D. E.; Merritt, C. D.; Perry, D. L.; Scott, G. W.; Talley, L. D. *J. Chem. Phys.* **1978**, *82*, 2268.

(2) Greene, B. I.; Hochstrasser, R. M.; Weisman, R. B. *J. Chem. Phys.* **1979**, *70*, 1247.

(3) Hamanoue, K.; Nakajima, K.; Hidaka, T.; Nakayama, T.; Teranishi, H. *Laser Chem.* **1984**, *4*, 287.

(4) Miyasaka, H.; Morita, K.; Kamada, K.; Mataga, N. *Bull. Chem. Soc. Jpn.* **1990**, *63*, 3385.

(5) McGarry, P. F.; Doubleday, C. E., Jr.; Wu, C-H.; Staab, H. A.; Turro, N. J. *J. Photochem. Photobiol. A* **1994**, *77*, 109.

(6) Prater, K.; Freund, W. L.; Bowman, R. M. *Chem. Phys. Lett.* **1998**, *295*, 82.

(7) Shah, B. K.; Rodgers, M. A. J.; Neckers, D. C. *J. Phys. Chem. A* **2004**, *108*, 6087.

(8) Turro, N. J. *Modern Molecular Photochemistry*; The Benjamin/Cummings Publishing Company: 1978.

(9) Yabumoto, S.; Sato, S.; Hamaguchi, H. *Chem. Phys. Lett.* **2005**, *100*, 416.

(10) El-Sayed, M. A.; Leyerle, R. *J. Chem. Phys.* **1975**, *62*, 1579.

(11) Wäckerle, G.; Bär, M.; Zimmermann, H.; Dinse, K.-P.; Yamauchi, S.; Kashmar, R. J.; Pratt, D. W. *J. Chem. Phys.* **1982**, *76*, 2275.

(12) Tauler, R. *Chemom. Intell. Lab. Syst.* **1995**, *30*, 133.

(13) Navea, S.; de Juan, A.; Tauler, R. *Anal. Chem.* **2003**, *75*, 5592.

(14) Ruckebusch, C.; Duponchel, L.; Sombret, B.; Huvenne, J. P.; Saurina, J. *J. Chem. Inf. Comput. Sci.* **2003**, *43*, 1966.

(15) Blanchet, L.; Mezzetti, A.; Ruckebusch, C.; Huvenne, J. P.; de Juan, A. *Anal. Bioanal. Chem.* **2007**, *387*, 1863.

(16) Von Frese, J.; Kovalenko, S. A.; Ernsting, N. P. *J. Chemom.* **2007**, *21*, 2.

(17) Zhang, L.; Quan, D.; Wang, L.; Yang, G.; Weng, Y. *Sci. China G* **2004**, *47*, 208.

(18) (a)Van Stokkum, I. H. M.; Scherer, T.; Brouwer, A. M.; Verhoeven, J. W. *J. Phys. Chem.* **1994**, *98*, 852. (b) Vengris, M.; Van Stokkum, I. H. M.; He, X.; Bell, A. F.; Tongue, P. J.; Van Grondelle, R.; Larsen, D. S. *J. Phys. Chem. A* **2004**, *108*, 4587.

(19) Plaza, P.; Mahet, M.; Martin, M. M.; Checcucci, G.; Lenci, F. *J. Phys. Chem. B* **2004**, *108*, 6087.

(20) Malinowski, E. R. *Factor Analysis in Chemistry*, 2nd ed.;Wiley-Interscience: New York, 1992.

(21) De Juan, A.; Casassas, E.; Tauler, R. In *Encyclopedia of Analytical Chemistry*; Meyers, R. A., Ed.; John Wiley and Sons Ltd: Chichester, 2000; p 9800.

(22) De Juan, A.; Maeder, M.; Martinez, M.; Tauler, R. *Chemom. Intell. Lab. Syst.* **2002**, *54*, 123.

(23) Amigo, J. M.; de Juan, A.; Coello, J.; Maspoch, S. *Anal. Chim. Acta* **2006**, *567*, 245.

(24) Boscà, F.; Cosa, G.; Miranda, M. A.; Scaiano, J. C. *J. Photochem. Photobiol. Sci.* **2002**, *1*, 704.

(25) Golub, G. H.; Van Loan, C. F. *Matrix computations*, 2nd ed.; John Hopkins University Press: Baltimore, 1990; Chapter 8.

(26) Maeder, M. *Anal. Chem.* **1987**, *59*, 527.

(27) Ruckebusch, C.; Aloïse, S.; Blanchet, L.; Huvenne, J. P.; Buntinx, G. *Chem. Intell. Lab. Syst.*, to be published, DOI:10.1016/j.chemolab.2007.05.007.

(28) Maeder, M.; Neuhold, Y. M. *Practical Data Analysis in Chemistry*, Rutan, S., Walczak, B., Eds.; Elsevier: New York, 2007; Chapter 4.

(29) Jaumot, J.; Gemperline, P. J.; Stang, A. *J. Chemom.* **2005**, *19*, 97.

(30) Kovalenko, S. A.; Schanz, R.; Farztdinov, V. M.; Hennig, H.; Ernsting, N. P. *Chem. Phys. Lett.* **2000**, *323*, 312.

(31) Sun, Y. P.; Sears, D. F.; Saltiel, J. *J. Am. Chem. Soc.* **1989**, *111*, 706.

(32) Batley, M.; Kearns, D. R. *Chem. Phys. Lett.* **1968**, *2*, 423.

(33) Nakayama, T.; Sakurai, K.; Ushida, K.; Kawatsura, K.; Hamanoue, K. *Chem. Phys. Lett.* **1989**, *164*, 557.

(34) Singh, A. K.; Bhasikuttan, A. C.; Palit, D. K.; Mittal, J. P. *J. Phys. Chem. A* **2000**, *104*, 7002.

(35) He, H-Y.; Fang, W-H.; Philips, D. L. *J. Phys. Chem. A* **2004**, *108*, 5386.

© 2016 Tous droits réservés.

doc.univ-lille1.fr

Annexe 4. Aloïse et al, J. Phys. Chem. A,111,10,2007

THE JOURNAL OF PHYSICAL CHEMISTRY A

HDR de Stéphane Aloïse, Lille 1, 2016

© Copyright 2007 by the American Chemical Society

VOLUME 111, NUMBER 10, MARCH 15, 2007

ARTICLES

Photochromism of Photoenolizable Ketones in Quinoline and 1,8-Naphthyridine Series Studied by Time-Resolved Absorption Spectroscopy

Stéphane Aloïse,* Julien Réhault, Baptiste Moine, Olivier Poizat, and Guy Buntinx

Laboratoire de Spectrochimie Infrarouge et Raman (UMR 8516 du CNRS), Centre d'études et de recherches Lasers et Applications (FR 2416 du CNRS), Université des Sciences et Technologies de Lille, Bat C5, 59655 Villeneuve d'Ascq Cedex, France

Vladimir Lokshin, Magalie Valès, and André Samat

Groupe de Chimie Organique et Matériaux Moléculaires (UMR 6114), Université de la Méditerranée, Faculté des Sciences de Luminy, Case 901, 13288 Marseille Cedex 09, France

Received: July 12, 2006; In Final Form: January 24, 2007

For the two photochromic molecules, 3-benzoyl-2-benzyl-1-methyl-1H-quinolin-4-one (QC1) and 3-benzoyl-1,2-dibenzyl-*1H*-1,8-naphthyridin-4-one (QC18a) as well as the nonphotochromic 3-benzoyl-1-benzyl-2-methyl-*1H*-1,8-naphthyridin-4-one (QC18b), the full photochemical mechanism, which is based on the photoenolization process, has been elucidated using stationary and time-resolved spectroscopy techniques. After photoexcitation, the $S_1(n,\pi^*)-T_1(n,\pi^*)$ ISC process involving the exocyclic carbonyl chromophore is demonstrated to occur. Subsequently, γ-hydrogen transfer proceeds very rapidly to give rise to the triplet photoenol with a probable 1,4-biradical structure. For all three molecules, the biradical is clearly detected and proved quantitatively to be the direct precursor of the colored form (photochromic compounds) or ground state starting material (nonphotochromic compound). Solvent effects for the three molecules studied may suggest the existence of intramolecular hydrogen bonding in both biradical and colored form species. Structural effects on the γ-hydrogen transfer rate and biradical decay are related to the photochromic performances.

Introduction

The first observation of photochromism in heterocyclic ketones was reported by Ullman et al.[1,2] The phototransformation principle was based on the photoenolization process (Norrish type II reaction) arising in *o*-alkylphenylketones via a [1,5]H sigmatropic shift[3] for which light excitation leads to colored but unstable *o*-xylylenols (ground state photoenol) photoproducts. To obtain photochromic materials with more stable colored forms, Ullman et al. proposed attaching a second carbonyl group to stabilize the enol form via intramolecular hydrogen bonding. This goal was successfully achieved by the replacement of a phenyl nucleus by a heterocyclic analogue possessing an additional carbonyl group. A series of such new compounds were synthesized. Some of them demonstrated photochromic behavior, and the photochemical mechanism was investigated by UV−visible absorption, phosphorescence emission at different temperatures, and deuterium exchange tests.[2] On the basis of this study, the authors suggested that the photochromism results from the occurrence of a thermally activated enolization taking place in an $n\pi^*$ triplet state of the

* To whom correspondence should be addressed. E-mail: stephane.aloise@univ-lille1.fr.

10.1021/jp064397q CCC: $37.00 © 2007 American Chemical Society
Published on Web 02/22/2007

© 2016 Tous droits réservés.

doc.univ-lille1.fr

HDR de Stéphane Aloïse, Lille 1, 2016

SCHEME 1

$$S_0 + h\nu \rightarrow {}^1K \rightarrow {}^3K \rightarrow {}^3E \rightarrow CF$$

CHART 1

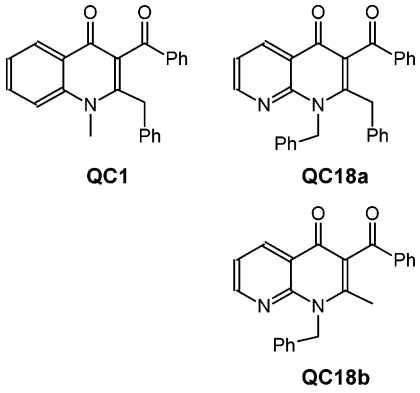

ketonic form (^{3}K). This latter species yields an enol triplet (^{3}E), which relaxes to the colored ground state form (CF) (see Scheme 1).

In fact, this reaction scheme, for which none of the chemical intermediates were directly identified, is in conformity with the well-known general mechanism, which is accepted to describe the photoenolization in simple carbonyl compounds[4,5] such as *o*-benzylbenzophenone[6] or *o*-methylbenzophenone[7] (MBP). Among transient species in photoenolization processes, the triplet photoenol, recognized for a long time to have a 1,4-biradical structure[4,8] (Norrish type II biradical), is of particular importance since its geometry determines the stereoselectivity of the *o*-xylylenol photoproducts.[9]

Recently, renewed interest in the photoenolization processes has emerged because of the possibility of achieving a better stabilization of the photoenol products via hydrogen bonding or electronic control.[10] Within this context and with the final goal of finding new stable photochromic materials,[11] the synthesis of new photoenolizable heterocyclic ketones has been undertaken as a continuation of the initial work of Ullman et al.[1,2] New synthesis routes were found, and approximately 50 compounds were obtained.[12] Preliminary steady state spectroscopic and chemical analyses[12,13] allowed the identification of the compounds, which are photochromic. Among them, two categories of molecules were distinguished depending on whether or not photoenolization is followed by a cyclization step.[13]

The aim of the present paper is to use various time-resolved spectroscopic techniques and standard photochemical methods (solvent and quenching effects) together with steady state absorption experiments under continuous irradiation to obtain better insight into the full photochemical mechanism responsible for the photochromism in these compounds. In particular, it was desired to check the validity of the proposed reaction Scheme 1 by characterizing the different chemical intermediates along the reaction pathway. With regard to this objective, we have chosen to focus our investigation on three molecules (Chart 1) that are representative of the simple photoenolization process (with no postenolization cyclization): 3-Benzoyl-2-benzyl-1-methyl-1H-quinolin-4-one (QC1), already investigated by Ullman et al. by conventional stationary spectroscopic techniques,[1] and two newly synthesized molecules of similar structures, 3-benzoyl-1,2-dibenzyl-1H-1,8-naphthyridin-4-one (QC18a) and 3-benzoyl-1-benzyl-2-methyl-1H-1,8-naphthyridin-4-one (QC18b). As will be seen, the first two are photochromic while QC18b is not. An attempt to understand some structural factors that govern the (non)photochromism of these compounds will be given at the end of this work.

Experimental Section

QC1 was synthesized using a modified procedure,[1] mp 175−176 °C (lit.[1] 177 °C). The synthesis of QC18a was described elsewhere,[12b] and its analogue QC18b was synthesized by the same method. White solid, mp 181 °C (from methanol). ^{1}H NMR ($CDCl_3$): 2.24 (3H, s, CH_3), 5.81 (2H, sl, CH_2), 6.97 (2H, m, H-arom.), 7.12−7.51 (7H, m, H-arom., H-6), 7.81 (2H, m, H-arom.), 8.60 (2H, m, H-5 and H-7). ^{13}C NMR ($CDCl_3$): 18.5 (q), 48.1 (t), 120.5 (d), 120.9 (s), 123.9 (s), 126.0 (d), 127.7 (d), 128.8 (d), 129.1 (d), 129.5 (d), 133.7 (d), 136.1 (d), 136.6 (s), 137.5 (s), 150.7 (s), 151.2 (s), 152.8 (d), 175.7 (s), 196.6 (s). Anal. calcd for $C_{23}H_{18}N_2O_2$: C, 77.95; H, 5.12; N, 7.90. Found: C, 78.10; H, 5.10; N, 7.83.

For the spectroscopic experiments, used were the following spectroscopic grade Sigma-Aldrich products: acetonitrile (CH_3-CN), methanol (CH_3OH), dimethylsulfoxide (DMSO), and trifluoroethanol (TFE). All solvents were used without further purification.

The pump−probe subpicosecond absorption experiments were carried out using an amplified Ti:sapphire laser (BMI Industry) delivering 0.8 mJ and 80 fs pulses at 800 nm with a repetition rate of 1 kHz. The pump pulses were obtained by frequency tripling the fundamental giving 30 μJ pulses at 266 nm. The probe beam was generated by focusing 1 μJ of the fundamental on a 1 mm CaF_2 plate giving a white light continuum with a spectrum covering the UV−vis and near IR range. The probe beam was split into signal and reference beams before crossing the sample, and the resulting beams were recorded on two different channels of a multichannel spectrograph. Transient absorbance was obtained by comparing signal and reference spectra for different time delays. The time delay between the pump and the probe could be varied by up to 1.5 ns (using a micrometric optical delay line), and the temporal resolution of the apparatus was better than 300 fs. Pump and probe beams, with relative linear polarizations at the magic angle, were focused in a 2 mm flowing sample cell with CaF_2 windows. The typical sample concentration used was 5×10^{-4} M.

A conventional laser flash photolysis apparatus was used to record nanosecond time-resolved absorbance data. Pump pulses (355 nm) of 7 ns and 1 mJ delivered by a nanosecond diode-pumped Q-switched laser (Thales) were focused onto a 10 mm optical path sample cell. The probe light was provided by a xenon lamp and analyzed with a photomultiplier via a spectrometer coupled to a digitalized oscilloscope (TDS540, Tektronics). This system allows a 50 ns time resolution. All solutions were prepared in such a way that the stationary optical density at 355 nm is about unity. Furthermore, all solutions were degassed by bubbling N_2. The quenchers *cis*-1,3-pentadiene and paraquat (Sigma-Aldrich) were used as received, and the latter was dissolved in wet acetonitrile (9:1). Quenching by O_2 was achieved by simply bubbling the gas through the deaerated solutions.

Steady state photolysis experiments were performed in a thermostated at 20 °C (±0.2 °C) copper block inside the sample chamber of a Cary 50 spectrometer. The optical path length of the cell was 10 mm. An Oriel 150W high-pressure Xe lamp was used for irradiation, and excitation wavelengths were selected by a monochromator tuned to the maximum absorbance of the uncolored form.

© 2016 Tous droits réservés.

doc.univ-lille1.fr

HDR de Stéphane Aloïse, Lille 1, 2016

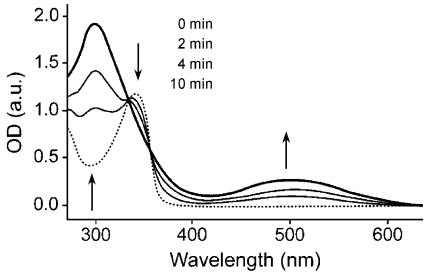

Figure 1. Absorption spectra of QC18a in acetonitrile under continuous UV irradiation acquired at different times as indicated on the graph.

TABLE 1: Spectrokinetic Parameters Obtained from Stationary Absorption Experiments for QC1, QC18a, and QC18b in Acetonitrile

	λ_{max}(nm)			
	uncolored form	colored form	k_Δ (s^{-1})	E_a (kJ mol^{-1})
QC1	338	490	2.6×10^{-3}	55.8 ± 0.9
QC18a	339	500	6.3×10^{-3}	55.3 ± 0.5
QC18b	338			

Results

Steady State Photolysis Experiments. UV−vis absorption spectra through continuous illumination acquired at regular temporal steps are shown for QC18a in acetonitrile in Figure 1. The initial spectrum, recorded in the absence of illumination, is due to the uncolored species (typical band at 339 nm). Subsequently, a gradual evolution is seen with irradiation time, with two clear isosbestic points at 330 and 355 nm, which gives evidence of the photochromic transformation. The final spectrum recorded after 10 min of irradiation shows a visible absorption band that corresponds to the colored form CF. Similar spectra and temporal behaviors were obtained for the QC1 molecule (not shown). The absorption maximum of CF in the visible region stands at 486 and 500 nm for QC1 and QC18a, respectively (Table 1). It provides a spectral reference for identifying the colored form in time-resolved data. In contrast to QC1 and QC18a, QC18b does not present any spectral evolution upon continuous photoexcitation, revealing the absence of photochromic behavior in this molecule. As thermal reversibility is an essential parameter of the photochromism effect, we have examined the ability of CF to return to the uncolored molecule when the irradiation is stopped. Indeed, by measuring the kinetic evolution at the characteristic CF absorbance, we observe that both QC1 and QC18a undergo a back reaction in the dark with thermal fading rates, k_Δ, of a few min^{-1}. By varying the temperature of the sample, the activation energy E_a of this fading process could also be determined. All of these spectrokinetic properties are summarized in Table 1.

Subpicosecond Time-Resolved Absorption Measurements. For QC18a in acetonitrile, transient absorption spectra recorded in the 320−690 nm spectral range within time windows of 2−10 and 20−500 ps following 267 nm excitation are shown in Figure 2a,b, respectively. The strong negative signal near 340 nm is due to bleaching as it corresponds to the λ_{max} of the uncolored form (see Table 1). This signal is nearly constant at all times, indicating that no significant repopulation occurs on this time scale. Apart from this bleaching signal, the shortest time spectrum (2 ps) is characterized by a UV-blue absorption peaking at 365 nm that will be ascribed in the following to a state named S. A rapid overview of the 2−10 ps spectral evolution shows the decrease of the 365 nm band while no increasing signal can be detected. Subsequently, in the 20−500 ps time domain, another type of spectral evolution occurs, which is characterized by concomitant absorption growths at $\lambda_{max} = 405$ and 655 nm and absorption decays in the 350−380 and 420−450 nm regions. The resulting spectrum is assigned to a new intermediate state named T_B. However, it is clear that the band S is not the direct precursor of the band T_B. Indeed, as it can be seen from Figure 3a), the absorption kinetic behavior at 365 nm is well-fitted with a biexponential function with decay times of 12 (band S decay; 68%) and 180 ps (decays of an intermediate species; 32%). On the contrary, the kinetics at 655 nm (band T_B growths) can be fitted by a monoexponential function with the same 180 ps characteristic time. The simpler way to describe our results is to assume a two-step process, S → T_A and T_A → T_B, even if it appears difficult to isolate clearly the new T_A intermediate. The second step of this mechanism is supported by the presence of one real isosbestic point at 417 nm that reveals the participation of two species kinetically linked (see the inset in Figure 2b). During the kinetic evolution, the shoulder peaking near $\lambda_{max} = 413$ nm (see the 20 ps trace) evolves until the new maximum, $\lambda_{max} = 405$ nm attributed to the band T_B, is reached (see the 500 ps trace). The 413 nm

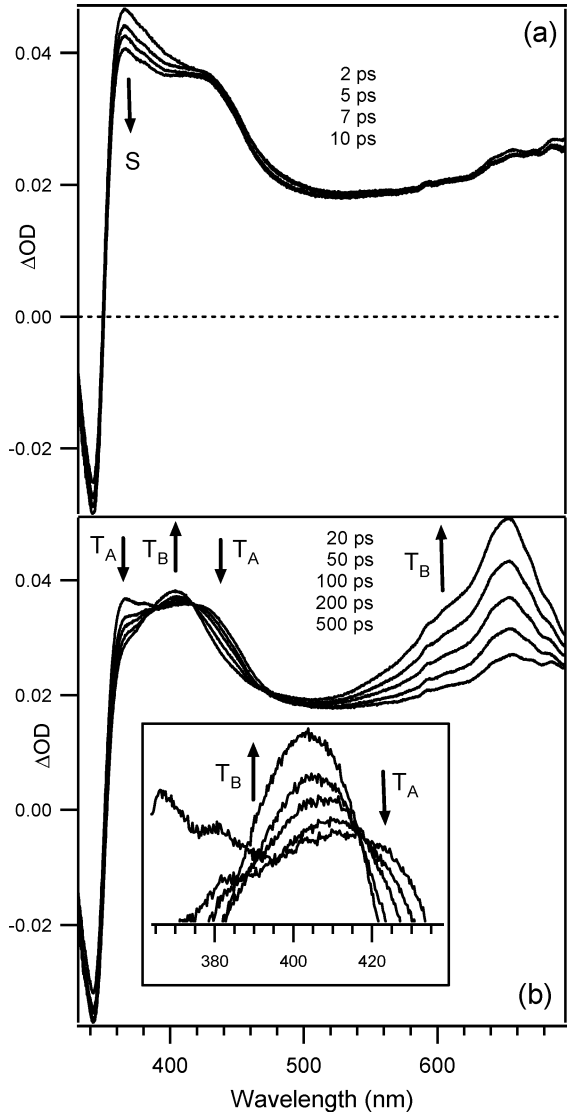

Figure 2. Subpicosecond time-resolved absorption spectra (267 nm excitation) of QC18a in acetonitrile in the 2−10 (a) and 20−500 ps (b) time domains. The time evolution is shown by arrows, and the band assignments to S, T_A, and T_B species are indicated. The inset is a zoom of the 365−465 nm region.

© 2016 Tous droits réservés.

doc.univ-lille1.fr

HDR de Stéphane Aloïse, Lille 1, 2016

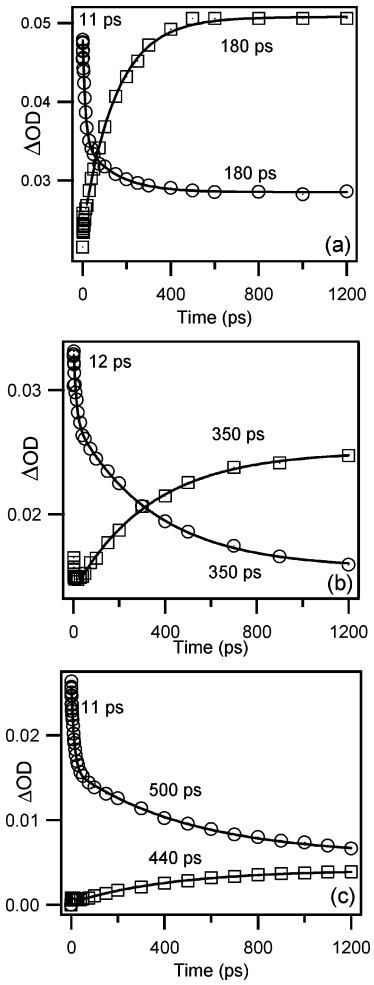

Figure 3. Kinetics obtained in acetonitrile during the 0−1200 ps time window at: (a) 365 (○) and 655 nm (□) for QC18a, (b) 365 (○) and 660 nm (□) for QC18b, and (c) 350 (○) and 640 nm (□) for QC1; in this latter case, the kinetics at 640 nm is obtained after subtraction of the kinetics of the background monitored at 560 nm. Solid lines are the results of exponential fitting.

TABLE 2: Spectral and Kinetic Data Defining Transient Species S, T_A, and T_B Detected during Subpicosecond Time-Resolved Absorption Experiments for QC1, QC18a, and QC18b (in Acetonitrile)[a]

	λ_{max} (nm)			τ_S (ps)	τ_1 (ps)
	S	T_A	T_B	S → T_A	T_A → T_B
QC18a	365	413	405 655	11 ± 2	180 ± 20
QC18b	365	425	404 660	12 ± 2	350 ± 40
QC1	350	-	395 640	12 ± 1	440 ± 30

[a] τ_S and τ_1 are the lifetimes of S and T_A, respectively.

band is therefore ascribed to T_A. In the following, lifetimes (decay rate constants) of S and T_A species will be denoted by τ_S (k_s) and τ_1 (k_1), respectively. For the three species S, T_A, and T_B, the λ_{max} and kinetic parameters are reported in Table 2.

For QC18b (spectra not shown), quite an identical spectral and kinetic behavior is found (see Table 2). Indeed, as shown in Figure 3b, the 365 nm kinetics displays a fast decay (12 ps; 33%) attributed to the S intermediate (λ_{max} = 365 nm) and a longer one (350 ps; 67%) attributed to the T_A intermediate. This latter time holds also for the growth of T_B (λ_{max} = 404 and 660 nm) monitored at 660 nm. The maximum of absorption of the

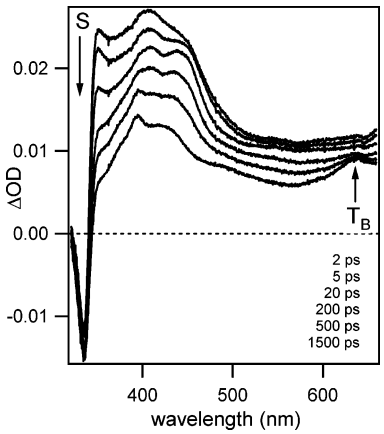

Figure 4. Subpicosecond time-resolved absorption spectra (267 nm excitation) of QC1 in acetonitrile in the 2−1500 ps time domain.

T_A species, determined as above, gives a maximum of absorption at λ_{max} = 425 nm. Note that the T_A lifetime (Table 2) is a factor of about two larger as compared to the value found in the case of QC18a.

Finally, for QC1, the spectral evolution (Figure 4) is somewhat less clear since no rising component is observed due to the presence of an additional decreasing broad background signal. However, common points with QC18a and QC18b molecules can be found. The absorption kinetics at 350 nm (λ_{max}) shown in Figure 3c can be still fitted with a biexponential function with decay times of 12 (50%) and 500 ps (50%). As previously, the shorter time can be assigned to the decay of the S species by analogy with QC18a and QC18b. Furthermore, the final spectrum (1500 ps) shows a weak absorption band near 640 nm and two maxima at 390 and 425 nm that can be considered to be analogous to the T_B bands in the above two compounds although their relative intensities appear quite different. A growth time of 440 ps can be estimated for the 640 nm band by subtracting the kinetics of the background monitored at 560 nm from the kinetics at 640 nm as shown in Figure 3c. This time correlates approximately to the longest decay time (500 ps) found at 350 nm and is therefore attributed to the growth of the T_B intermediate. In the case of QC1, the absence of isosbestic point makes the spectral identification of T_A difficult. No attempt to explain the additional decreasing background will be given in the following.

Finally, to better rationalize the initial photochemical events in the three studied molecules and to facilitate appropriate comparisons, time-resolved absorption measurements were also made on the photoenolizable MBP as well as the benzophenone (BP) molecule to obtain kinetic data under the same experimental conditions (see Discussion).

Nanosecond Laser-Flash Photolysis Experiments. Laser flash photolysis experiments were performed for 355 nm laser excitation in various deaerated solvents. The spectra recorded for QC1 in acetonitrile in the 340−670 nm spectral domain are displayed in Figure 5. Note the bad signal-to-noise ratio below 340 nm that prevents a good acquisition of the bleaching signal (expected at 338 nm). At short times (70 ns), the spectrum corresponds to that observed above for T_B (1500 ps trace in Figure 4) with absorption bands at 390 and 640 nm. This spectrum decreases exponentially with a characteristic time of 255 ns (value measured at 640 nm) until a final spectrum is observed with a peak at 355 nm and a broad band around 490 nm. This last spectrum is characteristic of the colored form (CF) identified in the steady state measurements (see Table 1).

© 2016 Tous droits réservés.

doc.univ-lille1.fr

HDR de Stéphane Aloïse, Lille 1, 2016

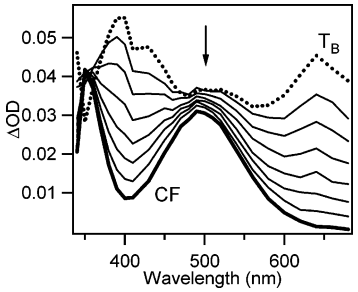

Figure 5. Laser flash photolysis spectra (355 nm excitation) obtained for QC1 in acetonitrile between 340 and 680 nm. The arrows indicate the evolution of the spectra. The delay times are 0.06 (dashed line), 0.14, 0.2, 0.28, 0.38, 0.5, 0.7, and 1.6 μs (bold).

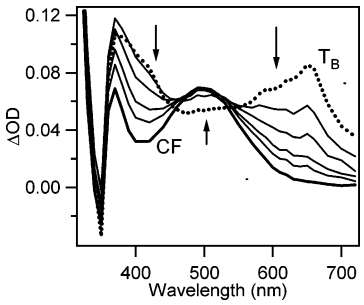

Figure 6. Laser flash photolysis spectra (355 nm excitation) obtained for QC18a in acetonitrile between 320 and 720 nm. The arrows indicate the evolution of the spectra. The delay times are 0.06 (dashed line), 0.09, 0.12, 0.16, 0.20, and 1.6 μs (bold).

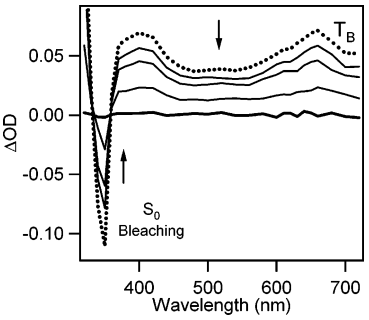

Figure 7. Laser flash photolysis spectra (355 nm excitation) obtained for QC18b in acetonitrile between 320 and 720 nm. The arrows indicate the evolution of the spectra. The delay times are 0.06 (dashed line), 0.14, 0.2, 0.4, and 1.6 μs (bold).

For QC18a, as shown in Figure 6, besides the clear bleaching signal around 340 nm, the spectrum of T_B is clearly identified by comparison with the picosecond data (see the 500 ps trace in Figure 2b) and seems to lead to the CF species (see Figure 1 and Table 1) within 45 ns. However, as in the case of QC1, the kinetic sequence $T_B \rightarrow$ CF is not supported by the presence of unambiguous isosbestic points (only a slight rising component is noticed around 500 nm). This kinetic sequence will be confirmed below by quenching experiments.

Finally, for QC18b (Figure 7), the T_B spectrum can still be observed at short times, but unlike the two other molecules, it disappears completely with a characteristic time of 285 ns without yielding any new absorption signal. The 340 nm bleaching signal disappears simultaneously with the same time constant, and clear isosbestic points are observed near 330 and 360 nm. These observations indicate clearly that T_B relaxes to the ground state instead of producing the colored form, in agreement with the fact that no photochromism was observed for QC18b from steady state measurements. For the three

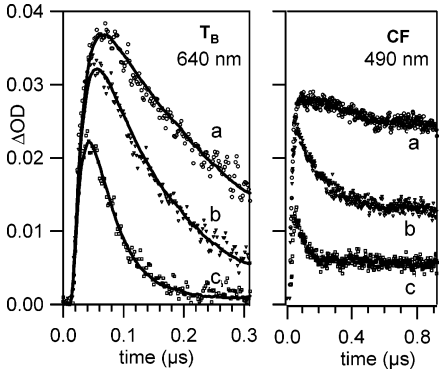

Figure 8. Kinetics obtained from laser flash photolysis at 640 (left) and 490 nm (right) for QC1 in wet acetonitrile for increasing concentrations of *cis*-1,3-pentadiene: (a) no quencher, (b) 0.004 M, and (c) 0.023 M. Bold lines are fitting curves.

TABLE 3: Lifetimes (τ_2) and Quenching Rate Constants (*cis*-1,3-Pentadiene and Paraquat) of Transient Species T_B Obtained from the Laser Flash Photolysis Experiment

	τ_2 (ns)[a]	k_2^Q (10^9 M^{-1} s^{-1})[a]	k_2^{PQ2+} (10^9 M^{-1} s^{-1})[b]
QC1	255 ± 5	0.86 ± 0.05	10.1 ± 0.3
QC18a	45 ± 1	1.74 ± 0.02	
QC18b	285 ± 3	1.72 ± 0.04	7.5 ± 0.6

[a] In acetonitrile. [b] In wet acetonitrile.

molecules, the lifetime (decay rate) of the T_B species, denoted τ_2 (k_2), is reported in Table 3.

Quenching Results. To gain more information about the T_B species, we studied the effect of different types of quenchers. First, we observed for the three molecules a clear shortening of the T_B lifetime in the presence of oxygen in the solution, indicating either a triplet[14] or biradical nature for this species (biradicals are known to be very sensitive to paramagnetic substances[5,15]). Next, as shown for example for QC1 in Figure 8, adding 1,3-pentadiene also shortens the T_B decay time (640 nm kinetics) and reduces simultaneously the final CF yield (as measured by the intensity of the long time "plateau" absorption at 490 nm). Note that the 640 nm kinetics is well fit by a monoexponential function convoluted with the apparatus response function.[16] Therefore, on the one hand, the triplet nature of T_B is thus confirmed while on the other hand T_B seems to be a precursor of the CF species. We can prove quantitatively that these two species are directly related. As seen in Figure 9a for the three molecules, the observed decay rate, k_{exp}, at 640 nm depends linearly on the quencher concentration according to the Stern−Volmer equation:

$$k_{exp} = k_2 + k_2^Q[Q] \quad (1)$$

The corresponding quenching rate k_2^Q values are given in Table 3. On the other hand, in the above assumption that T_B is the direct precursor of CF (QC1 and QC18a), the intensity of the long time absorbance plateau at 490 nm (A_∞^Q) is also expected to vary linearly with the inverse of the quencher concentration according to:

$$\frac{A_\infty^0}{A_\infty^0 - A_\infty^Q} = 1 + \frac{k_2}{k_2^Q} \cdot \frac{1}{[Q]} \quad (2)$$

where A_∞^0 is the final absorption at 490 nm in the absence of 1,3-pentadiene. Linear fits are indeed observed for both QC1 and QC18a (Figure 9b) and lead to values of the slope of 0.0043

© 2016 Tous droits réservés.

doc.univ-lille1.fr

HDR de Stéphane Aloïse, Lille 1, 2016

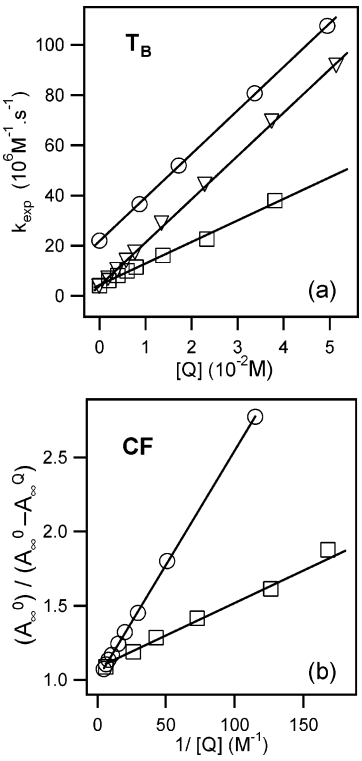

Figure 9. Sterm−Volmer plots concerning QC1 (□), QC18a (○), and QC18b (▽) in acetonitrile solvent. (a) Experimental decay rate, k_{exp}, of T_B species (eq 1) obtained from kinetics at 640 nm wavelength detection (Figure 8, left) function of 1,3-pentadiene concentration [Q]. (b) Calculated ratio (eq 2) obtained from long time plateau absorbance of CF (QC1 and QC18a only) at 490 nm wavelength detection (Figure 8, right) function of the inverse of quencher concentration.

and 0.015, respectively, in excellent accordance with the k_2/k_2^Q ratios of 0.0045 and 0.013, respectively, calculated from the values found from the 640 nm fits (Table 3). This result definitively confirms the sequence:

$$T_B(\sim 640\ \text{nm}) \rightarrow CF(\sim 490\ \text{nm}) \qquad (3)$$

As photoenolization processes are known to involve 1,4-biradicals,[5,8] the effect of adding paraquat PQ^{2+} (methylviologen), which is one of the best quenchers of such biradicals,[17] has also been checked following the method[17] given by Das et al. Effective quenching was observed for all three compounds, but quenching constants of the T_B intermediate (see Table 3) were obtained quantitatively only for QC1 and QC18b because of the too short T_B lifetime of QC18a. These last results indicate that T_B is a biradical species.

Solvent effects. To identify enol type products among the transient species involved in the photoenolization process, solvent influence has been tested. Indeed, as first demonstrated by Haag et al. in the case of simple photoenolizable compounds,[18] lifetimes of photoenols in the singlet or triplet manifold are substantially enhanced in solvents having strong hydrogen bond acceptor (HBA) basicity (related to the β parameter[19] that measures the solvent's ability to accept a proton in a solute-to-solvent hydrogen bond). Such an effect, explained by a better solvation of the enol function,[18] is usually not accompanied by any spectral modification. In the present case, various unexpected results were obtained. First, for the three molecules, the T_B triplet species lifetime measured at 640 nm does not display any enhancement with the HBA basicity of the solvent as shown in Table 4. In fact, almost the opposite situation occurs since a maximum lifetime is obtained for CH_3CN, which has a moderate HBA basicity value as compared to DMSO. Then, in the case of the CF species, a drastic hypsochromic shift is observed as a function of the increasing HBA basicity of the solvent. In Figure 10, the CF spectrum of QC18a acquired at 1600 ns peaks at 505, 500, 480, and 440 nm in TFE, CH_3CN, CH_3OH, and DMSO, respectively. A similar effect is found for QC1, and all values are reported in Table 4. Therefore, it is clear that the general approach given by Haag et al. cannot be applied directly for the molecules studied here and the apparent discrepancies will be discuss in the following section.

TABLE 4: Spectrokinetic Parameters Related to the CF (λ_{max}) and T_B Species (Lifetime) for Various Solvents[a]

		QC**1**		QC**18a**		QC**18b**
	β[b]	CF λ_{max} (nm)[c]	T_B τ_2 (ns)[d]	CF λ_{max} (nm)[c]	T_B τ_2 (ns)[e]	T_B τ_2 (ns)[e]
TFE	0.00	510	190	505	15	15
CH_3CN	0.31	490	255	500	45	285
CH_3OH	0.62	470	135	480	15	70
DMSO	0.76	450	160	440	20	40

[a] HBA basicity parameters (β) are indicated. [b] From ref 18. [c] ±5 nm. [d] ±5 ns. [e] ±3 ns.

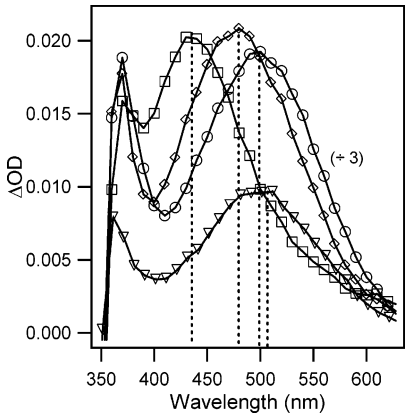

Figure 10. Laser flash photolysis spectra of the QC18a molecule in DMSO (□), CH_3CN (○), CH_3OH (◊), and TFE (▽) for time delays Δt = 1600 ns (CF species). Scaling factors concern the acetonitrile case.

SCHEME 2

QC1 and QC18a: $S_0 + h\nu \rightarrow S \rightarrow T_A \rightarrow T_B \rightarrow CF$

QC18b: $S_0 + h\nu \rightarrow S \rightarrow T_A \rightarrow T_B \rightarrow S_0$

To obtain a synthetic view of the kinetic mechanism, the reaction Scheme 2 summarizes the results obtained for the three molecules from the femtosecond and nanosecond measurements including the quenching experiment results.

Discussion

Our results reveal extensive analogies between the reaction Scheme 2 proposed for the studied compounds and the reaction Scheme 1 suggested by Ullman et al. since the same number of reaction intermediates are involved in both cases. In light of the agreement between both schemes, we propose in the following to identify all of the species involved in the photochemical process. After some comments about the CF compound and the global photochromic process, first the transient species T_B will be discussed and then the species S and T_A. After discussing the full photochemical mechanism, additional comments concerning the structural factors that influence the photochromism will end this section.

© 2016 Tous droits réservés.

doc.univ-lille1.fr

HDR de Stéphane Aloïse, Lille 1, 2016

SCHEME 3

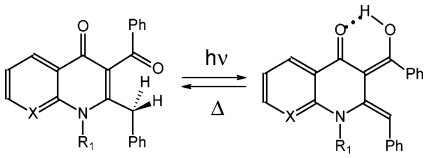

Colored Form Species Stabilized by Intramolecular Hydrogen Bonding. First, as suggested by Ullman et al.,[1,2] the final product for the photochromic heterocyclic ketones has to be the same type of ground state *ortho*-xylylenol, thermally unstable in most common ketones but stabilized by intramolecular hydrogen bonding for the colored form CF in the case of QC1 and also for QC18a compounds. In fact, the global photochromic mechanism (Scheme 3) postulated in the past has only recently been confirmed by structural analysis using the time-resolved NMR technique.[20] From the present results, the stabilization of the colored forms, i.e., the ground state photoenols, is first confirmed by the comparison of its lifetimes, in the order of few minutes (Table 1), with the 2.9 ms value reported for the most stable photoenol of MBP[7] (trans isomer).

Furthermore, the unexpected and drastic hypsochromic effect observed on increasing the HBA character of the solvent (Figure 10) is probably related to the presence of the enol function stabilized by an intramolecular hydrogen bond. Indeed, progressively stronger hydrogen bond acceptor solvents compete more and more efficiently with the initial intramolecular hydrogen bond, which decreases the planarity of the CF molecule and consequently the extension of the electronic π-conjugation system. This effect can therefore explain the observed blue shift of CF spectra upon increasing the β-parameter. Such a competition between intra- and intermolecular hydrogen bonds inducing a blue shift has been reported for the 2-hydroxybenzophenone,[21] which supports the hypothesis outlined above. If this interpretation is correct, the hypsochromic shift could be taken as a particularly elegant signature of the presence of an intramolecular hydrogen-bonded enol group in the colored form species.

Identification of the T_B Species. In this section, we will discuss the nature of the direct precursor of the CF species. It has been clearly shown using a Sterm−Volmer approach (see eqs 1−3) that this precursor is the T_B species. The latter has been identified as the 1,4-biradical species (oxygen and paraquat quenching) frequently invoked during the photoenolization process displaying an excited triplet state behavior[23,24] (oxygen and 1,3-pentadiene quenching).

If the T_B species is recognized as being the 1,4-biradical intermediate, it implies that the $T_A \rightarrow T_B$ kinetic step corresponds to the [1,5]H sigmatropic shift. On the other hand, the rate of γ-hydrogen transfer is known to depend on the nature of the intramolecular hydrogen donor group.[25] In our case, the appearance rate of the T_B intermediate (i.e., $k_1 \approx 1/\tau_1$; see Table 2) is reduced by a factor of about two on going from QC18a to QC18b in accordance with the fact that the γ C−H bond is more weakened by the adjacent phenyl than by the adjacent hydrogen substituent. This structural effect is therefore in accordance with the above assignment.

The lack of enhancement of the T_B lifetime in strong HBA solvents (Table 4), which appears to be in contradiction with the prediction of Haag et al., can be explained by the fact that the solvation of the enol group by intermolecular hydrogen bonding cannot take place. Indeed, as in the case of CF species, the enol group may already be stabilized by intramolecular hydrogen bonding.

In summary, for the T_B intermediate, reliable information has been obtained about the triplet multiplicity, the biradical nature, and the occurrence of an enol group engaged in intramolecular hydrogen bonding. Accordingly, we can denote this species as ^{3}BR-E, notation that summarizes more precisely the three above characteristics of T_B in comparison with the ^{3}E notation found in the Ullman et al. reaction scheme (Scheme 1).

Identification of the S and T_A Species. At this point, it is desirable to characterize more precisely the two prior precursors of ^{3}BR-E noted S and T_A. In this regard, it is interesting to compare our time-resolved spectroscopic data on the photophysics of QC1, QC18a, and QC18b with similar data reported for typical molecules undergoing such photoenolization processes (e.g., MBP[7]) that have been studied by ultrafast absorption spectroscopy. Data concerning the photophysics of the neighboring benzophenone molecule (BP)[26] that does not undergo photoenolization are also worthy of comparison. After photoexcitation, the lowest excited singlet state $S_1(n,\pi^*)$ of BP as well as MBP relaxes through an ISC process to the first triplet state $T_1(n,\pi^*)$ with characteristic times of between 10 and 13 ps for BP in acetonitrile[26] and 5 ps for MBP in ethanol solvent.[7] Under our experimental conditions and in acetonitrile solvent, we found values of 11 ps for BP and 12 ps for MBP. By comparing these two characteristic lifetimes with the ones in Table 2, one can deduce that the (n,π^*) nature of the BP S_1 state is maintained in all molecules. Thus, the precursor S can be assigned to the first excited state $S_1(n,\pi^*)$ (^{1}K in Scheme 1) while the T_A state can be ascribed to the $T_1(n,\pi^*)$ state (^{3}K in Scheme 1). As in the case of MBP, because the hydrogen transfer has not yet occurred, a keto structure is assumed for $T_1(n,\pi^*)$.

Full Photochemical Mechanism. Having identified all transient species, the full photochemical mechanism of the photoenolizable heterocyclic ketones, displayed in Figure 11, can now be discussed. After the photooexcitation, the $S_1(n,\pi^*)$ state relaxes through an ISC process to the first excited triplet state $T_1(n,\pi^*)$. The photophysics engaged at this stage, localized on the exocyclic carbonyl, mimics the BP behavior. In this sense, the participation of a $T_2(\pi,\pi^*)$ state,[27] at the origin of the very fast ISC process (10^{11} s^{-1}) in benzophenone-like molecules (explaining the apparent violation of El-Sayed rules[14]), is therefore strongly expected also in the case of heterocyclic ketones. After formation of the $T_1(n,\pi^*)$ triplet state, the intramolecular[1,5] H sigmatropic shift proceeds very rapidly. Indeed, all values obtained from the Table 2 ($k_1 > 10^9$ s^{-1}) are higher than the 5×10^8 s^{-1} value for MBP[7]. This fast H atom transfer, which is sensitive to structural effects (QC18a vs QC18b as already discussed), points to an ideal conformation for γ-hydrogen abstraction and may reveal quantum tunneling[28] as is accepted for totally constrained photoenolizable molecules.[29] The most important reaction pathway for $T_1(n,\pi^*)$ is thus the production of the 1,4-biradical triplet photoenol species, ^{3}BR-E, and one would expect a two-step process: The sigmatropic shift forms a first biradical species (see the dashed line state in Figure 11) that evolves through bond rotation to allow the formation of an intramolecular hydrogen bonding with the adjacent carbonyl (suggested by solvent effects). However, the monoexponential kinetic appearance of ^{3}BR-E may indicate that H atom transfer is the limiting kinetic step while the bond rotation proceeds, therefore without encountering any significant potential barrier. The ^{3}BR-E is the precursor of CF in the case of QC1 and QC18a while for QC18b a back process to the

© 2016 Tous droits réservés.

doc.univ-lille1.fr

HDR de Stéphane Aloïse, Lille 1, 2016

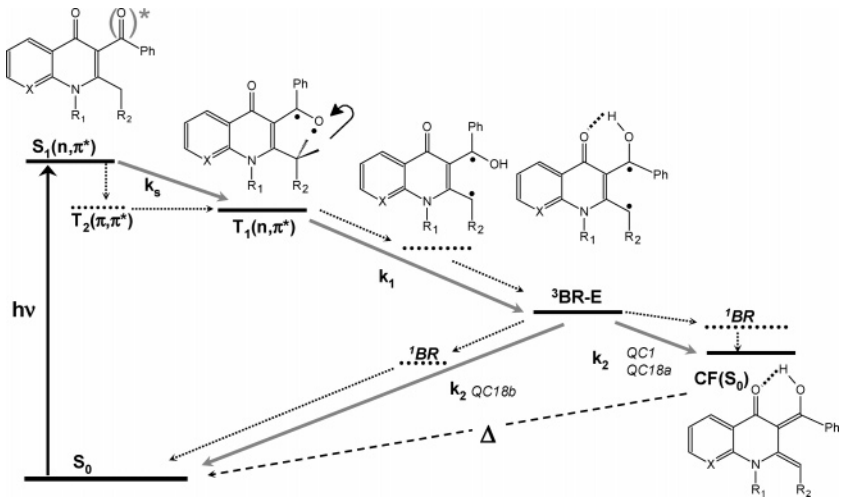

Figure 11. Overall reaction schemes describing the photoenolization process. Dashed line states and dashed line transitions (represented by arrows) are assumed to be involved in the reaction scheme but are not detected experimentally in this study.

CHART 2

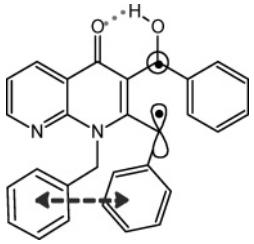

ground state of starting material (disproportionation process) is observed. It is well-known that the decay mechanism of a triplet biradical consists on the irreversible interconversion to a singlet biradicals (^{1}BR, on the Figure 11) that then yields products in a very fast process.[30] In our cases and for both deactivation channels (i.e., CF production or disproportionation), the experimental monoexponential decay of ^{3}BR-E of the three studied molecules (Table 3) is in conformity with the negligible lifetime (<1 ns[27,30]) of such singlet biradicals. However, a fundamental question still remains: Why is QC18b not photochromic even though ^{3}BR-E is clearly detected? Obviously, the comparison of QC18a and QC18b 1,4-biradicals is appropriate because the decisive role of the phenyl substituent in position 4 is clearly revealed. However, a simple substituent effect cannot be invoked to explain the different behavior of these two molecules if one reminds the example of *o*-methyl[7] and *o*-benzylbenzophenone[6] that give rise to 1,4-biradical upon photoexcitation as the precursor of the ground state photoenol. Alternatively, we think that additional conformational effects may play a decisive role in the fact that CF species is produced in QC18a but not in QC18b. Indeed, it is surprising that in spite of the presence of the supplementary stabilizing phenyl group (stabilization due to conjugation effect[31]), the lifetime of QC18a biradical is clearly shortened as compared to that of QC18b (Table 3). By analogy with previous results on simple photoenolizable valerophenone,[32] the steric interaction between the QC18a N-benzyl group and the other contiguous benzyl group may favor a molecular conformation allowing an ideal orientation of the atomic orbital at positions 1 and 4 maximizing the ISC process toward the CF species. In conformity with the classical picture of ISC process, such an ideal conformation corresponds to a perpendicular orientation of atomic p orbitals[31] as illustrated in Chart 2. The lack of photochromism of QC18b is a challenging question; therefore, theoretical calculations[9,27] would be very helpful to definitively address an answer.

Once it is produced, the CF species possesses a long lifetime due to intramolecular hydrogen bond stabilization and displays slow thermal back reactions in the dark.

Structural Factors Influencing the Photochromism. Finally, it is interesting to compare qualitatively the photochromic performances of QC1 and QC18a. According to the reaction scheme in Figure 11, the quantum yield for production of the colored form ϕ(CF) is proportional to $k_s \times k_1 \times k_2$. From the values located in Tables 2 and 3 for the different lifetimes, one estimates a ratio of 15:1 for the photochromic quantum yield in favor of QC18a. This drastic effect may be due to different (complementary) effects. First, the k_1 value for γ-hydrogen transfer is lower in QC1 as compared to that in QC18a. This difference suggests that (i) the biradical species is produced less efficiently in QC1 and (ii) structural effects should also play a non-negligible role in the rate of hydrogen transfer. In this sense, both steric (N−Me vs N−CH_2Ph) and electronic (quinolin-4-one vs naphthyridin-4-one) effects can be expected. Next, as proposed above, phenyl−phenyl interactions are absent (see Chart 2) for the biradical of QC1, which may explain its lower ISC rate (i.e., $k_2 \approx 1/\tau_2$) as compared with the more favorable value for QC18a. From the above example, it is clear that a better understanding of the photochemical step related to the photochromic yield can lead to intelligent optimization of photochromic performance. We conclude that QC18a is a better photochromic compound as compared to QC1.

Conclusions

Within the framework of a photochromism study, three photoenolizable heterocyclic ketones with the unique possibility of stabilizing the ground state photoenol by intramolecular hydrogen bond have been studied. For both the nonphotochromic QC18b molecule and the two photochromic QC18a and QC1 compounds, a clear picture of the full photochemical mechanism through the detection of all transient species has been established and summarized in Figure 11. Strong similarities between heterocyclic and simple photoenolizable ketones are found within the number, the nature of the transient species, and the processes involved. After photoexcitation, the first excited state $S_1(n,\pi^*)$ relaxes through an ISC process to the first excited triplet state $T_1(n,\pi^*)$ in which a [1,5]H sigmatropic shift takes place. This gives rise to 1,4-biradical species, identified also as a triplet photoenol species ^{3}BR-E. Either the CF species (for QC18a and QC1) or the ground state starting molecule (for

© 2016 Tous droits réservés.

doc.univ-lille1.fr

HDR de Stéphane Aloïse, Lille 1, 2016

QC18b) is then produced. For both CF and ^{3}BR-E species, unexpected solvent effects are explained in terms of competition between intermolecular (solvent) and intramolecular (endo carbonyl group) hydrogen bonding. Because ^{3}BR-E is detected for all three compounds, it appears that the reactivity of this species controls the photochromism. Furthermore, it has been found that structural effects influence the γ-hydrogen abstraction as well as the biradical decay by ISC. With the idea of better controlling such effects to optimize the photochromic yield, the synthesis and investigation of new compounds are in course in our laboratories.

Acknowledgment. We are grateful to P. O'Keeffe for help with the revision of the English version. We thank the Groupement de Recherche GDR 2466 from CNRS and the Centre d'études et de Recherches Lasers et Applications (CERLA) for their help in the development of this work. CERLA is supported by the Ministère chargé de la Recherche, Région Nord/Pas de Calais, and the Fonds Européen de Développement Economique des Régions.

References and Notes

(1) Huffman, K. R.; Loy, M.; Ullman, E. F. *J. Am. Chem. Soc.* **1965**, *87*, 5417.

(2) Henderson, W. A., Jr.; Ullman, E. F. *J. Am. Chem. Soc.* **1965**, *87*, 5424.

(3) Yang, N. C.; Rivas, C. J. *J. Am. Chem. Soc.* **1961**, *83*, 2213.

(4) Sammes, P. G. *Tetrahedron* **1976**, *32*, 405.

(5) (a) Scaiano, J. C. *Acc. Chem. Res.* **1982**, *15*, 252. (b) Johnston, L. J.; Scaiano, J. C. *Chem. Rev.* **1989**, *89*, 521.

(6) (a) Netto-Ferreira, J. C.; Wintgens, V.; Scaiano, J. C. *Can. J. Chem.* **1994**, *72*, 1565. (b) Ohzeki, T.; Ohgusa, H.; Isaka, H.; Suzuki, S.; Takahashi, H. *Chem. Phys. Lett.* **1988**, *149*, 379.

(7) Nakayama, T.; Torii, Y.; Nagahara, T.; Hamanoue, K. *J. Photochem. Photobiol. A* **1998**, *119*, 1.

(8) Wagner, P. J.; Kelso, P. A.; Zepp, R. G. *J. Am. Chem. Soc.* **1972**, *94*, 7480.

(9) Wagner, P. J.; Sobczak, M.; Park, B. S. *J. Am. Chem. Soc.* **1998**, *120*, 2488.

(10) (a) Mal, P.; Lourderaj, U.; Venugopalan, P.; Moorthy, J. N.; Sathyamurthy, N. *J. Org. Chem.* **2003**, *68*, 3446. (b) Koner, A. L.; Singhal, N.; Nau, W. M.; Moorthy, J. N. *J. Org. Chem.* **2005**, *70*, 7439.

(11) Bouas-Laurent, H.; Dürr, H. *Photochromism*; Elsevier Science B. V.: Amsterdam, The Netherlands, 2003.

(12) (a) Valès, M. Ph.D. thesis, Université de Luminy, Marseille, 2001. (b) Valès, M.; Lokshin, V.; Pepe, G.; Guglielmetti, R.; Samat, A. *Tetrahedron* **2002**, *58*, 8543.

(13) Lokshin, V.; Valès, M.; Samat, A.; Pèpe, G.; Metelista, A.; Khodorkovsky, V. *Chem. Commun.* **2003**, 2080.

(14) Turro, N. J. *Modern Molecular Photochemistry*; The Benjamin/Cummings Publishing Co.: 1978.

(15) Redmond, R. W.; Scaiano, J. C. *J. Phys. Chem.* **1989**, *93*, 5347.

(16) Note that the reduction of the initial intensity in both the 640 and the 490 nm kinetics as the quencher concentration is raised, satisfactorily reproduced by the fits in Figure 8, is not due to a lowering of the initial T_B concentration but results from an effect of the convolution of the constant apparatus response with the increasingly rapid exponential decay kinetics of T_B (as the timescale of these kinetics are similar to the apparatus response time, its short-time region appears truncated).

(17) (a) Das, P. K.; Encinas, M. V.; Small, R. D., Jr.; Scaiano, J. C. *J. Am. Chem. Soc.* **1979**, *101*, 6965. (b) Baral-Tosh, S.; Chattopadhyay, S. K.; Das, P. K. *J. Phys. Chem.* **1984**, *88*, 1404.

(18) (a) Haag, R.; Wirz, J.; Wagner, P. J. *Helv. Chim. Acta* **1977**, *60*, 2595. (b) Lutz, H.; Bréhéret, E.; Lindqvist, L. *J. Chem. Soc. Faraday Trans. 1* **1973**, *69*, 2096.

(19) Kamlet, M. J.; Abboud, J. L.; Abraham, M. H.; Taft, R. W. *J. Org. Chem.* **1983**, *48*, 2877.

(20) Berthet, J.; Lokshin, V.; Valès, M.; Samat, A.; Vermeersch, G.; Delbaere, S. *Tetrahedron Lett.* **2005**, *46*, 6319.

(21) Delling, W. L. *J. Org. Chem.* **1966**, *31*, 1045.

(22) Scaiano, J. C. *J. Photochem.* **1973**, *2*, 81.

(23) If the triplet of the photoenol and the 1,4-biradical are one and the same species, the dominant character between radical-like or excited triplet state behavior (see ref 5) has to be determined although this information can only be precisely deduced from time-resolved ESR experiments. (a) Ikoma, T.; Akiyama, K.; Tero-Kubota, S.; Ikegami, Y. *J. Phys. Chem.* **1989**, *93*, 7087. (b) Akiyama, K.; Ikegami, Y.; Tero-Kubota, S. *J. Am. Chem. Soc*. **1987**, *109*, 2538.

(24) Quenching of type II biradical with β-carotene by triplet energy transfer is an example of excited state triplet behavior characterization. Kumar, C. V.; Chattopadhyay, S. K.; Das, P. K. *J. Am. Chem. Soc*. **1983**, *105*, 5143.

(25) De Feyter, S.; Diau, E. W.-G.; Zewail, A. H. *Angew. Chem. Int. Ed*. **2000**, *39*, 260.

(26) (a) Shah, B. K.; Rodgers, M. A. J.; Neckers, D. C. *J. Phys. Chem. A* **2004**, *108*, 6087. (b) McGarry, P. F.; Doubleday, C. E., Jr.; Wu, C.-H.; Staab, H. A.; Turro, N. J. *J. Photochem. Photobiol. A* **1994**, *77*, 109.

(27) The participation of the $T_2(\pi,\pi^*)$ state during Norrish type I and II reactions has been recently demonstrated by CASSCF calculation. He, H.-Y.; Fang, W.-H.; Philips, D. L. *J. Phys. Chem. A* **2004**, *108*, 5386.

(28) Wagner, P. J.; Giri, B. P.; Scaiano, J. C.; Ward, D. L.; Gabe, E.; Lee, F. E. *J. Am. Chem. Soc*. **1985**, *107*, 5490.

(29) (a) Sreedhara Rao, V.; Chandra, A. K. *Chem. Phys.* **1997**, *214*, 103. (b) Al-Soufi, W.; Eychmüller, A.; Grellmann, K. H. *J. Phys. Chem.* **1991**, *95*, 2022.

(30) Scaiano, J. C. *Tetrahedron* **1982**, *38*, 819.

(31) (a) Salem, L.; Rowland, C. *Angew. Chem., Int. Ed. Engl.* **1972**, *11*, 92. (b) Caldwell, R. A. *Pure Appl. Chem.* **1984**, *56*, 1167. The conjugation effect occurring during the biradical decay can be explained in the following terms: Increased delocalization should increase the average distance between the unpaired electrons of the biradical, thus lowering their spin-orbit coupling and consequently decreasing the yield of the ISC process responsible for the decay.

(32) Caldwell, R. A.; Majima, T.; Pac, C. *J. Am. Chem. Soc*. **1982**, *104*, 629.

© 2016 Tous droits réservés.

doc.univ-lille1.fr

Annexe 5. JACS.Aloïse et al,132,7379-7390,2010

JACS ARTICLES

Published on Web 05/10/2010

Bridged Photochromic Diarylethenes Investigated by Ultrafast Absorption Spectroscopy: Evidence for Two Distinct Photocyclization Pathways

Stéphane Aloïse,*,† Michel Sliwa,† Zuzanna Pawlowska,† Julien Réhault,†,|| Julien Dubois,† Olivier Poizat,† Guy Buntinx,† Aurélie Perrier,*,‡ François Maurel,‡ Shouhei Yamaguchi,§ and Michinori Takeshita§

Laboratoire de Spectrochimie Infrarouge et Raman (UMR 8516 du CNRS), Centre d'études et de recherches Lasers et Applications (FR 2416 du CNRS), Université des Sciences et Technologies de Lille, Bat C5, 59655 Villeneuve d'Ascq Cedex, France, Laboratoire Interfaces, Traitements, Organisation et Dynamique des Systèmes (ITODYS), CNRS UMR 7086, Université Paris 7 - Paris Diderot, Bâtiment Lavoisier, 15 rue Jean Antoine de Baif, 75205 Paris Cedex 13, France, and Department of Chemistry and Applied Chemistry, Faculty of Science and Engineering, Saga University, Honjo1, Saga 840-8502, Japan

Received December 22, 2009; E-mail: stephane.aloise@univ-lille1.fr; aurelie.perrier-pineau@univ-paris-diderot.fr

Abstract: Two photochromic diarylethenes blocked by alkyl bridges in an ideal conformation for photocyclization are studied by stationary and femtosecond transient spectroscopy in order to depict the photocyclization processes: the bistable 1,2-dicyano[2.*n*]metacyclophan-1-ene with $n = 2$, abbreviated as [2.2], and its non-bistable analogue with $n = 4$, abbreviated as [2.4]. The data are interpreted in the light of AM1-CIS calculations and state correlation diagrams based on conclusive TD-DFT calculations. For [2.2], a solvent-sensitive excitation wavelength threshold governing the photocyclization yield is clearly evidenced between the S_1 and S_2 singlet states. Excitation above and beyond this threshold induces two distinct photochemical pathways. The S_1 vertical excitation induces direct efficient ($\phi \approx 0.9-1$), and ultrafast ($\sim$120 fs) photocylization from S_1 open form that leads to a ground-state transition structure, probably through a conical intersection, then to a hot cyclized ground state that relaxes by vibrational cooling. Upon higher excitation energy, the system undergoes internal conversion to the hot S_1 state, then evolves toward the cyclized S_1 state and relaxes by ultrafast S_1-S_0 internal conversion. Alternatively, the possibility for a second conical intersection near hot S_1 state is discussed. This second photoclosure reaction is less efficient and both the photocylization yield and overall kinetics depend on solvent polarity ($\phi = 0.49$, $\tau = 2.5$ ps in nonpolar solvent; $\phi = 0.7$, $\tau = 1.5$ ps in polar solvent). In the case of [2.4], for which the distance between the two reactive carbons is larger, a unique photoclosure mechanism is found and a structural effect is reported. Indeed, this mechanim is similar to the above second reaction of [2.2] but characterized by much slower kinetics ranging from 12 to 20 ps (depending on the excitation wavelength and solvent polarity). All polarity effects are rationalized in terms of stabilization of the transient states of charge-transfer character involved in the photocyclization process.

1. Introduction

Photochromism is a photoinduced reversible transformation between two chemical forms having different absorption spectra.[1] This reaction is of great importance due to its actual implications for the development of photomemory and photoswitching materials.[1] Among all photochromic families, diarylethenes are some of the most efficient compounds used for photoswitching applications because of their thermal irreversibility, high fatigue resistance, and good photoconversion yield between an open form (OF) and a closed form (CF).[2a] For those reasons, numerous recent advances based on diarylethene photochemistry have been reported.[2b] However, the photocyclization (OF→CF) yield, a fundamental photochemical parameter for applications, is seriously limited in classical diarylethenes by the existence of two OF conformers having anti and syn configurations and among which only the former is photoactive.[1,2] An attractive approach to overcome this limitation is to lock the molecule in an ideal conformation by incorporating a rigid link. Recently, Takeshita et al. succeeded

† Université des Sciences et Technologies de Lille.
‡ Université Paris 7 - Paris Diderot.
§ Saga University.
|| Current address: Universität Zürich Physikalisch Chemisches Institut Winterthurerstrasse 190 CH-8057 Zürich.

(1) Bouas-Laurent, H.; Dürr, H. *Photochromism*; Elsevier Science B.V.: Amsterdam, 2003.

(2) (a) Irie, M. *Chem. Rev.* **2000**, *100*, 1685. (b) Tsuboi, Y.; Shimizu, R.; Shoji, T.; Kitamura, N. *J. Am. Chem. Soc.* **2009**, *131*, 12623. (c) Al-Atar, U.; Fernandes, R.; Johnsen, B.; Baillie, D.; Branda, N. R. *J. Am. Chem. Soc.* **2009**, *131*, 15966. (d) Morimoto, M.; Miyasaka, H.; Yamashita, M.; Irie, M. *J. Am. Chem. Soc.* **2009**, *131*, 9823. (e) Wing-Wah Yam, V.; Ka-Wai Lee, J.; Ko, C. C.; Nianyong, Z. *J. Am. Chem. Soc.* **2009**, *131*, 912.

10.1021/ja910813x © 2010 American Chemical Society

© 2016 Tous droits réservés.

doc.univ-lille1.fr

HDR de Stéphane Aloïse, Lille 1, 2016

Chart 1

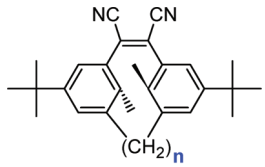

n= 2 [2.2]

n=4 [2.4]

in performing such challenging synthesis of a series of metacyclophan-1-ene photochromic compounds in which the two reacting aryl groups are maintained in an antiparallel conformation by the presence of an additional alkyl bridge of variable length *n* (see Chart 1).[3]

Interest in these bridged compounds was stimulated by preliminary results.[3] First, it was shown that the thermal stability of the metacyclophan-1-ene CF can be varied by changing the length of the alkyl bridge.[3] Then, an improvement for the photocyclization yield was reached but not as significant as could be expected.[3] In order to understand the reason for this moderate improvement and the parameters controlling the photoswitching efficiency, we have undertaken a thorough investigation of the photochemical reactivity of representative bridged diarylethenes by ultrafast pump−probe spectroscopy and quantum chemical calculations.

In this paper, we focus our attention on two specific bridged photochromic compounds among those previously studied,[3] the 1,2-dicyano[2.*n*]metacyclophan-1-enes with alkyl chain lengths $n = 2$ and 4, abbreviated as [2.2] and [2.4], respectively (Chart 1): [2.2] is a bistable photochromic compound since the thermal back reaction is very slow (CF lifetime of the order of 50 days at 273 K).[3] A total recovery of the starting OF material can be readily achieved by visible light irradiation without any significant photodegradation.[3] As already mentioned, the improvement of the photocyclization yield has reached only a few percent: $\phi_{OF\rightarrow CF} = 0.39$ for [2.2] vs 0.35 for the unconstrained analogue (upon 313 nm excitation in nonpolar solvent).[3] In contrast, [2.4] is not stable in the CF and undergoes thermal back reaction to the OF so rapidly that the spectral characterization of the CF by stationary spectroscopy is not possible even at low temperature.[3] As a consequence, its photocyclization yield cannot not be determined.

Concerning the photochemistry of unconstrained diarylethenes, it has been established that the fundamental processes occur on a picosecond time scale, photoopening reaction (CF→OF) occurring in more than 10 ps and photocyclization in a faster 1 − 10 ps time domain, depending on the molecular structure.[4−10,13] Note that for this latter process, direct identification of CF precursor by transient spectroscopy has never been achieved due to the lack of isosbestic points related to its formation. Alternatively, theoretical investigations including CASSCF calculations have attempted to describe the overall photochemical pathway. These studies concluded, for model diarylethenes, the participation of S_0/S_1 conical intersections in the photocyclization process,[14−16] a result often generalized to most of the diarylethenes. However, recent experimental studies pointed out the fact that the knowledge of the S_1 photochemical pathway was not sufficient anymore to fully understand the photoreversion and photocyclization reactions of the diarylethene family. Indeed, investigating the ring-opening reactions, Miyasaka et al. demonstrated that the photoreversion yield can be enhanced through multiphoton absorption, which suggests that the photoconversion process could be more efficient in higher singlet states S_n than in the S_1 state via one-photon absorption.[17] However, such additional S_n photoactive pathways are not yet characterized. Fukaminato et al. recently performed photocyclization yield measurements as a function of the excitation wavelength and observed a threshold wavelength effect that they explain in terms of distinct singlet and triplet photoreactivity.[18] Additionally, Irie et al. discovered the possibility to tune the photochromic yields by changing the polarity of the solvent through charge-transfer (CT) excited-state conformations.[19]

By analogy with unbridged diarylethenes and with particular attention to the photoinduced ring-closure process in [2.2] and [2.4], we performed photocyclization yield measurements, subpicosecond time-resolved absorption experiments for various excitation wavelengths and for various solvents. We discovered important effects that might be of fundamental importance for the photochromism's community: (i) constraining the diarylethene with an alkyl bridge opens two distinct photochemical channels (Kasha's rule violations) that lead to the same colored form; (ii) the branching ratio between the two channels would be dependent on the solvent polarity; (iii) faster (few hundred

(3) (a) Takeshita, M.; Yamato, T. *Tetrahedron Lett.* **2001**, *42*, 4345. (b) Takeshita, M.; Inoue, M.; Hisasue, H.; Maekawa, S.; Nakamura, T. *J. Phys. Org. Chem.* **2007**, *20*, 830.
(4) Tamai, N.; Saika, T.; Shimidzu, T.; Irie, M. *J. Phys. Chem.* **1996**, *100*, 4689.
(5) Owrutsky, J. C.; Nelson, H. H.; Baronavski, A. P.; Kim, O. K.; Tsivgoulis, G. M.; Gilat, S. L.; Lehn, J.-M. *Chem. Phys. Lett.* **1998**, *293*, 555.
(6) (a) Hania, P. R.; Telesca, R.; Lucas, L. N.; Pugzlys, A.; Van Esch, J. H.; Feringa, B. L.; Snijders, J. G.; Duppen, K. *J. Phys. Chem. A* **2002**, *106*, 8498. (b) Hania, P. R.; Pugzlys, A.; Lucas, L. N.; De Jong, J. J. D.; Telesca, R.; Feringa, B. L.; Van Esch, J. H.; Duppen, K. *J. Phys. Chem. A* **2005**, *109*, 9437.
(7) (a) Miyasaka, H.; Nobuto, T.; Itaya, A.; Tamai, N.; Irie, M. *Chem. Phys. Lett.* **1997**, *269*, 281. (b) Miyasaka, H.; Nobuto, T.; Murakami, M.; Itaya, A.; Tamai, N.; Irie, M. *J. Phys. Chem. A* **2002**, *106*, 8096.
(8) Okabe, C.; Nakabayashi, T.; Nishi, N.; Fukaminato, T.; Kawai, T.; Irie, M.; Sekiya, H. *J. Phys. Chem. A* **2003**, *107*, 5384.
(9) Shim, S.; Eom, I.; Joo, T.; Kim, E.; Kim, K. S. *J. Phys. Chem. A* **2007**, *111*, 8096.
(10) Ern, J.; Bens, A. T.; Martin, H.-D.; Mukamel, S.; Schmid, D.; Tretiak, S.; Tsiper, E.; Kryschi, C. *J. Lumin.* **2000**, *87−89*, 742.
(11) (a) Ern, J.; Bens, A. T.; Bock, A.; Martin, H.-D.; Kryschi, C. *J. Lumin.* **1998**, *76−77*, 90. (b) Ern, J.; Bens, A. T.; Martin, H.-D.; Mukamel, S.; Schmid, D.; Tretiak, S.; Tsiper, E.; Kryschi, C. *Chem. Phys.* **1999**, *246*, 115.
(12) Shim, S.; Joo, T.; Bae, S. C.; Kim, K. S.; Kim, E. *J. Phys. Chem. A* **2003**, *107*, 8106.
(13) Bens, A. T.; Ern, J.; Kuldova, K.; Trommsdorff, H. P.; Kryschi, C. *J. Lumin.* **2001**, *94−95*, 51.
(14) Nakamura, S.; Irie, M. *J. Org. Chem.* **1988**, *53*, 6136.
(15) Boggio-Pasqua, M.; Ravaglia, M.; Bearpark, M. J.; Garavelli, M.; Robb, M. A. *J. Phys. Chem. A* **2003**, *107*, 11139.
(16) (a) Asano, Y.; Murakami, A.; Kobayashi, T.; Goldberg, A.; Guillaumont, D.; Yabushita, S.; Irie, M.; Nakamura, S. *J. Am. Chem. Soc.* **2004**, *126*, 12112. (b) Nakamura, S.; Kobayashi, T.; Takata, A.; Uchida, K.; Asano, Y.; Murakami, A.; Goldberg, A.; Guillaumont, D.; Yokojima, S.; Koatake, S.; Irie, M. *J. Phys. Org. Chem.* **2007**, *20*, 821. (c) Uchida, K.; Guillaumont, D.; Tsuchida, E.; Mochizuki, G.; Irie, M.; Murakami, A.; Nakamura, S. *THEOCHEM* **2002**, *579*, 115.
(17) (a) Miyasaka, H.; Murakami, M.; Itaya, A.; Guillaumont, D.; Nakamura, S.; Irie, M. *J. Am. Chem. Soc.* **2001**, *123*, 753. (b) Miyasaka, H.; Murakami, M.; Okada, T.; Nagata, Y.; Itaya, A.; Kobatake, S.; Nakamura, S.; Irie, M. *Chem. Phys. Lett.* **2003**, *371*, 40. (c) Ishibashi, Y.; Tani, K.; Miyasaka, H.; Kobatake, S.; Irie, M. *Chem. Phys. Lett.* **2007**, *437*, 243. (d) Tani, K.; Ishibashi, Y.; Miyasaka, H.; Kobatake, S.; Irie, M. *J. Phys. Chem. C* **2008**, *112*, 11150.
(18) Fukaminato, T.; Doi, T.; Tanaka, M.; Irie, M. *J. Phys. Chem. C* **2009**, *113*, 11623.
(19) Irie, M.; Sayo, K. *J. Phys. Chem.* **1992**, *96*, 7671.

© 2016 Tous droits réservés.

doc.univ-lille1.fr

HDR de Stéphane Aloïse, Lille 1, 2016

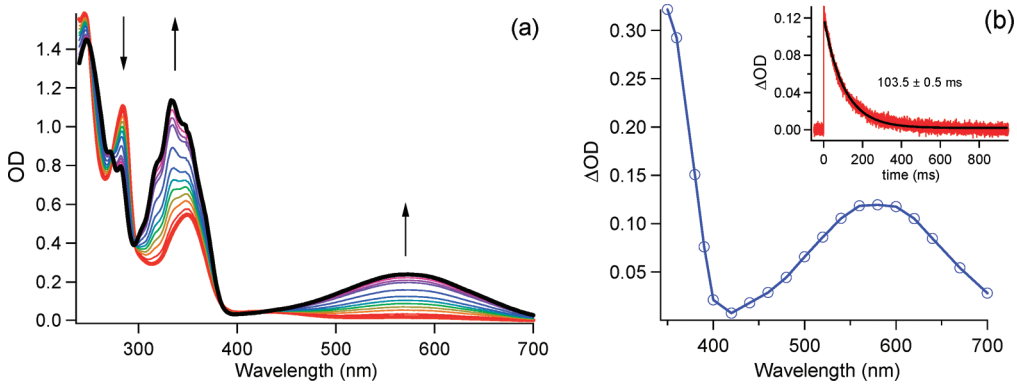

Figure 1. (a) Absorption spectra of [2.2] in acetonitrile under continuous UV irradiation acquired every 1 min; the arrows indicate the temporal evolution. (b) Transient absorption spectrum of [2.4] in acetonitrile (20 μs delay time) under 355 nm laser excitation. The inset shows the decay of the 595 nm absorption band.

femtoseconds) processes are found compared with unbridged diarylethenes; (iv) depending on the excitation wavelength and solvent polarity, the photocylization quantum yield can be optimized for appropriate conditions. In the following, we will demonstrate with the help of theoretical calculations that all these findings can be interpreted in terms of two distinct photochromic singlet pathways, and we believe that such results would be of extended importance for the general understanding of diarylethene molecules and related applications.

2. Experimental and Theoretical Methods

The syntheses of [2.2] and [2.4] are published elsewhere.[3] Typical sample concentrations used in time-resolved experiments were 5×10^{-4} M. The Sigma-Aldrich acetonitrile (ACN), hexane (HX), and ethanol (EtOH) solvents were used as received, and spectroscopic measurements were performed in pure ACN and mixed solvents (HX/EtOH 12:1).

2.1. Spectroscopic Measurements. Stationary absorption was recorded with a CARY-100B Bio absorption spectrometer. Two different experiments were performed for the bistable [2.2] molecule to evaluate its photocoloration yield (for [2.4] see below). First, the photocoloration yield ϕ(313 nm) was determined according to a standard procedure using the 313 nm line of a Mercury lamp and bis(2-methyl-1-benzothien-3-yl)hexafluorocyclopentene as reference molecule.[20] Additionally, the photocoloration yields at various wavelengths were performed using an ORIEL Xe lamp (1000 W) equipped with a monochromator. In order to correlate these measurements with previous ones, all data ϕ (λ) were normalized with respect to the 313 nm excitation wavelength measurement according to

$$\phi(\lambda) = \frac{I_0(313\text{ nm})}{I_0(\lambda)} \times \frac{1 - 10^{-A_{OF}(313\text{ nm})}}{1 - 10^{-A_{OF}(\lambda)}} \times \frac{(\dot{A}_{CF})_\lambda}{(\dot{A}_{CF})_{313\text{ nm}}} \phi(313\text{ nm}) \quad (1)$$

where I_0 denotes the incident light power, A_{OF} is the open form absorbance at irradiation wavelength λ, and $\dot{A}_{CF} = dA_{CF}/dt$ is determined by fitting with linear slope the time evolution of the closed form absorption maximum under continuous irradiation, i.e., $A_{CF} = f(t)$ (see Figure 1). Only the first 30 min was acquired in order to avoid exponential curvatures.

The nanosecond laser (Nd:YAG)-flash photolysis apparatus used for the determination of the [2.4] back-thermal reaction and photocoloration yields ratio has been described elsewhere.[22] The measurements consist of acquiring the kinetics of appearance of CF either for 266/355 nm excitations in a given solvent or for a given excitation in different solvents and then computing the intensity ratio after normalizing all data according to the benzophenone triplet reference signal.

The pump−probe subpicosecond absorption experiments were carried out using an amplified Ti:sapphire laser (BM Industries) delivering 0.8 mJ and 80 fs pulses tunable between 766 and 800 nm with a repetition rate of 1 kHz.[22] The 390 nm pump pulses were obtained by frequency doubling the fundamental at 780 nm, while the 266 nm pump pulses were obtained by frequency tripling the fundamental at 800 nm. About 3 mJ·cm^{-2} was provided by the pump in both cases. The probe beam was generated by focusing 1 μJ of the fundamental on a 1 mm CaF_2 plate giving a white light continuum with a spectrum covering the UV−vis and near IR range. The probe beam was split into signal and reference beams before crossing the sample, and the resulting beams were recorded on two different channels of a multichannel spectrograph equipped with a CCD camera. Transient absorbance was obtained by comparing signal and reference spectra for different time delays. The time delay between the pump and probe was varied up to 1.5 ns (using a micrometric optical delay line), and the temporal resolution of the apparatus was better than 300 fs. All of the transient traces presented in this paper are GVD corrected according to the typical extrapolation method.[21] Furthermore, the characteristic times deduced from kinetics are obtained by fitting the uncorrected data with the result of a multiexponential function convolved with a Gaussian pulse (which approximates the pump−probe correlation function) and taking into account GVD and OD due to thickness of the sample (see eq 16 of ref 21).[21] Pump and probe beams, with relative linear polarizations set at the magic angle, were focused in a 2 mm flow cell equipped with CaF_2 windows. Note that an additional Xe lamp with green filter is continuously lighting the sample reservoir for a maximum regeneration of the OF species after its conversion into the CF by the action of the laser pump excitation.

2.2. Theoretical Calculations. The spectral properties of [2.2] and [2.4] were simulated following a three-step methodology[23a] based on density functional theory (DFT) and time-dependent DFT (TD-DFT): (i) the ground-state geometry of each structure was optimized without symmetry constraints in the gas phase with DFT; (ii) the vibrational spectrum is computed at the same level of theory to confirm that the optimized structures correspond to true minima

(20) Uchida, K.; Tsuchida, E; Aoi, Y.; Nakamura, S.; Irie, M. *Chem. Lett.* **1999**, *28*, 63.

(21) (a) Nakayama, T.; Amijima, Y.; Ibuki, K.; Hamanoue, K. *Rev. Sci. Instrum.* **1997**, *68*, 4364. (b) Ziőlek, M.; Lorenc, M.; Naskręcki, R. *Appl. Phys. B: Laser Opt.* **2001**, *72*, 843.

(22) Aloïse, S.; Réhault, J.; Moine, B.; Poizat, O.; Buntinx, G.; Lokshin, V.; Valès, M.; Samat, A. *J. Phys. Chem. A* **2007**, *111*, 1737.

(23) (a) Jacquemin, D.; Perpète, E. A.; Ciofini, I.; Adamo, C. *Acc. Chem. Res.* **2009**, *42*, 326. (b) Maurel, F.; Perrier, A.; Perpète, E. A.; Jacquemin, D. *J. Photochem. Photobiol. A* **2008**, *199*, 211.

© 2016 Tous droits réservés.

doc.univ-lille1.fr

HDR de Stéphane Aloïse, Lille 1, 2016

on the potential energy surface; and (iii) the vertical transition energies to the excited states are computed with TD-DFT. All calculations were performed using the Gaussian 03 package.[24]

For steps i and ii, we have used the 6-311G(d) triple-ξ polarized basis set, while for step iii, the more extended 6-311+G(d) basis set has been used to obtain converged transition energies. For the geometry optimizations, we have used the PBE0 functional[25] that provides accurate ground-state structure for most organic systems and particularly for photochromic molecules.[23] For TD-DFT calculations, four hybrid functions with different percentages of exact exchange were tested: B3LYP (20% of exact exchange),[25a] PBE0 (25%),[25b] BMK (42%),[25c] and BHandHLYP (50%).[25d] For vertical transition energy calculations, solvent effects were introduced by using the polarizable continuum model (PCM).[26] Most of the theoretical results are reported in the Supporting Information. Table SI1 (Supporting Information) lists the wavelengths computed for the first transitions of [2.2] and [2.4] open-ring isomers with B3LYP, PBE0, BMK, and BHandHLYP functionals. These four functionals actually provide the same qualitative results. Quantitatively, if we focus on the intense $S_0 \rightarrow S_2$ transition, the excitation wavelength calculated with the BMK functional is in closer agreement with experimental results (absolute error of 0.13 eV for [2.2] and 0.03 eV for [2.4]). Consequently, in the following text we will stick to the PCM-TD-BMK/6-311+G(d)//PBE0/6-311G(d) calculation scheme.

To investigate the ring-closure/ring-opening mechanism, we should determine some characteristic properties of the ground state as well as the excited-state potential energy surfaces (PES). The description of the excited states PES at the ab initio level requires the use of a multiconfigurational self-consistent field (MC-SCF) method such as the complete active-space SCF (CASSCF) approach. Unfortunately, the correct description of the excited states of the considered molecule requires CASSCF calculations involving the distribution of 18 π electrons in 18 π orbitals (18e, 18o), which is not feasible at the present time for such a large system. Calculations with a reduced (14e, 14o) active space, excluding the cyano groups, have led to significant differences in the frontier orbitals delocalization and in the nature of the excited singlet states. This underlies the crucial role of CN substituents on the excited state properties of [2.2] and [2.4]. Alternatively, semiempirical calculations using configuration interaction (CI) have proven to be useful to obtain the approximate wave function and molecular geometry of the electronic excited states.[27] Therefore, the semiempirical configuration interaction using all possible single excitations (AM1-CIS) available in the AMPAC 8.0 package[28] was used for the optimization of the excited states. All singly excited configurations involving the nine highest occupied and nine lowest unoccupied orbitals, which correspond to the π and π^* orbitals, were included in the CIS expansion. The reliability of the AM1-CIS method has been extensively tested for conjugated molecules: this method was shown to reproduce qualitatively the geometry of ground and excited states.[29] For spectroscopic results, Tables SI1 and SI2 (Supporting Information) show that the vertical energy transitions of the low-lying excited states (S_1 and S_2) are in good agreement with TD-DFT calculations and experiments. For [2.2] (respectively [2.4]), TD-DFT calculations underestimate the $S_0 \rightarrow S_1$ transition by −0.19 eV (−0.05 eV), while CIS overestimates this transition by 0.31 eV (0.41 eV). For the $S_0 \rightarrow S_2$ excitation, TD-DFT provides a signed error of +0.13 eV for [2.2] (−0.03 eV for [2.4]), while CIS is in close agreement with experiment (−0.04 eV for [2.2] and 0.0 eV for [2.4]). In the latter case, the exceptional agreement between CIS and experimental features certainly partially originates in error cancellation. An inspection of the molecular orbitals has shown that excitations calculated at the CIS level imply the same orbitals as TD-DFT calculations. Nevertheless, the oscillator strengths calculated at the semiempirical level are in discrepancy with TD-DFT and experiments: the CIS $S_0 \rightarrow S_1$ transition is predicted to be more intense than the $S_0 \rightarrow S_2$ transition. For the higher energetic states (S_3 to S_5), comparison between CIS calculations and experimental features is no longer straightforward. AM1-CIS calculations will thus be used to investigate the geometries and energetic profiles of the S_1 and S_2 low-lying excited states, and particular precaution will be taken concerning the predicted oscillator strength.

Table 1. Spectrokinetic Properties and Photochromic Quantum Yields (Absolute and Relative Values) for [2.2] and [2.4] in ACN and HX/EtOH (12:1)

		λ_{max} (nm)		ϕ(OF→CF)			
		OF	CF	$\lambda = 313$ nm	$\lambda > 400$ nm	ratio ϕ	τ_Δ (ms)
[2.2]	HX/CH_2Cl_2 9:1	340[a]	555[a]	0.39[a]			
	HX/EtOH 12:1	345	560	0.49	0.9	0.71−0.90[b]	
	ACN	350	575	0.69	1		
[2.4]	HX/EtOH 12:1	330	575			0.93[c]	62.5
	ACN	335	595				103.5

[a] Reference 3. [b] Ratio = ϕ(HX/EtOH 12:1)/ϕ(ACN), computed from absolute values. [c] From laser flash photolysis measurement at 355 nm excitation.

Scheme 1

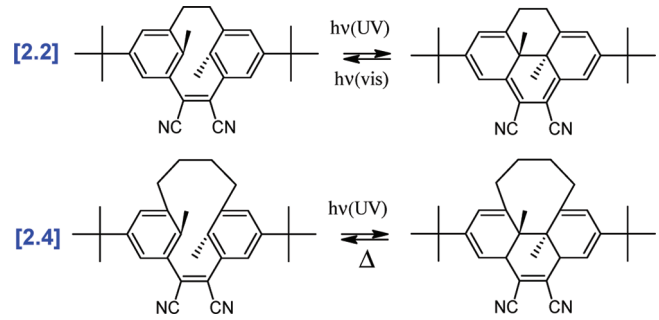

3. Results

3.1. OF and CF Spectrokinetic Characterizations. Upon UV irradiation, a colorless solution of [2.2] in either acetonitrile or HX/EtOH (12:1) becomes rapidly purple. All spectrokinetic data are tabulated for both solvents in Table 1. For the ACN case, Figure 1a shows the evolution of the UV−vis absorption spectra of [2.2] under continuous broad band UV excitation during 15 min.

The initial spectrum, recorded before irradiation, shows a band at 350 nm typical of the uncolored OF. Then a gradual evolution is seen with irradiation time: this modification is characterized by two isosbestic points at 274 and 297 nm and is related to the photochromic photocyclization (Scheme 1) between OF and CF, the latter species being well recognized with the new visible absorption band maximizing at 570 nm (note also a sharp UV band with vibrational structure peaking at 325, 335, and 345

(24) *Gaussian 03, Revision C.02*. Frisch, M. J. et al. Gaussian, Inc., Wallingford, CT, 2004.
(25) (a) Becke, A. D. *J. Chem. Phys.* **1993**, *98*, 5648. (b) Adamo, C.; Barone, V. *J. Chem. Phys.* **1999**, *110*, 6158. (c) Boese, A. D.; Martin, J. M. L. *J. Chem. Phys.* **2004**, *121*, 3405. (d) Becke, A. D. *J. Chem. Phys.* **1993**, *98*, 1372.
(26) Tomasi, J.; Mennucci, B.; Cammi, R. *Chem. Rev.* **2005**, *105*, 2999.
(27) Maurel, F.; Aubard, J.; Millie, P.; Dognon, J. P.; Rajzmann, M.; Guglielmetti, R.; Samat, A. *J. Phys. Chem. A* **2006**, *110*, 4759.
(28) AMPAC 8, 1992−2004 Semichem, Inc., PO Box 1649, Shawnee, KS 66222.
(29) (a) Agmon, N.; Rettig, W.; Groth, C. *J. Am. Chem. Soc.* **2002**, *124*, 1089. (b) Gedeck, P.; Schneider, S. *J. Photochem. Photobiol. A: Chem* **1999**, *121*, 7. (c) Lambert, C.; Risko, C.; Coropceanu, V.; Schelter, J.; Amthor, S.; Gruhn, N.; Durivage, J.; Bredas, J. L. *J. Am. Chem. Soc.* **2005**, *127*, 8508.

© 2016 Tous droits réservés.

doc.univ-lille1.fr

HDR de Stéphane Aloïse, Lille 1, 2016

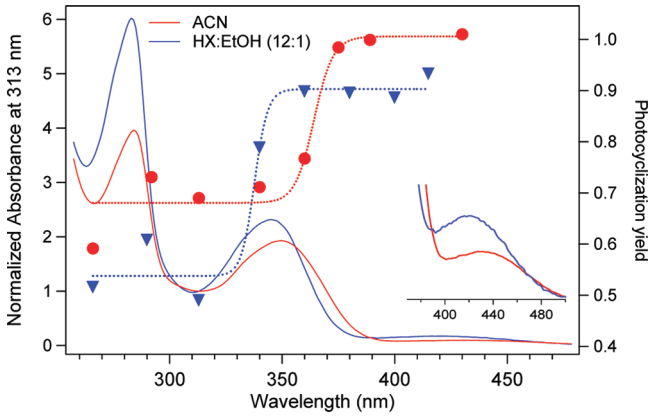

Figure 2. Photocoloration quantum yields of [2.2] for different excitation wavelengths in ACN and (HX/EtOH 12:1). The absorption spectrum of [2.2] is also included (inset: spectra × 20). The sigmoid functions (dashed lines) are purely illustrative.

nm). In the less polar solvent, a moderate hypsochromic effect is noticed for both OF and CF (see Table 1). Additionally, a hyperchromic effect is observed for OF (see Figure 2) but not for CF (not shown).

In the case of [2.4], it was not possible to follow the time evolution of the absorption spectrum by the above procedure due to too fast thermal back-reaction, and nanosecond flash photolysis measurements were performed consequently. Figure 1b shows the presence of a photoinduced broad transient visible absorption band peaking at ca. 595 nm in ACN that can be likely ascribed to the CF of [2.4] by analogy with the 570 nm stationary absorption band of [2.2]. In HX/EtOH (12:1), a similar hypsochromic effect is observed for OF and CF, as seen in Table 1, while in regard to the intensity spectra, a hyperchromic effect is also obtained for OF but not CF. A solvent polarity effect is found also for the lifetime of [2.4] CF at ambient temperature, which decreases from 103.5 ms in ACN to 62.5 ms in HX/EtOH (12:1).

3.2. Wavelength- and Polarity-Dependent Photocoloration Yields. Because CT character appears preeminent from stationary data, new photocoloration yield measurements upon 313 nm excitation were achieved for [2.2] in both ACN and HX/EtOH (12:1). As shown in Table 1, the new photocoloration yield increases with the solvent polarity from 0.49 in HX/EtOH (12:1) to 0.69 in ACN. To gain more information on the fundamental photochromic processes, the photocoloration yield measurements were extended to different excitation wavelengths between 266 and 430 nm in both solvents (Figure 2). Striking effects are clearly detected. Indeed, in ACN, the photocoloration yield suddenly raises from a value of about 0.7 in the UV region to a value of 1 at excitation wavelengths longer than a threshold value around 360 nm. In the less polar solvent, this threshold wavelength is lowered (around 330 nm) and the photocoloration yield variation is larger, increasing from 0.5 below the threshold to 0.9 beyond it. Note that those effects are nicely parallel to the hyperchromic trend found for OF.

Trying to study in more detail the excitation wavelength dependency in [2.4] was tricky due to the nonaccordability of our laser source. Measurements at 355 and 266 nm excitation, using benzophenone as actinometer, allowed us to assess a ratio $\phi(355)/\phi(266) = 0.93$, indicating that, unlike [2.2], no significant excitation wavelength effect characterizes [2.4]. To investigate the solvent effect, time-resolved measurements were realized in HX/EtOH (12:1) and ACN. A photocoloration yield ratio of

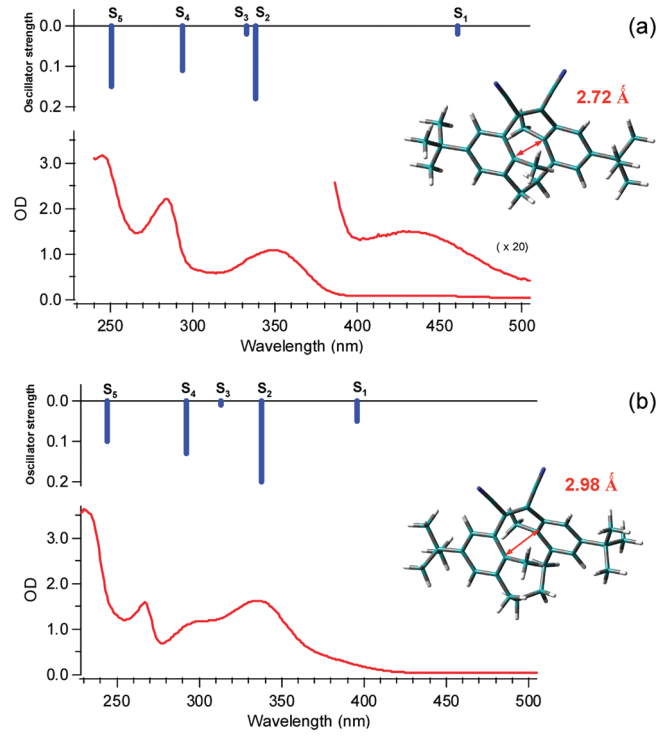

Figure 3. Absorption spectra of the open form of [2.2] (a) and [2.4] (b) in acetonitrile (red curve) together with TD-DFT excitation energies and oscillator strength (bold blue sticks). Theoretical DFT geometries are included indicating the increasing distance between the two reactive carbons (r_{cc}).

0.94 was determined, pointing out some lack of solvent polarity influence on the photocyclization process in [2.4].

3.3. OF and CF Theoretical Characterizations. From a structural point of view, the OF-optimized DFT geometries, included in Figure 3, underline the notable difference for the distance between the two reactive carbons in the ground state: 2.72 Å for [2.2] vs 2.98 Å for [2.4]. One can also notice that, from [2.2] to [2.4], the torsion between the two sides of the molecule (see Table SI3, Supporting Information) increases, leading to a conjugation loss. In contrast, no such differences are found for the CF geometries (see Table SI3, Supporting Information) with both reactive carbon distances close to 1.57 Å. Consequently, comparing the photophysics of the two molecules (see below), structural effects are mostly expected for the OF species.

The TD-DFT-computed wavelengths and oscillator strengths for [2.2] and [2.4] open forms in acetonitrile are compared to experimental spectra as shown in Figure 3 (see also Table SI1 (Supporting Information), where electronic transition attributions are also given). The noticeable agreement between experiments and calculations enables us to attribute with confidence the [2.2] and [2.4] absorption spectra to transitions from the S_1 up to the S_5 singlet excited state.

Influence of Alkyl Bridge Length on OF Absorption Spectra. On going from [2.2] to [2.4], a hypsochromic shift (−40 nm in ACN) is observed for the $S_0 \rightarrow S_1$ transition while the $S_0 \rightarrow S_2$ and $S_0 \rightarrow S_3$ bands, which cannot be distinguished for [2.2], are separated for [2.4] with a wavelength difference of 38 nm in ACN. These two structural effects can be explained by an inspection of the molecular orbitals involved in the electronic excitations. Indeed, in [2.2] and [2.4], the OF first excited state, S_1^{FC}(OF), corresponds to a charge transfer (CT)

© 2016 Tous droits réservés.

doc.univ-lille1.fr

HDR de Stéphane Aloïse, Lille 1, 2016

Chart 2. HOMO and LUMO Orbitals (BMK/6-311G(d), Contour Threshold of 0.03 au)

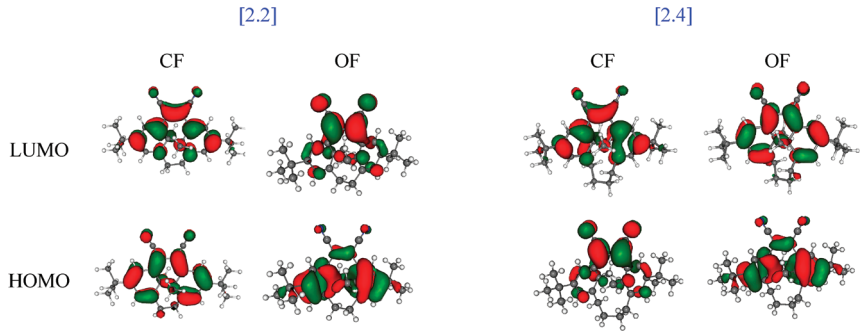

from the HOMO, essentially localized on the central double bond, to the LUMO, rather involving the cyano substituents. The latter can be assumed to be quite insensitive to alkyl bridge modifications, while the HOMO shows an antibonding character between the two reactive carbons and will thus be stabilized by a longer distance. As a consequence, from [2.2] to [2.4], the HOMO stabilization combined with the LUMO insensitivity leads to an increase of the HOMO−LUMO gap and thus to a hypsochromic effect for the HOMO→LUMO transition. Additionally, the strong structural effect found for the $S_0 \rightarrow S_3$ (HOMO-2→LUMO) transition energy is likely rationalized by observing the HOMO-2 orbital (see Table SI4, Supporting Information). For [2.2], this orbital presents a strong and unexpected contribution of the σ alkyl bridge orbital which leads to an antibonding interaction between the σ and π systems. For [2,4], the larger distance between the two reactive carbons lessens this antibonding interaction and stabilizes the HOMO-2 orbital. Therefore, the σ/π coupling yields an increase of the HOMO-2/LUMO gap, the corresponding electronic transition is tuned toward smaller wavelength, and the S_2-S_3 states are split up.

Solvent Polarity Effects on OF and CF Absorption Spectra. The hypsochromic solvent effect that shifts the OF absorption bands with increasing solvent polarity (Figure 2) can be well predicted by TD-DFT calculations (Table SI1, Supporting Information). For instance, for the S_0 (HOMO)→S_1 (LUMO) transition of [2.2] ([2.4]), calculations foresee a hypsochromic shift of −26 nm (−20 nm) in agreement with the −10 nm (−10 nm) displacement experimentally observed. This effect results from the stabilization of the LUMO by polar solvents, which thus reduces the HOMO−LUMO gap. The same conclusion holds for the S_2 state which corresponds, for both [2.2] and [2.4], to an electron promotion from the HOMO-1, centered on the photochromic core, to the LUMO. The hyperchomic effect on intensity is likely related with the strong CT character for the OF as indicated on Table 3.

For both CF molecules (Table SI2, Supporting Information), the visible band can be assigned to the S_0 (HOMO)→S_1 π,π^* (LUMO) transition while the UV band near 350 nm is ascribed to the S_0 (HOMO)→S_3 (LUMO+1) transition. These frontier orbitals are delocalized on the photochromic unit with small contributions of the cyano groups, accounting for the moderate solvatochromic effect experimentally observed.

3.4. Subpicosecond Transient Absorption Measurements at Different Excitation Wavelengths. To better understand the photocyclization process, time-resolved experiments were performed both below and beyond the characteristic threshold of [2.2], using 266 and 390 nm excitations. For comparison, similar transient measurements were performed for [2.4]. According to the assignment of the absorption spectra established above (Figure 3b), the 266 and 390 nm excitations are respectively expected to populate up to the S_5 and S_1 excited states (S_2 state foot band as well) in the case of [2.2], up to the S_4 and S_1 excited states in the case of [2.4].

[2.4] OF Excited at 266 and 390 nm. For [2.4] in acetonitrile, transient absorption spectra recorded in the 300−670 nm spectral range within time windows of 0.5−1.1 and 1.4−400 ps following 266 nm excitation are shown in parts a and b, respectively, of Figure 4. Similar measurements following 390 nm excitation (for 400−750 nm spectral range) are shown in parts c and d of Figure 4. The description of these transient spectra is straightforward and can be done globally for both excitation cases. At early times (Figure 4a,c) a broad signal covering the entire spectral range increases and evolves toward a more structured spectrum with three well-defined bands peaking at 350 nm (band A), 470 nm (band B), and 700 nm (band C). The growth times are identical for the three bands and equal to 190 ± 50 fs and 480 ± 80 fs for 390 and 266 nm excitation, respectively (see Table 2). At longer times (Figure 4b,d), these bands decay concomitantly with a similar time constant of ∼20 ps (see Table 2), leading to a final spectrum showing two bands at 360 and 595 nm, stable on the 100−1500 ps time range. This last spectrum is readily ascribable to the ground-state CF of compound [2.4] as it is undeniably similar to the spectrum observed for this species in the flash photolysis experiment (Figure 1b). Strictly similar spectra were obtained in HX/EtOH (12:1) (see Table 2), the characteristic times of bands A/B/C displaying, however, lower values. Some excitation wavelength dependency of these times is also noticed. For example, on going from ACN to HX/EtOH (12:1), the decay time of bands A/B/C decreases from ∼20 to ∼16 ps at 390 nm excitation and from ∼17 to ∼12 ps at 266 nm excitation.

[2.2] OF Excited at 266 nm. For [2.2] in acetonitrile, transient absorption spectra following 266 nm excitation, recorded in the 300−670 nm spectral range, within time windows of 0.6−1.2 and 1.4−200 ps, are shown in parts a and b, respectively, of Figure 5. A clear analogy is observed between these spectra and those previously discussed for [2.4] (Figure 4a,c). At short times, the transient spectrum includes two absorption bands peaking at about 480 and 635 nm analogous to band B and band C of [2.4] and a highly structured spectral frame with positive and negative sharp peaks in the 300−370 nm region (rather than the unique band A seen for [2.4]). All features appear first with a characteristic time of 400 ± 40 fs (see Table 2). The decay of these bands involves two exponential contributions. In the 450−700 nm region, bands B and C decay with a single exponential time constant 1.5 ± 0.1 ps. At the end of this decay, a broad band maximizing around 560 nm is apparent and keeps constant intensity at longer times. This band is unambiguously ascribed to the ground-state CF species by

© 2016 Tous droits réservés.

doc.univ-lille1.fr

HDR de Stéphane Aloïse, Lille 1, 2016

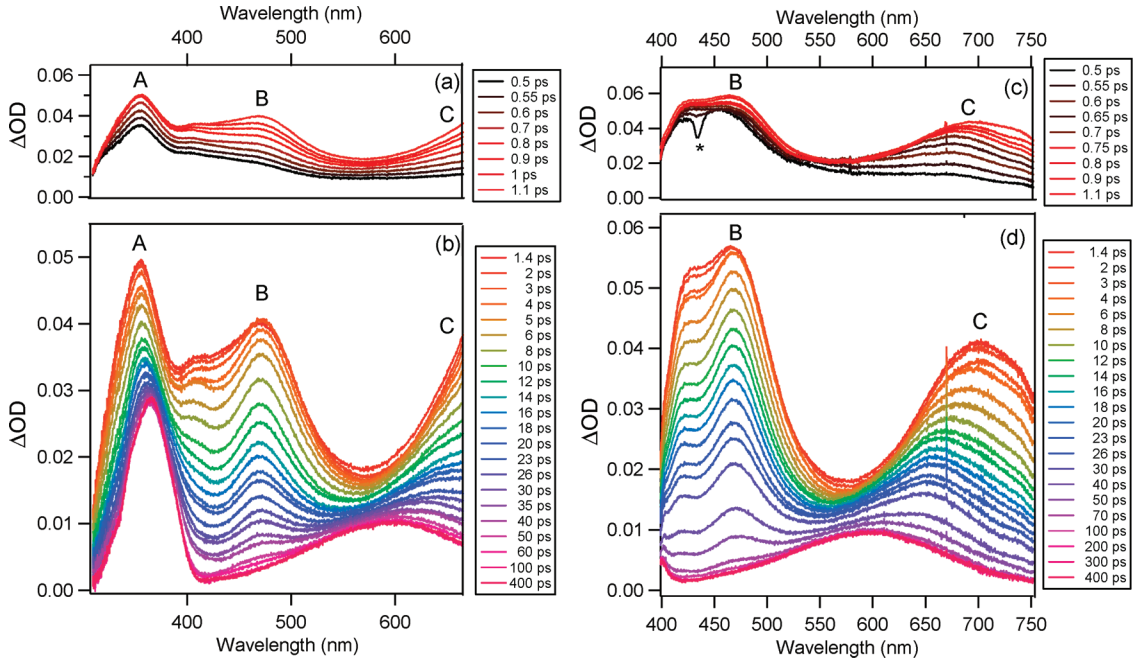

Figure 4. Subpicosecond time-resolved absorption spectra of [2.4] in acetonitrile using 266 nm (left) and 390 nm (right) excitation wavelengths within the 0.5−1.1 ps (a, c) and 1.4−400 ps (b, d) temporal windows. All spectra are corrected from the GVD. The star indicates stimulated Raman peak.

Table 2. Characteristic Times for [2.2] and [2.4] in ACN and (HX/EtOH 12:1) Obtained from the Best Fits of the Subpicosecond Time-Resolved Absorption Kinetics Measured at Appropriate Wavelengths

			growth A/B/C (ps)	decay A/B/C (ps)	growth D (ps)	decay D (ps)
[2.2]	390 nm	HX/EtOH 12:1			<0.1	0.11 (2)
		ACN			<0.1	0.12 (4)
	266 nm	HX/EtOH 12:1	0.25 (4)	2.5 (1)[a]		
		ACN	0.40 (4)	1.5 (1)[a]		
[2.4]	390 nm	HX/EtOH 12:1	0.13 (2)	16.4 (7)		
		ACN	0.19 (5)	20.5 (2)		
	266 nm	HX/EtOH 12:1	0.34 (4)	11.5 (5)		
		ACN	0.48 (8)	17 (1)		

[a] Only bands B and C.

analogy with the steady-state spectrum (Figure 1a). On the basis of the structural effect on the ring-closure reaction (predicted in section 3.3), it is tempting to propose that the CF of [2.2] is thus formed with a time constant of 1.5 ps, while this process requires 20 ps for [2.4]. Besides the temporal evolution of bands B and C, the 380 nm absorption band decays biexponentially (time constants 1.5 and 13 ps) concomitantly with the disappearance of the 300−370 nm sharp structure and the growth of a new absorption band peaking at 335 nm (an isosbestic point is seen at 355 nm). The remaining 335 nm band corresponds, as does the 560 nm feature, to the ground state CF species. If the 1.5 ps decay is already assigned, the 13 ps contribution reveals the presence of an additional photoinduced process. The band structure observed in the 300−370 nm region shows two sharp minima at 330 and 350 nm that correspond approximately to the position of the vibronic maxima in the UV absorption band of CF (see the black curve in Figure 1a). It reveals the probable presence of some bleaching of the CF ground state of [2.2] superimposed on the transient absorption band. Such a bleaching contribution can be explained by the high stability of both forms for [2.2] and consequently the presence of some amount of steady-state CF during the measurement. As a confirmation, the CF bleaching contribution was found to notably increase for long acquisition periods, i.e., after long irradiation times. We thus propose that the 13 ps dynamic processes corresponds to the overall excited-state decay of CF including the $S_1 \rightarrow S_0$ deactivation and photoreversion processes. Similar data have been obtained in HX/EtOH (12:1) except for an exponential time of 2.5 ps for the decay of bands A/B/C (see Table 2).

[2.2] OF Excited at 390 nm. In ACN, spectra recorded in the 400−750 nm spectral range within time windows of 0.3−0.5 and 0.525−10 ps following 390 nm excitation are presented in parts c and d, respectively, of Figure 5. In contrast to the similarity of the spectral evolution observed for [2.4] upon photolysis at 390 and 266 nm, a clear excitation wavelength effect is seen for [2.2]. At short times (Figure 5c), a broad band covering the entire 400−750 nm region undergoes a notable red-shift from about 450 nm at 300 fs to 700 nm at 650 fs. This ultrafast band shift, clearly apparent in the contour plot representation of Figure 6b, is completed at 650 fs and has a characteristic time evaluated to be less than 100 fs (see Table 2). The 650 fs trace is representative of a transient band noted band D in the following. A simultaneous decay of band D is observed up to 1.2 ps and leads to a final spectrum characterized by a broad absorption maximizing at 570 nm typical of the ground state CF but with broader width. The final CF spectrum (see Figure 1a) is finally recovered within about 10 ps via a process that can be safely attributed to vibrational relaxation of the colored form (we will not try to fit this last process because of its minor spectral contribution). The global fitting analysis of the ultrafast band D decay, performed using the deconvolution approach of Ziolek et al. (see, for example, the 500 and 690 nm traces in Figure 6a) leads to a characteristic time of 120 ± 40 fs. As a consequence, we provide clear spectroscopic evidence for the existence of two different ring closure dynamics. Similar data were obtained in HX/EtOH (12:1) (see Table 2).

[2.2] CF Excited at 390 nm. In order to investigate the CF excited-state dynamics, we performed similar time-resolved

© 2016 Tous droits réservés.

doc.univ-lille1.fr

HDR de Stéphane Aloïse, Lille 1, 2016

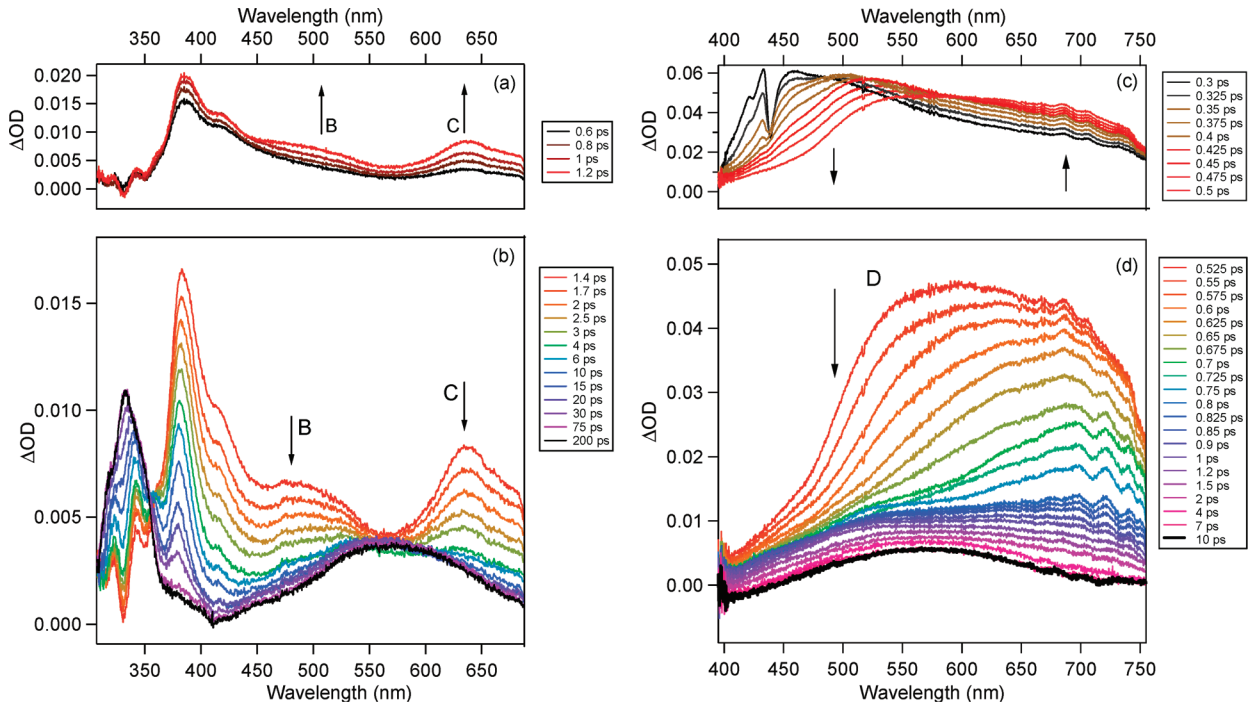

Figure 5. Subpicosecond time-resolved absorption spectra of [2.2] in acetonitrile using 266 nm (left) and 390 nm (right) excitation wavelengths. The temporal windows are different: 0.6−1.2 ps (a) and 1.4−200 ps (b); 0.3−0.5 ps (c) and 0.525−10 ps (d). All spectra are corrected from the GVD. The sharp peak in part c is due to stimulated Raman diffusion.

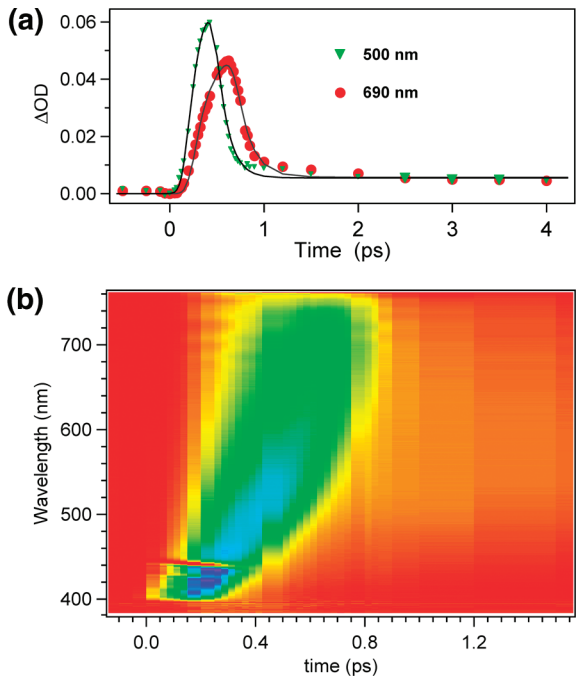

Figure 6. (a) 500 and 690 nm kinetic traces obtained for molecule [2.2] with 390 nm and best fits to exponentials evolutions (see the Experimental and Theoretical Methods for more details); (b) contour plot obtained from Figure 5 and expanded between 0 and 1.4 ps.

experiments on a [2.2] purple solution (photostationary state achieved after 30 min UV irradiation) with a CF proportion estimated to be higher than OF proportion (results shown in Figure SI2a, Supporting Information). According to Table SI2 (Supporting Information), the 390 nm excitation populates the S_1 state of CF. Within the 0.3−0.9 ps time window, an initial broad negative signal is likely assigned to CF bleaching superimposed to some OF* excited state absorption (probably band D) resulting from the direct excitation of the OF population present in the initial sample in addition to CF. The decay of this broad signal gives rise to the hot CF, S_0(CF, v*), spectrum, which decays via vibrational relaxation during the 1−20 ps time window (Figure SI2b, Supporting Information). The characteristic times for these two processes are 250 fs and 2.5 ps, respectively. Considering the nonnegligible contribution of OF*, it appears difficult to assign precisely those times. However, they provide upper estimations of the characteristic times related to the S_1(CF)→S_0(CF, v*) internal conversion, i.e., 250 fs, and vibrational relaxation of S_0(CF, v*), i.e., 2.5 ps.

3.5. Ground and Excited Potential Energy Surfaces. For [2.2] and [2.4], the first (S_1 and S_2) singlet excited-state potential energy surfaces (PES) calculated at the AM1-CIS level are shown in Figure 7. The reaction coordinate is represented by the distance between the two reactive carbons r_{cc} as shown in Figure 3. For [2.2], the geometry of the S_0(CF) and S_0(OF) isomers has been optimized at the AM1-CIS level leading to a trifling difference with TD-DFT-optimized structures (see Table SI3, Supporting Information). The S_0(CF)−S_0(OF) energy path, obtained by using the CHAIN method,[30] shows the existence of a transition state S_0(TS) with a r_{cc} distance of 1.99 Å and a barrier of activation for ring closure of 1.67 eV (39 kcal·mol^{-1}). S_0(TS) geometrical parameters are closer to the S_0(CF) geometry than to the S_0(OF) structure. For the first excited state, from the Franck−Condon geometry S_1^{FC}(OF), the system relaxes to its minimum energy structure S_1(OF). The value of the reaction coordinate is considerably shortened on going from S_1^{FC}(OF) (r_{cc} = 2.70 Å) to S_1(OF) (r_{cc} = 2.18 Å). On the ring-closure reaction path, the system then reaches a transition state S_1(TS) for a r_{cc} distance of 1.94 Å. The energy barrier to ring closure on the S_1 PES is very small 0.03 eV (0.7 kcal·mol^{-1}). After

(30) (a) Liotard, D. A.; Penot, J. P. *Numerical Methods in the Study of Critical Phenomena*; Springler-Verlag: Berlin, 1981; p 213. (b) Liotard, D. A. *Int. J. Quantum Chem.* **1992**, *44*, 723.

© 2016 Tous droits réservés.

doc.univ-lille1.fr

HDR de Stéphane Aloïse, Lille 1, 2016

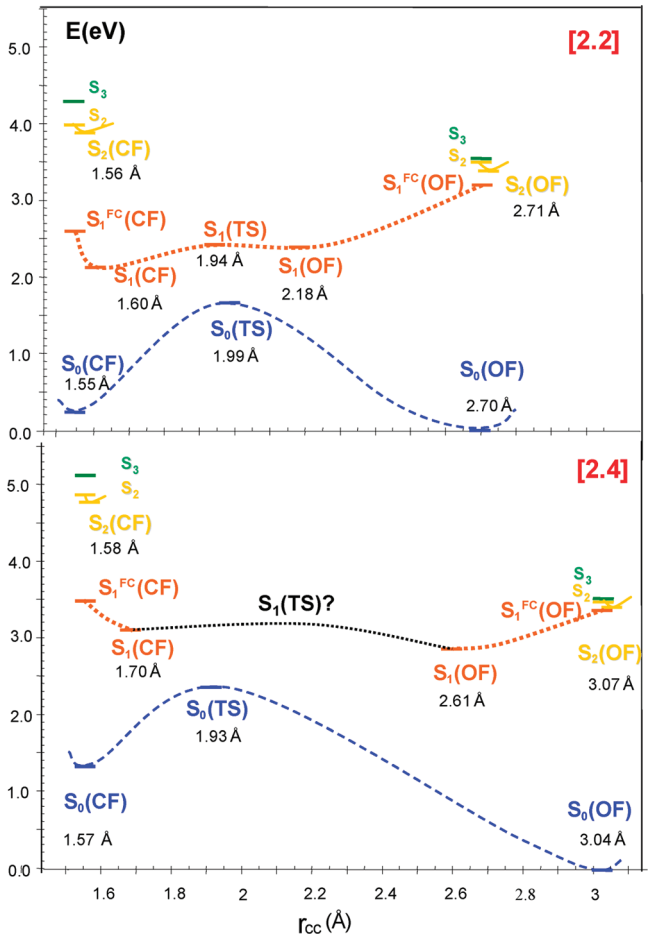

Figure 7. Ground- and first excited-state potential energy surfaces of [2.2] and [2.4] calculated at the AM1-CIS level. For both systems, the reference energy corresponds to S_0(OF).

reaching this transition state, a decrease in the potential energy leads to the closed-ring region of the PES and to the S_1(CF) minimum. This critical point (r_{cc} = 1.60 Å) is close to the S_1^{FC}(CF) geometry (r_{cc} = 1.55 Å). It is worth noting that the geometries of the different critical points on the PES are close to C_2 symmetry (Table SI3, Supporting Information). For the S_2 state, following the gradient in the Franck−Condon region leads to the S_2(OF) minimum with r_{cc} slightly stretched on going from S_2^{FC} (OF) (2.70 Å) to S_2(OF) (2.71 Å). Unfortunately, since AM1-CIS vertical excitations for the S_3, S_4, S_5 states did not provide satisfying comparisons with experiment and TD-DFT, we could not investigate the PES of these excited states.

To investigate the structural effect observed in section 3.3, we then compare the ground-state and excited-state PES of [2.2] and [2.4]. For the ground state, the transition state S_0(TS) of [2.4] is still localized in the closed-ring region as it was the case for [2.2] (Figure 7), and the energy barrier for ring-closure on the S_0 PES (2.62 eV, i.e., ~60.5 kcal·mol^{-1}) is much higher than the barrier for [2.2]. The optimization of the S_1(OF) structure from the FC region shortens the r_{cc} distance compared with the S_1(OF) structure of [2.2]. This indicates that the first intermediate on the S_1 PES of [2.4] is alike the OF geometry in contrast with [2.2]. The transition state search on the S_1 PES failed, which suggests that the PES is rather flat between S_1(OF) and S_1(CF). The dotted black line in Figure 7 is an illustration of this hypothesis.

State Correlation Diagrams. Since the AM1-CIS calculations could not provide information concerning the more energetic S_n potential energy surfaces and could not locate topological features (conical intersections, etc.), we have built the state correlation diagrams between OF and CF (Figure 8) for both [2.2] and [2.4]. These qualitative diagrams have been drawn according to usual procedure and assuming a C_2 symmetry (asymmetric and symmetric correlation lines are displayed in blue and black, respectively).[31] In the past, such diagrams have been successfully used by Irie et al. for the rationalization of thermal irreversibility[16] or the cycloreversion quantum yield.[7] Concerning the state energies, we took advantage of the TD-DFT results which are in good agreement with experiments (see Table SI1 (Supporting Information) and Figure 3) in order to derive state correlation diagrams. Note that the molecular orbitals (MO) used to build this correlation diagram[31] are displayed in Table SI3 (Supporting Information). Two main effects have to be commented for those diagrams. First, one recognizes the well-known S_0/S_n avoided crossing (hereafter CI_1) with adiabatic curves joining OF(S_0) and CF(S_0) states. This is consistent with known diarylethene photochemistry in which ultrafast dynamics is a result of such conical intersection.[14−18] However, unexpected correlation lines within the asymmetric manifold are found for the bridged diarylethene. Indeed, rather than the well-known correlation between the S_0 and S_1 states of OF and CF (due to HOMO→LUMO correlation) encountered for standards diarylethenes,[32] the CF S_1 state is correlated with the OF S_5 state (HOMO→LUMO+1 excitation) and S_8 state (HOMO→LUMO+3 excitation) in the case of [2.2] and [2.4] respectively. More details on these correlations are reported in the Supporting Information. As a consequence, two avoided crossings, named CI_2 and CI_3, arise after taking into account S_1-S_n(OF) and S_2-S_n(OF) asymmetric correlation lines.

4. Discussion

The spectrokinetic properties of the two bridged 1,2-dicyano[2,*n*]metacyclophan-1-enes studied in this paper display strong dependence on with solvent polarity conferred by the two acceptor cyano groups. The inspection of the molecular orbitals described in section 3.3 provides a straightforward rationalization of these main effects, underlining the charge-transfer character of the low-lying excited states of [2.2] and [2.4]. Furthermore, two separate results have demonstrated the existence of two distinct photocyclization pathways in the case of [2.2]: (i) a strong dependence of the photocoloration yield on the excitation wavelength is observed with a significant increase at a threshold wavelength lying between the $S_0\rightarrow S_1$ and $S_0\rightarrow S_2$ transitions, identified by TD-DFT (the wavelength threshold and the magnitude of the yield increase are both dependent on solvent polarity); (ii) the transient signal of [2.2] is totally different for an excitation below or beyond this threshold. Indeed, the complex and ultrafast 120 fs photocyclization dynamics arising upon 390 nm excitation ($S_0\rightarrow S_1$ transition), related to the observation of the transient absorption band D, is totally different from the 1.5 ps dynamics observed upon 266 nm excitation ($S_0\rightarrow S_n$ transition), related to the transient bands A/B/C. The latter transient absorption bands are also found to be involved in the photoreactivity of [2.4], which

(31) Rauk, A. *Orbital Interaction Theory of Organic Chemistry*; John Wiley & Sons, Inc.: New York, 2001.
(32) Perrier, A.; Maurel, F.; Aubard, J. *J. Photochem. Photobiol. A* **2007**, *189*, 167.

© 2016 Tous droits réservés.
doc.univ-lille1.fr

HDR de Stéphane Aloïse, Lille 1, 2016

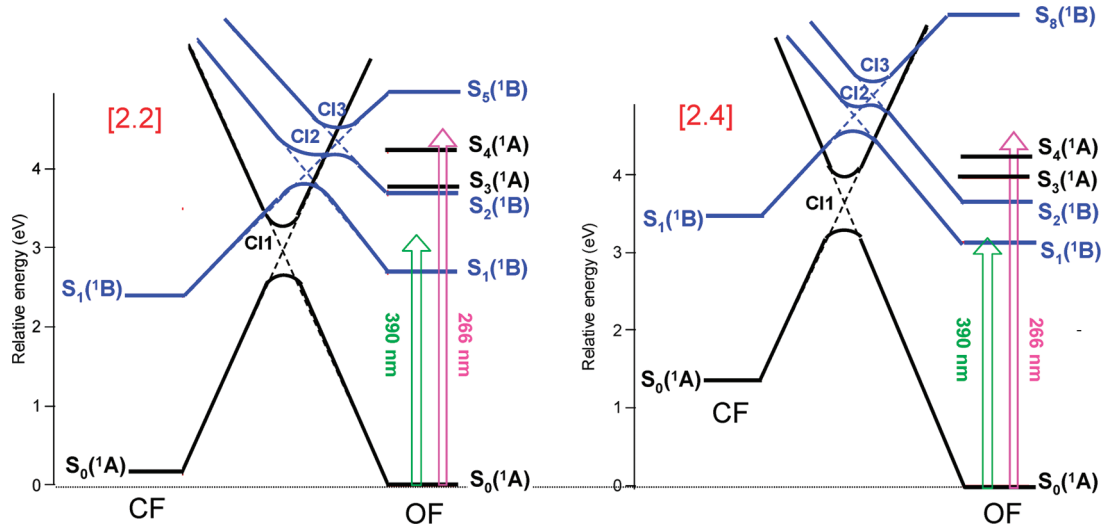

Figure 8. State correlation diagrams for [2.2] and [2.4] using TD-DFT vertical excitation energies where the OF ground-state level is taken as the reference energy. Black lines refer to symmetric states and blue lines for antisymmetric states (some correlation lines are not included for sake of simplicity). Laser excitations at 390 nm (green arrow) and 266 nm (pink arrow) are shown.

appears only moderately dependent on the excitation wavelength as well as the solvent polarity, and is characterized by time constants of ∼12−20 ps that are much longer than those measured for [2.2]. This comparison gives evidence for a photocyclization process notably dependent on the reactive carbon interdistance. We will now focus on the identification of these two distinct photocyclization pathways with the help of AM1-CIS calculations (Figure 7) and correlation diagrams (Figure 8).

4.1. Two Distinct Photochemical Pathways. Let us consider first the reaction channel available within S_1 state excitation (390 nm excitation case), which is efficient for [2.2] (ϕ(355 nm)/ϕ(266 nm) > 1.4) but does not seem to be efficient for [2.4] (ϕ(355 nm)/ϕ(266 nm) = 0.93). The early cyclization dynamics, characterized by a substantial and ultrafast spectral shift occurring within less than 100 fs (Figure 5c) can be assigned to an electronic relaxation from the Franck−Condon S_1^{FC} states to the S_1(OF) along the S_1 potential surface as indicated in Figure 7. Note that the spectral shift may be likely correlated with the drastic geometric change calculated along the ring closure coordinate (Δr_{cc} = 0.52 Å) during this ultrafast electronic relaxation. At this stage, the extremely fast 120 fs decay of S_1(OF) (Band D) can be understood by i) the strikingly similar geometries of S_1(OF) (2.18 Å) and S_0(TS) (1.99 Å); ii) the avoided crossing CI_1 on the state correlation diagram linking the ground and excited PES. In summary, the ultrafast photoclosure reaction is expected to occur through a conical intersection, noticed CI_1, between S_1(OF) and S_0(TS), allowing efficient production of hot ground-state CF, {S_0,(CF),v*}. Finally, in accordance with experimental observations, fast vibrational relaxation is the final step in the photocyclization reaction. The whole photocyclization pathway can be cast, assuming an adiabatic transition from a totally relaxed singlet state S_1(OF), in the following way

$$S_0(OF) \rightarrow S_1^{FC}(OF) \rightarrow S_1(OF) \rightarrow (CI_1) \rightarrow \{S_0,(CF),v^*\} \rightarrow S_0(CF) \quad (2)$$

As further validation of this mechanism, relevant similarities have been found with the results of Hania et al. that report a 900 fs time closure through a conical intersection.[6b] Their conclusion was based on transient data exhibiting a strong spectral shift. The excellent photocylization yield measured for excitation above the energy threshold (near unity) is consistent with the striking proximity for the S_1(OF) minimum and transition state S_0(TS) predicted from AM1/CIS calculations (see Figure 7). Similarly, one can foresee in the case of [2.4] that the inefficiency of this mechanism is due to drastic geometrical differences between those two decisive topological features (Δr = 0.68 Å, see Figure 7). It seems more reasonable that, once the system has reached S_1(OF), it finds an appropriate funnel to relax toward the starting OF ground state.

Complete identification of the second photocyclization process and its solvent dependency is more challenging due to the need to rationalize two seemingly opposite results: on one hand, a similar photoreactive mechanism, different from the S_1 photochemical pathway, occurs for both molecules (similar spectral bands A/B/C); on the other hand, violation of Kasha's rules is observed only in the case of [2.2]. As a first hypothesis for solving this dilemma, S_2 state photoreactivity can be ruled out at first glance. Indeed, the AM1-CIS geometry of S_2 denotes an additional expansion of the molecule rather than an evolution in the ring closure direction. As a matter of fact, because the abrupt threshold for the photocyclization yield of [2.2] is lying between the S_1 and S_2 states, it seems reasonable to envisage the second photoreactive channel as originating from a topological region of the S_1(OF) potential curve located at higher energy compared to the S_1(OF) potential minimum. In this sense, AM1-CIS calculation predict the existence of a transition state S_1(TS) accessible only from a vibrationally excited S_1 state, abbreviated {S_1,(OF),v*}. We thus propose that the transient bands A/B/C arise, for both molecules, from this hot state. Within this hypothesis, the precyclization dynamics can be suggested to result from a fast population of the {S_1(OF),v*}from the initially excited Franck−Condon region by internal conversion, with a dynamics obeying the energy gap law as seen in Table 2 for the A/B/C bands growth time (the higher the excitation, the slower the internal conversion). Identification of the following step in the ring closure dynamics has to take into account the structural effect reported in section 3.4, i.e., a monoexponential A/B/C bands decay of 1.5−2.5 ps and 12−20 ps for [2.2] and [2.4], respectively. Inspection of AM1-CIS results indicates that

© 2016 Tous droits réservés.

doc.univ-lille1.fr

HDR de Stéphane Aloïse, Lille 1, 2016

only OF excited species could be responsible for such effect rather than CF excited species (see below). Furthermore, no other intermediate is detected as precursor of CF, and it seems unlikely that photo-ring closure could occur neither directly from $\{S_1(OF),v^*\}$ nor through the conical intersection CI_1 discussed above. We suggest therefore the possible population of $S_1(CF)$ through $S_1(TS)$ followed by an ultrafast internal conversion (probably few hundreds of femtosecond) leading to $S_0(CF)$. As a confirmation, we assessed internal conversion of $S_1(CF)$ to be less than 250 fs (see Figure SI2 in the Supporting Information); this is also consistent with the 300 fs characteristic time reported by Ern et al.[11b] As a consequence, because one cannot distinguish such fast process compared to picosecond processes, the direct detectable precursor of CF (responsible for transient bands A/B/C) would be $\{S_1(OF),v^*\}$ rather than $S_1(CF)$. Summarizing the above propositions and assuming a light excitation to excited singlet state $S_n(OF)$, the second photocyclization pathway can be cast in the following form:

$$S_0(OF) \rightarrow S_n(OF) \rightarrow \{S_1(OF),v^*\} \rightarrow S_1(TS) \rightarrow S_1(CF) \rightarrow S_0(CF) \quad (3)$$

The structural effect reported in this study has to be rationalized by eq 3 and AM1-CIS results. Regarding the final electrocyclization process, it is worthwhile to corroborate the increasing decays from [2.2] (1.5−2,5 ps) to [2.4] (12−20 ps) to the drastic increasing distances between the reactive carbons in $S_1(OF)$, i.e. 2.18 Å and 2.61 Å respectively. (Obviously, one considers that hot S_1 state would has similar geometry compared to $S_1(OF)$.) Additionally, faster photoclosure process found for [2.2] can be likely related to the negligible 0.7 kcal.mol^{-1} potential barrier to overpass to go from $\{S_1(OF),v^*\}$ to $S_1(CF)$ (see $S_1(TS)$). In this sense, the longer photoclosure process for [2.4] can be related with the substantial endothermicity predicted between $S_1(OF)$ and $S_1(CF)$. Finally, note that the 1.5/2.5 ps closure time found for [2.2] is consistent with the 1−10 ps time set published by other groups for more conventional unbridged diarylethenes.[4,10−13]

Because no clear isosbestic point involving CF visible band has been reported in our transient spectra, it is still possible to find alternative mechanism for eq 3. In this sense, even if theoretical computations of advanced topological keypoints are not feasible in our case, correlation diagrams of Figure 8 predict unusual avoided crossing due to unusual S_1-S_5 or S_1-S_8 correlation lines. From the low energy avoided crossing (see CI_2 on figure 8) due to antisymmetric manifold, one can predict the existence of a conical intersection, abbreviated CI_2 as well, that would be responsible for direct CF production without any CF* species involved. It would allow rewriting eq 3 as

$$S_0(OF) \rightarrow S_n(OF) \rightarrow \{S_1(OF),v^*\} \rightarrow CI_2 \rightarrow S_0(CF) \quad (4)$$

Within this hypothesis, the energy position of CI_2 would be logically sensitive to solvent polarity. Final distinction between eq 3 and eq 4 could be achieved with the aid of CASSCF calculations for model bridged diarylethenes.

4.2. Rationalization of Solvent Effects on Transient Data. Further validation of eq 3 can be attempted by examining the solvent effect on the femtosecond data of [2.2] and [2.4] in light of the theoretical results (such an approach is impossible for eq 4 without precise conical intersection calculations). For [2.2] after 266 nm excitation, as seen in Table 2, the lifetime of the assumed precursor of CF decreases from 2.5 to 1.5 ps while the absolute CF yield increases from 0.49 to 0.69 on going from HX/EtOH (12:1) to ACN. To account for these solvent effects, the relative CT character of the low-lying excited states has been evaluated by analyzing the percentage of electronic delocalization of the LUMO on the cyano groups (excitation of the S_1 and S_2 states corresponds to an electron promotion toward the LUMO). As indicated in Table 3, it is tempting to invoke a stronger polar stabilization for $S_1(TS)$ state compared to $S_1(CF)$, since these two states present respectively 9% and 4% electron density on the CN groups. Assuming that diabatic transition occurs through any high vibrational level, this polar stabilization is assumed to reduce the potential barrier to overcome and consequently to lower the CF precursor lifetime and enhance the photocyclization yield. Reversely, the characteristic time (Table 2) increases with polarity for [2.4] (from ∼12−16 ps to ∼17−20 ps) while the photocyclization yield (Table 1) is not really affected by polarity changes. Even if $S_1(TS)$ is still unknown, the strong CT character of $S_1(OF)$ (12% LUMO electron density on the CN groups) is expected to induce polar stabilization and thus greater endothermicity compared to $S_1(CF)$, which should increase the lifetime of the CF precursor. Similarly, one notes in Table 2 that the lifetime of the precursor of CF depends on the excitation wavelength. The reported lower lifetimes for more energetic excitation are totally consistent with a diabatic transition depending on the excess of electronic energy.

Table 3. Description of the LUMO at the AM1-CIS Level: Percentage of the Electronic Density of the LUMO Localized on the Cyano Groups Alone and on the Cyano Groups Plus the Adjacent Carbon Atoms

	cyano groups (%)		cyano groups + adjacent carbons (%)	
	[2.2]	[2.4]	[2.2]	[2.4]
$S_0(OF)$	16	17	69	72
$S_1^{FC}(OF)$	16	17	69	47
$S_1(OF)$	9	12	47	58
$S_1(TS)$	7		36	
$S_1(CF)$	4	4	20	20
$S_0(TS)$	6	7	33	34
$S_0(CF)$	5	5	23	23

4.3. Optimizing the Photocyclization Yield? To the best of our knowledge, this study is the first one reporting two distinct photochemical pathways within the singlet manifold accounting for the same photocyclization transformation in diarylethenes. From an application point of view, the enhancement of the photocyclization yield of [2.2] from 0.39 (nonpolar solvent, UV excitation) to almost unity (polar solvent, near-visible excitation) is of fundamental importance. Indeed, we finally demonstrate the ability of the bridging alkyl chain to effectively increase the photochromic yield, providing, however, that a photoexcitation beyond the threshold is used. Thus, one can conclude that the functionality expected for the alkyl bridge, i.e., blocking the molecule in a unique photoactive antiparallel conformation, is fully validated. Unfortunately, the addition of such alkyl bridge induces serious electronic changes and opens a less efficient photochromic channel (eq 3 or 4) for excitation just above the more effective one (eq 1), leading finally to a decrease of the photocyclization yield upon UV excitation.

From a structural point of view, it is interesting to remark that the threshold on Figure 2, delimiting the branching ratio between mechanisms (2) and (3) (or (4)) depends on the charge-transfer character of the molecule (electronic delocalization toward cyano groups) through the $S_1(TS)$ (or CI_2) energy level. Additionally, it has been demonstrated that, if the alkyl chain

© 2016 Tous droits réservés.

doc.univ-lille1.fr

HDR de Stéphane Aloïse, Lille 1, 2016

length influences the S_1 state energy level, a similar influence is logically expected for the CI_1 energy level as well. For too long alkyl chains, as is the case for [2.4], the more efficient mechanism (2) is totally quenched by the less efficient mechanism (3)/(4). New diarylethenes with novel bridges and ethylene substituents that maximize the photocyclization process through mechanism (2) for UV excitation should be a relevant approach to optimize bridged diarylethene.

5. Conclusions

Compared to standard diarylethenes, the lack of improvement found in previous studies[3] for the photocyclization yield of 1,2-dicyano[2.*n*]metacyclophan-1-ene diarylethenes with additional alkyl bridges locked in a favorable conformation has been rationalized in terms of two different photocyclization pathways. The two channels have been evidenced by femtosecond transient absorption spectroscopy and rationalized with the aid of state correlation diagrams and AM1-CIS calculations. Indeed, we demonstrate that changing the alkyl bridge length induces drastic changes within the OF and CF electronic states distribution allowing two different photocyclization pathways to be followed by the system. The first photocyclization pathway (eq 2) concerns mostly [2.2] and involves efficient $\phi \approx 1$ and ultrafast (120 fs) adiabatic transition through S_0/S_n conical intersection leading to hot S_0(CF) followed by vibrational relaxation. The unexpected second photocyclization pathway, displaying less efficiency and solvent dependent quantum yield ranging from ~0.4 to 0.7, can be explained through the reactivity of hot singlet state, $\{S_1$,(OF),v*$\}$. From this state, two possibilities are proposed: (i) a diabatic transition to S_1(CF) through a transition state S_1(TS) and followed by ultrafast internal conversion (eq 3) and (ii) an adiabatic transition through some conical intersection CI_2 leading to CF (eq 4). Polarity-dependent photocyclization quantum yields are explained in terms of some charge transfer character of either S_1(TS) or CI_2. Since the novel photophysical schemes found in this study have been related with structural features, alkyl chain length and charge transfer character, bridged diarylethene are good candidates to achieve a complete photocyclization yield optimization, i.e., $\phi = 1$ under UV excitation. In this sense, trying to generalize the two different photochemical paths evidenced in this study by investigating new bridged diarylethenes as well as some smaller model compounds allowing CASSCF theoretical calculations are now under investigation in our laboratories.

Acknowledgment. Part of this work is supported by a Grant-in-Aid for Science Research in a Priority Area New Frontiers in Photochromism (471) (No. 21021021) from the Ministry of Education, Culture, Sports, Science and Technology (MEXT), Japan, and a Grant-in-Aid for Scientific Research (C) (No. 21550119) from Japan Society for the Promotion of Science (JSPS), to whom M.T. feels grateful. We thank also the Groupement de Recherche PHENICS GDRI 93 from CNRS for its help in the development of this work.

Supporting Information Available: Table SI1: absorption spectra of [2.2] and [2.4] OF isomers computed with different functionals and with AM1-CIS. Table SI2: TD-DFT and AM1-CIS absorption spectra of [2.2] and [2.4] CF isomers. Table SI3: selected geometrical parameters of [2.2] and [2.4] CF and OF obtained from geometry optimization. Table SI4: relevant molecular orbitals. Figure SI1: Geometrical coordinate definitions. Figure SI2: Transient absorption spectra recorded for a photostationary mixture of CF and OF species. Additional description of the state correlation diagram. Full ref 24. This information is available free of charge via the Internet at http://pubs.acs.org/.

JA910813X

© 2016 Tous droits réservés.

doc.univ-lille1.fr

Annexe 6. Aloïse et al, PCCP, 16, 26762, 2014

PCCP

HDR de Stéphane Aloïse, Lille 1, 2016

PAPER

View Article Online
View Journal | View Issue

Cite this: *Phys. Chem. Chem. Phys.*, 2014, **16**, 26762

The photochemistry of inverse dithienylethene switches understood†

Stéphane Aloïse,*[a] Ruan Yibin,[a] Ismail Hamdi,[a] Guy Buntinx,[a] Aurélie Perrier,*[b] François Maurel,[b] Denis Jacquemin*[c] and Michinori Takeshita[d]

Received 14th August 2014,
Accepted 21st October 2014

DOI: 10.1039/c4cp03641g

www.rsc.org/pccp

The photophysical properties of a series of dithienylethenes, free or blocked in an ideal photoactive conformation by an alkyl bridge, have been investigated by stationary, ultrafast spectroscopy and state-of-the-art time-dependent density functional theory calculations. Thanks to the clear ultrafast transient signatures corroborating NMR results, we bring strong evidence that the unreactive parallel open form conformer has been efficiently removed by the chain. For the first time, the photophysics of this species, namely an internal conversion of 120 ps is highlighted. In contradiction to the main ideas in the literature, the photocyclization mechanism is rationalized by a direct photocyclization mechanism from the Franck–Condon region passing directly through a conical intersection within ≈100 fs (not few picoseconds) while a competitive mechanism occurs through the relaxed S_1 state. Relaxation processes (fluorescence and internal conversion) originating from this relaxed state are sensitive to the length of the blocking chain. Both concomitant pathways are necessary to rationalize: (i) the inverse relationship between emission and cyclization quantum yields and (ii) the non-unity value of the latter for bridged compounds.

Published on 22 October 2014. Downloaded by Univ Lille 1 on 31/08/2016 11:31:36.

Introduction

Photochromism is a reversible photoinduced transformation between two chemical forms presenting different absorption spectra.[1] Photochromic compounds attract ever-growing attention due to their potential applications in optoelectronics, *e.g.*, they can be used as building blocks for rewritable optical memory media[2] or optical switches allowing modulation of key physical properties of both molecules and materials.[3,4] Among the photochromes reported during the last thirty years, diarylethenes and more specifically dithienylethenes (DTEs), are often viewed as the most efficient compounds due to their thermal irreversibility, high fatigue resistance and good photocyclization quantum yield between the open (OF) and closed (CF) forms.[5–7] However, this yield is strongly limited for classical diarylethenes by the existence of two OF conformers presenting anti-parallel (AP) and parallel (P) configurations, only the former being photoactive toward cyclization. In most molecules, the AP : P ratio is close to 1 : 1, which limits the maximal quantum yield to *ca.* 50%. Overcoming this inherent limitation is the focus of various research studies relying on a purpose-designed synthetic approaches[8–11] or specific excited-state reactivities.[12–14]

Over the last two decades, our laboratories performed joint studies to probe photochemical reaction pathways of DTEs by combining state-of-the-art time-dependent density functional theory (TD-DFT) calculations with time resolved spectroscopy. Our goals were to clarify the rather large, and often inconsistent, panel of reported data, as well as to avoid improper generalization between normal (N-type) and inverse (I-type) DTEs. In 2010, we demonstrated that the addition of alkyl chains blocking diarylethene in an ideal photoactive conformation induces large variations of the excited-state features, and hence of the photochemical pathways.[15] Very recently, we have compared N-type and I-type switches, with the aim of ascertaining the relationship between the 50% yield and the 1 : 1 AP : P ratio. Surprisingly, in I-type DTEs, the percentage of P conformers is significantly smaller (10–25% range), but the cyclization quantum yield still does not exceed 50%.[16] A CASSCF/CASPT2 study demonstrated that the N-type and I-type DTEs follow different excited-state reaction pathways – for

[a] *Université de Lille 1, Sciences et Technologies, Lasir Umr 8516, Bât C5, 59655 Villeneuve d'Ascq Cedex, France. E-mail: stephane.aloise@univ-lille1.fr*
[b] *Université Paris 7 Denis Diderot, Sorbonne Paris Cité, ITODYS, UMR 7086, 15 rue Jean-Antoine de Baïf, 75205 Paris Cedex 13, France. E-mail: aurelie.perrier-pineau@univ-paris-diderot.fr*
[c] *CEISAM UMR CNRS 6230, Université de Nantes, 2, rue de la Houssinière, BP 92208 44322 Nantes and Institut Universitaire de France 103 blvd St Michel, 75005 Paris Cedex 05, France. E-mail: Denis.Jacquemin@univ-nantes.fr*
[d] *Department of Chemistry and Applied Chemistry, Faculty of Science and Engineering, Saga University, Honjo1, Saga 840-8502, Japan*

† Electronic supplementary information (ESI) available: Derivation of eqn (1) and (2); Table S1: experimental and PCM-TDDFT maximum of absorption for CF species. Calculated R_{CC} are listed as well; Table S2: the maximum absorption wavelength (in nm) for transient bands X, Y and Z. TDDFT vertical excitation from either (i) AP or P conformers, (ii) S0 or S1(opt) states; Fig. S1: transient absorption spectra of DTE (ACN/350 nm excitation) for 600 fs and 500 ps pump–probe delay; Fig. S2: DFT orbitals for OF and CF; Table S3: structural information (Cartesian coordinates; carbon–carbon distances and torsion angles) on the series including the ground and first excited states. See DOI: 10.1039/c4cp03641g

This journal is © the Owner Societies 2014

© 2016 Tous droits réservés.

doc.univ-lille1.fr

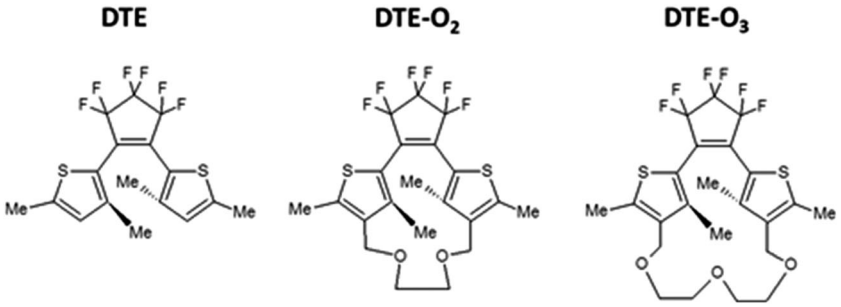

Scheme 1 Inverse dithienylethene, **DTE** (left), and two polyether bridged analogs **DTE-O2** (center) and **DTE-O3** (right).

Published on 22 October 2014. Downloaded by Univ Lille 1 on 31/08/2016 11:31:36.

the former, S_1 and S_2 excited states allow photocyclization, while for the latter, only the S_1 state yields photocyclization through a conical intersection (CI), whereas excitation of S_2 induces the formation of the P conformer.[17]

In the present contribution, we focus on one I-type **DTE**, bis(3,5-dimethyl-2-thienyl)-perfluorocyclopentene, denoted **DTE** ($C_{17}H_{14}F_6S_2$), and two analogs presenting a polyether bridge of variable length, **DTE-O2** ($C_{21}H_{20}F_6O_2S_2$) and **DTE-O3** ($C_{23}H_{24}F_6O_3S_2$) (see Scheme 1). These [2.*n*]thiophenophan-1-ene derivatives have been designed to constrain the molecule within the unique photoactive AP conformation, and, consequently to enhance the photochromic yields.[18] However, the measured cyclization quantum yields[18] are 0.40, 0.70 and 0.42 for **DTE**, **DTE-O2** and **DTE-O3**, respectively, and this evolution cannot be straightforwardly correlated to the relevant geometrical parameters, *e.g.*, to the distance separating the two reactive carbon atoms (R_{CC}). In short, the reason for the unexpected better efficiency of **DTE-O2** remains unknown. As we will demonstrate, this series is relevant to unravel the complex relationship between the photocyclization quantum yield and the AP *vs.* P photophysics.

Experimental and theoretical methods

Stationary techniques

DTE has been synthesized according to the procedure of Irie *et al.*[19] while the synthesis of bridged molecules has already been published.[18] Hexane (HX) solvent (spectroscopic grade, Sigma-Aldrich) was used as received. All stationary absorption and fluorescence spectra were recorded using double beam CARY 100bio and Jobin Yvon Div. FluoroMax 3 spectrometers, respectively. The spectral resolution is typically 2 nm in both experiments. Emission spectra were corrected for the lamp and detector response. Measurements were performed at ambient temperature using 1 cm quartz cells with about 10^{-5} to 10^{-6} M solutions, keeping the maximum absorbance at less than 0.1 in order to avoid any significant reabsorption effects.

Transient absorption experimental setup

The femtosecond transient absorption setup had already been described elsewhere.[20,21] Briefly, a 1 kHz Ti:sapphire laser system (Coherent oscillator and a BM Industries regenerative amplifier) delivered 100 fs (0.8 mJ) pulses at 800 nm. Pump pulses were set to 350 nm by using an OPA (Quantronix, Palitra), while probe pulses (white light continuum) were generated by focusing the fundamental beam in a CaF_2 rotating plate. The transient absorption measurements covered the 400–750 nm spectral range and the 0–500 ps temporal range. Sample solutions (about 10^{-4} M) were circulating in a flow cell equipped with a 100 μm thick CaF_2 entrance window and characterized by a 2 mm optical pathlength. The time-resolution of the experiment (about 200 fs) was estimated from pump–probe cross-correlation measurements.[20,21] The characteristic times deduced from kinetics were obtained by fitting the GVD corrected data (using the procedure proposed by Nakayama *et al.*[22]) with the result of a multi-exponential function convolved with a Gaussian function which approximates the pump–probe cross-correlation one. Within this approach, global fitting was systematically performed taking into account simultaneously four or five relevant wavelengths.

Theoretical calculations

All the calculations have been performed using the Gaussian 09 package[23] using density functional theory (DFT) and time dependent DFT (TD-DFT) calculations to model ground-state (GS) and excited-state (ES) properties, respectively. We have systematically applied the 6-31+G(d) atomic basis set which is known to yield converged results for both geometrical and optical properties of a wide range of solvated dyes.[24]

The critical points corresponding to minima on the potential energy surfaces (PES) of both GS and ES have been determined using the ωB97X range-separated hybrid functional.[25,26] Contrary to the conventional hybrid functionals, range separated hybrids are known to avoid inconsistencies for ES geometries.[24,27] The GS and ES minima have been determined using the Berny-GEDIIS algorithm[28] using a tight convergence criteria (residual RMS force smaller than 0.00001 a.u.). The geometry optimizations have been carried out in HX, applying the PCM model to quantify the impact of the environment.[29] The (GS and) ES geometry optimizations have been carried out in the equilibrium limit using the linear-response (LR) PCM scheme.[30,31]

To determine the spectroscopic parameters, we used the hybrid PBE0 functional[32,33] which was shown to provide fast and accurate predictions for the transition energies of conjugated molecules.[24] In fact, the only major drawback of PBE0 is its inability to describe long-range charge-transfer excited-states, but this limit is irrelevant in our case as we consider a compact molecule. For solvated systems, we selected the state-specific (SS) approximation[34] in

© 2016 Tous droits réservés. doc.univ-lille1.fr

Published on 22 October 2014. Downloaded by Univ Lille 1 on 31/08/2016 11:31:36.

its nonequilibrium limit to determine the total and transition energies of the ES. The SS model accounts more accurately than the LR model for the variations of the polarization of the medium following the electronic density rearrangement of the solute after absorption or emission. Within this framework, we have also determined the 0–0 energies that can be compared to the absorption/emission crossing point in a physically meaningful way. We determined the λ_{abs}^{max} and λ_{fluo}^{max} values which correspond to the longest wavelength of the vertical TD-DFT calculation computed, respectively, at the minimum of the GS and ES. We redirect the interested reader to the review of Mennucci *et al.*[35] (and references therein) which provides a detailed discussion on the solvent models that can be used to obtain the optical properties of solvated chromophores and to the study of Jacquemin *et al.*[24] which describes the protocol enabling to determine the absorption/fluorescence crossing point.

Results and discussion

AP *vs.* P conformers

To confirm the absence of the P conformer for the bridged DTEs, the temperature dependence of the ^{1}H-NMR signal has been investigated and compared to the free **DTE** features. Previously, for **DTE**, the P conformer proportion has been assessed between 10 and 25% at ambient temperature through subtle comparisons between DFT calculations and temperature dependence of the ^{1}H-NMR signal.[16] Focusing on the Me proton of the reactive carbons (involved in the σ bond formation), Fig. 1 shows that the temperature effect due to the existence of the AP/P thermal equilibrium is reduced by one order of magnitude for the bridged analogs compared to **DTE**, bringing a strong evidence that the methoxy bridge efficiently disables the P conformer formation in the ground state. Nevertheless, since we evidenced in the past that conformational changes can follow an AP* → P route,[17] the hypothesis of a non-negligible P conformer population in the excited states will not be discarded in the following.

Spectroscopic signatures of OF and CF

In Fig. 2, we present the measured and computed absorption spectra of **DTE**, **DTE-O2** and **DTE-O3** in HX still considering AP and P conformers. We observe no significant auxochromic effect (all peaks are in the 337–343 nm domain), though the **DTE-O2** extinction coefficient is smaller than its **DTE** and **DTE-O3** counterparts. In line with the NMR results, the positions of the absorption maxima are better reproduced by theory considering the AP conformer rather than the P one (Table 1). In addition, as seen in Fig. 2, by comparing the experimental extinction coefficients of **DTE**, **DTE-O2** and **DTE-O3** (1 : 0.63 : 1.21 ratio) with TD-DFT oscillator strengths, one also obtains a much better

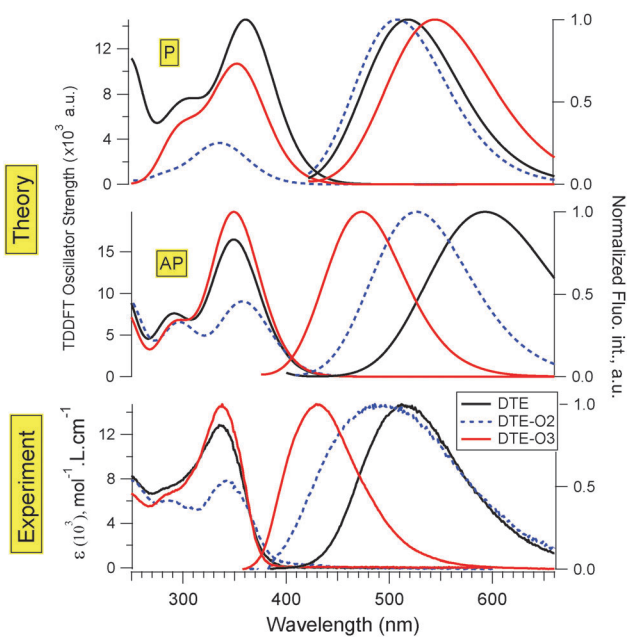

Fig. 2 (down) Experimental (in HX) and (up) calculated PCM-TD-DFT absorption and emission spectra of **DTE**, **DTE-O2** and **DTE-O3**. Both AP and P conformer calculations have been undertaken.

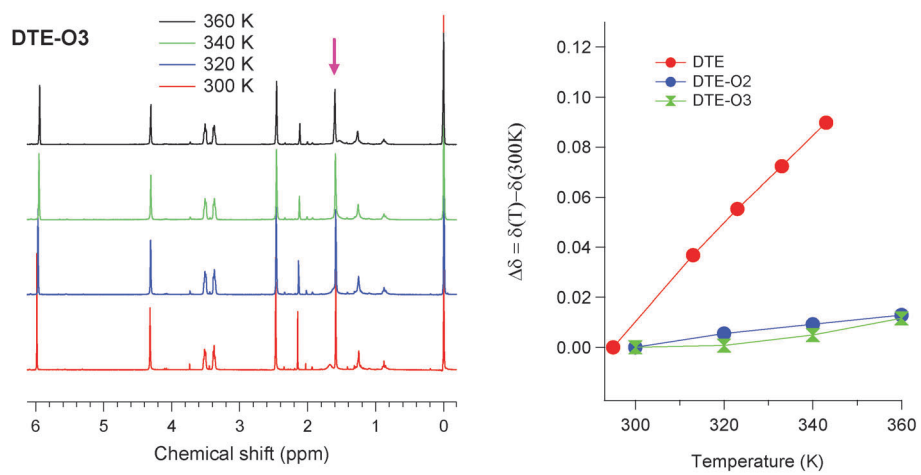

Fig. 1 (left) ^{1}H-NMR spectra in deuterated chloroform between 27 and 87 °C; (right) evolution of the chemical shift of the central Me proton (~1.6 ppm) as a function of temperature for **DTE** (ref. 15) and the bridged analogs (this work).

This journal is © the Owner Societies 2014
© 2016 Tous droits réservés.
doc.univ-lille1.fr

Published on 22 October 2014. Downloaded by Univ Lille 1 on 31/08/2016 11:31:36.

Table 1 Experimental quantum yields, absorption and emission parameters for OF conformers compared to PCM-TD-DFT results. All data in *n*-hexane (HX)

		λ_{abs}^{max} (nm)	ε, (10^4) mol^{-1} L cm^{-1} or oscillator strength	λ_{fluo}^{max} (nm)	ϕ (fluo)	ϕ (cycl)
DTE	Exp	337	1.29	507	0.008	0.40
	AP	353	0.34	589	—	—
	P	366	0.29	508	—	—
DTE-O2	Exp	343	0.81	492	0.004	0.70
	AP	365	0.19	523	—	—
	P	361	0.05	507	—	—
DTE-O3	Exp	338	1.56	426	0.011	0.42
	AP	357	0.41	465	—	—
	P	369	0.21	536	—	—

agreement considering AP (1 : 0.56 : 1.21) than P (1 : 0.17 : 0.72) isomers. More generally, the overall absorption spectra are successfully reproduced for AP species including the shoulder near 300 nm with constant intensity within the series. These excellent agreements seem to indicate that the P conformer represents a small or very small component of the experimental blend in the case of **DTE**, which is coherent with NMR results. From an orbital point of view, for the three molecules, the S_1 state responsible for absorption can be mainly attributed to a HOMO → LUMO transition. The analysis of the frontier orbitals (see ESI†) shows that there is logically no electronic delocalization on the polyether bridge, thus rationalizing the absence of auxochromic effects.

For the closed form (CF), TD-DFT qualitatively reproduces the structural effect observed for the experimental absorption spectra, that is, a bathochromic shift when the bridging chain extends. This shift can be rationalized by structural considerations: the polyether bridge induces an increase of the distance between the two reactive carbon atoms R_{CC} (see Table S1, ESI†) and thus provokes a concomitant destabilization of the HOMO (bonding between the two reactive C) and stabilization of the LUMO (antibonding).

Experimental emission spectra of OF (see Fig. 2) show an important hypsochromic shift from **DTE** (507 nm) to **DTE-O2** (492 nm) and **DTE-O3** (426 nm). Besides, as seen in the upper part of Fig. 2, the hypsochromic effect induced by the bridge is perfectly reproduced by TD-DFT calculations (see also Table 1) for the AP conformer while the P conformers do not follow the experimental trends. This corroborates the absorption results above and considering the overall DTE-On series, allows us to ascribe it to the experimental emission originating from the AP conformer rather than the P conformer. Actually, considering the **DTE** molecule alone, we recently advocated the inverse hypothesis based on theory–experiment comparison, *i.e.* the P conformer being responsible for the emission process.[16] Consequently, we face a contradiction if we follow this first idea because one would expect the extinction of the fluorescence signal for the bridged analogs, a fact not noticed experimentally. As we will see below, transient spectroscopy will help us to definitely confirm that the emission originates from the AP conformers.

Post-excitation ultrafast mechanisms

Ultrafast spectroscopic data following S_1 state excitation at 350 nm, in the 370–740 nm spectral range with a temporal evolution running up to 500 ps are presented in Fig. 3 for the three molecules. The transient absorption features are labeled X, Y and Z and Table 2 lists both their growing and decaying characteristic times determined through a global fitting method. We underline that the major photophysical events are very similar for all three molecules so that a global analysis is sufficient.

First, just after pump laser excitation, the signal is characterized by the rapid rise of the band X peaking at *ca.* 610 nm, the position of the band being surprisingly conserved irrespective of the considered photochrome. In parallel, with the same apparent rising kinetics, one notices the band Y peaking at the extreme blue region. Because this band Y lies at almost the same position of the CF spectra but is broader (see in particular **DTE** spectra) it allows us to tentatively ascribe it to the transient absorption of the hot CF(v*) species following thus an ultrafast photocyclization reaction. The very small amount of negative signal between the X and Y bands is attributed to Stimulated Emission (SE) coming from the emissive state. For the bridged DTEs, the importance of the SE band, recognized as the mirror of stationary emission spectra (see Fig. 2), is considerably higher which induces a modification of the shape of the band Y. As can be seen in Table 2, the respective growth kinetics of X and Y bands and of SE cannot be distinguished according to our temporal resolution, the characteristic times ranging from 90 fs for **DTE** to around 150 fs for the two bridged analogs.

Next, as can be seen in the central panels of Fig. 3, one observes the decay of bands X, Y and SE, with the clear apparition of the CF spectrum for the three molecules. Two interpretations can be proposed: (i) the species responsible for the transient band X/SE is also one precursor of CF species, *i.e.*, there exists a second and indirect photocyclization mechanism; or (ii) the CF was already formed by direct photocyclization, the subsequent decay of transient bands letting the spectrum appear. Actually, by close inspection of the transient data for **DTE** in Fig. S1 (ESI†) (less influenced by negative SE bands) one clearly notices that compared to the ''direct photocyclization'' signal (600 fs traces) there is no additional rise of CF intensity after the decay of the transient band X/SE (500 ps traces) strongly suggesting that there is no second mechanism for photocyclization, and hence supporting the second hypothesis.

An additional feature, specific to **DTE**, is the appearance of the transient Z band peaking at 570 nm. We highlight that the overall decay of the bands X and Y is monoexponential for **DTE** (τ_2 = 0.80 ps) but biexponential for the bridged analogs (τ_2 and τ_3 time constants in Table 2). Additionally, the decay of the band Z for **DTE** has a characteristic time τ_4 = 120 ps.

For the sake of clarity, all the transient band assignments and the related discussion of the photophysics of the **DTE** series are summarized in Scheme 2. The band Z can be straightforwardly attributed to the excited states of the P conformer as this conformer is absent in the bridged analogues (see NMR analysis above). To the best of our knowledge, this is the first

© 2016 Tous droits réservés. doc.univ-lille1.fr

Published on 22 October 2014. Downloaded by Univ Lille 1 on 31/08/2016 11:31:36.

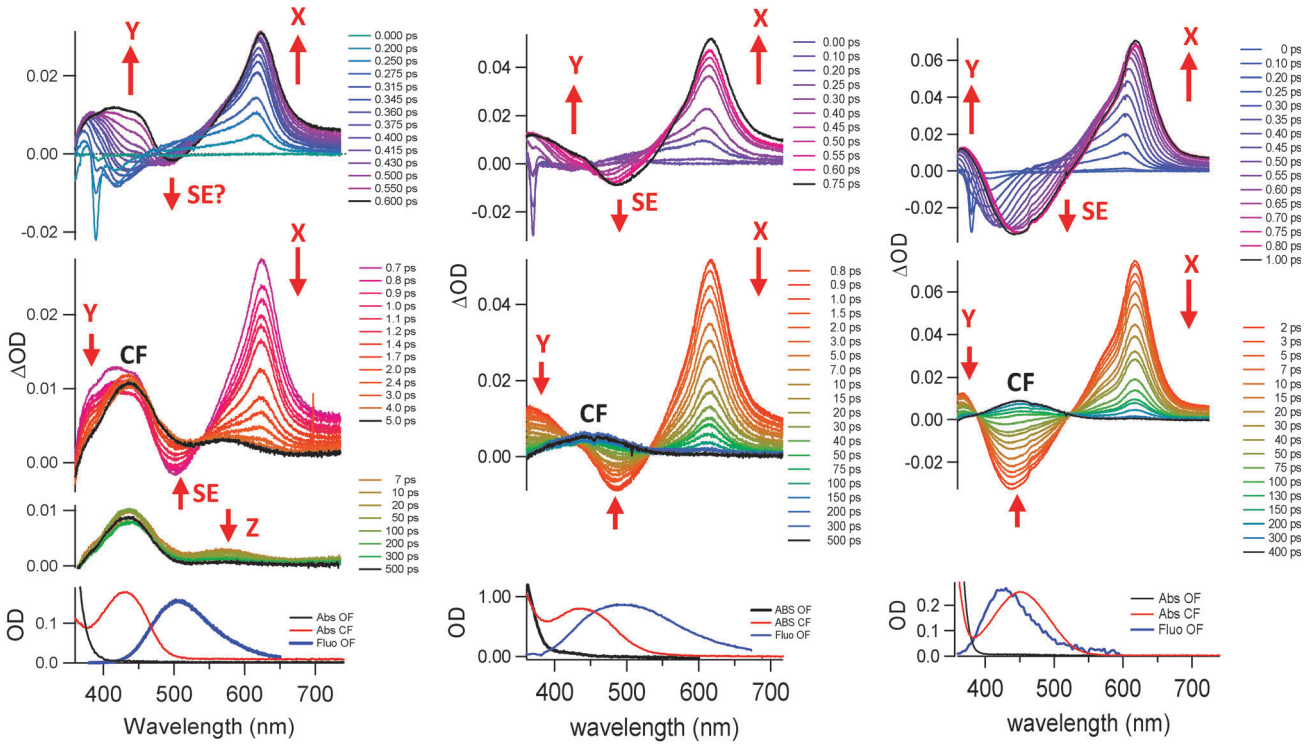

Fig. 3 Time-resolved spectra of **DTE** (left), **DTE-O2** (center), and **DTE-O3** (right) in HX for a 350 nm excitation. Data are displayed within distinct temporal windows. To help the identification of transient bands, stationary absorption spectra of OF and CF, and emission spectra of OF are given as well in the lower panel.

Table 2 R_{CC} calculated for the OF ground and excited states. Characteristic times deduced from the global fitting method applied to femtosecond transient data

	R_{CC} (Å)		Band X/Y growth	Band X decay		Band Z decay
	Ground state S0	Excited state S1(opt)	τ_1 (ps)	τ_2 (ps)	τ_3 (ps)	τ_4 (ps)
DTE	3.58	2.85	0.09(2)	0.8(1)		120(5)
DTE-O2	3.48	3.10	0.140(2)	4.7(6)	36(4)	—
DTE-O3	3.65	3.45	0.15(2)	15(5)	70(10)	—

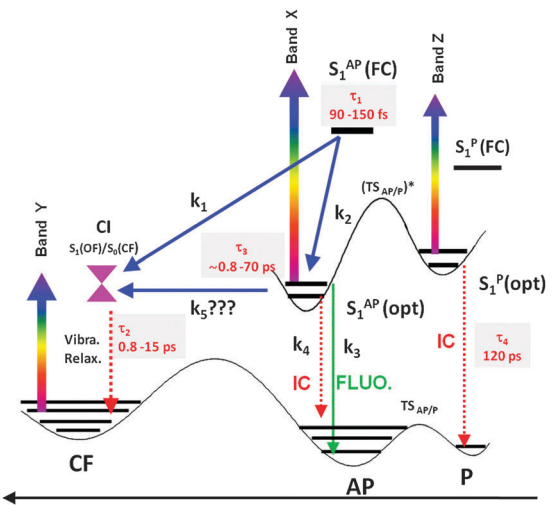

Scheme 2 Photophysical model displaying the two possible photocyclization pathways either from S1(FC) or S1(opt). The extreme right of this scheme dedicated to the P conformer states holds only for the (non-bridged) **DTE**. Transient bands are schematized as well even if one has to consider the spectral overlap with respect to each species contribution.

time that a weak but clear signature of the P conformer excited state has been identified. Furthermore, the experimental transient band Z at *ca.* 570 nm can be tentatively ascribed to the $S_1 \rightarrow S_n$ (with $n = 5$) absorption of S_1(opt) of the P conformer according to the TD-DFT calculations (see Table S3, ESI†). Therefore, we ascribe the decay of the band Z to an internal conversion (IC) from the S_1 state of the P conformer to the ground state without emission, the stimulated emission band being related to the AP conformer. There is no weak SE signal accompanying the decay of the P conformer excited state (band Z) giving a solid confirmation that the AP conformer is the only emissive species even for the "free" **DTE**. As a consequence, we thus show that the rapid interconversion AP* ↔ P* is not possible for the inverse type **DTE**, in clear contrast with the ground state situation.

Concerning the main photocyclization reaction, as already noticed for **DTE**, the transient band Y that rises with $\tau_1 = 90$ fs is similar in position to the CF spectrum, the final CF spectrum being recovered after a 800 fs decay (plus the band Z contribution). This is obviously a clear manifestation of the ultrafast photoclosure reaction giving rise to hot CF structures, CF(v*) with a broader spectrum, and the subsequent vibrational

This journal is © the Owner Societies 2014
© 2016 Tous droits réservés.
doc.univ-lille1.fr

Published on 22 October 2014. Downloaded by Univ Lille 1 on 31/08/2016 11:31:36.

relaxations (see also Fig. S1, ESI†). For bridged molecules, by direct analogy we ascribed $\tau_1 \approx 150$ fs to the photocyclization process. It is worth noting that the photoinduced mechanism is slower compared to **DTE** most probably because the bridged molecules are partially blocked in specific conformations, the presence of the chain implying that additional torsions are necessary to reach the conical intersection. Concerning the relaxation processes, among τ_2 and τ_3 the former is likely attributed to vibrational relaxation of CF(v*) because of the non-negligible signals of B and X for the longest delay. Note that the structural dependence of τ_2 (see Table 2) is tentatively ascribed to the dynamical effect related to the polyether bridge suggested by the structural effect affecting the CF species (see the rising R_{CC} in Table S1, ESI†). In addition the mono- *vs.* bi-exponential nature of the transient signal decay for the ''free'' and bridged analogues, respectively, can be rationalized considering that without the bridge one cannot distinguish the two processes ($\tau_2 \approx \tau_3$).

We now focus on the assignation of the intense transient band X evolving in parallel with the negative band SE and attribution of characteristic time τ_3. Gathering stationary and transient results together with TD-DFT calculations, this work evidences an impressive ''structural effect'' on the S_1 relaxed excited state potential energy surface (PES) of the AP conformer, denoted S_1(opt). First, the theoretical calculations indicate that the R_{CC} distance for the S_1(opt) structure gradually increases in the series, with a strong *ca.* 0.3 Å elongation between **DTE** and **DTE-O3**. We have also found a clear hypsochromic shift of the emission maxima, corroborating the increasing C–C distance of S_1(opt) predicted by calculations. Note that the hypsochromic shift of emission and the increase of τ_3 are straightforwardly related to the well-known ''energy gap'' law. Finally, when we measure the fading process of the transient band X, we notice the same trend in the series, which is an increasing characteristic time when going from **DTE** to **DTE-O3** (τ_3 in Table 2). This brings evidence that the species responsible for both SE and X bands is S_1(opt) of the AP conformer. Further confirmation of such assignation is found with the help of TD-DFT transitions (see Table S3, ESI†). Comparing the $S_1 \rightarrow S_n$ absorption in the three compounds for the S_1(CF) and S_1(opt) states, the former gives rise to an absorption at *ca.* 820 nm while the latter is located at *ca.* 560–670 nm in much better agreement with the experimental value. As seen in Tables 1 and 2, the relaxation of S_1(opt) likely corresponds to IC rather than emission, the predominance of the former being suggested by the low emission quantum yields and the structural effect affecting τ_3 related to either the chain dynamics relaxation or some additional solute–solvent frictional effects.

At this point, the final description of the overall mechanism has to account for the additional experimental findings of the **DTE** series: (i) the inverse relationship between photocyclization and emission quantum yields as one observes in Table 1, the photocyclization yield is larger for **DTE-O2**, ϕ(cycl) = 0.7, while the emission yield is minimal, ϕ(fluo) = 0.004 and (ii) despite the absence of P conformers, a perfect photocyclization (that is to say a quantum yield of 1) is not reached for bridged DTEs. To rationalize these results, one has to consider the possibilities of direct photocyclization through the CI(S_1/S_0) and indirect photocyclization *via* S_1(opt) (or a combination of these two possibilities). Let us consider a photophysical model including: (i) a direct mechanism (k_1) from S_1(FC) to the CI region as already reviewed through the transient band Y; (ii) the internal conversion (k_2) to S_1(opt); (iii) from the latter, the emission (k_3) or the IC (k_4) to the ground state; and (iv) a second photocyclization pathway (k_5) from S_1(opt). The relationship between the two quantum yields is given by (see ESI†):

$$\phi(\text{cycl}) \approx 1 - \frac{k_4}{k_3}\phi(\text{fluo}) \quad (1)$$

Reversely, if one considers only the indirect mechanism, *i.e.* $k_1 = 0$ and $k_5 \neq 0$, this equation becomes:

$$\phi(\text{cycl}) = \frac{k_5}{k_3}\phi(\text{fluo}) \quad (2)$$

Clearly, only the first equation is compatible with the inverse relationship between the emission and cyclization quantum yields and this definitively excludes the existence of an unique photocyclization pathway passing through S_1(opt). Apart from transient data evidence stated above, this is the second confirmation that, unexpectedly, a direct mechanism occurs for the classical I-DTE, the S_1 relaxed state being most likely responsible for emission and IC relaxations.

Therefore, to optimize the photocyclization quantum yield, we have shown that the synthetic approach consisting of proposing structural modifications to decrease the AP : P ratio is relevant but not sufficient. For **DTE-O3**, even if the population of the P conformer is negligible, the photocyclization quantum yield is comparable to the free **DTE**. The optimal quantum yield is obtained for **DTE-O2**, thanks to two concomitant effects: (i) like in **DTE-O3**, the AP population is close to 100%; and (ii) the chain length is small enough to maintain the two reactive carbon atoms at an optimal distance allowing the molecule to efficiently reach the CI. As an outlook, the optimization of a photochromic molecule should rely on the accurate knowledge of CI geometry, a feat attainable with *ab initio* calculations. We are currently attempting to enhance the direct photocyclization mechanism presented in this paper through appropriate structural modifications guided by first-principle CI calculations.

Acknowledgements

D.J. acknowledges the European Research Council (ERC) and Région des Pays de La Loire for financial support in the framework of a Consolidator Grant (Marches – 278845) and a recrutement sur poste stratégique, respectively. All authors acknowledge the IRG PHoto-switchablE orgaNIC molecular systems & deviceS (PHENICS) for support. This research used resources of the GENCI-CINES/IDRIS (Grant c2011086680).

© 2016 Tous droits réservés.
doc.univ-lille1.fr

Published on 22 October 2014. Downloaded by Univ Lille 1 on 31/08/2016 11:31:36.

References

1 H. Dürr and H. Bouas-Laurent, *Photochromism, Molecules, and Systems*, Elsevier, Amsterdam, 1990.
2 J. C. Crano and R. J. Guglielmetti, *Organic Photochromic and Thermochromic Compounds*, Plenum, New York, vol. 1 and 2, 1999.
3 K. Uno, H. Niikura, M. Morimoto, Y. Ishibashi, H. Miyasaka and M. Irie, *J. Am. Chem. Soc.*, 2011, **133**, 13558.
4 M. Morimoto and M. Irie, *J. Am. Chem. Soc.*, 2010, **132**, 14172.
5 M. Irie, *Chem. Rev.*, 2000, **100**, 1685.
6 M. Irie, *Chem. Rev.*, 2000, **100**, 1683.
7 M. Irie, *Bull. Chem. Soc. Jpn.*, 2008, **81**, 917.
8 S. Fukumoto, T. Nakashima and T. Kawai, *Eur. J. Org. Chem.*, 2011, 5047.
9 S. Fukumoto, T. Nakashima and T. Kawai, *Angew. Chem., Int. Ed.*, 2011, **50**, 1565.
10 W. Li, C. Jiao, X. Li, Y. Xie, K. Nakatani, H. Tian and W. Zhu, *Angew. Chem.*, 2013, **126**, 4691.
11 W. Li, C. Jiao, X. Li, Y. Xie, K. Nakatani, H. Tian and W. Zhu, *Angew. Chem., Int. Ed.*, 2014, **53**, 4603.
12 Y. Ishibashi, H. Miyasaka, S. Kobatake, M. Irie and Y. Yokoyama, *2007 Pacific Rim Conference on Lasers and Electro-Optics*, vol. 1–4, 2007, 1364.
13 Y. Ishibashi, M. Mukaida, M. Falkenstrom, H. Miyasaka, S. Kobatake and M. Irie, *Phys. Chem. Chem. Phys.*, 2009, **11**, 2640.
14 Y. Ishibashi, K. Okuno, C. Ota, T. Umesato, T. Katayama, M. Murakami, S. Kobatake, M. Irie and H. Miyasaka, *Photochem. Photobiol. Sci.*, 2010, **9**, 172.
15 S. Aloise, M. Sliwa, Z. Pawlowska, J. Rehault, J. Dubois, O. Poizat, G. Buntinx, A. Perrier, F. Maurel, S. Yamaguchi and M. Takeshita, *J. Am. Chem. Soc.*, 2010, **132**, 7379.
16 S. Aloise, M. Sliwa, G. Buntinx, S. Delbaere, A. Perrier, F. Maurel, D. Jacquemin and M. Takeshita, *Phys. Chem. Chem. Phys.*, 2013, **15**, 6226.
17 A. Perrier, S. Aloise, M. Olivucci and D. Jacquemin, *J. Phys. Chem. Lett.*, 2013, **4**, 2190.
18 M. Takeshita, C. Tanaka, T. Miyazaki, Y. Fukushima and M. Nagai, *New J. Chem.*, 2009, **33**, 1433.
19 K. Uchida and M. Irie, *Chem. Lett.*, 1995, 969.
20 G. Buntinx, R. Naskrecki and O. Poizat, *J. Phys. Chem.*, 1996, **100**, 19380.
21 B. Moine, J. Rehault, S. Aloise, J. C. Micheau, C. Moustrou, A. Samat, O. Poizat and G. Buntinx, *J. Phys. Chem. A*, 2008, **112**, 4719.
22 T. Nakayama, Y. Amijima, K. Ibuki and K. Hamanoue, *Rev. Sci. Instrum.*, 1997, **68**, 4364.
23 M. J. Frisch, G. W. Trucks, H. B. Schlegel, G. E. Scuseria, M. A. Robb, J. R. Cheeseman, G. Scalmani, V. Barone, B. Mennucci, G. A. Petersson, H. Nakatsuji, M. Caricato, X. Li, H. P. Hratchian, A. F. Izmaylov, J. Bloino, G. Zheng, J. L. Sonnenberg, M. Hada, M. Ehara, K. Toyota, R. Fukuda, J. Hasegawa, M. Ishida, T. Nakajima, Y. Honda, O. Kitao, H. Nakai, T. Vreven, J. A. Montgomery, Jr., J. E. Peralta, F. Ogliaro, M. Bearpark, J. J. Heyd, E. Brothers, K. N. Kudin, V. N. Staroverov, R. Kobayashi, J. Normand, K. Raghavachari, A. Rendell, J. C. Burant, S. S. Iyengar, J. Tomasi, M. Cossi, N. Rega, N. J. Millam, M. Klene, J. E. Knox, J. B. Cross, V. Bakken, C. Adamo, J. Jaramillo, R. Gomperts, R. E. Stratmann, O. Yazyev, A. J. Austin, R. Cammi, C. Pomelli, J. W. Ochterski, R. L. Martin, K. Morokuma, V. G. Zakrzewski, G. A. Voth, P. Salvador, J. J. Dannenberg, S. Dapprich, A. D. Daniels, Ö. Farkas, J. B. Foresman, J. V. Ortiz, J. Cioslowski and D. J. Fox, *Gaussian 09*, Gaussian, Inc., Wallingford, CT, 2009.
24 D. Jacquemin, A. Planchat, C. Adamo and B. Mennucci, *J. Chem. Theory Comput.*, 2012, **8**, 2359.
25 J.-D. Chai and M. Head-Gordon, *J. Chem. Phys.*, 2008, **128**, 084106.
26 N. Mardirossian, J. A. Parkhill and M. Head-Gordon, *Phys. Chem. Chem. Phys.*, 2011, **13**, 19325.
27 D. Jacquemin, E. Perpete, I. Ciofini and C. Adamo, *Theor. Chem. Acc.*, 2011, **128**, 127.
28 X. Li and M. J. Frisch, *J. Chem. Theory Comput.*, 2006, **2**, 835.
29 J. Tomasi, B. Mennucci and R. Cammi, *Chem. Rev.*, 2005, **105**, 2999.
30 M. Cossi and V. Barone, *J. Chem. Phys.*, 2001, **115**, 4708.
31 R. Cammi and B. Mennucci, *J. Chem. Phys.*, 1999, **110**, 9877.
32 C. Adamo and V. Barone, *J. Chem. Phys.*, 1999, **110**, 6158.
33 M. Ernzerhof and G. E. Scuseria, *J. Chem. Phys.*, 1999, **110**, 5029.
34 R. Improta, V. Barone and F. Santoro, *Angew. Chem., Int. Ed.*, 2007, **46**, 405.
35 B. Mennucci, *J. Phys. Chem. Lett.*, 2010, **1**, 1666.

This journal is © the Owner Societies 2014
© 2016 Tous droits réservés.
doc.univ-lille1.fr

Annexe 7. Lietard et al, PCCP, 16, 22262, 2014

HDR de Stéphane Aloïse, Lille 1, 2016

PCCP

PAPER

View Article Online
View Journal | View Issue

Cite this: *Phys. Chem. Chem. Phys.*, 2014, **16**, 22262

Competitive direct *vs.* indirect photochromism dynamics of constrained inverse dithienylethene molecules†

Aude Lietard,[abc] Giovanni Piani,[ab] Lionel Poisson,*[ab] Benoît Soep,[ab] Jean-Michel Mestdagh,[ab] Stéphane Aloïse,[d] Aurélie Perrier,[e] Denis Jacquemin[fg] and Michinori Takeshita[h]

Received 26th May 2014,
Accepted 28th August 2014

DOI: 10.1039/c4cp02310b

www.rsc.org/pccp

State-of-the-art experimental and theoretical tools were used to investigate the gas-phase relaxation dynamics of various photoexcited photochromic dithienylethene molecules in situations where several relaxation channels are simultaneously at play. Unconstrained and constrained dynamics were addressed by considering unbridged and bridged molecules with a polyether bridge of various sizes (from 2 to 4 units). Time-resolved ultrafast ionization spectroscopy techniques were used to probe the dynamics. This revealed the existence of several relaxation pathways from the first excited state to the ground-state. Characteristic times were determined for each process. These channels compete at an early stage of the dynamics only when the initial wavepacket splits into two parts. A striking excited state wavepacket oscillation is observed in bridged molecules. A general reaction mechanism is proposed which rationalizes the carbon–carbon distance rule which is widely used as an empirical tool to predict the photoactivity of photochromic molecules in crystals.

Published on 29 August 2014. Downloaded by Univ Lille 1 on 31/08/2016 14:53:47.

1 Introduction

A major part of femtochemistry studies on isolated molecules in the gas phase concerns situations where a series of non-adiabatic events occur sequentially.[1] Although the number of degrees of freedom is significant in large organic molecules, a single process often dominates each step of the sequential decay and competing relaxation processes can be neglected. Here, we aim to explore a significantly different situation where parallel and competing relaxation processes are simultaneously at play inside the same molecule. Although the present paper adopts a very general point-of-view with respect to parallel relaxation processes in molecules isolated in the gas phase, photochromic dithienylethene molecules will be considered in view of their practical impact. We consider it indeed important to examine whether in the intrinsic dynamics of these molecules the photochromic reaction pathway is in competition with relaxation pathways which reduce the photochromic yield.

The IUPAC Technical Report on ''Organic Photochromism''[2] defines photochromism as a reversible transformation of chemical species induced in one or the reverse direction by absorption of electromagnetic radiation between two forms, A and B, each one having a different absorption spectrum. Photochromic molecules present various optoelectronic applications such as optical memory devices and optical switches.[3]

Normal dithienylethene (N-DTE) and its substituted derivatives are often used as photochromic organic compounds. Numerous studies in condensed phases, solutions[4–6] or crystals[7,8] have revealed their outstanding properties: *e.g.* weak photodegradation, excellent thermal stability and high photoconversion yield. Theoretical investigations are also available.[9–13] The photochromic reaction pathway of these molecules corresponds to a switch between an open form (OF) and a closed form (CF) through a photoinduced electrocyclization process. The ring closure reaction is initiated by UV radiation while the reverse process occurs upon visible irradiation. The time scale of the OF–CF photoconversion

[a] *CNRS, IRAMIS, LIDyL, Laboratoire Francis Perrin, URA 2453, 91191 Gif-sur-Yvette, France*
[b] *CEA, IRAMIS, LIDyL, Laboratoire Francis Perrin, URA 2453, 91191 Gif-sur-Yvette, France. E-mail: lionel.poisson@cea.fr*
[c] *Université Paris Sud 11 – ED470 Chimie de Paris Sud, 91450 Orsay CEDEX, France*
[d] *Université Lille 1 – LASIR UMR 8516, 59655 Villeneuve d'Ascq CEDEX, France*
[e] *Université Paris 7 – Sorbonne Paris Cité – ITODYS UMR 7086, 75205 Paris CEDEX, France*
[f] *Laboratoire CEISAM – UMR CNRS 6230, Université de Nantes, 2 Rue de la Houssinière, BP 92208, 44322 Nantes Cedex 3, France*
[g] *Institut Universitaire de France, 103 Boulevard Saint Michel, 75005 Paris Cedex 5, France*
[h] *Department of Chemistry and Applied Chemistry, Faculty of Science and Engineering, Saga University, Honjo 1, Saga 840-8502, Japan*

† Electronic supplementary information (ESI) available: Full tables and molecular orbitals. See DOI: 10.1039/c4cp02310b

This journal is © the Owner Societies 2014

© 2016 Tous droits réservés.

doc.univ-lille1.fr

Published on 29 August 2014. Downloaded by Univ Lille 1 on 31/08/2016 14:53:47.

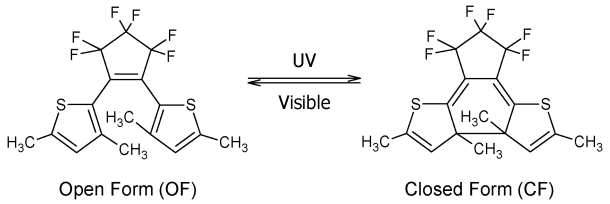

Fig. 1 Photochromic reaction of I-DTE.

falls in the picosecond range and varies with the molecular structure.[14,15] In crystals,[16,17] the photochromic yield is strongly dependent on the distance between the two carbon atoms which participate in the photocyclisation, hence offering a qualitative tool to rationalize photochromic efficiencies in view of applications.

The present paper addresses a slightly different class of molecules, derivatives of inverse dithienylethene (I-DTE), where a photoconversion between OF and CF is also responsible for the photochromic property. The OF and CF of I-DTE molecules are shown in Fig. 1. I-DTE differs from N-DTE by the bond location between the lateral thienyl substituents and the perfluorocyclopentene ring. One is in the β position of the sulfur atom in N-DTE whereas the other is in the α position in I-DTE. The latter configuration offers more flexibility to synthesize substituted I-DTE molecules.[18] I-DTE hence appears as the photochromic core of a new class of photochromic compounds which have not yet received as much attention as N-DTE molecules. The similarities and differences between I-DTE and N-DTE systems have been explored in several studies.[9,13,18–22]

The dithienylethene OF (both N-DTE and I-DTE) presents two conformations that are distinguished by the parallel (called P conformer of pseudo-C_s symmetry) or antiparallel (AP conformer of pseudo-C_2 symmetry) orientation of the thienyl groups. Condensed phase experiments on N-DTE revealed a very slow internal conversion between the two conformers with a much larger timescale than μs.[4] This suggests that the P and AP conformers are separated by large energy barriers. A lower barrier was observed for I-DTE.[9] The fact that the P conformer, where the thienyl groups do not have the proper orientation for the photocyclisation reaction, has no photochromic property is an indication that the landscape in the excited potential energy surface (PES) is also fairly complicated with basins and energy barriers which prevent finding the photochromic pathway to CF within the lifetime of the excited state. The existence of a non-reactive conformer is an important issue for the practical use of DTE molecules. Bridged variants of the I-DTE molecules have been synthesized, named I-DTE-O_x with x = 2, 3, 4, in order to lock the ground state I-DTE core with the reactive geometry (AP conformer); they are shown in Fig. 2 together with unbridged I-DTE molecule. Other kinds of I-DTE bridged molecules with chiral bridges were synthesized and NMR studies were done, which showed that 100% of these bridged molecules are locked in the AP conformer in $CDCl_3$ solvent.[20] In the present work I-DTE-O_x molecules are isolated in the gas phase, and we anticipate that the efficiency of bridges in these molecules may be reduced due to the flexibility of the bridge.

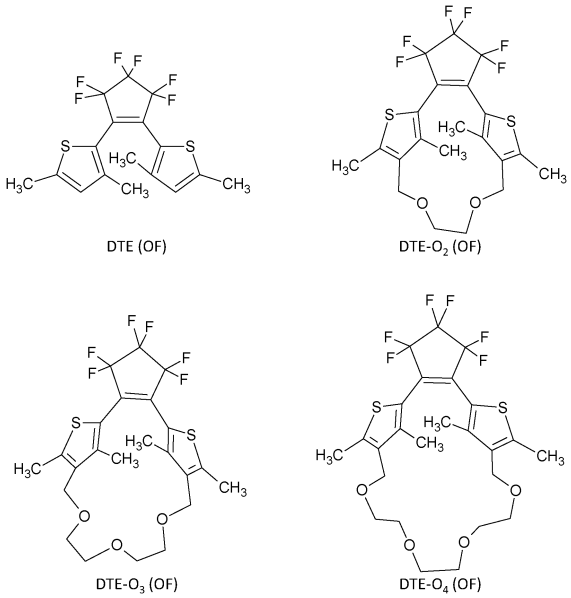

Fig. 2 Opened forms of basic and bridged molecules.

We mentioned above that the excited PES landscape in N-DTE is fairly complicated; this must be the case in I-DTE also. In the perspective of femtochemistry studies which are at the center of the present work, the presence of multiple energy basins and barriers may result in a splitting of the initial wavepacket and evolution along relaxation pathways which compete together. This offers a unique benchmark to explore dynamical regimes involving parallel relaxation pathways. The present experimental work complemented by theoretical calculations considers the I-DTE and I-DTE-O_x molecules, shown in Fig. 2, isolated in the gas phase. The basic idea is to launch the photochromic I-DTE core in different regions of the excited PES to explore how subsequent dynamics is affected by the initial geometry. Since the Franck–Condon principle precludes varying the region of excitation, the series of I-DTE-O_x bridged molecules is used to create a variety of initial geometries around the AP conformer and to observe the competition between the photochromic reaction pathway and non-reactive pathways.

On the experimental side, the gas phase reaction dynamics of I-DTE and I-DTE-O_x molecules is explored using the femtosecond pump–probe approach in a detection scheme which couples photoelectron spectrometry and ion mass spectrometry. This documents directly the relaxation of the initial electronic excitation within electronic states as a function of the time delay between the photoexcitation pump and photoionization probe. The interpretation of these results is supported by density functional theory (DFT) and time dependent-DFT (TD-DFT) calculations, which give an overview of the isomers which can be present in the experiment and document their excitation and ionization energies. Besides revealing the evidence of the parallel relaxation pathway, joint experiment/theory allows us to propose a general model which accounts for the cyclisation reaction mechanism in isolated I-DTE compounds.

© 2016 Tous droits réservés.
doc.univ-lille1.fr

Published on 29 August 2014. Downloaded by Univ Lille 1 on 31/08/2016 14:53:47.

2 Experimental details

The setup used for the present femtosecond pump–probe experiments has been described elsewhere[23,24] and is shown in Fig. 3. Shortly a pulsed valve operating at 20 Hz creates a supersonic jet in the source chamber ($P_{source} \sim 10^{-5}$ mbar). Helium is used as the carrier gas at a pressure of *ca.* 2 bars. An oven is mounted on the orifice plate of the valve. The solid sample is introduced in the oven and maintained at a temperature between 320 K and 350 K, below the limit of the decomposition of the molecule which is to be evaporated. The latter is checked experimentally by mass spectrometry.

After passing through a 1 mm diameter conical skimmer, the molecular beam enters the detection chamber ($P_{detection} \sim 10^{-7}$ mbar) where it perpendicularly crosses the pump and probe femtosecond laser beams. The pump laser wavelength is the third harmonic of a Ti:sapphire laser and was measured at 265 nm, with ~3 nm full-width-at-half-maximum (fwhm). The probe laser wavelength was measured at 795 nm (Ti:sapphire laser), with ~20 nm fwhm. The measured cross correlation between the laser pulses is 120 fs. The probe pulse is delayed by a variable time with respect to the pump pulse. The pump–probe delay is varied up to 60 ps, enough to cover the entire dynamics.

The probe operates by multiphoton ionization. The resulting photoions (PIs) and photoelectrons (PEs) are extracted along a vertical axis. The PIs are monitored using a Time-of-Flight Mass Spectrometer (TOF-MS) and the PEs are monitored independently using a Velocity Map Imaging (VMI) device[25] which documents their kinetic energy and angular distribution.

Raw images of the 2D projection of the PE distribution are recorded using a CCD camera. To recover the 3D distribution, they are inverted according to the pBASEX algorithm[26] using the LV_pBASEX inverse Abel Transform software.[27] Since raw images suggest an isotropic distribution of the PEs, the inversion procedure was limited to an isotropic decomposition. The energy calibration of the image was provided by the multiphoton ionization of the oxygen molecule.[28,29]

The I-DTE derivatives used in the present work (see Fig. 2) were synthesized and purified as described by Takeshita *et al.*[18] I-DTE 1,2-bis(3,5-dimethyl-2-thienyl)perfluorocyclopentene features the photochromic core which is presented in the bridge molecules. The latter are constrained with a polyether bridge and are named I-DTE-O_x where x corresponds to the number of oxygen atoms in the polyether bridge.

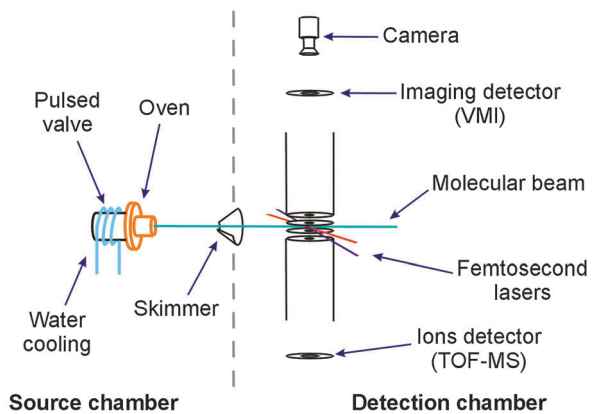

Fig. 3 Schematic of the experimental setup.

3 Computational methods

The photochromic core of the I-DTE molecules is composed of three rigid rings. Hence, a reduced number of flexible coordinates need to be explored to identify the possible conformers. Nevertheless, due to the flexibility of the polyether bridge a large number of rotamers are accessible to the bridged I-DTE-O_x molecules. For this reason, a two-step protocol was used to explore the ground state PES. In the first step, molecular dynamics (MD) simulations were performed to identify a panel of structures and the results reflect the chemical intuition (see the ESI,† for details). At this stage, various conformers, including P and AP conformers, were identified. In the second step, molecular structures, selected from MD trajectories, were optimized using the Gaussian 09 package.[30] These optimizations have been performed both for the ground-state (S_0) and excited-state (S_n) using DFT and TD-DFT approaches, respectively. The 6-31G+(d) atomic basis set was used since it was found to yield valuable results for both the geometrical and optical properties of a rich variety of conjugated molecules.[31] Because of the size of these molecules the calculation was limited to I-DTE-O_x, $x \leq 3$.

In line with previous DFT calculations dedicated to N-DTE,[9] the minima of the S_0 and S_n PES of the I-DTE-$O_{2,3}$ molecules have been determined using the ωB97X range-separated hybrid functional.[32,33] Unlike conventional hybrid functionals, these hybrids avoid the common overtwisting problem of the excited-state structure[31] and produce valid S_n geometries. A tight convergence criterion (residual RMS force smaller than 10^{-5} a.u.) was used. Hereafter, the $S_{n,opt}$ geometry refers to the structure of the molecule optimized in the S_n state. To ascertain the nature of the optimized structures, vibrational frequencies have been systematically computed using analytical and numerical derivatives for the S_0 and S_n critical points, respectively.

The PBE0 hybrid functional has been used to determine the UV-vis optical properties.[34,35] It was chosen for its fast and accurate predictions of the absorption and emission properties of I-DTE in the condensed phase.[9]

The calculation results are detailed in the ESI† where optimized geometry of the conformers is given together with vertical and adiabatic transition energies of the first lowest excited states. Information on theoretically determined ionization energies is also provided in the ESI.† Results which are directly relevant to the present experimental work are listed in Table 3.

4 Experimental results

4.1 Photoelectron spectrometry

PE images were recorded up to a pump–probe delay of 60 ps for I-DTE and I-DTE-$O_{2,3}$ molecules. After inversion, the radial distribution in each image reflects a PE spectrum. Given that

This journal is © the Owner Societies 2014
© 2016 Tous droits réservés.
doc.univ-lille1.fr

Published on 29 August 2014. Downloaded by Univ Lille 1 on 31/08/2016 14:53:47.

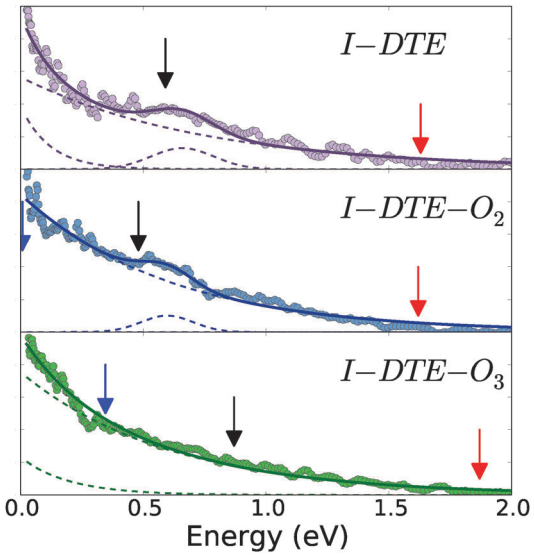

Fig. 4 Summed PE spectra. The dotted lines represent the contributions to the fit performed with the parameter listed in Table 1. The arrows indicate the maximum PE energy expected from a vertical [1 pump + 3 probe photon] ionization scheme from the S_0 optimized geometry $S_{0,opt}$ (in red); from a 3 probe photon ionization of the S_1 state with the $S_{0,opt}$ geometry (in black); and from a 3 probe photon ionization of the S_1 state with the $S_{1,opt}$ geometry (in blue) (out of the figure range for I-DTE in the top panel). The arrows are located with the theoretical calculations reported in Section 3.

the measured signals are fairly low, the section below reports various summations within these spectra to get reliable information.

4.1.1 Summed photoelectron spectra. To increase substantially the signal/noise ratio and to identify clearly the shape of PE spectra, all those measurements performed at various pump–probe delays are summed together. Summed spectra are shown in Fig. 4 for I-DTE and I-DTE-$O_{2,3}$. The PE signal is too low with I-DTE-O_4 to deserve a reliable PE spectrum. This is due to a very small lifetime of the product under the temperature conditions in the oven which cannot be compensated by using large product quantities, given the low yield of its synthesis.

Although broad and apparently structureless, the spectra in Fig. 4 can be decomposed as a combination of two exponential decay functions and a Gaussian function centred at about 0.6–0.7 eV which mimics a broad peak. Nevertheless, a single exponential decay is observed in the middle panel for I-DTE-O_2 and the Gaussian peak is visible for I-DTE and I-DTE-O_2 only. The fit parameters which define the exponential decay and Gaussian functions are reported in Table 1. Given the location of the black arrows in Fig. 4, the broad Gaussian peak can be assigned to a 3 probe photon ionization of the S_1 state in the $S_{0,opt}$ geometry, *i.e.* prior to any structural relaxation.

4.1.2 Time resolved photoelectron signals. Summation over the radial distribution in each image leads to the total PE signal as a function of the pump–probe delay. This is shown in Fig. 5 up to 6 ps and in the inserts up to 20 ps. For each molecule, a multiexponential evolution is observed: first, a rapid decay (few hundreds of femtoseconds); then a longer one (few picoseconds); and finally the signal does not go to zero at very long time scales (see inserts at ~20 ps) and stabilizes to ~5–10% of the maximum. The PE signals in Fig. 5 were fitted by two exponential decay functions $\left(\exp\left(-\frac{t}{t_i}\right) \text{with } i = 1,2\right)$ convoluted by the cross correlation function of the pump and probe laser pulses. For reasons that will appear later, the plateau is represented by a step function at time zero, also convoluted by the cross-correlation function. The time constant of the exponential functions is given at the top of Table 2 for each molecule. The interpretation model which justifies this fit is presented later.

4.1.3 Time resolved PE signal at low and high PE energies. When inspecting the PE images recorded at pump–probe delays between 0 and 60 ps, the shape of the PE spectra does not change significantly, and does not need to be presented thoroughly. However, the behavior at a time delay below 1 ps reveals small differences, at the limit of sensitivity of the experiment, when comparing the PE signals corresponding to low (<0.25 eV) and high (>1.2 eV) PE kinetic energies. Evolution of the PE signals as a function of the pump–probe time delay is reported in Fig. 6. The increasing time of the low energy signal (in purple) is apparently slower by ~25 fs in I-DTE and I-DTE-O_3. This corresponds to a 25 fs delay to reach the maximum, and this extra delay shows up also in the decay after the signal has reached its maximum.

4.2 Photoion experiments

4.2.1 Mass spectra. Time-of-Flight (TOF) mass spectra have also been collected for each molecule as a function of the pump–probe delay. Fig. 7 shows the sum of all TOF spectra recorded during an experiment. In each spectrum, the parent

Table 1 Parameters defining the two exponential decay $\left(\exp\left(-\frac{E}{E_i}\right)\right)$ and the Gaussian $\left(\exp\left(-\frac{(E-E_0)^2}{2\sigma^2}\right)\right)$ functions used to fit the PE spectra displayed in Fig. 4. The last two columns give the location of the red and black arrows in Fig. 4 (E_{PE} is the expected energy of the ejected PE. [X,Y′] correspond respectively to the number of pump and probe photons)

	Exponential 1	Exponential 2	Gaussian			
	E_1 (eV)	E_2 (eV)	fwhm (eV)	E_0 (eV)	Max E_{PE} from $S_{0,opt}$[1,3′] (eV)	Max E_{PE} from $S_{1,opt}$[3′] (eV)
I-DTE	0.120	0.750	0.180	0.660	1.63	0.59
I-DTE-O_2	—	0.600	0.150	0.600	1.62	0.48
I-DTE-O_3	0.200	0.600	—	—	1.87	0.87

© 2016 Tous droits réservés.
doc.univ-lille1.fr

Published on 29 August 2014. Downloaded by Univ Lille 1 on 31/08/2016 14:53:47.

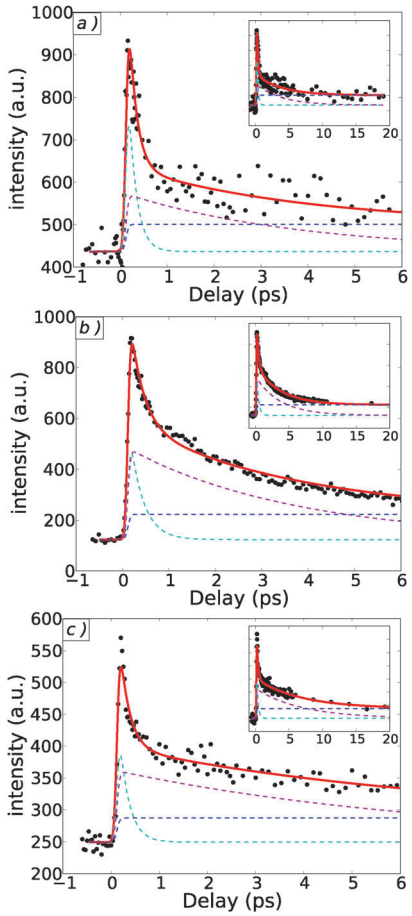

Fig. 5 Total PE signal as a function of the pump–probe delay for the I-DTE (a), I-DTE-O_2 (b) and I-DTE-O_3 (c) molecules. The pump and probe wavelengths are 265 and 795 nm respectively. The full curve running through the experimental points is a fit using the parameters listed in Table 2. The dashed curve shows the contribution of the two exponential decays and step function used in the fit (see text for details).

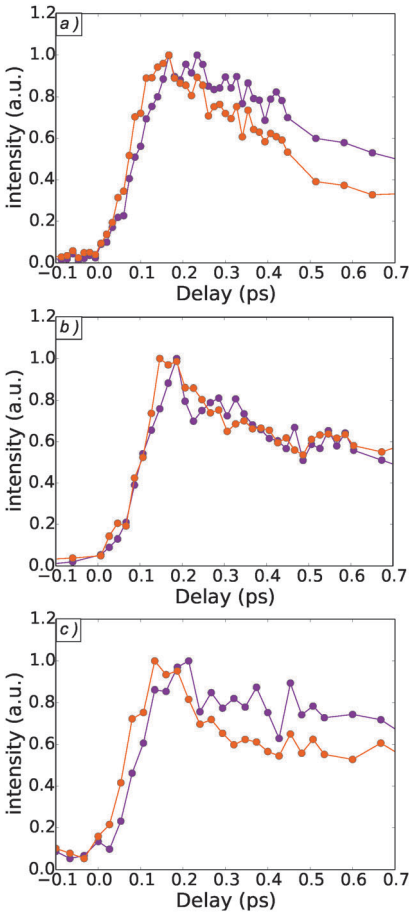

Fig. 6 PE signal corresponding to low (<0.25 eV, in purple) and high (>1.2 eV, in orange) PE kinetic energy as a function of the pump–probe time delay for the I-DTE (a), I-DTE-O_2 (b) and I-DTE-O_3 (c) molecules. The pump and the probe wavelengths are at 265 and 795 nm respectively.

Table 2 Relaxation time constants of I-DTE, I-DTE-O_2, I-DTE-O_3 and I-DTE-O_4 from the PE signal and oscillation period of each bridged molecule from the TOF signal

	I-DTE	I-DTE-O_2	I-DTE-O_3	I-DTE-O_4
t_1	170 ± 4 fs	290 ± 3 fs	200 ± 3 fs	120 ± 5 fs
t_2	3.8 ± 0.1 ps	3.70 ± 0.01 ps	6.80 ± 0.03 ps	1.75 ± 0.04 ps
Period	—	1.03 ± 0.01 ps	1.20 ± 0.03 ps	1.1 ± 0.1 ps

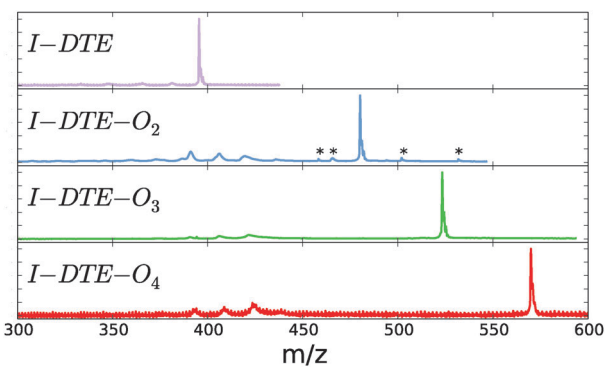

Fig. 7 Mass spectrum of the I-DTE, I-DTE-O_2, I-DTE-O_3 and I-DTE-O_4 molecules as labeled in the figure. Peaks marked with an asterisk (*) are due to impurities.

mass is assigned to the narrow peak with the characteristic sulfur and carbon isotopic distribution. Fragment peaks are observed at lower masses. They are broader than the parent peak, due to the recoil velocity along the fragmentation coordinate. Note that the fragmentation likely occurs during the ionization process, when the absorption of extra photons above the ionization limit gives enough internal energy to stimulate its fragmentation.[23]

The parent peak is observed at 396, 482, 526 and 570 amu in the mass spectra of I-DTE, I-DTE-O_2, I-DTE-O_3 and I-DTE-O_4, respectively. No other intense narrow peak is observed, indicating both the purity of the sample used in these experiments and the absence of the thermal degradation in the oven. Nevertheless, impurities are observed in small quantities with I-DTE-O_2; they are labeled with stars in the figure.

A very small fragmentation is observed with I-DTE, compared to the other molecules. The fragments correspond to a loss of methyl groups. For the three bridged molecules, fairly

This journal is © the Owner Societies 2014
© 2016 Tous droits réservés.
doc.univ-lille1.fr

Published on 29 August 2014. Downloaded by Univ Lille 1 on 31/08/2016 14:53:47.

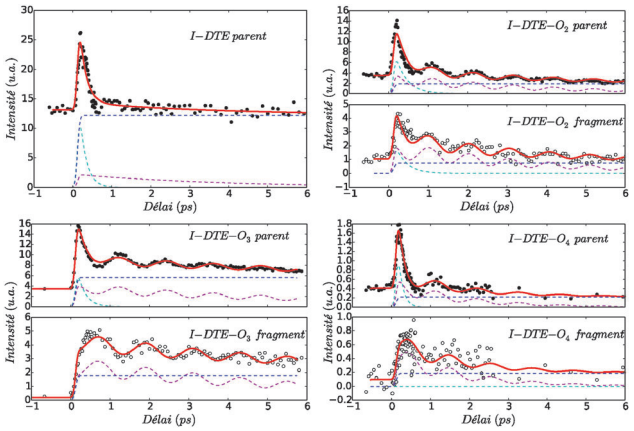

Fig. 8 Ion peak intensity as a function of the pump–probe time delay as labelled in the figure. The pump and the probe wavelengths are at 265 and 795 nm respectively. The full line is a fit running through the experimental points and the dotted lines are the contributions (see text for details).

large intensity fragments are measured at 394, 409 and 424 amu. They correspond to the partial or total loss of the polyether bridge. No other fragment is observed with I-DTE-O_3 and I-DTE-O_4. In contrast a close inspection of the I-DTE-O_2 spectrum reveals barely visible fragments between 300 and 370 amu. Another fragment, which does not appear with the scale of Fig. 7, is also observed at 60 amu for I-DTE-O_2. This corresponds to the ionized polyether bridge.

4.2.2 Time resolved PI signals. The intensity of each peak in the above mass spectra was monitored as a function of the pump–probe delay. Summing the signal for all fragments leads to the full PI signal. It has been checked that its time dependence has the same shape as observed in Fig. 5 for the corresponding PE signals. Since no charged particule, electron or ion is lost in the detection, the full PI signal is indeed the exact counterpart of the PE signal.

Time dependent PI signals are shown in Fig. 8 for a few peaks: the I-DTE, I-DTE-O_2, I-DTE-O_3, I-DTE-O_4 parents and for the bridged molecules, the fragment of largest mass (m/z = 424). As observed in Fig. 5 for the PE signals but with a different ratio, a rapid decay is followed in each parent peak by a longer decay. The very striking observation with the bridged molecules is that an oscillation regime, which does not show up at first glance in the PE signals, is superimposed on the longer decay for both the parent and the fragment. Apparently in-phase oscillations are observed between the parent and fragment of I-DTE-O_2 whereas the oscillations are very distinctly out-of-phase for I-DTE-O_3. Given the signal/noise ratio, it is hard to conclude for I-DTE-O_4.

For technical reasons, it was not possible to reduce the 2-photon ionization of the parent molecule by the pump pulse alone. Hence, the parent peak intensity is not zero at negative time when the probe pulse precedes the pump pulse. In turn at positive time, both photo-excited and ionized parent molecules are present and interact with the probe pulse. The former lead to the time dependent signal and reflect the desired excited state dynamics of the parent molecule whereas the latter may absorb a probe photon and fragment subsequently. Calculations on the electronically excited I-DTE ions show indeed that energy levels are present in the 1 to 2 eV excitation range of the I-DTE-O_x ions. The excess energy due to the absorption of a probe photon (1.5 eV) may induce fragmentation, thus reducing the amount of parent ion. This explains why for a long time delay, the parent ion signal goes below that measured at negative time. This effect is clearly observed for I-DTE-O_2 and I-DTE-O_4, barely visible for I-DTE and not at all for I-DTE-O_3. Since 2-pump-photon ionization is likely to form the molecular ion out of its equilibrium geometry, the subsequent absorption of a probe photon can depend on the pump–probe delay, due to the structural relaxation of the molecular ion about its equilibrium geometry. When observed, *i.e.* for I-DTE-O_2 and I-DTE-O_4, this effect is superimposed on (and likely hard to disentangle from) the time dependent photoionization signal which reflects the excited state dynamics of the parent molecule.

5 Data analysis and discussion

5.1 Initial excited state

Table 3 indicates that the transition to the S_1 state of the OF-AP conformers of I-DTE, I-DTE-O_2 and I-DTE-O_3 presents a strong oscillator strength and corresponds to a HOMO → LUMO electron promotion. In contrast, transition to S_2 and S_3 states presents smaller oscillator strengths, reduced by a factor 4. Hence, the pump pulse at 265 nm (∼4.6 eV) is likely to populate the S_1 state rather than S_2 or S_3 although it has enough energy to promote transitions above the S_3 state.

The molecular orbitals corresponding to the S_0–S_1 excitation are shown in the ESI.† Their shape is typical of open-ring dithienylethenes[36] and indicates that the electronic excitation corresponds to a transitions of ππ* character mainly localized on the double bonds of the central ring. It has been shown that such a characteristic is required to induce the cyclisation reaction which is responsible for the photochromic property of DTE.[37]

Table 3 Vertical excitation energy calculated at the TD-PBE0/6-31+G(d)//ωB97X/6-31+G(d) level for OF-AP conformer in the $S_{0,opt}$ geometry, corresponding oscillator strengths f and state description. D_0 is the ground state of the ion. The complete table is presented in the ESI

Molecule	State	Excitation energy (eV)	f	State description
I-DTE	S_1	3.63	0.28	HOMO → LUMO
	S_2	4.23	0.07	HOMO − 1 → LUMO
	S_3	4.45	0.06	HOMO − 2 → LUMO
	D_0	7.72	—	—
I-DTE-O_2	S_1	3.53	0.15	HOMO → LUMO
	S_2	4.16	0.05	HOMO − 1 → LUMO
	S_3	4.31	0.04	HOMO − 2 → LUMO
	D_0	7.73	—	—
I-DTE-O_3	S_1	3.67	0.34	HOMO → LUMO
	S_2	4.27	0.07	HOMO − 1 → LUMO
	S_3	4.35	0.01	HOMO − 2 → LUMO
	D_0	7.48	—	—

© 2016 Tous droits réservés.
doc.univ-lille1.fr

HDR de Stéphane Aloïse, Lille 1, 2016 View Article Online

Published on 29 August 2014. Downloaded by Univ Lille 1 on 31/08/2016 14:53:47.

5.2 Gas phase dynamics: an enhanced complexity

Four dynamical features characterize the gas phase dynamics of I-DTE and I-DTE-O_x: two time constants in the order of 120–290 fs and 1–7 ps, and a plateau which might reflect a very slow decay in the $\gg$100 ps regime. These three dynamical features might be compared to decays observed by Ishibashi *et al.*[4] and Sangdeok *et al.*[6] in time resolved studies in the condensed phase. A fourth, very important dynamical feature exists in the gas phase dynamics of bridged I-DTE-O_x molecules: an oscillation regime which is superimposed on the few picosecond delay. These 4 dynamical features are discussed hereafter.

5.2.1 Two competitive relaxation mechanisms. The photochromism of dithienylethene molecules is associated with the photoinduced electrocyclization reaction shown in Fig. 1. The distance between the two C-atoms forming the CC bond during the cyclisation process is larger in the OF than in the CF. This appears as a convenient order parameter to examine the photoinduced OF-to-CF switch. We define as the ''*OF–CF distance*'' the distance between the two C-atoms involved in the σ-bond formation.

The OF–CF distance of the optimized S_0 state is larger than the one of the S_1 state. This suggests that slopes exist on the S_1 surface, which can move the molecule out of the Franck–Condon region of excitation and drive it to a region of shorter OF–CF distance. Note that the σ-bond is not formed at the geometry of the S_1 state. The two carbon atoms, which will be eventually bound together, are simply in better position to do so than at the S_0 equilibrium geometry. This suggests that the OF–CF distance cannot be identified directly as the reactive coordinate even if it is involved in the reaction mechanism. Likely, deformations along several coordinates associated with a non-adiabatic energy transfer to the ground state PES participate simultaneously to the photocyclisation process.

Calculations performed on a model skeleton of the I-DTE molecules showed that conical intersections (CIs) exist between the S_1 and the S_0 PES which could drive a fast relaxation from the S_1 state to the ground state,[10,13] finally promoting the electrocyclization reaction on the ground state surface. Importantly CIs cannot be reached from the Franck–Condon region of the S_0–S_1 excitation by simply varying the OF–CF distance, but through multidimensional dynamics.

We have seen that the S_0–S_1 excitation corresponds to a ππ* transition localized on the C=C double bond of the central ring. An analogy can be drawn with the behavior of mono-alkenes and cyclic alkenes. The ππ* excitation in these molecules results in multidimensional dynamics where torsion about the C=C double bond is combined with pyramidalization about one of the carbon atoms. Then the molecule reaches a CI which funnels the electronic excitation as vibration of the ground state.[38] The same kind of behavior is likely at play in the initial step of the excited state dynamics of the I-DTE and I-DTE-O_x molecules. Accordingly, the ππ* transition launches a vibrational wavepacket on the S_1 PES, which will undergo multidimensional propagations, initially along torsion and pyramidalization coordinates. As it spreads on the excited PES, the wavepacket can reach the CI mentioned above. A rapid transfer to the ground state and subsequent photocyclisation would proceed. The faster time constant which appears in Table 2 documents the early dynamics of excited I-DTE and I-DTE-O_x molecules and must be assigned to this pathway. This falls in the 120–290 fs range for those molecules studied in the present work. This makes the initial step of the gas phase dynamics much faster by at least a factor 3 than observed in the condensed phase on BTF6.[4] This is probably realistic since this step involved large amplitude movements that are likely constrained and slowed down in the condensed phase.

As stated in the Introduction, a majority of femtochemistry studies concern a series of non-adiabatic events occurring sequentially. When bi-exponential behavior is observed, the initial population rapidly decays into a level which decays more slowly. This picture does not apply here since S_1 is populated initially and the 120–290 fs time constants correspond to a transfer to the ground state through a CI. The ionization potential of I-DTE and I-DTE-O_x molecules is too large indeed (see Table 3) to expect detection by the probe laser after the molecules have reached the ground state through the CI. We are left with the conclusion at this point that the excited state dynamics of these molecules is much more complicated than anticipated above, when comparing these molecules to mono-alkenes and cyclic alkenes. The number of deformation coordinates where the initial wavepacket can spread is indeed larger in the present case. Hence it is conceivable that a part of the wavepacket which does not find the CI at early time spreads over deformation degrees of freedom which are not involved in the access to the CI. Hence, the time constant which falls in the 1.75–6.8 ps range in Table 3 is assigned to the evolution of this component of the wavepacket.

The picture with two parallel relaxation channels which emerges in the present gas phase experiment has also been encountered in condensed phase experiments that will be described elsewhere. This is discussed now in terms of coupling efficiency between vibrational modes. The two decays which appear in Table 3 are assigned to the reactive AP isomer, excited to the S_1 electronic state, but in two different classes of vibrational modes among those that are populated by vertical excitation from the ground state. Those associated with the movement toward the CIs lead to the short time constant and the other modes to the long time constant. Actually this suggests that the two classes of modes are essentially uncoupled at a time scale of a few picoseconds corresponding to the slow time constant; otherwise intramolecular vibrational repopulation of the modes stimulating movement toward the CIs would be at play and a single time constant would be observed. This seems surprising at first glance, but the discussion of the oscillation regime in the next section indicates that such mode uncoupling exists in the I-DTE-O_x molecules. Let us mention also that the existence of two relaxation pathways is supported by the calculations on the model diarylethene.[10] One can figure out that part of the wavepacket is composed by modes directly coupled to the ground state after the photoexcitation, whereas the other part is composed by

 This journal is © the Owner Societies 2014

© 2016 Tous droits réservés. doc.univ-lille1.fr

Published on 29 August 2014. Downloaded by Univ Lille 1 on 31/08/2016 14:53:47.

other modes poorly coupled to the ground state and beating in the S_1 funnel. The observed decay figures out the coupling with modes involved in the CIs and thus to the ground state. The separation of the modes in two operative classes has been involved very often in the radiationless decay of molecules to explain different dynamical behaviors operating in parallel.[39]

5.2.2 The plateau observed after the transient decays. The energetics of the OF-AP and OF-P conformers of I-DTE, which is provided by the DFT calculations, suggest a relative Boltzmann population at the nozzle temperature (~340 K) ranging between 75% and 90% in favor of the OF-AP conformer. At the final expansion temperature, 200 K, the AP : P ratio would reach 98 : 2. However, a supersonic expansion with helium as the carrier gas is likely to freeze configurations rather than thermalize them.[40,41] Hence, the actual conformer ratio is expected to be between the two limiting values, anyway strongly dominated by the photoactive OF-AP conformer. Nevertheless, this leaves a maximum of 25% of the I-DTE molecule in the non-reactive isomer OF-P. Table 1 in the ESI† indicates that the OF-P conformer can absorb the pump laser light at 265 nm. Hence, a possibility is that the plateau observed in I-DTE in Fig. 5 (left panel) reflects the OF-P conformers which are present in the beam. The latter indeed would be excited by the pump laser at 265 nm and probed by multiphoton ionization using the probe laser at 795 nm as for the OF-AP conformer.

Fig. 5 reveals also that a plateau exists for I-DTE-O_2 and I-DTE-O_3 in about the same amount as for I-DTE. At first glance, this could be attributed to the occurrence of OF-P conformers in the beam as just discussed for I-DTE. However this does not fit with NMR studies which showed that other kinds of I-DTE bridged molecules with chiral bridges are present exclusively as the OF-AP conformer in $CDCl_3$ solvents,[20] whereas the height of the plateau is about the same for the three molecules and represents ~5–10% of the full signal. This might reveal that a suprathermal barrier exists between the two isomers, which prevents their thermal equilibration in the condensed phase environment whereas the barrier would be accessible in the gas phase.

An alternative interpretation of the plateau in Fig. 5 is provided by a theoretical investigation at the CASPT2/CASSCF(10,10)/6-31G(d) level of the S_0, S_1 and S_2 surfaces of the N-DTE and I-DTE molecules.[13] It appears that a CI exists between the S_2 state of the OF-AP I-DTE conformer and the S_1 state of the OF-P I-DTE conformer which provides a downhill path from S_2 OF-AP I-DTE to S_1 OF-P I-DTE which is non-reactive. It was suggested in Section 5.1 that the excitation by the pump laser is toward S_1. Nevertheless the oscillator strength to S_2 and S_3 is only a factor 4 smaller than that to S_1. As the energy of the pump photon (4.68 eV) is large enough to reach the S_2 and S_3 levels, a small initial population into these states can be anticipated with the possibility that the downhill path mentioned above populates the non-reactive S_1 OF-P I-DTE.

This alternative interpretation of the plateau in I-DTE can be extended to the I-DTE-O_2 and I-DTE-O_3 molecules. Hence we would be facing a third relaxation pathway of the initial wavepacket in parallel to the two that have been unraveled in the previous section. Of course, the energetics of this new pathway is very constrained to provide a downhill path from S_2 OF-AP I-DTE to S_1 OF-P I-DTE. Hence, we anticipate that the branching ratio to this relaxation pathway, *i.e.* height of the plateau with respect to the minimum intensity of the full signal, is very sensitive to the energy of the pump photon. Unfortunately with the present design of the laser facility, it was not possible to vary the excitation wavelength and to probe accordingly the presence of this new relaxation channel.

5.2.3 Oscillating wavepacket. The oscillation regime of bridged molecules is observed in the PI signal almost exclusively. This appears clearly when comparing Fig. 5 and 8: large amplitude and fully resolved oscillations are observed in Fig. 8. Only very dim oscillations, close to the experimental limit, are observed in Fig. 5 for I-DTE-O_2 whereas the signal/noise ratio does not allow us to conclude for the other bridged molecules. The oscillation regime which is observed on the PI signal corresponds to a modulation of the second decay discussed above in the PE spectra by 1.1 ps (~35 cm^{-1}) oscillations.

When considering the total PI signal of I-DTE-O_2, it appears that the contribution of numerous small fragments, which are

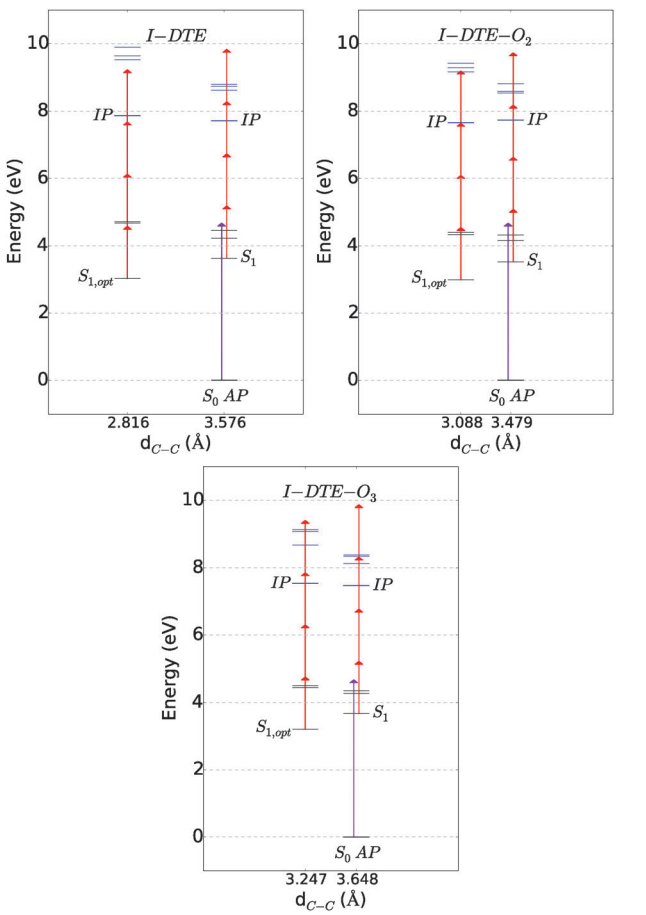

Fig. 9 Energy diagram of I-DTE, I-DTE-O_2 and I-DTE-O_3, made from data in Table 3. The purple arrows correspond to 265 photon (*i.e.* 4.67 eV) and red arrows correspond to a 795 photon (*i.e.* 1.56 eV).

© 2016 Tous droits réservés.
doc.univ-lille1.fr

Published on 29 August 2014. Downloaded by Univ Lille 1 on 31/08/2016 14:53:47.

not (or poorly) modulated, is smoothing the oscillations and reducing their relative amplitude. This is a strong indication that the oscillations are associated with a periodic variation of the ionization efficiency as a function of the pump–probe time delay due to a modulation of the ionization cross section with the geometry of the molecule. This observation is consistent with the energy diagram in Fig. 9 which shows that a quasi-resonance for the 3-probe photon ionization of I-DTE-O_2 (middle panel) from the equilibrium geometry of the S_1 state ($S_{1,opt}$ in the figure) is not preserved at other geometries (for instance in the Franck–Condon region which is also shown in the figure). Oscillation about the equilibrium geometry of the S_1 state thus likely results in a modulation of the ionization cross section. Unfortunately, it is difficult to discuss further the I-DTE-O_2 oscillations because of the scrambling effect that was revealed at the end of Section 4.2.2. The oscillations observed in the PI signal of I-DTE-O_3 are much more interesting because this scrambling effect is not at play.

The energetics of the I-DTE-O_3 molecule is qualitatively similar to that of I-DTE-O_2, but significant quantitative differences exist, which prevent the ionization resonance mentioned in the above paragraph. In contrast a resonance exists in the ion which allows the absorption of a fourth probe photon at specific geometries. Hence, when the excited I-DTE-O_3 molecule oscillates about the equilibrium geometry of the S_1 state, it can be ionized by the 4 or 3-probe photon whether this resonance is active or not. When the fourth photon is absorbed, enough energy is brought in the ion for fragmentation, hence transferring the population from the parent ion to fragments. Since this mechanism acts as a switch between the parent and fragments, it is likely to generate the out-of-phase oscillations observed in Fig. 8 between the I-DTE-O_3 parent and its fragment.

The oscillating regime observed in Fig. 8 is damped with the same time constant as that of the second decay. Two mechanisms can be proposed for such coupled relaxation: (i) direct vibronic relaxation to the ground state[42] and (ii) coupling of the oscillating vibrational mode to the deformation mode which targets the CIs. In the latter case the vibrational coupling also induces a relaxation to the ground state but it is not direct and implies an intramolecular vibrational energy redistribution toward modes that are active regarding the photochromic reaction. Note that the situation is somehow different from the beating observed formally on *cis*-stilbene[43] or TDMAE,[44] where vibrational modes orthogonal to the reaction pathway are populated.

In general, an oscillation regime occurs in a molecule when the wavepacket describing its vibrational motion overlaps several vibrational levels which beat together. These levels may belong to the same vibrational mode[45] or to different modes.[24] In the former case the 35 cm^{-1} energy which is associated with the 1.1 ps oscillation would correspond to the mode energy, whereas in the second case it would correspond to the energy difference between the two modes. Both situations can be anticipated from calculations performed in the present work: the vibrational spectrum calculated at the $S_{1,opt}$ equilibrium geometry reveals indeed low energy modes that are consistent with the 35 cm^{-1} value; three modes also exist in the region of 1270–1370 cm^{-1}, which are separated by $\sim$35 cm^{-1}. Although no final answer can be given to determine which situation is at play, a tentative explanation can be given because the implications in terms of oscillation damping are not the same in both cases.

In the situation where the oscillations are due to the excitation of several quantas of a single large amplitude motion mode, the full vibrational wavepacket is also likely composed of modes which are higher in energy. Indeed, the excess energy provided by the excitation is *ca.* 12 500 cm^{-1} and can hardly be fully accommodated by the low energy mode. Moreover, the energy stored in the low energy mode is probably not large enough to overcome the barrier toward the CIs. Hence the observed decay of the electronic excitation is likely due to the coupling of one or several modes of higher energy with a coordinate targeting the CIs. Alternatively a direct coupling with the ground state cannot be precluded. Since the oscillations within the low energy mode are damped at the same rate as the electronic excitation, this mode is essentially uncoupled to other modes, otherwise its decay would be faster.

In the second situation, where three high energy modes are populated coherently, the redistribution of the oscillations would be faster than that of the electronic excitation. Interestingly oscillations were also observed in the cycloreversion (ring opening) of 1,2-bis(2-methylbenzo[*b*]thiophen-3-yl)hexafluorocyclopentene (BTF6) in *n*-hexane.[46] This behavior is apparently similar to that observed in the present work, although it is not clear which vibrational mode is involved.

As a final remark, the fact that no oscillation appears in the PI signal of unbridged I-DTE molecule does not mean that no oscillating wavepacket is present in the excited state dynamics of this molecule. The bridge in the bridged molecules is not at the origin of the oscillation regime. Through its partial loss after ionization, it simply reveals that an oscillation regime exists within the molecule. Its absence in I-DTE precludes the observation of possible oscillation.

6 Conclusion

The relaxation dynamics of electronically excited photochromic inverse dithienylethene (I-DTE) derivatives was investigated by time-resolved photoelectron and photoion spectroscopy, using a velocity map imaging device and a time of flight mass spectrometer respectively. A femtosecond pump (@265 nm)–probe (@795 nm) arrangement coupled to beam setup was used in a scheme where the system under investigation, which is isolated in the gas phase, is probed by multiphoton ionization. Both the unbridged I-DTE molecule and three derivatives bridged by methoxy groups of various lengths were studied. The experimental results were complemented by first-principles calculations. Information on the low energy electronic states of these molecules, both in their neutral and ionized forms, at various geometries was provided by TD-DFT, whereas the

 This journal is © the Owner Societies 2014

© 2016 Tous droits réservés.
doc.univ-lille1.fr

Published on 29 August 2014. Downloaded by Univ Lille 1 on 31/08/2016 14:53:47.

ground-state structures have been sampled through molecular dynamics calculations.

We found that the electronic excitation decays with two time constants. This was not interpreted as a two step relaxation along a single reaction path as usual in femtochemistry. Instead, two parallel paths were assumed as suggested by calculations of the model diarylethene molecules,[10] after the initial wavepacket has split into two parts, each one having its own decay rate. The faster one (several femtoseconds) is assigned to the wavepacket relaxation through a conical intersection leading to the ground state of the closed form. The longer one (several picoseconds) is attributed to a relaxation of the other part of the wavepacket to the ground state through vibronic coupling. The latter is either direct or indirect after intramolecular vibrational energy transfer has populated modes which are coupled to the CIs. An oscillation regime is created by the pump laser excitation.

The central part of the present work is the splitting of the initial wavepacket which opens two parallel paths for the relaxation of the electronic excitation. Most probably, this situation applies to the whole family of dithienylethene molecules and to other classes of molecules such as diarylethene and beyond.

Furthermore one can assume that in the crystalline phase, the distortion of the molecules to reach the CIs is not possible. The only mechanism being available is the vibronic coupling. The condition for photochromism in the solid phase also becomes a condition for the relative location of the S_1 minimum and the barrier on the S_0 between the OF and CF.

Acknowledgements

L.P. thanks the ANR for support through the contract ANR-09-JCJC-0090-01 ''CHROMADYNE''. D.J. acknowledges the European Research Council (ERC) and the Région des Pays de la Loire for financial support in the framework of Starting Grants (Marches-278845) and a recrutement sur poste stratégique, respectively. This research used resources of the GENCI-CINES/IDRIS, of the CCIPL, and of a local Troy cluster. All authors are grateful to the GDRI-PHENICS international network. Furthermore, we thank the CEA/SLIC staff, in particular Olivier Gobert and Michel Perdrix, for technical support.

References

1 A. Stolow and J. Underwood, in *Time-resolved Photoelectron Spectroscopy of Nonadiabatic Dynamics in Polyatomic Molecules*, ed. S. A. Rice, John Wiley & Sons Inc., New York, 2008, vol. 139, pp. 497–583.
2 H. Bouas-Laurent and H. Durr, *Pure Appl. Chem.*, 2001, **73**, 639–665.
3 M. Irie, *Chem. Rev.*, 2000, **100**, 1685–1716.
4 Y. Ishibashi, M. Fujiwara, T. Umesato, H. Saito, S. Kobatake, M. Irie and H. Miyasaka, *J. Phys. Chem. C*, 2011, **115**, 4265–4272.
5 M. Murakami, H. Miyasaka, T. Okada, S. Kobatake and M. Irie, *J. Am. Chem. Soc.*, 2004, **126**, 14764–14772.
6 S. Sangdeok, E. Intae, J. Taiha, K. Eunkyoung and K. S. Kwang, *J. Phys. Chem. A*, 2007, **111**, 8910–8917.
7 S. Kobatake and M. Irie, *Bull. Chem. Soc. Jpn.*, 2004, **77**, 195–210.
8 M. Morimoto, S. Kobatake and M. Irie, *J. Am. Chem. Soc.*, 2003, **125**, 11080–11087.
9 S. Aloise, M. Sliwa, G. Buntinx, S. Delbaere, A. Perrier, F. Maurel, D. Jacquemin and M. Takeshita, *Phys. Chem. Chem. Phys.*, 2013, **15**, 6226–6234.
10 M. Boggio-Pasqua, M. Ravaglia, M. J. Bearpark, M. Garavelli and M. A. Robb, *J. Phys. Chem. A*, 2003, **107**, 11139–11152.
11 M. J. Bearpark, M. Deumal, M. A. Robb, T. Vreven, N. Yamamoto, M. Olivucci and F. Bernardi, *J. Am. Chem. Soc.*, 1997, **119**, 709–718.
12 F. Bernardi, M. Olivucci and M. A. Robb, *J. Photochem. Photobiol., A*, 1997, **105**, 365–371.
13 A. Perrier, S. Aloise, M. Olivucci and D. Jacquemin, *J. Phys. Chem. Lett.*, 2013, **4**, 2190–2196.
14 S. Aloise, M. Sliwa, Z. Pawlowska, J. Rehault, J. Dubois, O. Poizat, G. Buntinx, A. Perrier, F. Maurel, S. Yamaguchi and M. Takeshita, *J. Am. Chem. Soc.*, 2010, **132**, 7379–7390.
15 N. Tamai, T. Saika, T. Shimidzu and M. Irie, *J. Phys. Chem.*, 1996, **100**, 4689–4692.
16 S. Kobatake, K. Uchida, E. Tsuchida and M. Irie, *Chem. Commun.*, 2002, 2804–2805, DOI: 10.1039/b208419h.
17 H. Jean-Ruel, R. R. Cooney, M. Gao, C. Lu, M. A. Kochman, C. A. Morrison and R. J. D. Miller, *J. Phys. Chem. A*, 2011, **115**, 13158–13168.
18 M. Takeshita, C. Tanaka, T. Miyazaki, Y. Fukushima and M. Nagai, *New J. Chem.*, 2009, **33**, 1433–1438.
19 M. Takeshita, M. Nagai and T. Yamato, *Chem. Commun.*, 2003, 1496–1497.
20 H. Jin-nouchi and M. Takeshita, *Chem. – Eur. J.*, 2012, **18**, 9638–9644.
21 Y. Tatsumi, J.-i. Kitai, W. Uchida, K. Ogata, S. Nakamura and K. Uchida, *J. Phys. Chem. A*, 2012, **116**, 10973–10979.
22 K. Uchida, H. Sumino, Y. Shimobayashi, Y. Ushiogi, A. Takata, Y. Kojima, S. Yokojima, S. Kobatake and S. Nakamura, *Bull. Chem. Soc. Jpn.*, 2009, **82**, 1441–1446.
23 L. Poisson, K. D. Raffael, B. Soep, J.-M. Mestdagh and G. Buntinx, *J. Am. Chem. Soc.*, 2006, **128**, 3169–3178.
24 L. Poisson, R. Maksimenska, B. Soep, J.-M. Mestdagh, D. H. Parker, M. Nsangou and M. Hochlaf, *J. Phys. Chem. A*, 2010, **114**, 3313–3319.
25 A. T. Eppink and D. H. Parker, *Rev. Sci. Instrum.*, 1997, **68**, 3477–3484.
26 G. A. Garcia, L. Nahon and I. Powis, *Rev. Sci. Instrum.*, 2004, **75**, 4989–4996.
27 L. Poisson, *LV_pBASEX*, 2009.
28 L. Poisson, P. Roubin, S. Coussan, B. Soep and J.-M. Mestdagh, *J. Am. Chem. Soc.*, 2008, **130**, 2974–2983.
29 S. Awali, L. Poisson, B. Soep, M. A. Gaveau, M. Briant, C. Pothier, J. M. Mestdagh, M. Ben El Hadj Rhouma, M. Hochlaf, V. Mazet and S. Faisan, *Phys. Chem. Chem. Phys.*, 2013, **16**, 516–526.

© 2016 Tous droits réservés. doc.univ-lille1.fr

Published on 29 August 2014. Downloaded by Univ Lille 1 on 31/08/2016 14:53:47.

30 M. J. Frisch, G. W. Trucks, H. B. Schlegel, G. E. Scuseria, M. A. Robb, J. R. Cheeseman, G. Scalmani, V. Barone, B. Mennucci, G. A. Petersson, H. Nakatsuji, M. Caricato, X. Li, H. P. Hratchian, A. F. Izmaylov, J. Bloino, G. Zheng, J. L. Sonnenberg, M. Hada, M. Ehara, K. Toyota, R. Fukuda, J. Hasegawa, M. Ishida, T. Nakajima, Y. Honda, O. Kitao, H. Nakai, T. Vreven, J. J. A Montgomery, J. E. Peralta, F. Ogliaro, M. Bearpark, J. J. Heyd, E. Brothers, K. N. Kudin, V. N. Staroverov, R. Kobayashi, J. Normand, K. Raghavachari, A. Rendell, J. C. Burant, S. S. Iyengar, J. Tomasi, M. Cossi, N. Rega, J. M. Millam, M. Klene, J. E. Knox, J. B. Cross, V. Bakken, C. Adamo, J. Jaramillo, R. Gomperts, R. E. Stratmann, O. Yazyev, A. J. Austin, R. Cammi, C. Pomelli, J. W. Ochterski, R. L. Martin, K. Morokuma, V. G. Zakrzewski, G. A. Voth, P. Salvador, J. J. Dannenberg, S. Dapprich, A. D. Daniels, O. Farkas, J. B. Foresman, J. V. Ortiz, J. Cioslowski and D. J. Fox, *Gaussian 09 Revision A2*, 2009.

31 D. Jacquemin, A. Planchat, C. Adamo and B. Mennucci, *J. Chem. Theory Comput.*, 2012, **8**, 2359–2372.

32 J.-D. Chai and M. Head-Gordon, *J. Chem. Phys.*, 2008, **128**, 084106, DOI: 10.1063/1.2834918.

33 N. Mardirossian, J. A. Parkhill and M. Head-Gordon, *Phys. Chem. Chem. Phys.*, 2011, **13**, 19325–19337.

34 M. Ernzerhof and G. Scuseria, *J. Chem. Phys.*, 1999, **110**, 5029–5036.

35 C. Adamo and V. Barone, *J. Chem. Phys.*, 1999, **110**, 6158–6170.

36 A. Fihey, A. Perrier and F. Maurel, *J. Photochem. Photobiol., A*, 2012, **247**, 30–41.

37 A. D. Laurent, J.-M. Andre, E. A. Perpete and D. Jacquemin, *J. Photochem. Photobiol., A*, 2007, **192**, 211–219.

38 J. M. Mestdagh, J.-P. Visticot, M. Elhanine and B. Soep, *J. Chem. Phys.*, 2000, **113**, 237–248.

39 A. Frad, F. Lahmani, A. Tramer and C. Tric, *J. Chem. Phys.*, 1974, **60**, 4419–4430.

40 L. Poisson, P. Pradel, F. Lepetit, F. Reau, J. M. Mestdagh and J. P. Visticot, *Eur. Phys. J. D*, 2001, **14**, 89–95.

41 L. Poisson, L. Dukan, O. Sublemontier, F. Lepetit, F. Reau, P. Pradel, J. M. Mestdagh and J. P. Visticot, *Int. J. Mass Spectrom.*, 2002, **220**, 111–126.

42 J. Jortner, R. D. Levine and S. A. Rice, *Level Structure and Dynamics from Diatomics to Clusters*, 1988, vol. 70, pp. 1–34.

43 S. Pedersen, L. Baares and A. H. Zewail, *J. Chem. Phys.*, 1992, **97**, 8801–8804.

44 E. Gloaguen, J. Mestdagh, L. Poisson, F. Lepetit, J. Visticot, B. Soep, M. Coroiu, A. Eppink and D. Parker, *J. Am. Chem. Soc.*, 2005, **127**, 16529–16534.

45 P. Cong, G. Roberts, J. Herek, A. Mohktari and A. Zewail, *J. Phys. Chem.*, 1996, **100**, 7832–7848.

46 H. Miyasaka, M. Murakami, T. Okada, Y. Nagata, A. Itaya, S. Kobatake and M. Irie, *Chem. Phys. Lett.*, 2003, **371**, 40–48.

This journal is © the Owner Societies 2014
© 2016 Tous droits réservés.
doc.univ-lille1.fr

View Article Online / Journal Homepage / Table of Contents for this issue
Dynamic Article Links

PCCP

Annexe 8. Aloïse et al, PCCP, 13, 13185, 2011

Cite this: *Phys. Chem. Chem. Phys.*, 2011, **13**, 13185–13195

HDR de Stéphane Aloïse, Lille 1, 2016

www.rsc.org/pccp

PAPER

The excited state dipole moments of betaine pyridinium investigated by an innovative solvatochromic analysis and TDDFT calculations†

Zuzanna Pawlowska,[a] Aude Lietard,[a] Stéphane Aloïse,*[a] Michel Sliwa,[a] Abdenacer Idrissi,[a] Olivier Poizat,[a] Guy Buntinx,[a] Stéphanie Delbaere,[b] Aurélie Perrier,[c] François Maurel,[c] Patrice Jacques[d] and Jiro Abe[e]

Received 25th March 2011, Accepted 30th April 2011
DOI: 10.1039/c1cp20920e

This work reports on the solvatochromic properties of a simple heterocyclic betaine pyridinium, 2-(1-pyridinio)benzimidazolate (SBPa), having promising potentialities in non-linear optics. From advanced PCM-TDDFT calculations, the solvatochromism of SBPa was found to be unusual, involving two different electronic states for absorption ($S_0 \rightarrow S_2$) and emission ($S_1 \rightarrow S'_0$). To account for this behavior, we developed an innovative physical treatment which consists in a non-linear fit of the solvatochromic data using the Bilot–Kawski theoretical model and visualizing the least-square coefficient χ^2 on a 2D map as a function of the solute polarizability and gas phase absorption energy. In parallel, Kamlet–Taft correlations were undertaken to select a propitious set of electrostatic solvents usable in this treatment. Protic solvents that lead to specific interactions and nonpolar solvents that favor dimerization processes were excluded. From a choice of aprotic solvents with sufficiently high polarity, 4 dipole moments $\mu_g(S_0) = +9.1$ D, $\mu_e(S_2) = -1.5$ D, $\mu_e(S_1) = 0$ D and $\mu_g(S'_0) = +3.31$ D were determined, the 3 former values being in close agreement with TDDFT values, although the solute polarizability values seem underestimated. Anyhow, disregarding this discrepancy, we evaluated the static hyperpolarizability to $\beta(0) = -64 \times 10^{-30}$ esu from the solvatochromic data in close agreement with DFT calculations.

Published on 22 June 2011. Downloaded by Univ Lille 1 on 31/08/2016 15:13:09.

I. Introduction

Within the last two decades, heterocyclic betaine pyridinum molecules have received considerable attention for their potential utilization in the development of new organic materials for nonlinear optics. Indeed, it has been shown that the hyperpolarizability (β) of betaine pyridinium is particularly high due to an inversion of the dipole moment upon photo-excitation. Within the framework of dipole approximation and using the two-state model,[1,2] the static β value, $\beta(0)$, can be expressed as

$$\beta(0) = \frac{3(M_{ge})^2 \Delta\mu}{2(\hbar\omega_{ge})^2} \quad (1)$$

where M_{ge}, $\hbar\omega_{ge}$ and $\Delta\mu = \mu_g - \mu_e$ are the transition moment, energy gap and dipole moment change between the ground state and the excited state, respectively. Accurate knowledge of the dipole moments at ground and excited states is thus essential to better evaluate the macroscopic hyperpolarizability in view of applications.

Among the various betaine pyridinium molecules investigated in the past,[3–7] 2-(1-pyridinio)benzimidazolate (SBPa), presented in Chart 1, has been extensively studied due to its attractive hyper-Rayleigh scattering properties that result from a large negative first-order hyperpolarizability, $\beta = (115 \pm 25)10^{-30}$ esu.[3,4,7] As an example, this value is 5-fold larger than that of 4-nitroaniline in chloroform.[3,4] In order to correlate this parameter with the dipole moments of the molecule, a series of theoretical studies have been devoted to the calculation of the $S_1(\pi,\pi^*)$ excited state structure using the various approaches from Hartree–Fock to Single excitation Configurations Interactions (CIS) levels of calculation.[3,4]

[a] *Laboratoire de Spectrochimie Infrarouge et Raman (UMR 8516 du CNRS), Université des Sciences et Technologies de Lille, Bat C5, 59655 Villeneuve d'Ascq Cedex, France. E-mail: stephane.aloise@univ-lille1.fr*
[b] *Université Lille Nord de France, UDSL, Laboratoire de Spectrochimie Infrarouge et Raman (UMR 8516 du CNRS), 3 rue du Professeur Laguesse BP83, F-59006 Lille, France*
[c] *Laboratoire Interfaces, Traitements, Organisation et Dynamique des Systèmes, CNRS UMR 7086, Université Paris Diderot, Bât. Lavoisier, 15 rue Jean Antoine de Baif, 75205 Paris Cedex 13, France*
[d] *Ecole Nationale Supérieure de Chimie de Mulhouse, Université de Haute-Alsace, 3 rue Alfred Werner, 68093 Mulhouse, France*
[e] *Department of Chemistry, School of Science and Engineering, Aoyama Gakuin University, 5-10-1 Fuchinobe, Sagamihara, Kanagawa 229-8558, Japan*
† Electronic supplementary information (ESI) available. See DOI: 10.1039/c1cp20920e

© 2016 Tous droits réservés.
doc.univ-lille1.fr

HDR de Stéphane Aloïse, Lille 1, 2016 View Article Online

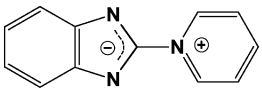

Chart 1 2-(1-Pyridinio)benzimidazolate (abbreviated as SBPa).

For this state, an intramolecular charge transfer (CT) character has been identified, which involves a displacement of the π charge from the betaine (donor) to the pyridinium (acceptor) part of the molecule. Advanced MP2 calculations[3,4] have successfully reproduced the experimental dipole moment value for the ground state, $\mu_g(\text{exp}) = 10.33$ D.[7] In parallel, CIS calculations of the excited state have predicted the preservation of the ground state molecular symmetry group (namely C_{2v}) and an enhancement of the overall quinoid character of the molecule accompanied with a decrease and inversion of the dipole moment, with a calculated value around $\mu_e \sim -3$ D.[3,4] No experimental data are presently available for this quantity.

It is known that experimental estimation of excited state dipole moments can be provided from solvatochromic analysis.[8–13] Surprisingly, although this type of analysis needs inexpensive equipment, a thoughtful solvatochromism study of SBPa has never been reported except for some sparse data.[14] In general, the procedure for analyzing solvatochromic data, first proposed by Lippert and Mataga,[15–18] consists in evaluating $\Delta\mu$ through a plot of the Stokes shift as a function of a solvent polarity parameter and deducing μ_e from a second independent measurement of μ_g by conventional electrotechnics. However, great care has to be taken with regard to the different assumptions made in the theoretical treatment of the solvatochromism, such as the choice of the solute polarizability.[19,20] It is worth mentioning here that the α_g and α_e values of the solute polarizability in both the ground and excited states are *a priori* important physical parameters to be considered. Practically, it is a challenging task that is much debated in the literature.[8,19–22] One can be easily convinced of this problem through the very recent controversy about the polarizability difference $\Delta\alpha = \alpha_g - \alpha_e$ in Reichardt's betaine B30.[19,20] Thus, it is not surprising that most often this parameter is not considered at all or simply approximated to a dimensionless constant value $\alpha_g = \alpha_e = \kappa/a_0^3$ where κ depends on the molecule and a_0 is the Onsager cavity radius.[11] As recently discussed by Renge,[19,20] another important aspect to consider in solvatochromic analyses is the proper evaluation of the gas phase transition energy—a quantity hardly accessible for chemists—but this problem is skipped when dealing with Stokes shift quantities.

In this paper, we present a detailed solvatochromic analysis of SPBa to get a reliable evaluation of the SBPa dipole moments involved in the CT transition. This analysis has involved not less than 19 different solvents but has been carried out successively for several restricted groups of them to prevent possible misinterpretation of the data due to the presence of solvent–solute specific interactions or solute stacking phenomena often arising with polar species. For each group of solvents, Kamlet–Taft correlations[23] were established to detect the eventual presence of such undesirable processes. A lot of decisive results were deduced: (i) the SBPa solvatochromism appeared unusual in the sense that it is strongly negative for absorption whereas it is moderately positive for fluorescence; (ii) comprehensive comparison of the absorption and emission data with the theoretical transitions predicted from TDDFT calculations revealed that both the S_1 and S_2 excited singlet states have to be considered to really understand the photophysics of SBPa, the intense CT absorption being related with the second excited state; (iii) with regard to this complex situation, an original approach considering separately the solvent-dependent shifts of the absorption band ($S_0 \rightarrow S_2$ CT transition) and emission band ($S_1 \rightarrow S_0$ transition) has been adopted and the four dipole moments involved in the absorption and emission transitions were assessed and compared with the calculated TDDFT values. An attempt to evaluate the hyperpolarizability of SBPa from this innovative treatment of the solvatochromism has been finally proposed.

II. Experimental

The SBPa molecule has been synthesized according to the procedure reported by Alcalde *et al.*[7] The 19 solvents including toluene, dioxane, anisole, tetrahydrofuran (THF), ethylacetate (EtOAc), methylacetate (MeOAc), dichloromethane (DCM), hexamethylphosphoramide (HMPA), acetone, butyronitrile, dimethylformamide (DMF), acetonitrile (ACN), 2-butanol (BuOH), 1-propanol, ethanol (EtOH), methanol (MeOH), trifluoroethanol (TFE), water and hexafluoroisopropanol (HFIP) were used as received without further purification (Aldrich).

All stationary absorption and fluorescence spectra were recorded using double beam CARY 100bio and Jobin Yvon Div. FluoroMax 3 spectrometers, respectively. Measurements were performed at ambient temperature using 1 cm quartz cells with about 10^{-5}–10^{-6} M solutions, keeping the maximum absorbance at less than 0.1 in order to avoid reabsorption effects. The spectral resolution is typically 2 nm in both experiments. Emission spectra were corrected for the lamp and detector response.

All ^{1}H and ^{13}C NMR data were acquired on Bruker AVANCE NMR spectrometers equipped with a QNP or TXI probe, and operating at 300 MHz or 500 MHz for ^{1}H and 75 or 125 MHz for ^{13}C. Solutions of SBPa were prepared in methanol-d_4, acetonitrile-d_3, tetrahydrofuran-d_8, toluene-d_8 (concentration 10^{-2}–10^{-3} M).

III. Theoretical calculations

Different calculations were done to compute stationary absorption, emission and NMR spectra as well as polarizabilities and static/dynamic hyperpolarizabilities, all of them being based on the Density Functional Theory (DFT) and/or Time-Dependent DFT (TD-DFT) formalisms according to the Jacquemin *et al.* methodology[24] to compute the excited state properties of conjugate molecules. For the overall calculations, solvent contributions were introduced by using the Polarizable Continuum Model (PCM).[25] All these calculations were performed using Gaussian 09 packages.[26]

For all geometry optimizations, we used the PBE0/6-311G(d) level of calculation that provides accurate ground-state structures for most organic systems.[24] For the vertical absorption transition energy calculated with TDDFT, especially for

 This journal is © the Owner Societies 2011

Published on 22 June 2011. Downloaded by Univ Lille 1 on 31/08/2016 15:13:09.

© 2016 Tous droits réservés.

doc.univ-lille1.fr

Published on 22 June 2011. Downloaded by Univ Lille 1 on 31/08/2016 15:13:09.

the $S_0 \rightarrow S_1$(FC) and $S_0 \rightarrow S_2$ (FC) transitions, four hybrid functions with different percentages of exact exchange were tested with the 6-311G++(2d,p) basis set: B3LYP (20% of exact exchange),[27] PBE0 (25%),[28,29] BMK (42%),[30] and BHandHLYP (50%).[31] The full comparison between computed transition energies and experimental absorption spectra of SBPa is reported in the ESI.† Fig. SI1 (ESI†) displays the experimental spectrum for acetonitrile (ACN) together with the TDDFT oscillator strength and wavelength values computed for the first transitions with the B3LYP, PBE0, BMK and BHandHLYP functionals. The detailed transition characteristics are displayed in Table SI1 (ESI†) for the ACN case. Quantitatively, if we focus on the intense CT band, the excitation wavelength calculated with the PBE0 functional is in closest agreement with experimental data. Consequently, in the following, we will stick to the PCM-TD-PBE0/6-311++G(2d,p)//PBE0/6-311G(d) calculation scheme for all the analysis of the solvatochromism effect. In the case of the vertical emission transitions, an optimization of the excited state geometry was necessary. Starting from the Franck–Condon (FC) geometry, a complete optimization procedure was accomplished following the TD-DFT analytical gradients available in Gaussian09 software.[26] During the exploration of the excited state potential energy surfaces, we used the equilibrium linear response (LR) solvation scheme.[32] True minima were validated by ensuring that no imaginary frequencies are present in the computed vibrational spectra. Starting from S_1(FC) and S_2(FC), we obtained two optimized structures, named, respectively, S_1(opt) and S_2(opt). For each optimized state, the emission to the final ground state was obtained by exploiting the corrected LR scheme (cLR).[33] Within the cLR approach, a "state-specific" correction to LR excitation energies was introduced by using a solvent reaction field created in response to the excited state charge distribution. The emission wavelength was then simply deduced from the energy gap between the optimized excited state S_1(opt) and S_2(opt) and the corresponding lower vertical state, respectively, abbreviated as S_0' and S_0''. At this stage, the ground state energy was computed with non-equilibrium solvation, at the excited state geometry and with the static solvation reaction field from the excited state.

Evaluation of the Onsager cavity size has been made by DFT calculations using the PBE0 functional with different basis sets for both polar (ACN) and nonpolar (THF) solvents. All results, reported in ESI† (Table SI2), give the Onsager radius comprised in a restricted interval with a medium value a_0 = 4.75 Å, which will be used in the solvatochromic data treatment (see below).

In order to investigate thoroughly the geometry of SBPa in solution, in particular determining whether the molecule is planar or not, theoretical NMR spectra were computed on the basis of the above conclusive PBE0 results but with an extended basis set, as required to obtain satisfactory accordance with experimental NMR spectra.[34] Thus, for an imposed planar geometry (near C_{2v}) and for various twisted geometries differing by the value of the fixed dihedral angle between the betaine and pyridinium parts, PCM-PBE0/6-311+G(d,p) geometry optimization was followed by PBE0/6-311++G(2d,p) NMR spectra computation. Additionally, for comparison, full PCM-DFT calculations were performed for the SBPa molecule surrounded with 4 explicit solvent molecules.

IV. Solvatochromic data treatment

Our innovative solvatochromic data treatment is based on the theory of Bilot and Kawski[35,36] that we first summarize to focus on the important parameters to consider.

IV.1 Theory of solvatochromism

According to the dielectric continuum formalism of Bilot and Kawski,[35,36] the transition energy (absorption/emission) between the ground and excited states of a free molecule (gas phase) is derived from quantum-mechanical first-order perturbation theory, in which the influence of solvation is introduced according to Onsager's model.[37] By taking into account the dimensionless polarizability[38] α of the solute and considering a solvent with dielectric constant ε and refractive index n, Bilot and Kawski define two relevant solvent functions:

$$g(n,\varepsilon,\alpha) = \frac{1}{1-\alpha f(n^2)}\left[\frac{f(\varepsilon)}{1-\alpha f(\varepsilon)} - \frac{f(n^2)}{1-\alpha f(n^2)}\right] \quad (2)$$

$$h(n,\alpha) = \frac{2-\alpha f(n^2)}{1-\alpha f(n^2)}\left[\frac{f(n^2)}{1-\alpha f(n^2)}\right] \quad (3)$$

where $f(x) = \frac{x-1}{2x+1}$. These two functions are involved in the first order expression of the difference of absorption/emission band maximum on going from the gas phase, $\nu^{gas}_{abs/fluo}$, to the solution, $\nu^{gas}_{abs/fluo}$, according to:

$$k\pi\varepsilon_0 hca_0^3\left(\nu^{gas}_{abs/fluo} - \nu^{gas}_{abs/fluo}\right) = \vec{\mu}_{g/e}(\vec{\mu}_e - \vec{\mu}_g)g(n,\varepsilon,\alpha) - \frac{(\vec{\mu}_e)^2 - (\vec{\mu}_g)^2}{2}h(n,\alpha) \quad (4)$$

where a_0 is the Onsager cavity radius and the subscripts g and e refer to the ground and excited states, respectively (the other constants having the usual meanings). For the sake of simplicity this equation can be rewritten as:

$$\left(\nu^{sol}_{abs/fluo} - \nu^{gas}_{abs/fluo}\right) = K_1 g(n,\varepsilon,\alpha) - K_2 h(n,\alpha) \quad (5)$$

where $K_1 = \vec{\mu}_g(\vec{\mu}_e - \vec{\mu}_g)$ and $K_1 = \vec{\mu}_e(\vec{\mu}_e - \vec{\mu}_g)$ for absorption and emission, respectively, and $K_2 = 0.5\,((\vec{\mu}_e)^2 - (\vec{\mu}_g)^2)$ in both cases. K_1 and K_2 can be deduced from a non-linear fit of the solvatochromic data according to eqn (5).

IV.2 Algorithm for solvatochromic data treatments

The originality of the treatment proposed here arises from the combination of the following three aspects: (i) absorption and emission solvatochromic data are considered separately. Thus, the four dipole moments (Chart 2), $\mu_g(S_0)$ and $\mu_e(S_2)$, on one hand, and $\mu_g(S_0')$ and $\mu_e(S_1)$, on the other hand, can be

© 2016 Tous droits réservés.

doc.univ-lille1.fr

Published on 22 June 2011. Downloaded by Univ Lille 1 on 31/08/2016 15:13:09.

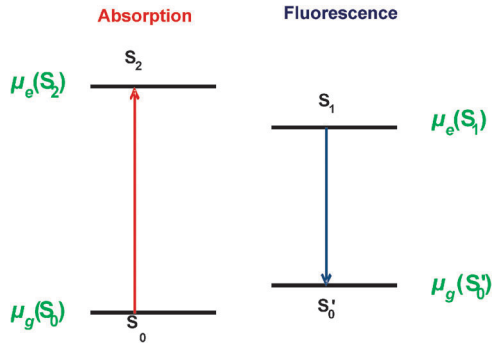

Chart 2 Dipole moments concerned by the solvatochromic effect.

determined from the K_1 and K_2 values obtained from the absorption and emission data, respectively, according to:

$$\mu_g(S_0) = \frac{1}{\sqrt{4\pi\varepsilon_0 a_0^3}} \frac{K_1}{\sqrt{2(K_1 - K_2)}} \quad (6)$$

$$\mu_e(S_2) = \frac{(\cos\theta)^{-1}}{\sqrt{4\pi\varepsilon_0 a_0^3}} \frac{K_2}{\sqrt{2(K_1 - K_2)}} \quad (7)$$

$$\mu_g(S_0') = \frac{1}{\sqrt{4\pi\varepsilon_0 a_0^3}} \frac{2K_2 - K_1}{\sqrt{2(K_1 - K_2)}} \quad (8)$$

$$\mu_e(S_1) = \frac{(\cos\theta)^{-1}}{\sqrt{4\pi\varepsilon_0 a_0^3}} \frac{K_1}{\sqrt{2(K_1 - K_2)}} \quad (9)$$

where $\theta = (\vec{\mu}_g, \vec{\mu}_e)$ is the angle between the ground and excited state dipole moments considered in the above equations; (ii) the polarizability of the solute is explicitly included as an adjustable parameter with the approximation that it has the same value in the ground and excited states, *i.e.*, $\alpha_g \approx \alpha_e = \alpha$; (iii) the gas phase absorption/emission band maxima $\nu^{gas}_{abs/fluo}$ are also considered as adjustable parameters. The involvement of these adjustable parameters emphasizes the drastic importance of carefully adjusting the analysis. For that task, from the solvatochromic $\nu^{sol}_{abs/fluo}$ data and solvent properties (n, ε), together with the two adjustable parameters α and $\nu^{gas}_{abs/fluo}$, one computes $\Delta\nu$, $g(n,\varepsilon,\alpha)$ and $h(n,\alpha)$ in order to perform non-linear fit according to eqn (5). The main idea of this innovative approach is thus based on the plot of 2D map of χ^2, (mean square coefficient) deduced from these non-linear fits, as a function of the $\nu^{gas}_{abs/fluo}$ and α values in order to visualize the presence of minima or of regions of least amplitude. By this procedure, the 4 dipole moments can be successively assessed for the different points chosen on the 2D map, providing a simple way for discussing the right choice of the adjustable parameters and/or set of solvents. The overall algorithm is illustrated in ESI† in Fig. SI2.

V. Results and discussion

The solvatochromic data comprising the absorption and emission transition maxima and Stokes shifts measured in the 19 solvents investigated are tabulated in Table 1 while theoretical results including TDDFT data for 4 representative solvents are gathered in Table 2.

V.1 Identification of the CT and emissive band

Fig. 1 presents the steady-state absorption and fluorescence spectra of SBPa in toluene, THF, ACN and MeOH, together with the TDDFT results (same color code) concerning the two absorption transitions $S_0 \rightarrow S_1$ and $S_0 \rightarrow S_2$ and the emission transition $S_1 \rightarrow S_0$ (see also Table 2). The experimental absorption spectrum shows essentially one band in the 300–600 nm domain, characterized by a clear negative solvatochromism contrasting with a lack of such an effect for the emissive band in the 500–750 nm domain. At first glance, the hypsochromic shift noticed on the absorption band upon increasing the solvent polarity is not observed for the emission band.

Table 1 SBPa absorption and emission peak frequency (ν_{abs}, ν_{fluo}) and wavelength (λ_{abs}, λ_{fluo}) and corresponding Stokes shift ($\Delta\nu_{st}$) in different solvents. Solvent properties (dielectric constant ε, refractive index n, Dimroth–Reichardt $E_T(30)$ parameter, and Kamlet–Taft α_{KT}, β_{KT}, and π^*_{KT} parameters) are also given

No	Solvent	$E_T(30)$/kcal mol^{-1}	ε	n	α_{KT}	β_{KT}	π^*_{KT}	λ_{abs}/nm	λ_{fluo}/nm	ν_{abs}/cm^{-1}	ν_{fluo}/cm^{-1}	$\Delta\nu_{st}$/cm^{-1}
1	Toluene	33.9	2.38	1.4941	0	0.11	0.49	446	669	22 421	14 948	7473
2	Dioxane	36	2.21	1.4203	0	0.37	0.49	424	671	23 585	14 903	8682
3	Anisole	37.1	4.33	1.5143	0	0.32	0.7	429	674	23 310	14 837	8473
4	THF	37.4	7.58	1.405	0	0.55	0.55	421	675	23 753	14 815	8938
5	EtOAc	38.1	6.02	1.3698	0	0.45	0.45	415	680	24 096	14 706	9390
6	MeOAc	38.9	6.68	1.3589	0	0.42	0.49	412	683	24 271	14 641	9630
7	DCM	40.7	8.93	1.421	0.13	0.1	0.82	415	672	24 096	14 881	9215
8	HMPA	40.9	29.3	1.457	0	1	0.87	404	677	24 752	14 771	9981
9	Acetone	42.2	20.56	1.356	0.08	0.48	0.62	402	681	24 876	14 684	10 192
10	Butyronitrile	42.5	24.83	1.382	0	0.45	0.63	405	680	24 691	14 705	9986
11	DMF	43.2	36.71	1.428	0	0.69	0.88	399	685	25 062	14 598	10 464
12	ACN	45.6	35.94	1.341	0.19	0.4	0.66	393	687	25 445	14 556	10 889
13	2-BuOH	47.1	16.56	1.3953	0.69	0.8	0.4	401	642	24 937	15 576	9361
14	1-Propanol	50.7	20.45	1.3837	0.84	0.9	0.52	397	654	25 189	15 290	9899
15	EtOH	51.9	24.55	1.3594	0.86	0.75	0.54	393	662	25 445	15 105	10 340
16	MeOH	55.4	32.66	1.3265	0.98	0.66	0.6	385	665	25 974	15 037	10 937
17	TFE	59.8	26.67	1.2907	1.51	0	0.73	370	592	27 027	16 891	10 136
18	H_2O	63.1	78.36	1.3325	1.17	0.47	1.09	361	643	27 700	15 552	12 148
19	HFIP	65.3	16.62	1.277	1.96	0	0.65	349	558	28 653	17 921	10 732

This journal is © the Owner Societies 2011

© 2016 Tous droits réservés.
doc.univ-lille1.fr

HDR de Stéphane Aloïse, Lille 1, 2016 View Article Online

Published on 22 June 2011. Downloaded by Univ Lille 1 on 31/08/2016 15:13:09.

Table 2 PCM-TDDFT calculated absorption wavelength (λ_{abs}) and oscillator strength (f) and emission wavelength (λ_{fluo}) compared to the experimental data. The transition moment (M_{ge}) is deduced from the experimental absorption band (see also Fig. SI3, ESI)

	M_{ge}/D	λ_{abs}/ nm (f)			λ_{fluo}/ nm	
	Exp	Exp	TDDFT $S_0 \rightarrow S_2$	TDDFT $S_0 \rightarrow S_1$	Exp	TDDFT $S_1 \rightarrow S_0$
MeOH	10.8	385	397 (0.4576)	416 (0.0092)	665	—
ACN	9.0	393	406 (0.4669)	432 (0.0094)	687	714
THF	7.7	421	422 (0.4815)	453 (0.0091)	675	709
Toluene	5.4	446	462 (0.5198)	510 (0.0082)	669	703

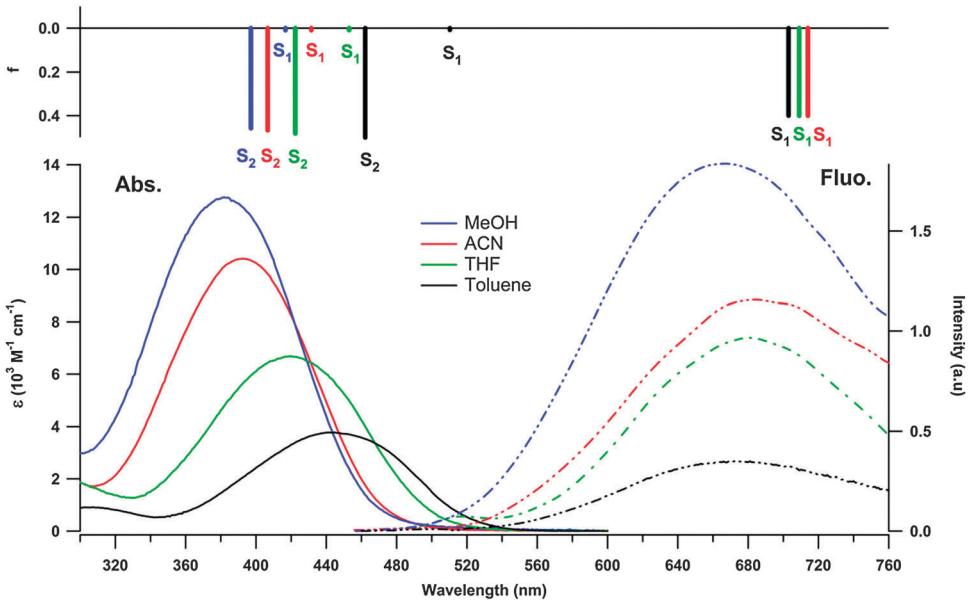

Fig. 1 Stationary absorption (solid line) and fluorescence (dashed line) spectra of SBPa in ACN (red), MeOH (blue), THF (green), and toluene (black) and TDDFT position of the $S_0 \rightarrow S_1$, $S_0 \rightarrow S_2$, and $S_1 \rightarrow S_0$ transitions in the same solvents. The predicted electronic oscillator strength of the absorption transitions is given by the size of the corresponding stick.

It suggests that the absorption transition has a specific CT character and thus does not involve the same excited state as the emissive transition. The TDDFT results (Fig. 1 and Table 2) indicate that the two transitions of lowest energy are close together but only the $S_0 \rightarrow S_2$ transition has significant oscillator strength and can reasonably be ascribed to the observed absorption band. This assignment is supported by the high-quality agreement between the calculated and observed peak maxima in the four solvents and an excellent prediction of the experimental solvatochromic behavior (see Fig. 1). Note that the hyperchromic effect noticed for the absorption band is not reproduced by calculations. However, TDDFT oscillator strengths are known to be less accurate than the corresponding transition energies.[39] After a PCM-TDDFT optimization of the first excited state, the emission band position is correctly predicted and assigned to the $S_1 \rightarrow S_0$ transition. Note that even the moderately positive solvatochromism of the emission band (λ_{max} = 669, 675, and 687 nm in toluene, THF, ACN, respectively) is well reproduced by calculations (703, 709 and 714 nm respectively). A further thorough analysis of theoretical results will be the object of another publication in the near future. As a main result, it is important to insist on the fact that two distinct electronic states S_1 and S_2 have to be considered for the analysis of SBPa solvatochromic data.

V.2 Geometry of SBPa in solution

In order to make an appropriate solvatochromic data treatment, the question of the solute geometry has to be addressed. The geometry of the ground state SBPa molecule is planar in the solid state with a near C_{2v} symmetry, as measured by X-ray spectroscopy.[7] This planar configuration is responsible for strong stacking effects. Indeed, head-to-tail dimeric entities have been identified by X-ray spectroscopy with a distance of 3.29 Å between monomers. As expected, in non-polar solvents, a strong tendency for dimerization has been proposed to explain the variation of the experimental dipole moment with increasing solute concentration.[7] Moreover, dimer formation was confirmed by MM2/AM1 calculations that predicted a satisfying distance of 3.4 Å between the planar monomeric units.[40] Obviously, a planar geometry of the ground state can be suspected in solution as already predicted by PCM-PBE0//6-311G(d) geometry optimizations. In order to confirm theses results, we compared experimental and PCM-DFT calculated NMR chemical shifts. The ^{1}H NMR spectra for SBPa in MeOD, ACN, THF and toluene are displayed in Fig. 2. The full assignment of these spectra has been established from 1D and 2D NMR experiments (^{1}H, ^{13}C, ^{1}H-^{1}H COSY, ^{1}H-^{13}C HSQC, ^{1}H-^{13}C HMBC). As expected, the proton H3, in the *ortho* position to the pyridinium nitrogen, is always the most

© 2016 Tous droits réservés.

doc.univ-lille1.fr

HDR de Stéphane Aloïse, Lille 1, 2016 View Article Online

Published on 22 June 2011. Downloaded by Univ Lille 1 on 31/08/2016 15:13:09.

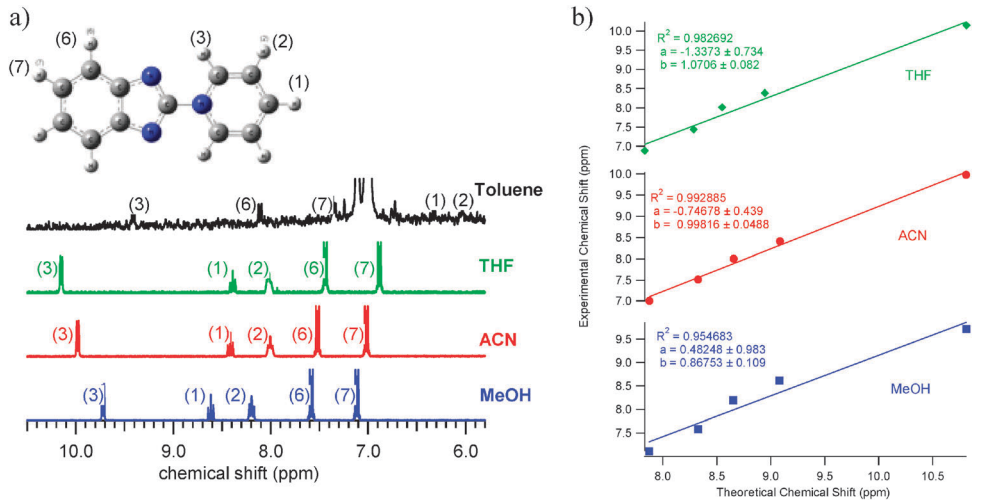

Fig. 2 (a) ^{1}H-NMR spectra of SBPa in toluene, THF, ACN, and MeOH. (b) Linear correlation of experimental and PCM-DFT NMR peak position considering a planar geometry for SBPa.

deshielded. Its chemical shift increases on going from MeOD (9.72 ppm) to ACN (9.98 ppm), then THF (10.15 ppm). In contrast, the four other protons show an inverse solvent dependency, with always the H6 (δ_{MeOD} = 7.58 ppm, δ_{ACN} = 7.52 ppm, δ_{THF} = 7.44 ppm) and H7 (7.10/7.02/6.88 ppm) couple lying at lower frequency than the H1 (8.62/8.41/8.39 ppm) and H2 (8.19/8.00 /8.02 ppm) couple. Different is the behaviour in toluene solution where the protons H6 (δ_{Tol} = 8.10 ppm) and H7 (δ_{Tol} = 8.34 ppm) have higher values of chemical shifts than those observed for H1 (δ_{Tol} = 6.32 ppm) and H2 (δ_{Tol} = 6.03 ppm). Such an effect likely arises from the magnetic anisotropy induced by toluene molecules but can be enhanced also by a head-to-tail dimerization of SBPa molecules. Anyhow, both effects cannot be accounted within the PCM approach and the toluene case is thus excluded from the experiment–theory comparison. It is worth to notice that the deshielding noticed for protons H1, H2, H6, and H7 correlates perfectly with the solvent polarity, which points at a pure electrostatic contribution. Reversely, the proton H3 deshielding correlates with the hydrogen bond accepting ability of the solvent (β_{KT} parameter in Table 1) balanced with the hydrogen bond donor strength (α_{KT} parameter in Table 1). More exactly, the proton H3 chemical shift position correlates with the $\beta_{KT} - \alpha_{KT}$ quantity, which strongly suggests the presence of specific interaction with this proton.

The linear correlation between the experimental and PCM-DFT NMR data, measured by its least square χ^2 parameter, is excellent for a planar geometry, as shown in Fig. 2b. We tried to further improve the correlation by changing gradually the dihedral angle between the betaine and pyridinium moieties but, actually, the difference of total energy between the planar and twisted geometries was found weaker than the thermal energy (0.025 eV), indicating the probable existence of a distribution of molecules with various angles controlled by the Boltzmann law. To further confirm the quasi planarity of SBPa, additional PCM-DFT calculations were performed with 4 explicit solvent molecules. According to this approach, a small torsion of the SBPa dihedral angle of 2°, 3° and 10° is found in MeOH, THF and ACN, respectively. In conclusion, it is probable that the SBPa conformation in solution deviates only slightly from planarity, with a dihedral angle that is not correlated to the solvent polarity. Note finally that, from additional theoretical investigation that will be published elsewhere, the geometry of S_1 and S_2 optimized with TDDFT methods has been found planar.

V.3 The solvatochromic analysis of SBPa

As discussed above, the SBPa absorption and fluorescence data show strongly different dependence on the solvent polarity, which excludes a safe treatment of the solvatochromism simply based on Stoke's shifts (Lippert–Mataga approach). Thus, the absorption and fluorescence data have to be considered separately.

Empirical approach $\nu_{abs/fluo}$ = *f*(ET30). The analysis of the solvatochromic data cannot be done directly on the whole set of solvents but, instead, it appears crucial to distinguish different families of solvents depending on the type of interaction with the solute. In particular, great care has to be taken in considering separately solvents that favour specific interactions. A manifest evidence of the existence of this type of interaction is shown in Fig. 3 where the absorption and fluorescence band maxima are plotted as a function of the solvent polarity index $E_T(30)$. Undeniably, a clear distinction appears between protic and aprotic solvents for both absorption and emission processes. As discussed above, the presence of solute–solvent hydrogen bonding interaction was already suggested from PCM-DFT geometry optimization performed for SBPa with 4 specific MeOH molecules added (Chart 3) and from the behaviour of proton H3 in NMR spectra (Fig. 2b). Concerning the fluorescence data, besides the separation between protic and aprotic solvents, we can distinguish in Fig. 3 two sub-groups of aprotic solvents depending on whether they are weakly or strongly polar. We suggest that this partition occurs in the less polar solvents due to the dimerization effect discussed previously that probably interfere with the emission process. Within the semi-empirical framework, a more advanced analysis is

 This journal is © the Owner Societies 2011

© 2016 Tous droits réservés.

doc.univ-lille1.fr

Published on 22 June 2011. Downloaded by Univ Lille 1 on 31/08/2016 15:13:09.

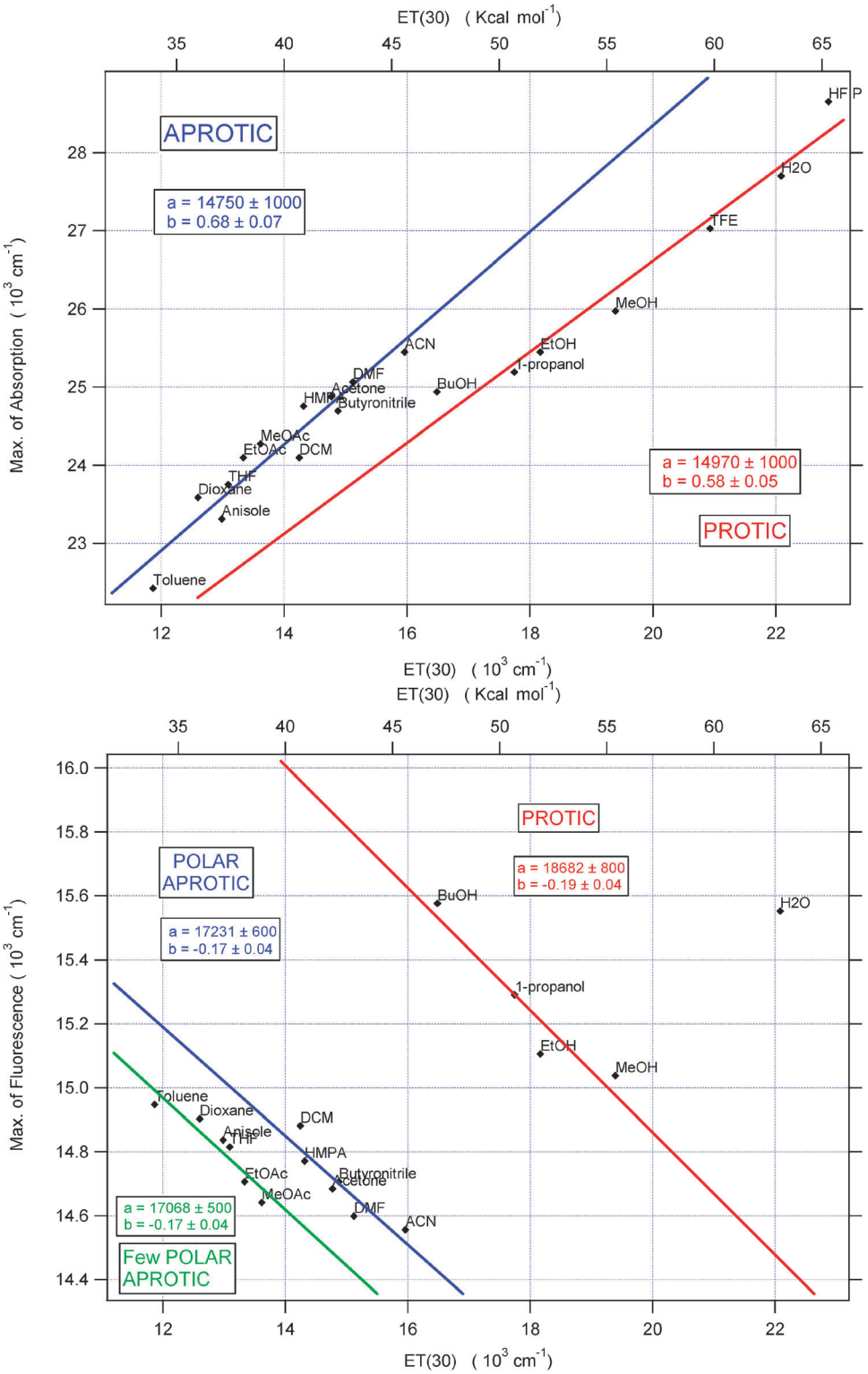

Fig. 3 Solvatochromic plots of absorption (lower panel) and fluorescence (upper panel) as a function of the $E_T(30)$ polarity index. Slopes of linear correlations are indicated.

achievable by comparison with the B30 molecule[41] and it is worth to notice that such a split of the overall correlation between aprotic and protic solvents is intriguing, as to the best of our knowledge, such an effect has never been reported.

As a conclusion from the empirical representation, three distinct sets of solvents have to be considered independently (see the numbering given in Table 1): (i) all aprotic solvents no 1–12; (ii) polar aprotic solvents no 4, 8–12, *i.e.*, a sub-group of the latter restricted to the most polar solvents ($\varepsilon > 7$) for

© 2016 Tous droits réservés.

doc.univ-lille1.fr

HDR de Stéphane Aloïse, Lille 1, 2016 View Article Online

Published on 22 June 2011. Downloaded by Univ Lille 1 on 31/08/2016 15:13:09.

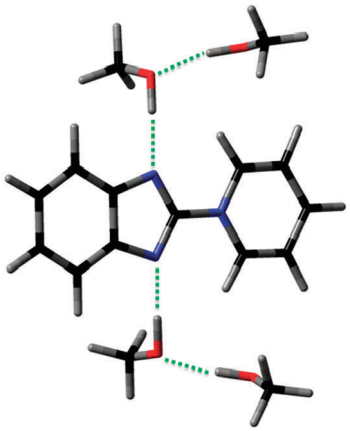

Chart 3 (SBPa + 4MeOH) geometry optimized by PCM-DFT calculations. Hydrogen bonds are indicated with dotted lines.

which dimerization is not expected; (iii) protic solvents no 13–16, 18, expected to inform on the role played by solvent–solute hydrogen bonding interactions on the solvatochromism. However, at this point, a determination of the Kamlet–Taft correlations[42] is necessary, as it can provide an adequate way to ensure, within each set of solvents used for the determination of the dipole moments, whether solvent–solute interactions are mainly electrostatic or involve specific interactions.

Kamlet–Taft correlation. According to this approach, the solvent-dependent spectral shift ν can be linearly correlated with the empirical Kamlet–Taft solvatochromic parameters π^*_{KT}, α_{KT}, and β_{KT}:

$$\nu = \nu_0 + a\alpha_{KT} + b\beta_{KT} + p\pi^*_{KT} \quad (10)$$

Where π^*_{KT} is a measure of the nonspecific solvent polarity and polarizability, α_{KT} and β_{KT} characterize the solvent hydrogen bond donating and accepting properties, and p, a, and b are related to solute properties: dipole moment, ability to donate a hydrogen bond to the solvent and ability to accept a hydrogen bond/lone pair from the solvent, respectively. In practice, a set of solvents for which the p coefficient is higher than the a and b ones can be considered as having minor specific interactions with the solute.

For the three groups of solvents selected above the Kamlet–Taft correlation coefficients were determined for absorption and emission solvatochromic data and the results of these six correlations are given in Table 3. First, considering the first group of solvents for both absorption and emission data, it is clear that specific interactions dominate the correlations since the electrostatic coefficient is lower than the hydrogen bond related coefficients (a, $b \gg p$). For the second group of solvents, the correlation are acceptable for both absorption and emission ($R^2 > 0.91$) even if some aspects of the results are somewhat surprising, such as the observation of a non-negligible contribution obtained for coefficient a in aprotic solvents (in both the absorption and fluorescence correlations). This effect is a consequence of the fact that the solvatochromic data are correlated with coefficient α_{KT} rather than π^*_{KT} and that, in the aprotic solvent set, only ACN and acetone have non-zero α_{KT} values. Anyhow, the best correlation coefficients are obtained for the polar aprotic set (4, 8–12), which is thus relevant for a physical treatment of solvatochromism. This group of solvents can be considered as electrostatic, because $p > a$ and b (even if a and b are still not negligible). Note that for the third group (protic solvents) the correlations are of less quality ($R^2 < 0.88$) and the electrostatic condition is achieved only for the absorption case.

Thus, even if the limited number of solvents for each sets ($N < 6$) does not allow a quantitative discussion of the numerical values of a, b, and p, an important qualitative information can be deduced from their sign. In the case of absorption, coefficients a and p are positive but b is negative, which is the hallmark of a zwitterionic structure in the ground state, whereas for fluorescence, the respective signs are reversed, indicating a moderate polar emitting species.

The innovative physical approach. We now apply, for each one of the three groups of solvents, the detailed solvatochromic analysis described in Section IV.2 (and ESI†). For comparison, (TD)DFT polarizability values are computed for the ground and excited states. A most interesting aspect of this approach is that it allows scanning a large interval of values for the polarizability as proposed recently by several authors.[13,43] Also interesting is the fact that, apart from a recent paper by Renge,[20] there has never been any discussion in the literature about the importance of choosing with caution the $\nu^{gas}_{abs/fluo}$ value (such a value is not easily accessible) within a solvatochromic approach that does not deal with Stokes shift quantities.

For the group of aprotic solvents no 1–12, as seen in Fig. 4a, the optimum χ^2 value related to the absorption data is found for $\alpha \approx 0.93$ and $\nu^{gas}_{abs} \approx 25\,000$ cm^{-1}, which corresponds to dipole moments $\mu_g(S_0) = +0.38$ D and $\mu_e(S_2) = -6.8$ D. This result is totally irrational because, on the one hand, the ν^{gas}_{abs} value is manifestly too large compared to the 22 400 cm^{-1} absorption maximum measured in nonpolar toluene, and, on the other hand, the +0.38 D dipole moment value determined for the ground state is in total disagreement with the experimental value (+10.33 D[7]). This arises probably from SBPa aggregation effects, as evidenced above from the Kamlet–Taft correlations.

This aggregation effect is supposed to be reduced in the group of polar aprotic solvents as expected from the Kamlet–Taft correlations (prevailing p coefficient, although the a and b coefficients are still not negligible). The χ^2 map (Fig. 4b) established from the absorption data shows a slight minimum near $\alpha \approx 0.95$ as for the previous group (Fig. 4a), which leads to an unrealistically weak $\mu_g(S_0)$ value. Because the true minimum on the 2D map does not give reliable results, we decided to explore the region corresponding to the well defined tail of χ^2 values that are only slightly higher than at the minimum. At the value $\alpha = 0.5$ currently used in the literature and in conformity with calculations (see Table 3), the dipole moment found for the ground state (+4.2 D) is not consistent with the experimental value. However, by further extending the χ^2 tail until $\alpha = 0$ for a reasonable value of $\nu^{gas}_{abs} = 17\,200$ cm^{-1}, a value of $\mu_g(S_0) = +9.1$ D is predicted in quite good agreement with the experimental value of +10.33 D. Moreover, the corresponding excited state dipole moment has an opposite

 This journal is © the Owner Societies 2011

© 2016 Tous droits réservés.

doc.univ-lille1.fr

HDR de Stéphane Aloïse, Lille 1, 2016 View Article Online

Published on 22 June 2011. Downloaded by Univ Lille 1 on 31/08/2016 15:13:09.

Table 3 Dipole moments determined through the solvatochromism method for 3 groups of solvents together with the corresponding Kamlet–Taft correlation coefficients. The last column states whether the dipole moments are determined from a true minimum on the 2D map (see text)

			Kamlet–Taft correlations					Innovative solvatochromism treatment			
	Solvent group		ν_0	a	b	P	R^2	μ_g	μ_e	$2\alpha/a^3$	True minimum on 2D map?
Abs.	Aprotic	[1–12]	22 750 ± 666	9010 ± 2770	2666 ± 797	−63 ± 1230	0.7304	0.3	−6.8	0.93	Yes
	Polar aprotic	[4,8–12]	22 437 ± 668	4191 ± 1880	−1628 ± 1010	4428 ± 1410	0.9105	0.2	−6.5	0.97	Yes
								4.2	−12.3	0.5	No
								9.1	−1.5	0	No
	Protic	[13–16,18]	24 716 ± 755	963 ± 697	−1828 ± 558	2490 ± 504	0.8231	1.7	−0.61	0.97	Yes
Fluo.	Aprotic	[1–12]	14 823 ± 143	−1103 ± 595	−369 ± 171	207 ± 264	0.8169	2.7	0	1.034	Yes
	Polar aprotic	[4,8–12]	15 021 ± 17	−484 ± 48	506 ± 26	−872 ± 36	0.9981	3.3	0	0.01	Yes
								3.9	−1.2	0.5	No
	Protic	[13–16,18]	17 186 ± 1600	−3695 ± 1480	−153 ± 1180	2527 ± 1070	0.8769	7.5	0.005	1.015	Yes

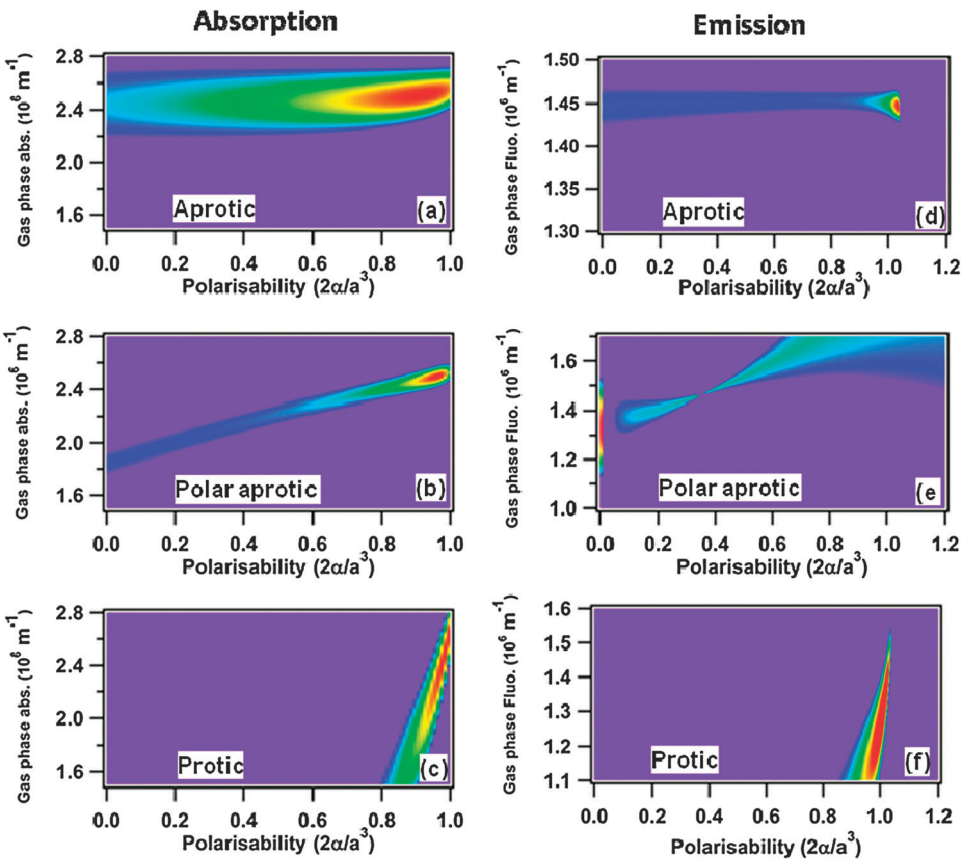

Fig. 4 Maps of the χ^2 values deduced from the non-linear fits of the 3D solvatochromic data (eqn (5)) $\nu_{abs/fluo} = f[g(n,\varepsilon,\alpha), h(n,\alpha)]$ for absorption (a–c) and fluorescence (d–f), for three distinct sets of solvents (aprotic, polar aprotic, and protic) defined in the text.

and much weaker value of $\mu_e(S_2) = -1.5$ D consistent with expectations. The excellent correlation (0.9981) obtained for the emission data (Fig. 4f) confirms this result, with a p coefficient notably higher than the a and b coefficients and a χ^2 minimum clearly located at $\alpha = 0.01$. The two dipole moments values related to this minimum, $\mu_e(S_1) = 0$ and $\mu_g(S_0') = 3.31$ D, are consistent with regard to the range fixed by solvatochromism absorption results. These 4 dipole moments are represented in Chart 4.

Finally, data in protic solvents are likely affected by the strong specific interactions as predicted by the Kamlet–Taft analysis (see Chart 3). The 2D χ^2 maps obtained from both the absorption and emission data (Fig. 4c and g, respectively) have similar shapes with a minimum near $\alpha = 1$. We suggest that this region concerns mostly a solute in interaction with solvent molecules (see Chart 3) rather than the solute alone.

Discussion of the dipole moment values. Calculation of the hyperpolarizability. To the best of our knowledge, this study provides the first confrontation of experimental and theoretical dipole moment values for 4 different electronic configurations. Despite the complex photophysics of SBPa and the problems of dimerization and specific interactions, this confrontation leads to very encouraging results. As seen in Table 4, the S_0

© 2016 Tous droits réservés.

doc.univ-lille1.fr

HDR de Stéphane Aloïse, Lille 1, 2016 View Article Online

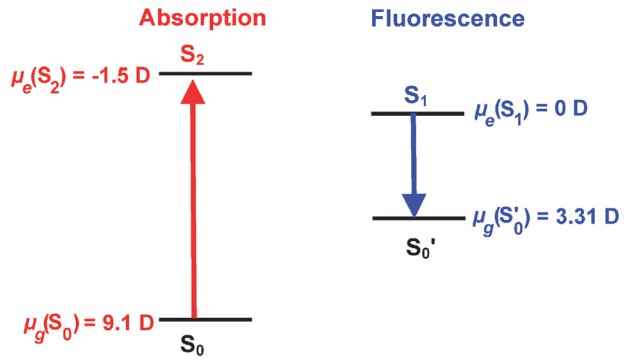

Chart 4 Dipole moments deduced from the solvatochromic analysis restricted to the set of polar aprotic solvents in the assumption of a $\alpha = 0$ polarizability.

dipole moment of +9.1 D correlates well with the TDDFT prediction (+8.2 D) and is close to the experimental value of +10.33 D[7] (measured in dioxane). By the way, the HF values[3–5] apparently in better agreement with experiment are likely overestimated as the actual experimental value in vacuum has to be less than 10 D . For the emissive excited state S_1, the TDDFT value (−1.4 D) is in much closer agreement with the experimental value (0 D), confirming a flip of the dipole moment in the excited state (already predicted by CIS calculations).[3,4] For the first time, an absolute dipole moment value of −1.5 D is determined for the S_2 state from the solvatochromic analysis, qualitatively comparable to the TDDFT value (+2.7 D). As an example of the difficulties encountered for reproducing the proper sign of excited state dipole moments, the PCM-TDDFT $\mu_e(S_2)$ value, unlike the $\mu_e(S_1)$ one, was found sensitive to the polarity of the surrounding medium. This effect will be analyzed in a future report. Finally, as negative results, we failed to determine a reasonable dipole moment value for S'_0 as well as proper values for the polarizability, mainly due to our difficulty to define a solvent set free of any specific interactions. The failure to correctly reproduce the solute polarizability can also arise from the rough approximation $\alpha_g = \alpha_e$ used within the Bilot and Kawski formalism, which cancels out the second order term in eqn (5), this term taking into account specifically α_g and α_e. Indeed, as seen in Table 4, the change in polarizability predicted by DFT on going from S_0 (0.49) to S_1 (0.42) or S_2 (0.34) is not negligible.

Anyhow, with our approach, all relevant quantities required to compute the hyperpolarizability according to eqn (1) are extracted but great care is recommended in this procedure. First, the transition moment M_{ge} and transition energy $\hbar\omega_{ge}$ (Table 2) related to the solvatochromic CT absorption band (S_2 state) are plotted as a function of the polarity and values in vacuum are estimated by extrapolation (see ESI†). Consequently, the excited state to consider within the two-state model framework of Oudar[1] is S_2 rather than S_1 ($\Delta\mu_{ge} = -10.6$ D). So, gathering all quantities, we were able to determine a static hyperpolarizability value of $\beta(0) = -64 \times 10^{-30}$ esu, which corroborates nicely the theoretical value of $-51.7\ 10^{-30}$ esu predicted from TDDFT computation. Considering the dynamic value computed at 1064 nm, our new DFT value is somewhat in closer agreement with the experimental value in chloroform (probably overestimated relative to the true vacuum value) than the former MP2 value.[3,4]

VI. Conclusions

The 2-(1-pyridinio)benzimidazolate SBPa is still an interesting molecule for the non-linear optics field but the solvatochromism governing its absorption and emission is rather complex to analyze for various reasons. First, as found with the help of advanced PCM-TDDFT calculations, two distinct electronic transitions have to be considered for absorption ($S_0 \rightarrow S_2$) and emission ($S_1 \rightarrow S'_0$), which excludes the use of Lippert–Mataga treatment. Then, dimerization and specific interactions, highlighted by Kamlet–Taft correlations, are important for this molecule. Despite these difficulties, we propose an innovative physical treatment which consists in a non-linear fit of the solvatochromic data using the Bilot–Kawski theoretical equation and a visualization of the corresponding χ^2 values on a 2D map in which the solute polarizability and gas phase absorption are defined as varying parameters. By treating absorption and emission separately, we deduced the values of the 4 dipole moments characterizing the S_0, S'_0, S_1, and S_2 levels, respectively, and compared them with (TD)-DFT values. Three of these dipole moments have reliable values but the solute polarizability seems underestimated. Anyhow, disregarding this discrepancy, we could successfully evaluate the static hyperpolarizability in close

Table 4 Theoretical and experimental values for the SBPa dipole moments and hyperpolarizability (static and dynamic values). Values in brackets are the polarizabilities computed by TDDFT

		INDO/S		CIS			
		HF/6-31G**	MP2/6-31G**	HF/6-31G**	TDDFT PBE0/6-311G* (vacuum)	Solvatochromism	Exp.
μ_g/D (α_g)	S_0	+10.27	+10.14[a]	+10.50[a]	+8.2 (0.49)	+9.1 —	10.33[b] —
	S_0'	—	—	—	+8.8 (0.49)	+3.3 —	
μ_e/D (α_e)	S_1	−5.01[a]	−4.50[a]	−6.24[a]	−1.4 (0.42)	0 —	
	S_2	—	—	—	+2.7 (0.34)	−1.5 —	
$\Delta\mu_{ge}$/D			−14.64	−16.74	−5.5	−10.6	115 ± 25[a]
$\beta_{vec}(0)$[c]			−36.0	−35.4	−51.7	−64.0	
$\beta_{vec}(1064)$[c]			−165.5	—	−75.0	—	

[a] Ref. 3–5. [b] Ref. 7. [c] All β are in units of 10^{-30} cm^5 esu^{-1}.

This journal is © the Owner Societies 2011

Published on 22 June 2011. Downloaded by Univ Lille 1 on 31/08/2016 15:13:09.
© 2016 Tous droits réservés.
doc.univ-lille1.fr

HDR de Stéphane Aloïse, Lille 1, 2016 View Article Online

Published on 22 June 2011. Downloaded by Univ Lille 1 on 31/08/2016 15:13:09.

agreement with DFT calculations. New measurements on modified betaines with low ability to specific interaction are now in progress in our group.

References

1 J. L. Oudar, *J. Chem. Phys.*, 1977, **67**, 446–457.
2 F. Meyers, J. L. Bredas and J. Zyss, *J. Am. Chem. Soc.*, 1992, **114**, 2914–2921.
3 J. Abe, N. Nemoto, Y. Nagase and Y. Shirai, *Chem. Phys. Lett.*, 1996, **261**, 18–22.
4 J. Abe and Y. Shirai, *J. Am. Chem. Soc.*, 1996, **118**, 4705–4706.
5 J. Abe, Y. Shirai, N. Nemoto, F. Miyata and Y. Nagase, *J. Phys. Chem. B*, 1997, **101**, 576–582.
6 J. Abe, Y. Shirai, N. Nemoto and Y. Nagase, *J. Phys. Chem. B*, 1997, **101**, 1910–1915.
7 E. Alcalde, I. Dinares, J. Elguero, J.-P. Fayet, M.-C. Vertut, C. Miravitlles and E. Molins, *J. Org. Chem.*, 1987, **52**, 5009–5015.
8 N. G. Bakhshiev, *J. Opt. Technol.*, 2001, **68**, 184–188.
9 C. Reichardt, *Solvents and Solvent effects in Organic Chemistry*, Wiley-VCH, 2003.
10 P. Suppan, *J. Photochem. Photobiol., A*, 1990, **50**, 293–330.
11 P. Suppan and N. Ghoneim, *Solvatochromism*, RSC, 1997.
12 J. Catalan, J. L. G. de Paz and C. Reichardt, *J. Phys. Chem. A*, 2010, **114**, 6226–6234.
13 M. Jozefowicz, P. Milart and J. R. Heldt, *Spectrochim. Acta, Part A*, 2009, **74**, 959–963.
14 G. V. Boyd, *Tetrahedron Lett.*, 1966, **29**, 3369–3371.
15 E. Lippert, *Z. Naturforsch.*, 1955, **109**, 571.
16 E. Lippert, *Z. Elektrochem.*, 1957, **61**, 962.
17 N. Mataga, Y. Kaifu and M. Koizumi, *Bull. Chem. Soc. Jpn.*, 1955, **28**, 690–691.
18 N. Mataga, Y. Kaifu and M. Koizumi, *Bull. Chem. Soc. Jpn.*, 1956, **29**, 465–470.
19 I. Renge, *Chem. Phys. Lett.*, 2008, **459**, 124–128.
20 I. Renge, *J. Phys. Chem. A*, 2010, **114**, 6250–6254.
21 A. Kawski, *Progress in Photochemistry and Photophysics*, CRC Press, vol. V, 1992.
22 R. A. Marcus, *J. Chem. Phys.*, 1965, **43**, 1261.
23 M. J. Kamlet and R. W. Taft, *Acta Chem. Scand., Ser. B*, 1985, **39**, 611–628.
24 D. Jacquemin, E. A. Perpete, I. Ciofini and C. Adamo, *Acc. Chem. Res.*, 2009, **42**, 326–334.
25 J. Tomasi, B. Mennucci and R. Cammi, *Chem. Rev.*, 2005, **105**, 2999–3093.
26 M. J. Frisch, G. W. Trucks, H. B. Schlegel, G. E. Scuseria, M. A. Robb, J. R. Cheeseman, G. Scalmani, V. Barone, B. Mennucci, G. A. Petersson, H. Nakatsuji, M. Caricato, X. Li, H. P. Hratchian, A. F. Izmaylov, J. Bloino, G. Zheng, J. L. Sonnenberg, M. Hada, M. Ehara, K. Toyota, R. Fukuda, J. Hasegawa, M. Ishida, T. Nakajima, Y. Honda, O. Kitao, H. Nakai, T. Vreven, J. A. Montgomery, Jr., J. E. Peralta, F. Ogliaro, M. Bearpark, J. J. Heyd, E. Brothers, K. N. Kudin, V. N. Staroverov, R. Kobayashi, J. Normand, K. Raghavachari, A. Rendell, J. C. Burant, S. S. Iyengar, J. Tomasi, M. Cossi, N. Rega, J. M. Millam, M. Klene, J. E. Knox, J. B. Cross, V. Bakken, C. Adamo, J. Jaramillo, R. Gomperts, R. E. Stratmann, O. Yazyev, A. J. Austin, R. Cammi, C. Pomelli, J. W. Ochterski, R. L. Martin, K. Morokuma, V. G. Zakrzewski, G. A. Voth, P. Salvador, J. J. Dannenberg, S. Dapprich, A. D. Daniels, Ö. Farkas, J. B. Foresman, J. V. Ortiz, J. Cioslowski and D. J. Fox, *GAUSSIAN 09 (Revision A.01)*, Gaussian, Inc, Wallingford, CT, 2009.
27 A. D. Becke, *J. Chem. Phys.*, 1993, **98**, 5648–5652.
28 C. Adamo and V. Barone, *Chem. Phys. Lett.*, 1999, **314**, 152–157.
29 C. Adamo, M. Cossi and V. Barone, *THEOCHEM*, 1999, **493**, 145–157.
30 A. D. Boese and J. M. L. Martin, *J. Chem. Phys.*, 2004, **121**, 3405–3416.
31 A. D. Becke, *J. Chem. Phys.*, 1993, **98**, 1372–1377.
32 M. Caricato, B. Mennucci, J. Tomasi, F. Ingrosso, R. Cammi, S. Corni and G. Scalmani, *J. Chem. Phys.*, 2006, **124**, 520–533.
33 B. Mennucci, C. Cappelli, C. A. Guido, R. Cammi and J. Tomasi, *J. Phys. Chem. A*, 2009, **113**, 3009–3020.
34 C. J. Cramer, *Essentials Of Computational Chemistry: Theories And Models*, John Wiley & Sons Ltd, West Sussex, 2004.
35 L. Bilot and A. Kawski, *Z. Naturforsch., A: Astro. physik. Chem*, 1962, **17**, 621.
36 L. Bilot and A. Kawski, *Z. Naturforsch., A: Astro. physik. Chem*, 1963, **18**, 10.
37 L. Onsager, *J. Am. Chem. Soc.*, 1936, **58**, 1486–1493.
38 The dimensionless polarizability α is derived from the molecular polarizability α' as follows: $\alpha = \frac{2\alpha'[A^3]}{a_0^3}$, where a_0 is the Onsager cavity radius.
39 I. Ciofini and C. Adamo, *J. Phys. Chem. A*, 2007, **111**, 5549–5556.
40 I. Dinares, C. Jaime and E. Alcalde, *J. Mol. Struct.*, 1993, **291**, 105–121.
41 A more advanced analysis of $E_T(30)$ plots can be made by comparison with Reichardt's pyridinium *N*-phenoxide betaine dye B30 that has some kind of zwitterionic structure as the SBPa molecule. It is well-known that the huge blue shift of B30 absorption with increasing polarity is linked to the two following synergetic effects: (i) a large decrease of the dipole moment upon excitation, (ii) a strong specific interaction between the hydroxyl groups of protic solvents and the highly localized negative electronic charge on the oxygen atom. Regarding the latter point for SBPa, it can be verified that absorption maxima is well linearly correlated with $E_T(30)$ for aprotic solvents, the slope being positive and high (0.7). This implies that μ_e has to be substantially lower than μ_g in qualitative agreement with the early assumption proposed by Abe *et al.* Concerning the role played by specific interactions, inspection of hydroxylic solvents points in Fig. 2 is instructive on two points at least. First, the slope is still high (0.6), but significantly lower than for non-hydroxylic solvents, introducing a discontinuity in the overall plot. This can be easily explained by the fact unlike B30, the negative charge in SBPa is delocalized on the imidazole group (–N–C–N–), resulting in a weaker interaction with the HO– group of the solvent than for B30. Note also the 2-butanol point is lower by 1000 cm^{-1} than expectation. The resulting disruption of the overall correlation is intriguing, as to the best knowledge of the authors, such an example was never reported.
42 M. J. Kamlet, J.-L. M. Abboud, M. H. Abraham and R. W. Taft, *J. Org. Chem.*, 1983, **48**, 2877–2887.
43 S. Krawczyk, B. Jazurek, R. Luchowski and D. Wiacek, *Chem. Phys.*, 2006, **326**, 465–470.

© 2016 Tous droits réservés.

doc.univ-lille1.fr

View Article Online / Journal Homepage / Table of Contents for this issue
Dynamic Article Links

PCCP

Annexe 9.Aloïse et al, PCCP,14,1945-1956,2012

Cite this: *Phys. Chem. Chem. Phys.*, 2012, **14**, 1945–1956

HDR de Stéphane Aloïse, Lille 1, 2016

www.rsc.org/pccp

PAPER

A two-step ICT process for solvatochromic betaine pyridinium revealed by ultrafast spectroscopy, multivariate curve resolution, and TDDFT calculations†

Stéphane Aloïse,*[a] Zuzanna Pawlowska,[a] Cyril Ruckebusch,[a] Michel Sliwa,[a] Julien Dubois,[a] Olivier Poizat,[a] Guy Buntinx,[a] Aurélie Perrier,[b] François Maurel,[b] Patrice Jacques,[c] Jean-Pierre Malval,[d] Lionel Poisson,[e] Giovanni Piani[e] and Jiro Abe[f]

Received 11th July 2011, Accepted 30th November 2011
DOI: 10.1039/c2cp22254j

Published on 09 January 2012. Downloaded by Univ Lille 1 on 31/08/2016 15:00:41.

This work deals with the photophysics of a pyridinium betaine, 2-pyridin-1-yl-1*H*-benzimidazole (**SBPa**), based on a combination of steady-state, femtosecond photoionization (gas phase) and femtosecond transient absorption (solution) spectroscopic measurements, supported by (LR)-PCM-(TD)DFT calculations. Preliminary and new electrochemical results have revealed a strongly negative solvatochromic charge transfer (CT) absorption due to a $S_0 \rightarrow S_2$ vertical transition and a weakly-solvatochromic emission due to $S_1 \rightarrow S_0$ transition. Advanced TDDFT optimizations of the Franck–Condon states S_2(FC) and S_1(FC) led to two additional CT levels with planar geometry, S_2(CT) and S_1(CT), respectively, allowing prediction of a two-step photoinduced ICT process, *i.e.*, $S_0 \rightarrow S_2$(FC) and S_2(CT) $\rightarrow S_1$(CT), separated by a S_2(FC) $\rightarrow S_2$(CT) back charge transfer relaxation. While the pyridinium ring is the acceptor group in both steps, two different donor groups, the benzene ring and the imidazole bridge, are involved in the excitation and internal conversion processes, respectively. Femtosecond transient absorption experiments supported by MCR-ALS decomposition confirmed indeed the contribution of two distinct CT states in the photophysics of **SBPa**: following excitation to the S_2(CT) state, ultrafast production of the emissive S_1 state (the only channel observable in the gas phase) was observed to occur in competition with a further ICT process toward the S_1(CT) state, with a time constant ranging from 300 fs to 20 ps depending on the solvent. While in aprotic media this ICT process was found to be purely solvent controlled (double polarity and viscosity dependency), in protic solvents, the influence of the hydrogen bond network has to be taken into account. Comparison with data obtained for a pre-twisted **SBPa** analogue led us to exclude the presence of any large-amplitude geometrical change during ICT. Analyzing the solvent dependency using the power law approach, we concluded that the S_1(CT) state decays essentially through IC in the 3–40 ps time range whereas the emissive S_1 state decays within 130–260 ps *via* IC, ISC and fluorescence.

[a] *Laboratoire de Spectrochimie Infrarouge et Raman CNRS UMR 8516, Université de Lille1 Sciences et Technologies, Université Lille Nord de France, Bat C5, 59655 Villeneuve d'Ascq Cedex, France. E-mail: stephane.aloise@univ-lille1.fr*
[b] *Université Paris Diderot, Sorbonne Paris Cité, ITODYS, CNRS UMR 7086, 15 rue Jean Antoine de Baif, 75205 Paris Cedex 13, France*
[c] *Ecole Nationale Supérieure de Chimie de Mulhouse, Université de Haute-Alsace, 3 rue Alfred Werner, 68093 Mulhouse, France*
[d] *Institut de Sciences des Matériaux de Mulhouse, LRC CNRS 7228, Université de Haute Alsace, 15 rue Jean Starcky, 68057 Mulhouse, France*
[e] *CNRS, IRAMIS, SPAM, Laboratoire Francis Perrin, URA 2453, F-91191 Gif-sur-Yvette, France*
[f] *Department of Chemistry, School of Science and Engineering, Aoyama Gakuin University, 5-10-1 Fuchinobe, Sagamihara, Kanagawa 229-8558, Japan*

† Electronic supplementary information (ESI) available: Table SI1: preexponential factors deduced from global fits of data in Fig. 3d–e; Fig. SI1: cyclic voltammogram of **SBPa** in ACN; Fig. SI2: femtosecond transient absorption spectra of **SBPa** in EtOH; Fig. SI3: femtosecond transient absorption spectra of **Br$_2$SBPa** in ACN; Fig. SI4: plots of the CT time constant τ_2 as a function of the average solvation time τ_{solv}; Fig. SI5: stationary absorption spectra of **TwSBPa** in ACN and methylacetate; Fig. SI6: molecular orbitals for **TwSBPa** and **SBPa** molecules; full ref. 47. See DOI: 10.1039/c2cp22254j

© 2016 Tous droits réservés.
doc.univ-lille1.fr

HDR de Stéphane Aloïse, Lille 1, 2016 View Article Online

Published on 09 January 2012. Downloaded by Univ Lille 1 on 31/08/2016 15:00:41.

I. Introduction

Intramolecular charge transfer (ICT) organic molecules are of great interest in numerous scientific fields but especially in the domain of non-linear optics (NLO).[1] One of the most remarkable characteristics of CT excited states is undeniably the solvatochromism affecting the absorption and/or emission bands involving these states.[2–4] Extensively studied representative cases of ICT molecules are Reichardt betaine (abbreviated as B30), showing a negative solvatochromism,[3,5–7] *p*-nitroaniline (PNA), with positive solvatochromism,[8,9] and *p*-*N*,*N*-dimethylaminobenzonitrile (DMABN), characterized by the well-known dual fluorescence signal[10] from two distinct emissive singlet states, a localized excited state (LE) and an intramolecular charge transfer state (ICT).[11] Time-resolved spectroscopic investigations revealed that ICT reactions are ultrafast, ranging from ~100 fs to ~2 ps for B30,[6,12–18] until 4 ps for DMABN[19–23] with a characteristic time depending on the solvent polarity and viscosity. The back CT reaction, also solvent dependent, is a slower process ranging from ~1 ps for B30[6,12–18] to few ns for DMABN.[19–23] However, major controversies are still present in the literature, in particular concerning the DMABN excited state geometry where the well-known Twisted ICT (TICT) hypothesis[11,24–28] is in opposition with Planar ICT (PICT) one. The PICT model, defended preliminarily by Zachariasse and his group,[29] takes into account the fact that the donor and acceptor parts of the molecule are strongly coupled in the CT state, coupling proportional to the small energy gap between the S_2 and S_1 excited states.[11,29–31] Note that a recent CASSCF/CASPT2 study of Boggio-Pasqua *et al.*[32] suggests a planar geometry of both the LE and CT excited states and describes the ICT reaction as a non-adiabatic process occurring through a conical intersection for which a relevant reaction coordinate would be the quinoidality rather than the torsional angle.[32]

In order to go further towards a thoughtful rationalization of complex ICT processes, novel approaches as well as new tools appear as essential. For example, our group has demonstrated that the treatment of ultrafast transient absorption data with an advanced chemometrics tool such as Multivariate Curve Resolution–Alternative Last Square (MCR-ALS) is a suitable approach to help distinguishing transient species with similar spectral signatures and/or temporal dynamics,[33] and for testing the relevance of hypothetical kinetic models.[33,34] In a complementary approach aiming at detangling the intrinsic dynamics of a molecule from the solvent influence, time-resolved mass spectrometry can be performed on a cold molecular beam of an isolated organic molecule.[34,35] For example, Fuß *et al.* have investigated DMABN and constrained analogues by femtosecond resonant multiphoton ionization following S_2 state excitation.[36–38] During the S_2 state relaxation dynamics (~70 fs) populating in parallel S_1(LE) and S_1(CT) and during the subsequent S_1(LE) → S_1(CT) transition (~1 ps), they observed some oscillating signal allowing identification of some relevant normal modes coupled to the ICT transition. They proposed a unified model in which either the TICT or the PICT mechanism arises depending on the steric hindrance of the molecule. Finally, Time-Dependent Density Functional Theory (TDDFT) calculations introducing the solvent by means of the Polarized Continuum Model (PCM)[39] have been recently used as an efficient way of reproducing the solvatochromism of DMABN[22] and B30.[6] Since a few years, TDDFT optimization of the excited state geometry from the Franck–Condon (FC) configuration has been possible and, consequently, emissive transitions to the ground state can now be predicted.[40,41]

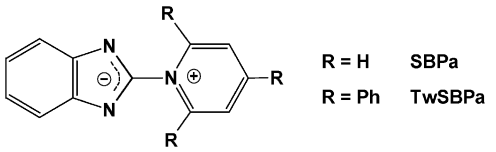

Chart 1 2-Pyridin-1-yl-1*H*-benzimidazole (**SBPa**) and its phenyl substituted analogue (**TwSBPa**).

Among all these families of molecules exhibiting strong photoinduced ICT properties that related to the 2-pyridin-1-yl-1*H*-benzimidazole molecule, abbreviated as **SBPa** (Chart 1), has been the object of precursor investigations in the past pointing out a solvatochromic behaviour of the absorption spectra,[42] a large change of dipole moment upon photoexcitation[43,44] and consequently a high first-order hyperpolarizability value.[44] For this reason, we have recently reinvestigated the solvatochromism of **SBPa** by using an innovative approach allowing us to deduce the dipole moments of various electronic states involved in the photophysics and the related hyperpolarizability.[45] Furthermore, we have achieved a full PCM-TDDFT description of the ground state as well as the low-lying excited states.[46] From the two first vertical excitations, S_0 → S_1(FC) and S_0 → S_2(FC), a complete optimization procedure was accomplished following the TD-DFT analytical gradients[47] including the equilibrium linear response (LR) solvation scheme and exploiting the state specific model to assess vertical emission transitions as well. Starting from S_1(FC) and S_2(FC), we obtained two optimized structures with planar geometries named, respectively, S_1(opt) and S_2(opt) with distinct Merz–Kollman (MK) charges.[46] It has been found that the S_0 → S_2(FC) transition is responsible for the largely negative solvatochromic absorption band, while the S_1(opt) → S_0 transition is related with the moderate positive solvatochromic emission band.[45,46] Convinced by the potential interest of **SBPa** from a fundamental point of view in providing new information on ICT molecules, we decided to explore more deeply the photophysics of this molecule with special attention to the roles played by both the S_1 and S_2 states.

In this paper, we propose to go further in the comprehension of the ultrafast photoinduced ICT reactions of **SBPa** in solution by combining experiments with various advanced techniques as a key strategy. First, the ground and CT excited state properties will be commented on the basis of previous stationary spectroscopy results supported by PCM-(TD)DFT calculations[45,46] and new electrochemical measurements. Afterward, time-resolved absorption studies of **SBPa** in acetonitrile will allow depicting the photochemical pathway related with ICT processes as well as competitive reactions. Data treatment will include multivariate analyses using the MCR-ALS approach and complementary multiexponential global fitting. Testing various solvents polarity/viscosity or studying twisted analogue **TwSBPa** (Chart 1) will allow rationalizing the contribution from the external medium or the effect of geometrical changes during ICT dynamics respectively. Complementarily, femtosecond pump–probe mass

 This journal is © the Owner Societies 2012

© 2016 Tous droits réservés.

doc.univ-lille1.fr

HDR de Stéphane Aloïse, Lille 1, 2016 View Article Online

Published on 09 January 2012. Downloaded by Univ Lille 1 on 31/08/2016 15:00:41.

spectrometry for the isolated molecule (gas phase) will be analyzed. As we will see, the overall set of results will allow proposing a complete reaction scheme in which not less than three distinct singlet states are involved in a two-step ICT mechanism.

II. Experimental section

II.1. Materials

The synthesis of **SBPa** and **TwSBPa** has been previously published.[43] All solvents, acetonitrile (ACN), butyronitrile, octanenitrile, decanenitrile, tetrahydrofuran (THF), methylacetate (MeOAc), ethylacetate (EtOAc), methanol (MeOH), trifluoroethanol (TFE), ethanol (EtOH), 2-butanol, and 2-pentanol (Aldrich), were used without any further purification.

II.2. Stationary experiments

Stationary absorption spectra were recorded using a double beam CARY 100bio with 10^{-5} M solutions contained in 10 × 10 mm quartz cells. Cyclic voltammetry experiments were performed with a computer-controlled Princeton 263A potentiostat and a three-electrode single-compartment cell for which a saturated calomel reference electrode was placed in a separate compartment maintained at room temperature. Samples were dissolved in an Ar-degassed ACN solution containing 0.1 M n-Bu_4BF_4. Ferrocene was used as an internal reference.

II.3. Femtosecond time-resolved spectroscopy

II.3.1 Transient photo-ion experimental set up (gas phase). The experimental set-up devoted to gas phase studies had been described in a previous paper.[48] Briefly, the compounds were mixed and compressed in a graphite pill that was introduced into an oven. In the present study, the molecule was found to be very sensitive to the way it was introduced in the gas phase. The oven was kept below 150 °C to avoid sample degradation. A pulsed expansion of helium as carrier gas was blowing in the oven to create a supersonic molecular beam. The molecular beam went through a skimmer to reach the laser interaction region. Femtosecond lasers were provided by the European facility LASERLAB/SLIC/LUCA. Pump excitation was set at 266 nm or 400 nm. Probing was achieved by multiphoton ionization at 800 nm. Both laser polarizations were adjusted so as to be parallel to the detector. The laser cross-correlation time was 75 fs. The generated ions were dispersed in mass by a time-of-flight spectrometer.

II.3.2 Transient absorption experimental set up (solution). The femtosecond transient absorption set up had already been described elsewhere.[49,50] Briefly, a 1 kHz Ti:sapphire laser system (coherent oscillator and a BM Industries regenerative amplifier) delivered 100 fs (0.8 mJ) pulses at 800 nm. Pump pulses were set at 390 nm or 266 nm by frequency doubling or tripling the fundamental beam, respectively, while probe pulses (white light continuum) were generated by focusing the fundamental beam on a CaF_2 rotating plate. The transient absorption measurements covered a 400–750 nm spectral range and a 0–3 ns temporal range. Sample solutions (about 10^{-3} M, absorbance of 0.2) were circulating in a flow cell equipped with 1 mm thick CaF_2 windows and characterized by a 2 mm optical path length. The laser cross-correlation time has been evaluated to be about 200 fs and 300 fs at 390 nm and 266 nm, respectively.[49,50] The characteristic times deduced from kinetics were obtained by fitting the uncorrected data with the result of a multiexponential function convolved with a Gaussian pulse (which approximates the pump–probe correlation function) taking into account the GVD and OD phenomena originating from the sample thickness (see eqn (16) in Ziolek *et al.* paper.)[51] Within this approach, global fitting was systematically performed taking into account simultaneously four relevant wavelengths. (Note that for graphs presentation, transient data were GVD corrected using a procedure proposed by Nakayama *et al.*[52])

II.4. Analysis of the transient absorption data

Multivariate analysis of the transient absorption spectra was performed using MCR-ALS[33,53–58] which aims at decomposing the spectrokinetic matrix $\boldsymbol{D}$, *i.e.*, m transient spectra (corresponding to m time delays) recorded at n wavelengths, into k pure spectral components with the respective k concentration profiles. As detailed description of the method can be found elsewhere,[37,56] only the main points of the procedure are given here. The alternating least-squares optimization algorithm decomposes data according to the bilinear model given in eqn (1).

$$\boldsymbol{D} = \boldsymbol{C}\boldsymbol{S}^{\mathrm{T}} + \boldsymbol{E} \quad (1)$$

where the matrix $\boldsymbol{C}(m \times k)$ contains the time-dependent concentration profiles of the k pure contributions at m delays and the matrix $\boldsymbol{S}^{\mathrm{T}}(k \times n)$ contains the corresponding transient spectra at n wavelengths. The matrix $\boldsymbol{E}(m \times n)$ contains the residuals not explained by the k components. Applying adequate constraints during the alternating least-squares optimization warrants some physical meaning to the resolved profiles. For transient absorption data, suitable constraints can be for example the non-negativity and unimodality (only one maximum) of the time-dependent concentration profiles, each one being expected to reflect a growth-and-decay type evolution of one of the chemical species involved in the reaction dynamics. All the calculations were performed using Matlab 7.1 (The Mathworks, Massachusetts, USA). MCR-ALS routines are freely available at http://www.ub.es/gesq/mcr/mcr.htm.

II.5. Theoretical calculations

PCM-TDDFT calculations have been performed for **TwSBPa** in order to reproduce the absorption spectra in ACN and MeOAc solvents and compare the electronic excitations with those previously calculated for **SBPa**.[45,46] Geometry optimizations and TDDFT calculations for both molecules were done at the PBE0/6-311++G(d,p) level of calculation using the Gaussian 09 package.[47]

III. Results and discussion

We will first review the previously reported basic stationary spectroscopic results of **SBPa**[45,46] completed with new electrochemical measurements and (LR)-PCM-(TD)DFT calculations[45,46] to give a first picture of the overall photochemical scheme (Section III.1). Then, time-resolved femtosecond spectroscopic measurements in solution (Section III.2.1) and

© 2016 Tous droits réservés.

doc.univ-lille1.fr

Published on 09 January 2012. Downloaded by Univ Lille 1 on 31/08/2016 15:00:41.

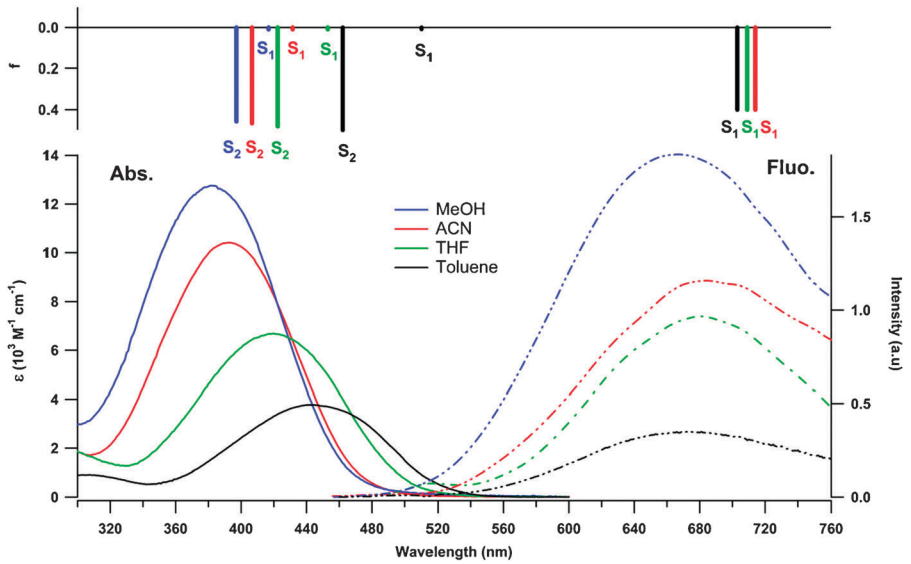

Fig. 1 Stationary absorption (solid lines) and fluorescence (dash-dotted lines) spectra of **SBPa** in MeOH (blue), ACN (red), THF (green), and toluene (black) together with the TDDFT wavelengths of the $S_0 \rightarrow S_1$(FC), $S_0 \rightarrow S_2$(FC), and S_1(opt) $\rightarrow S_0$ transitions in the same solvents. The theoretical oscillator strengths are quantitative only for the absorption transitions. (Reproduced from ref. 45 by permission of the Royal Society of Chemistry.)

in the gas phase (Section III.2.2) will be discussed to enable us to refine the detailed mechanisms.

III.1. Stationary spectroscopy and calculations

Fig. 1 summarizes the recently reported[45] absorption and fluorescence spectra of **SBPa** in toluene, THF, ACN, and MeOH, together with (LR)-PCM-TDDFT results (same color code). It has been established that the $S_0 \rightarrow S_2$(FC) transition with notable CT character is responsible for the intense solvatochromic absorption observed around 400 nm. On the other hand, the optimized S_1 state, S_1(opt), is predicted to be the emissive state, with a theoretical S_1(opt) $\rightarrow S_0$ transition energy well fitting the observed emission band position ($\sim$680 nm) and its moderately positive solvatochromism.[45,46] Cyclic voltammetry measurements interpreted by using the Weller expression[59–61] (see Fig. SI1 and all details in ESI†) confirm that an ICT process is thermodynamically allowed upon excitation within the solvatochromic absorption band, which can thus be classified as a CT band. In summary, the analysis of stationary solvatochromic data points out the involvement of at least two distinct singlet excited states in the **SBPa** photophysics, S_2(FC), related with the CT absorption band, and S_1(opt), related with the emission band. As we will see below, this couple of singlet excited states will not be sufficient to propose a convincing interpretation of the complex transient absorption data.

Lets us consider now in more detail the geometrical characteristics and MK charges predicted by the (LR)-PCM-TDDFT methodology.[45,46] We recall here that optimization of both the S_1(FC) and S_2(FC) states has led to planar geometries, as the S_0 state, and all attempts to find an eventual twisted or bended stable conformation failed.[46] By comparison with S_0, a common change in geometry of S_1(opt) and S_2(opt) concerns mostly

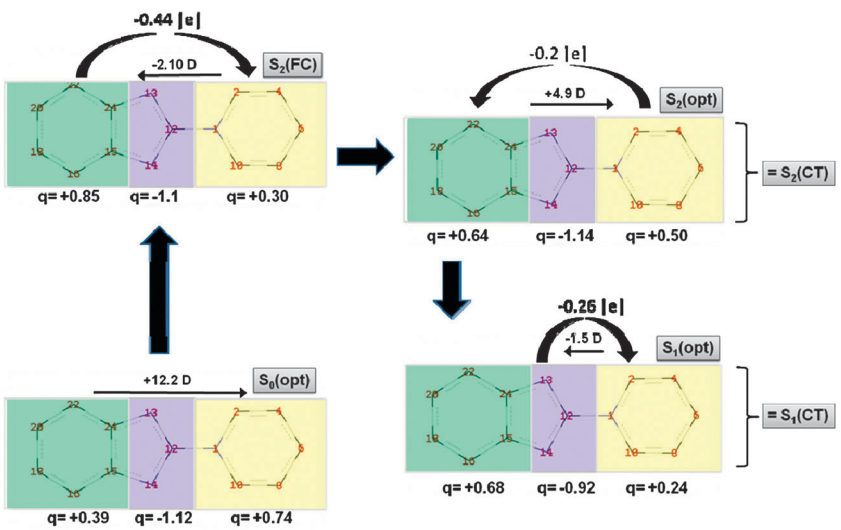

Fig. 2 Computed MK charges (ACN case) summed over three parts of **SBPa** (benzene, imidazole and pyridinium groups) for the S_0(opt), S_2(FC), S_2(opt) and S_1(opt) states. The molecular dipole moments of each state and fractions of charge transferred in each transition are also indicated.

 This journal is © the Owner Societies 2012

© 2016 Tous droits réservés.

doc.univ-lille1.fr

HDR de Stéphane Aloïse, Lille 1, 2016 View Article Online

Published on 09 January 2012. Downloaded by Univ Lille 1 on 31/08/2016 15:00:41.

the quinoidality of the pyridinium ring (weakly dependent on the solvent polarity) while the quinoidality changes of the betaine moiety are different. The question of the excited state geometry will be discussed in more detail later by taking into account the **TwSBPa** transient data.

Fig. 2 presents the electronic charges repartition for the S_0, S_2(FC), S_2(opt) and S_1(opt) states restricted to the partial sums of MK charges for clarity. Unexpectedly, three different parts of the **SBPa** molecule have to be considered: two distinct donor groups, the benzene ring and the imidazole bridge (N–C–N), and an acceptor group, the pyridinium ring. With the aim to focus on a photochemical process, we first examine the excitation from S_0 to S_2(FC) that induces a drastic diminution of the dipole moment due to the transfer of about $-0.44|e|$ from the benzene to the pyridinium ring. Then, unexpectedly, the relaxation of S_2(FC) toward the corresponding potential well minimum S_2(opt) causes some weak back electron transfer (about $-0.2|e|$) from the pyridinium to the benzene, in such a way that the overall charge transfer from S_0 to S_2(opt) is limited to $-0.24|e|$. This still non-negligible CT character of S_2(opt) incites us to call it S_2(CT) hereafter. Finally, the S_2(opt) → S_1(opt) relaxation is correlated with a further charge transfer of $-0.26|e|$ from the imidazole part to the pyridinium ring, which suggests that S_1(opt), related with the emissive state, can be renamed as S_1(CT). An overall charge transfer of $(-0.44 + 0.2 - 0.26) = -0.5|e|$ is thus predicted from S_0 to S_1(opt), which decreases with the solvent polarity.[46] Based on this last result, probable solvent polarity dependence can be predicted during time resolved experiments aiming to determine the S_2(CT) → S_1(CT) ICT transient signal.

At this point, on the basis of stationary results supported by (LR)-PCM-TDDFT calculations, a two-step ICT process can be predicted for **SBPa**, one step being directly related with the S_0 → S_2(FC) excitation and the second one associated with the S_2(CT) → S_1(CT) relaxation, both leading essentially to

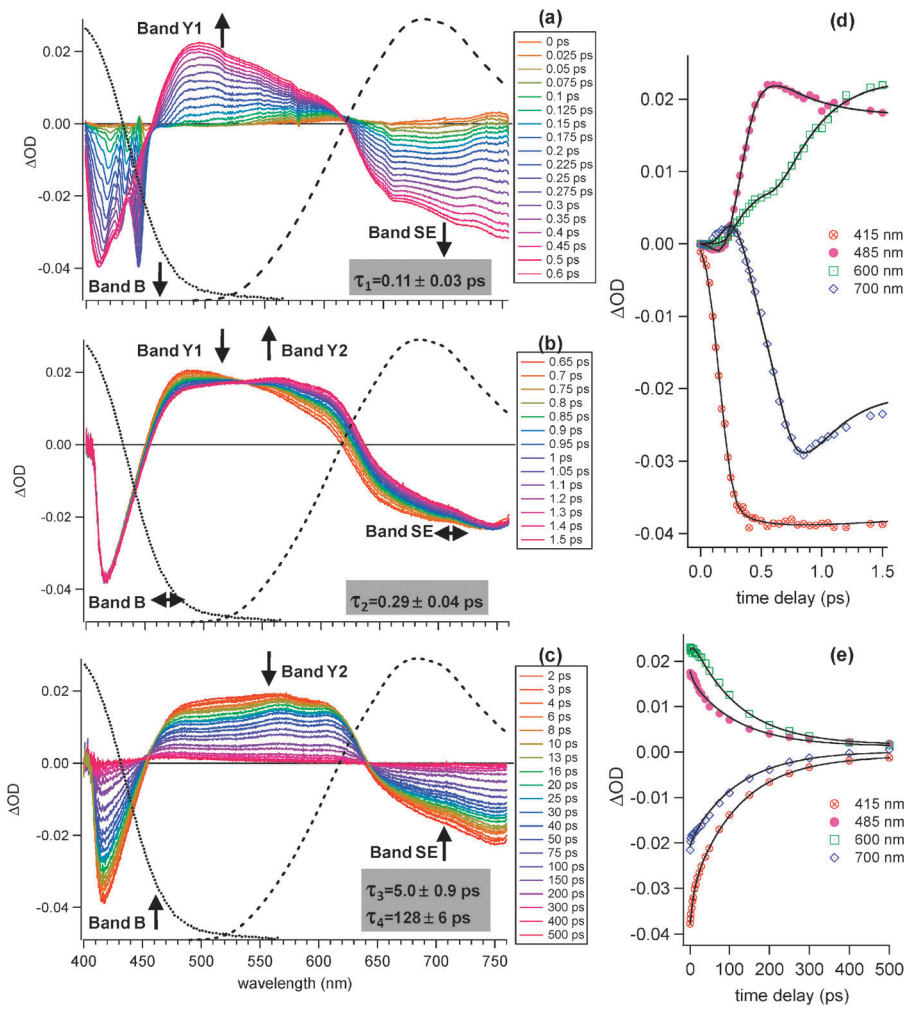

Fig. 3 (left) Femtosecond transient absorption spectra of **SBPa** in ACN following laser excitation at 390 nm, divided into three temporal windows: (a) 0–0.6 ps, (b) 0.65–1.5 ps, and (c) 2–500 ps; transient stimulated Raman peaks of the solvent are noticed below 450 nm for time delays <0.5 ps; the stationary absorption (dotted line) and emission (dashed line) spectra are also shown for comparison. (right) Kinetics monitored at 415 nm (band B), 485 nm (band Y_1), 600 nm (band Y_2), and 700 nm (band SE) related to the (d) 0–1.5 ps and (e) 2–500 ps temporal windows; global fit is performed using four exponential functions convolved with an absorption/GVD modified Gaussian function; pump–probe correlation time: 180 fs; sample OD at 390 nm: 0.2; the four characteristic times are indicated in insets of parts a–c and the corresponding preexponential factors are gathered in Table SI1 (ESI†).

© 2016 Tous droits réservés.

doc.univ-lille1.fr

Published on 09 January 2012. Downloaded by Univ Lille 1 on 31/08/2016 15:00:41.

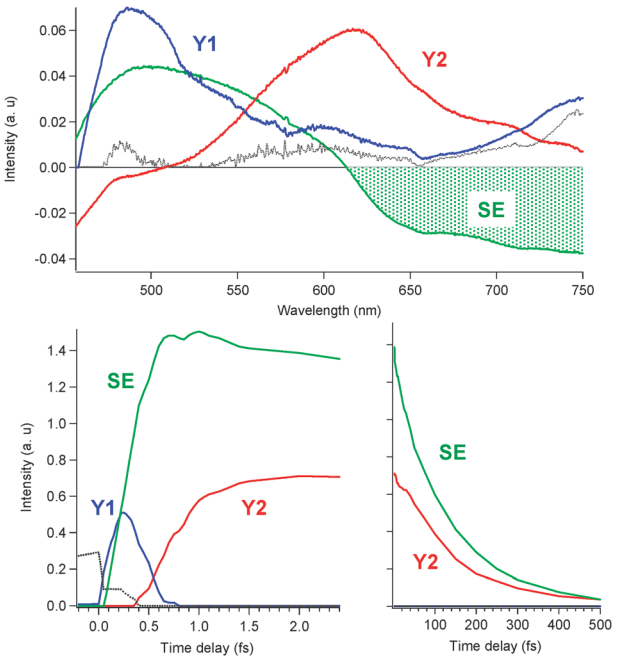

Fig. 4 MCR-ALS decomposition of the transient absorption spectra of **SBPa** in ACN shown in Fig. 3. Pure component spectra (upper panel) and concentration profiles (lower panels) follow the same color code and denoted as Y_1 (blue lines), Y_2 (red lines) and SE (green lines). A negligible contribution at ultrashort time delays ($t < 400$ fs) in grey was required for data decomposition (probably laser induced artifact, see ref. 62).

variations of the quinoidality rather than to twisting motion, as found by Boggio-Pasqua *et al.* for DMABN.[32] In this scheme, if S_1(CT) is the emissive state we will see that this attribution is no longer valid to take into consideration time resolved data.

III.2. Femtosecond spectroscopy

III.2.1 Investigation in solution. The 0–500 ps time evolution of the femtosecond transient absorption spectra of **SBPa** in ACN following pump excitation at 390 nm is presented in Fig. 3 with the corresponding global fitting characteristic times τ_1, τ_2, τ_3 and τ_4 (preexponential factors are gathered in Table SI1 (ESI†)). For clarity, the evolution is divided into 3 stages qualified as "initial dynamics", "ICT dynamics" and "post ICT dynamics". The corresponding MCR-ALS decomposition of this data set is displayed in Fig. 4. (Similar femtosecond spectra of **SBPa** in the EtOH case are presented in Fig. SI2 (ESI†).) Table 1 gives the $\tau_1 - \tau_4$ values found in 11 solvents. Times τ_2, τ_3 and τ_4 vary strongly with the solvent polarity and/or viscosity, as displayed in Fig. 5.

Initial dynamics (Fig. 3a). Just after excitation, the simultaneous growth of three bands is observed. A first negative band in the 400–450 nm range is easily recognized as a bleaching component (band B), as it corresponds approximately to the negative image of the absorption spectrum of **SBPa** (dotted trace). A second negative band between 610 and 760 nm is likely attributed to stimulated emission (band SE) by analogy with the steady-state fluorescence spectrum (dashed trace). Finally, a positive band, labelled as band Y_1, located between 450 and 610 nm, is related with absorption of excited species. Two isosbestic points are observed at 450 nm and 610 nm, confirming that all three signals appear simultaneously, at least within our temporal resolution. In EtOH solvent (Fig. SI2, ESI†), the early dynamics ($\tau_1 \approx 120 \pm 50$ fs) seems more complex, the growth of band Y_1 being apparently not concomitant with that of band SE. This divergence is due to the presence of an additional SE signal coming from the FC region. The τ_1 values in the eleven solvents are more or less comparable (see Table 1) but too close to the experimental resolution to be analyzed quantitatively.

In ACN, excitation at 390 nm is almost matching the maximum of the strong CT band (Fig. 1) ascribed to the $S_0 \rightarrow S_2$(FC) transition. Consequently, S_2(FC) is the state being populated at time zero. Band SE is evidently characterizing the emissive excited S_1 state. At first sight, it seems that band Y_1 also characterizes the emissive state. However, from the analysis of the full set of spectra at all time delays using MCR-ALS decomposition, it will be found that the situation is more complex and that band Y_1 results from the superimposition of two overlapped spectral components.

The ICT dynamics (Fig. 3b). Transient absorption spectra recorded in ACN between 0.65 and 1.5 ps show the decrease of the Y_1 band concomitantly with the increase of a new transient

Table 1 **SBPa** characteristic times (in ps) associated to the initial dynamics (τ_1), ICT dynamics (τ_2) and post-ICT dynamics (τ_3 and τ_4) obtained from the global fitting analysis of transient absorption spectra excited at 390 nm in various solvents. The solvent dielectric constant ε, viscosity η, and average solvation time $\langle\tau_{solv}\rangle$ are also given

Solvent	ε^a	η/cP	$\langle\tau_{solv}\rangle^b$/ps	τ_1/ps	τ_2/ps	τ_3/ps	τ_4/ps
Vacuum	—	—	—	0.09 ± 0.01	—	—	—
ACN	35.9	0.345	0.27	0.11 ± 0.05	0.29 ± 0.04	5.0 ± 0.9	128 ± 6
Butyronitrile	24.8	0.542	0.54	0.10 ± 0.05	1.2 ± 0.2	22 ± 8	146 ± 20
Octanenitrile	13.6	1.525	3.94	0.15 ± 0.05	4.0 ± 0.5	25 ± 10	172 ± 10
Decanenitrile	10.6	2.676	—		11 ± 4	—	200 ± 10
THF	7.58	0.575	0.94	0.17 ± 0.05	0.4 ± 0.1	2.6 ± 0.3	134 ± 8
MeOAc	6.68	0.364	0.61	0.10 ± 0.05	1.0 ± 0.1	9 ± 4	145 ± 10
EtOAc	6.02	0.426	0.86	0.10 ± 0.05	1.2 ± 0.4	12 ± 8	130 ± 20
MeOH	32.7	0.593	5	0.12 ± 0.09	0.3 ± 0.1	3.4 ± 0.4	109 ± 10
EtOH	24.6	1.2	16	0.12 ± 0.05	3.7 ± 0.3	14 ± 5	119 ± 7
2-Butanol	16.6	3.632	63	0.12 ± 0.05	12 ± 4	40 ± 20	250 ± 40
2-Pentanol	13.7	5.307	103	0.14 ± 0.09	19 ± 2		260 ± 30

[a] From ref. 68. [b] Determined in this work from femtosecond transient absorption data of C153.

 This journal is © the Owner Societies 2012

© 2016 Tous droits réservés.

doc.univ-lille1.fr

Published on 09 January 2012. Downloaded by Univ Lille 1 on 31/08/2016 15:00:41.

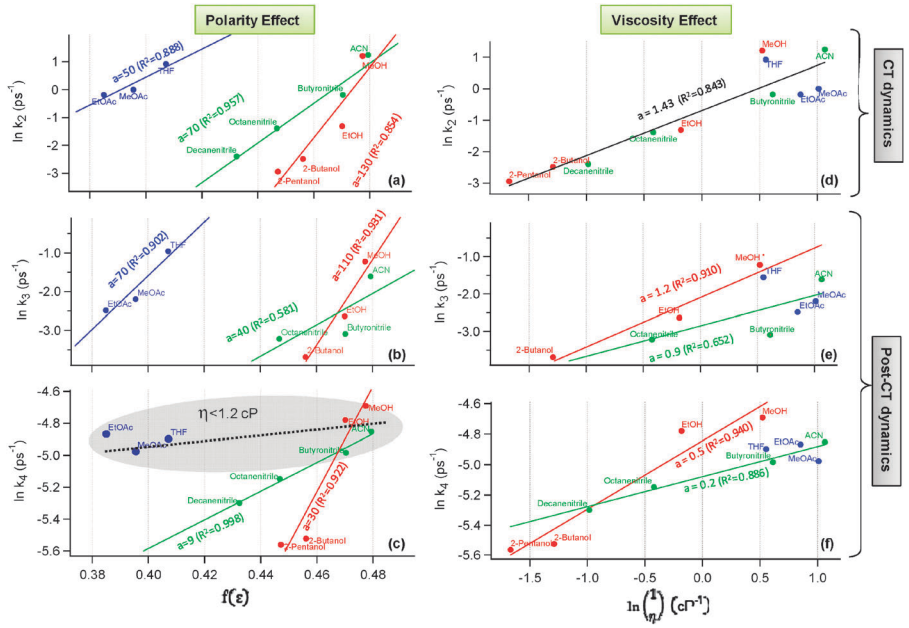

Fig. 5 Dependency of the characteristic decay rates k_2, k_3 and k_4 deduced from multiexponential global fitting of the transient absorption spectra of **SBPa** in ACN (shown in Fig. 3) on the solvent polarity $f(\varepsilon)$ (a–c) and viscosity (d–f). Slope and regression coefficients of linear correlation are indicated for each set of solvents. The shadow area in panel c indicates solvents of low or moderate viscosity.

absorption band peaking at ~570 nm, named as Y_2, with a clear isosbestic point in between, at 530 nm (characteristic time $\tau_2 = 0.29 \pm 0.04$ ps). During this process, the SE band keeps nearly constant intensity and shows only minor change in shape, which can be likely explained by the rise of the partially overlapped Y_2 absorption. It seems thus that the SE band is not affected by the $Y_1 \rightarrow Y_2$ process, *i.e.* the population of the emissive state does not vary significantly during this process. In addition, there is no perceptible recovery of the ground state, as revealed by the stability of the bleach band (B) intensity. In other words, the $Y_1 \rightarrow Y_2$ process can be classified as a transition between two excited states that are both distinct from the emissive state. Moreover, since the Y_1 and SE bands appear with the same kinetics, it can be concluded that both the excited state related to Y_1 and the emissive state are formed in parallel from a precursor state with kinetics faster than the experimental time resolution. The observed dynamics appears thus more complex than anticipated from the TDDFT calculations. We suggest that the precursor state, too short-lived to be detected in the present experiments, is the S_2(FC) level, and that the Y_1 band corresponds to the relaxed S_2(CT) state. According to this assumption, the S_2(FC) state relaxes in parallel toward the S_2(CT) state and the emissive state. Then, we propose to assign the $Y_1 \rightarrow Y_2$ process to the S_2(CT) $\rightarrow$ S_1(CT) transition, which implies that, contrary to our previous conclusion from the TDDFT results, S_1(CT) is not the emissive state, we call the emissive state S_1(E) hereafter.

The above assumption of a reaction scheme leading in parallel to the S_1(CT) and S_1(E) states is nicely corroborated by the four component MCR-ALS decomposition of the SBPa/ACN transient spectra (Fig. 3), as shown in Fig. 4. This analysis, restricted to the 450–750 nm spectral region, was assuming that only one state is responsible for the observed SE signal. Within this analysis, three main components labelled as Y_1 (blue traces in Fig. 4), Y_2 (red traces) and SE (green traces) explain 98% of the total variance. The remaining minor component (grey) extracted at very short time delays was left unaffected.[62] Clearly in Fig. 4, at early times the two components Y_1 and SE grow simultaneously while their spectra have distinct shapes, with a strong negative contribution above 600 nm exclusively for SE as anticipated, pointing for two distinct transient state signatures. In conclusion, by combining TDDFT calculations, time-resolved spectroscopy experiments, and MCR-ALS analysis, we have provided convincing evidence for the existence of two competing energy relaxation routes, S_2(FC) $\rightarrow$ S_2(CT) and S_2(FC) $\rightarrow$ S_1(E), responsible for the early dynamics of **SBPa** after excitation to the S_2(FC) level. In addition, the formation of S_2(CT) is followed by fast S_2(CT) $\rightarrow$ S_1(CT) relaxation that is accompanied by further ICT.

Solvent effects. First, the solvent polarity dependency of the ICT reaction rate ($k_2 = 1/\tau_2$) is illustrated in Fig. 5a for 3 groups of solvents (ethers/acetates, nitriles, and alcohols). If linear correlation (for one given group) is rationalized in terms of ICT reaction occurring within a normal Marcus region,[45,63,64] the clear partition between the three subgroups is likely ascribable to specific interactions, as discussed in our previous paper.[45] On the other hand, the viscosity dependency of k_2 (Fig. 5d) shows a good correlation for the complete set of solvents without any partition. This double dependence on polarity and viscosity indicates that the S_2(CT) $\rightarrow$ S_1(CT) dynamics is controlled by the solute–solvent shell electrostatic interaction including specific interactions as well as the solvent diffusion necessary for solvating of the S_1(CT) state. As a confirmation, the correlation in Fig. SI4 (ESI†) shows that the τ_2 values match reasonably well the mean solvation times $\langle\tau_{solv}\rangle$[65] in aprotic solvents ($\tau_2 \simeq 0.954\langle\tau_{solv}\rangle$), which indicates that an ICT process is effectively purely controlled by

© 2016 Tous droits réservés.

doc.univ-lille1.fr

Published on 09 January 2012. Downloaded by Univ Lille 1 on 31/08/2016 15:00:41.

the solvation dynamics in this medium.[65] Reversely, in protic solvents, the correlation (Fig. SI4, ESI†) reveals that an ICT process is much faster than the mean solvation time ($\tau_2 \simeq 0.182\langle\tau_{solv}\rangle$). This seems to indicate that, due to the hydrogen bond network only the fastest components of the solvent relaxation dynamics in protic medium have to be taken into account.

TICT or not?. To check an eventual role of the torsional angle between the pyridinium and betaine moieties during the ICT mechanism, femtosecond transient absorption measurements of the pretwisted **TwSBPa** molecule in ACN were done upon pump excitation at 266 nm (Fig. 6). Note that 390 nm excitation could not be used efficiently as the visible CT absorption is too weak (see Fig. SI5, ESI†). In the ground state, the X-ray structure of **TwSBPa**[43] shows a twist angle of 84.4° between the pyridinium and imidazole moieties due to steric hindrance. Similar CT transitions involving comparable

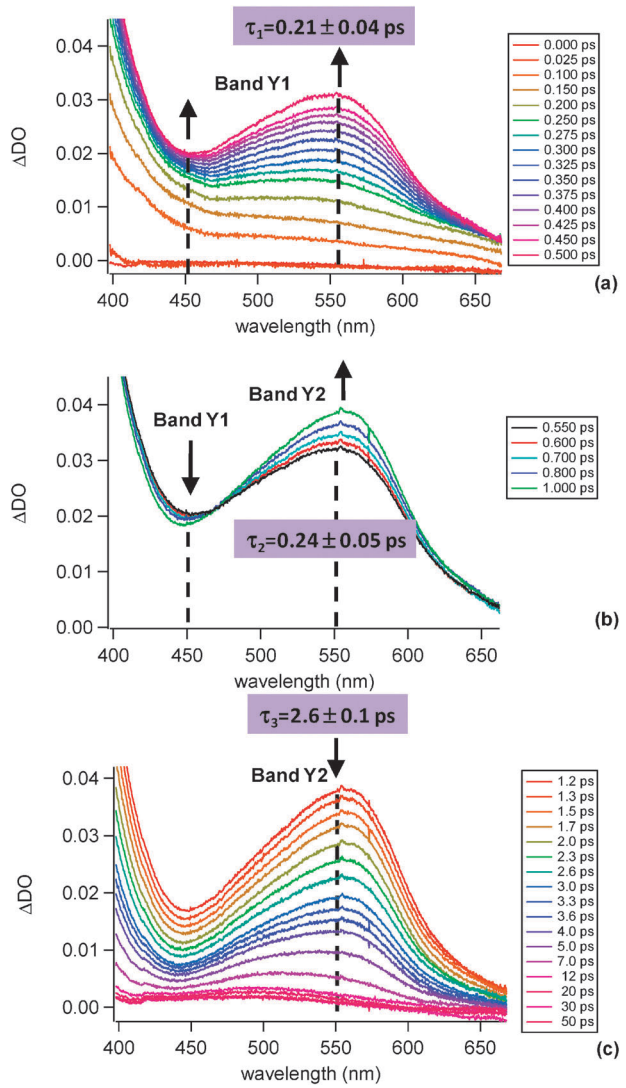

Fig. 6 Femtosecond transient absorption spectra of **TwSBPa** in ACN following laser excitation at 266 nm, for two temporal windows: (a) 0.9–1.3 ps and (b) 1.5–150 ps. Characteristic times are found by individual monoexponential fit at selected wavelengths (dashed lines).

orbitals are predicted by the calculations in **SBPa** and **TwSBPa** (Fig. SI6, ESI†). Note however that it was impossible to detect any stationary emission for **TwSBPa**. Assuming that the population at 266 nm of a high-lying S_n state is followed by efficient and ultrafast $S_n \rightarrow S_2$ relaxation, the photophysics of the pre-twisted molecule can be directly compared to that of **SBPa**. If the $S_2(CT) \rightarrow S_1(CT)$ transition (time constant τ_2) in **SBPa** does not induce a torsion around the dihedral angle, it should happen similarly in **TwSBPa**, and the spectral evolution should also be characterized by a Y_1/Y_2 band exchange. Reversely, if the torsion around the dihedral angle is involved in the reaction coordinate of the ICT process in **SBPa**, a different photophysics is expected in the case of **TwSBPa** that is blocked in a pretwisted geometry. In Fig. 6, the transient signals seem to be similar to those found for **SBPa** upon 390 nm excitation, which justifies the use of similar notations for both molecules. In the 0–0.5 ps temporal window (Fig. 6a), an ultrafast growth of band Y_1 ($\tau_1 = 0.21 \pm 0.04$ ps) is noticed. However, unlike for **SBPa**, there is no contribution from any bleaching signal below the 450 nm region or the SE signal above 600 nm, in agreement with the negligible intensity of the CT band of **TwSBPa** and its nonemissive character (Fig. SI5, ESI†). The shape of band Y_1 is thus not affected by the overlap with negative bands, in contrast to the situation of **SBPa** (Fig. 4). Next, within the 0.55–1 ps temporal window (Fig. 6b), one observes the decay of band Y_1 concomitantly with the increase of what we believe to be the new band Y_2, because an isosbestic point is noticed at 470 nm. By analogy with **SBPa**, we assign this evolution to the existence of a final charge transfer step that stabilizes the ICT process, *i.e.* $S_2(CT) \rightarrow S_1(CT)$. Even if during this process, only small variations of intensity are observed, the corresponding characteristic time of 0.22 ps is comparable to the 0.24 ps value found for the **SBPa** case. So, as a fundamental result, it seems that **SBPa** does not need an intramolecular twisting motion for the ICT to proceed because the similar two ICT steps arise for the pre-twisted analogue as well.

Post-ICT dynamics (Fig. 3c). The spectral evolution in the 2–500 ps temporal window shows the simultaneous bi-exponential fading of the negative bleach B and stimulated emission SE as well as the excited-state absorption band Y_2 with characteristic times $\tau_3 = 5.0 \pm 0.5$ ps and $\tau_4 = 128 \pm 6$ ps. At 500 ps a weak residual signal is noticed at 450 nm. The SE signal is present until 500 ps, which indicates that the decay of the emissive $S_1(E)$ state can be correlated to the longer decay time, τ_4. The shorter decay time τ_3 is likely characterizing the $S_1(CT)$ state associated with band Y_2, *i.e.*, it corresponds to a back electron transfer process. The bi-exponential decay is also confirmed by MCR-ALS decomposition (Fig. 4), showing distinct decaying concentration profiles for the two components Y_2 and SE. Note however that the time constant τ_3 of the shortest decay component is largely overestimated by the MCR-ALS decomposition compared to the value found by global analysis probably due to difficulties in isolating species contribution with high spectral and/or temporal overlapping (rotational ambiguity). The transient data of **TwSBPa** confirm nicely the above assignment made for SBPa: (i) rather than biexponential, monoexponential decay is observed for band Y_2 (Fig. 6c) with a characteristic time of

 This journal is © the Owner Societies 2012

© 2016 Tous droits réservés.

doc.univ-lille1.fr

Published on 09 January 2012. Downloaded by Univ Lille 1 on 31/08/2016 15:00:41.

τ_3 = 2.6 ps similar to the 5 ps reported for SBPa pointing out for a similar S_1(CT) state relaxation in both compounds; (ii) the absence of a long time decay τ_4, correlated to the lack of stationary emission and SE band, is consistent with the attribution in **SBPa** of time τ_4 to the decay of the S_1(E) state. Finally, to help us assigning the residual spectrum observed at time delays longer than 500 ps, we investigated by transient absorption spectroscopy the photophysics of a dibrominated analogue of **SBPa** (see Fig. SI3 and the related discussion in ESI†). The observation of a clear heavy atom effect on the intensity of this spectrum as well as a notable reduction of its lifetime in the presence of oxygen led us to definitely assign this residual spectrum to the lowest excited triplet state T and to identify its precursor state as being the emissive S_1(E) state rather than S_1(CT).

Solvent effects. To gain more information about these deactivation processes, it is instructive to analyze the solvent polarity and viscosity influence on τ_3 (Fig. 5c and f) and τ_4 (Fig. 5b and e). Such analysis has to be considered with caution because both solvent characteristics are interlinked. At first glance, some dependency can be found for τ_4 in protic and alkylnitrile solvents but these dependencies become insignificant if viscous solvents ($\eta < 1.2$) are neglected. This result is fully consistent with the weak solvatochromic emission of the S_1(E) state revealing an energy level not sensitive to polarity variations. The case of τ_3 is intriguing because good correlations are found for nonpolar (R^2 = 0.902) and protic (R^2 = 0.931) solvents, which contrast with a poor correlation for the alkylnitrile group (R^2 = 0.581). This observation highlights a higher sensitivity of back electron transfer to specific interactions (aggregation effects and hydrogen bonding) rather than to pure electrostatic interactions. Attempts to rationalize dependencies of τ_3 and τ_4 on solvent viscosity (η) are undertaken by adopting a power law approach[66,67] in Fig. 5e and f, respectively, for both protic and aprotic solvents. The linear correlation of τ_3 is excellent for protic solvents (R^2 = 0.961) and poor for aprotic solvents (R^2 = 0.652). However, both solvent groups give a slope close to 1: a small activation barrier has to be crossed (Kramers picture) and thus a strong dependency of τ_3 on the solvent viscosity is observable. This is in accordance with the influence of solute–solvent frictions in the back charge transfer process, the S_1(CT) $\rightarrow$ S_0 IC leading to the recovery of the starting molecule. Reversely, minor dependency was found for τ_4 (smaller slope values) in both protic and aprotic solvents, which suggests that, among the IC, ISC, and fluorescence processes contributing to the decay of the S_1(E) state, the last one is probably the major deactivation pathway (only IC and ISC are directly sensitive to solute–solvent frictions).

III.2.2 Gas phase investigation. Time resolved mass spectroscopy of **SBPa** was performed with 400 nm pump pulses and 800 nm probe pulses (multiphoton ionization). The pump–probe ionization did not induce any fragmentation, the parent mass (195 amu) being the only peak with noticeable intensity (> 5%) in the mass spectrum.

Considering that the absorption spectrum of isolated **SBPa** is close to that in a non-polar solvent, *i.e.* toluene (Fig. 1), pump excitation at 400 nm is expected to populate mainly the S_2 state, as in solution. This is also consistent with the TDDFT vertical transition energies calculated under vacuum: 600 nm (S_0 $\rightarrow$ S_1), 483 nm (S_0 $\rightarrow$ S_2), and 380 nm (S_0 $\rightarrow$ S_3). The kinetics of the parent peak (Fig. 7) shows an ultrafast single exponential decay (90 $\pm$ 10 fs) followed by a plateau stable for up to 5 ps (only the 0–2 ps time window is shown), according to a A $\rightarrow$ B process. Strongly different ionization efficiencies are found for species A ($\sigma_A \approx 95\%$) and B ($\sigma_B \approx 5\%$), which indicates an important charge redistribution on going from A to B, as already observed in the time-resolved dynamics of spiropyran molecules.[48] The ultrafast kinetics is attributed to the depopulation of the S_2(FC) state by internal conversion (IC) toward a lower energy excited state of lifetime > 5 ps. We have seen in the preceding section that, in aprotic solvents, the S_2(CT) $\rightarrow$ S_1(CT) process is kinetically controlled by the solvation dynamics implying that, for the isolated molecule, this process is expected to be much slower due to the lack of solvation. Since the 90 fs time constant found for the A $\rightarrow$ B process in the gas phase is notably shorter than the S_2(CT) $\rightarrow$ S_1(CT) time constant in any solvent, it cannot be assigned to this relaxation dynamics. This suggests thus that another excited state than S_1(CT) is formed in the gas phase, characterized by a lifetime higher than 5 ps and a charge distribution notably different from the precursor S_2(FC) state. By analogy with the results established in solution, we propose that, in the gas phase, the S_2(FC) state relaxes exclusively *via* ultrafast IC to the emissive state, S_1(E).

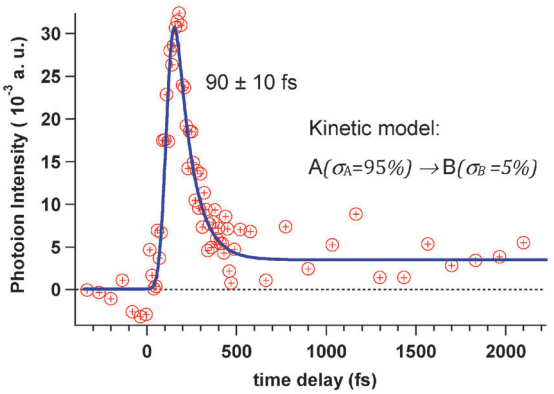

Fig. 7 Time evolution of **SBPa** ion signal followed on fragment mass 195 amu and best fit according to a first-order kinetic model A $\rightarrow$ B convolved with a Gaussian instrumental response function (FWHM = 75 fs).

IV. Conclusions

Combining various advanced techniques (femtosecond spectroscopies) and novel tools (MCR-ALS, TDDFT for excited states), we achieved a thorough characterization of the **SBPa** photophysics and related ICT processes. An overall summary of the results is presented in Chart 2 adopting diabatic and adiabatic representations.

The key point to understand the photophysics of **SBPa** is undeniably the two-step aspect of the photoinduced ICT process leading to the final S_1(CT) state. Indeed, vertical excitation from the planar ground state molecule, S_0 $\rightarrow$ S_2(FC), induces a first charge transfer from the benzene to the pyridinium

© 2016 Tous droits réservés.

doc.univ-lille1.fr

Published on 09 January 2012. Downloaded by Univ Lille 1 on 31/08/2016 15:00:41.

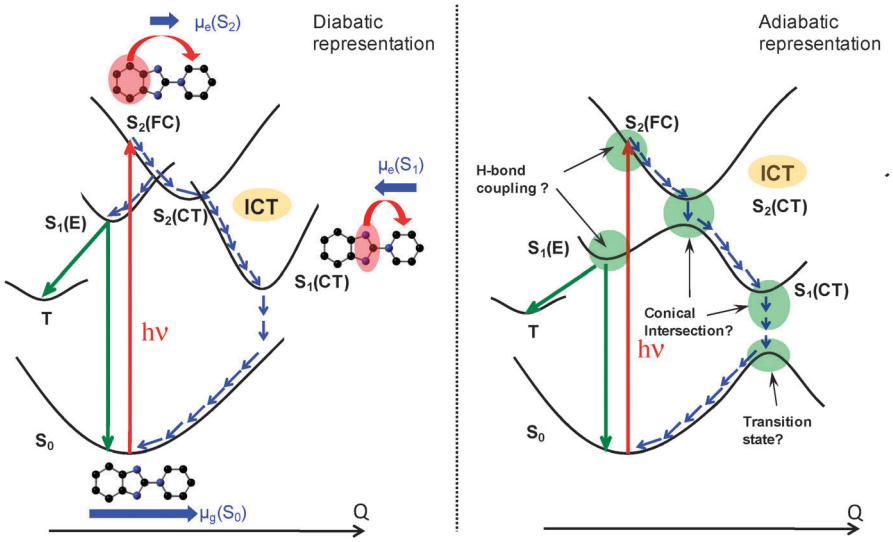

Chart 2 Possible photophysical scheme for **SBPa** (diabatic and adiabatic representations).

ring, which results in a drastic dipole moment reduction (inversion can even be expected in polar solvents).[46] An ultrafast $S_2(FC) \rightarrow S_2(CT)$ relaxation ($\sim$100 fs) leads to the stabilization of this CT state from its initial Franck–Condon geometry, which is accompanied by some reorganization of the electronic configuration (a weak fraction of charge is transferred back). Note that according to TDDFT calculations, the dipole moment difference between these two configurations is not negligible[46] giving a justification for the lack of such a process in the gas phase. Then, the system undergoes an internal conversion process, $S_2(CT) \rightarrow S_1(CT)$, which corresponds to a further ICT from the imidazole moiety to the pyridinium ring. The characteristic time τ_2 for this reaction ranges between $\sim$300 fs and 20 ps depending on the solvent nature. In aprotic solvents, it matches the mean solvation time $\langle\tau_{solv}\rangle$, pointing to a full control by the solvent dynamics. In protic solvents, a more complicated situation arises, with a relaxation rate notably faster than the mean solvation rate which is an evidence for an ICT process sensitive to the hydrogen bond network. From results related to the pre-twisted **TwSBPa** molecule, we definitively excluded the hypothesis of formation of a TICT state which suggests that the observed viscosity and polarity dependency on τ_2 is related to the $S_2(CT)$ excited-state solvation dynamics rather than internal twisting motion. Our study corroborates the PICT model[11,29–31] proposed for DMABN by Zachariasse *et al.* and confirmed recently by CASSCF calculations.[32] This agreement is consistent with the involvement of both the S_1 and S_2 states in the ICT process.[33–35] As an interesting result, the final $S_1(CT)$ dipole moment is found independent of the solvent polarity,[46] which could explain the lack of a clear polarity effect on the $S_1(CT)$ lifetime τ_3. In the future, to get a still better understanding of the **SBPa** photophysics, it would be fundamental to determine if the central ICT process, $S_2(CT) \rightarrow S_1(CT)$, and corresponding decay, $S_1(CT) \rightarrow S_0$, proceeds, respectively, through a S_2/S_1 and $S_1/S0$ conical intersection. Answer to this question will require in the future advanced CASSCF/CASPT2 calculations[32] in order to determine the different possible conical intersections and the related molecular geometries.

In parallel to the $S_2(CT) \rightarrow S_1(CT)$ ICT deactivation route, a competitive process has been found to occur from $S_2(FC)$, leading to the $S_1(E)$ state that is the only emissive state of **SBPa**. In the gas phase, the formation of $S_1(E)$ is probably the only deactivation route from the $S_2(FC)$. At the present time, our first attempts to properly predict this state from a theoretical point of view encountered some contradictions. On one hand, considering TDDFT emission predictions alone, the emissive state is identified to be the planar CT state, *i.e.*, $S_1(E) = S_1(CT)$. On another hand, as recalled above, time-resolved data led to the conclusion that, actually, an ICT process $S_2(CT) \rightarrow S_1(CT)$ arises independently of the $S_1(E)$ dynamics. This result implies logically that the $S_1(E)$ and $S_1(CT)$ states have to be reconsidered as distinct states. In order to overpass this apparent discrepancy, we proposed that there may exist a secondary minimum lying probably near the $S_1(CT)$ energy (with quite similar electronic distribution), which can account for the observed stimulated emission. This proposition is reasonable when considering the recent TDDFT study of Jacquemin *et al.* who succeeded to compute two neighbouring planar excited states accounting for the dual fluorescence of the Nile Red molecule.[41] In the future, other interesting points to explore concern: (i) the transient SE signal observed from the FC singlet state specifically in protic medium; (ii) the ISC process between $S_1(E)$ and the triplet states. As a consequence, the right prediction of the $S_1(E)$ structure, search for hydrogen bond induced couplings, and determination of the triplet state nature might be obtained by new TDDFT calculations testing other combinations of functional/basis sets including explicit surrounding solvent molecules. Such new TDDFT calculations are now in progress in our laboratories.

Acknowledgements

The authors are glad to acknowledge the financial support provided by the CNRS through the GDRI 91 "PHENICS". GP thanks the RTRA "Triangle de la physique" for support under the contract 2008-062T "DYNANEX". LP thanks the ANR for support through the contract ANR-09-JCJC-0090-01 "CHROMADYNE". This work was performed using HPC

 This journal is © the Owner Societies 2012

© 2016 Tous droits réservés.

doc.univ-lille1.fr

HDR de Stéphane Aloïse, Lille 1, 2016 View Article Online

Published on 09 January 2012. Downloaded by Univ Lille 1 on 31/08/2016 15:00:41.

resources from Geni-CINES (Grant 2011-C2011086626). The Centre de Ressources Informatiques de Lille1 is thankfully acknowledged for the CPU time allocation.

References

1 S. Mukamel, *Principles of nonlinear optical spectroscopy*, Oxford University Press, Inc, Oxford, 1995.
2 P. Suppan, *J. Photochem. Photobiol., A*, 1990, **50**, 293–330.
3 C. Reichardt, *Chem. Rev.*, 1994, **94**, 2319–2358.
4 C. Reichardt, *Solvents and Solvent effects in Organic Chemistry*, Wiley-VCH, 2003.
5 C. Reichardt, *Pure Appl. Chem.*, 2008, **80**, 1415–1432.
6 V. Kharlanov and W. Rettig, *J. Phys. Chem. A*, 2009, **113**, 10693–10703.
7 S. R. Mente and M. Maroncelli, *J. Phys. Chem. B*, 1999, **103**, 7704–7719.
8 T. P. Carsey, G. L. Findley and S. P. McGlynn, *J. Am. Chem. Soc.*, 1979, **101**, 4502–4510.
9 O. S. Khalil, C. J. Seliskar and S. P. McGlynn, *J. Chem. Phys.*, 1973, **58**, 1607–1612.
10 K. Rotkiewicz, K. H. Grellmann and Z. R. Grabowski, *Chem. Phys. Lett.*, 1973, **19**, 315–318.
11 Z. R. Grabowski, K. Rotkiewicz and W. Rettig, *Chem. Rev.*, 2003, **103**, 3899–4031.
12 S. A. Kovalenko, N. Eilers-Konig, T. A. Senyushkina and N. P. Ernsting, *J. Phys. Chem. A*, 2001, **105**, 4834–4843.
13 N. E. Levinger, A. E. Johnson, G. C. Walker and P. F. Barbara, *Chem. Phys. Lett.*, 1992, **196**, 159–165.
14 P. J. Reid and P. F. Barbara, *J. Phys. Chem.*, 1995, **99**, 3554–3565.
15 E. Akesson, A. E. Johnson, N. E. Levinger, G. C. Walker, T. P. Dubruil and P. F. Barbara, *J. Chem. Phys.*, 1992, **96**, 7859–7862.
16 P. J. Reid, S. Alex, W. Jarzeba, R. E. Schlief, A. E. Johnson and P. F. Barbara, *Chem. Phys. Lett.*, 1994, **229**, 93–100.
17 M. C. Beard, G. M. Turner and C. A. Schmuttenmaer, *J. Phys. Chem. A*, 2002, **106**, 878–883.
18 M. C. Beard, G. M. Turner and C. A. Schmuttenmaer, *J. Am. Chem. Soc.*, 2000, **122**, 11541–11542.
19 S. I. Druzhinin, S. R. Dubbaka, P. Knochel, S. A. Kovalenko, P. Mayer, T. Senyushkina and K. A. Zachariasse, *J. Phys. Chem. A*, 2008, **112**, 2749–2761.
20 S. I. Druzhinin, N. P. Ernsting, S. A. Kovalenko, L. W. Lustres, T. A. Senyushkina and K. A. Zachariasse, *J. Phys. Chem. A*, 2006, **110**, 2955–2969.
21 C. Chudoba, A. Kummrow, J. Dreyer, J. Stenger, E. T. J. Nibbering, T. Elsaesser and K. A. Zachariasse, *Chem. Phys. Lett.*, 1999, **309**, 357–363.
22 J.-K. Lee, T. Fujiwara, W. G. Kofron, M. Z. Zgierski and E. C. Lim, *J. Chem. Phys.*, 2008, **128**, 164512.
23 T. Gustavsson, P. B. Coto, L. Serrano-Andres, T. Fujiwara and E. C. Lim, *J. Chem. Phys.*, 2009, **131**, 4.
24 W. M. Kwok, C. Ma, M. W. George, D. C. Grills, P. Matousek, A. W. Parker, D. Phillips, W. T. Toner and M. Towrie, *Phys. Chem. Chem. Phys.*, 2003, **5**, 1043–1050.
25 T. Okada, M. Uesugi, G. Kohler, K. Rechthaler, K. Rotkiewicz, W. Rettig and G. Grabner, *Chem. Phys.*, 1999, **241**, 327–337.
26 W. M. Kwok, C. Ma, D. Phillips, P. Matousek, A. W. Parker and M. Towrie, *J. Phys. Chem. A*, 2000, **104**, 4188–4197.
27 A. L. Sobolewski and W. Domcke, *Chem. Phys. Lett.*, 1996, **250**, 428–436.
28 A. B. J. Parusel, W. Rettig and W. Sudholt, *J. Phys. Chem. A*, 2002, **106**, 804–815.
29 K. A. Zachariasse, S. I. Druzhinin, W. Bosch and R. Machinek, *J. Am. Chem. Soc.*, 2004, **126**, 1705–1715.
30 S. I. Druzhinin, S. A. Kovalenko, T. Senyushkina and K. A. Zachariasse, *J. Phys. Chem. A*, 2007, **111**, 12878–12890.
31 S. I. Druzhinin, P. Mayer, D. Stalke, R. von Bulow, M. Noltemeyer and K. A. Zachariasse, *J. Am. Chem. Soc.*, 2010, **132**, 7730–7744.
32 I. Gomez, M. Reguero, M. Boggio-Pasqua and M. A. Robb, *J. Am. Chem. Soc.*, 2005, **127**, 7119–7129.
33 S. Aloise, C. Ruckebusch, L. Blanchet, J. Rehault, G. Buntinx and J. P. Huvenne, *J. Phys. Chem. A*, 2008, **112**, 224–231.
34 M. Sliwa, N. Mouton, C. Ruckebusch, L. Poisson, A. Idrissi, S. Aloise, L. Potier, J. Dubois, O. Poizat and G. Buntinx, *Photochem. Photobiol. Sci.*, 2010, **9**, 661–669.
35 G. Gregoire, I. Dimicoli, M. Mons, C. Dedonder-Lardeux, C. Jouvet, S. Martrenchard and D. Solgadi, *J. Phys. Chem. A*, 1998, **102**, 7896–7902.
36 S. A. Trushin, T. Yatsuhashi, W. Fuß and W. E. Schmid, *Chem. Phys. Lett.*, 2003, **376**, 282–291.
37 W. Fuß, K. K. Pushpa, W. Rettig, W. E. Schmid and S. A. Trushin, *Photochem. Photobiol. Sci.*, 2002, **1**, 255–262.
38 W. Fuß, W. E. Schmid, K. K. Pushpa, S. A. Trushin and T. Yatsuhashi, *Phys. Chem. Chem. Phys.*, 2007, **9**, 1151–1169.
39 J. Tomasi, B. Mennucci and R. Cammi, *Chem. Rev.*, 2005, **105**, 2999–3093.
40 G. Scalmani, M. J. Frisch, B. Mennucci, J. Tomasi, R. Cammi and V. Barone, *J. Chem. Phys.*, 2006, **124**, 15.
41 C. A. Guido, B. Mennucci, D. Jacquemin and C. Adamo, *Phys. Chem. Chem. Phys.*, 2010, **12**, 8016–8023.
42 G. V. Boyd, *Tetrahedron Lett.*, 1966, **29**, 3369–3371.
43 E. Alcalde, I. Dinares, J. Elguero, J.-P. Fayet, M.-C. Vertut, C. Miravitlles and E. Molins, *J. Org. Chem.*, 1987, **52**, 5009–5015.
44 J. Abe, Y. Shirai, N. Nemoto, F. Miyata and Y. Nagase, *J. Phys. Chem. B*, 1997, **101**, 576–582.
45 Z. Pawlowska, A. Lietard, S. Aloïse, M. Sliwa, A. Idrissi, O. Poizat, G. Buntinx, S. Delbaere, A. Perrier, F. Maurel, P. Jacques and J. Abe, *Phys. Chem. Chem. Phys.*, 2011, **13**, 13185–13195.
46 A. Perrier, F. Maurel, Z. Pawlowska, M. Sliwa, S. Aloise and J. Abe, *Chem. Phys. Lett.*, 2011, **515**, 42–48.
47 M. J. Frisch, G. W. Trucks, H. B. Schlegel, G. E. Scuseria, M. A. Robb, J. R. Cheeseman, G. Scalmani, V. Barone, B. Mennucci, G. A. Petersson, H. Nakatsuji, M. Caricato, X. Li, H. P. Hratchian, A. F. Izmaylov, J. Bloino, G. Zheng, J. L. Sonnenberg, M. Hada, M. Ehara, K. Toyota, R. Fukuda, J. Hasegawa, M. Ishida, T. Nakajima, Y. Honda, O. Kitao, H. Nakai, T. Vreven, J. A. Montgomery Jr., J. E. Peralta, F. Ogliaro, M. Bearpark, J. J. Heyd, E. Brothers, K. N. Kudin, V. N. Staroverov, R. Kobayashi, J. Normand, K. Raghavachari, A. Rendell, J. C. Burant, S. S. Iyengar, J. Tomasi, M. Cossi, N. Rega, N. J. Millam, M. Klene, J. E. Knox, J. B. Cross, V. Bakken, C. Adamo, J. Jaramillo, R. Gomperts, R. E. Stratmann, O. Yazyev, A. J. Austin, R. Cammi, C. Pomelli, J. W. Ochterski, R. L. Martin, K. Morokuma, V. G. Zakrzewski, G. A. Voth, P. Salvador, J. J. Dannenberg, S. Dapprich, A. D. Daniels, Ö. Farkas, J. B. Foresman, J. V. Ortiz, J. Cioslowski and D. J. Fox, *R. A. Gaussian 09*, Gaussian, Inc., Wallingford, CT, 2009.
48 L. Poisson, K. D. Raffael, B. Soep, J. M. Mestdagh and G. Buntinx, *J. Am. Chem. Soc.*, 2006, **128**, 3169–3178.
49 G. Buntinx, R. Naskrecki and O. Poizat, *J. Phys. Chem.*, 1996, **100**, 19380–19388.
50 B. Moine, J. Rehault, S. Aloise, J. C. Micheau, C. Moustrou, A. Samat, O. Poizat and G. Buntinx, *J. Phys. Chem. A*, 2008, **112**, 4719–4726.
51 M. Ziolek, M. Lorenc and R. Naskrecki, *Appl. Phys. B: Lasers Opt.*, 2001, **72**, 843–847.
52 T. Nakayama, Y. Amijima, K. Ibuki and K. Hamanoue, *Rev. Sci. Instrum.*, 1997, **68**, 4364–4371.
53 R. Tauler, *Chemom. Intell. Lab. Syst.*, 1995, **30**, 133–146.
54 A. de Juan and R. Tauler, *CRC Crit. Rev. Anal. Chem.*, 2006, **36**, 163–176.
55 C. Ruckebusch, S. Aloise, L. Blanchet, J. P. Huvenne and G. Buntinx, *Chemom. Intell. Lab. Syst.*, 2008, **91**, 17–27.
56 C. Ruckebusch, M. Sliwa, J. Rehault, P. Naumov, J. P. Huvenne and G. Buntinx, *Anal. Chim. Acta*, 2009, **642**, 228–234.
57 N. Mouton, A. de Juan, M. Sliwa and C. Ruckebusch, *Chemom. Intell. Lab. Syst.*, 2010, **105**, 74–82.
58 N. Mouton, M. Sliwa, G. Buntinx and C. Ruckebusch, *J. Chemom.*, 2010, **24**, 424–433.
59 *Part one: Organic molecules*, ed. J. Mattay, WILEY-VCH Verlag GmbH, Weinheim, 2001.
60 K. A. Zachariasse, S. I. Druzhinin, V. A. Galievsky, S. Kovalenko, T. A. Senyushkina, P. Mayer, M. Noltemeyer, M. Boggio-Pasqua and M. A. Robb, *J. Phys. Chem. A*, 2009, **113**, 2693–2710.

© 2016 Tous droits réservés.

doc.univ-lille1.fr

HDR de Stéphane Aloïse, Lille 1, 2016 View Article Online

61 J. P. Malval, J. P. Morand, R. Lapouyade, W. Rettig, G. Jonusauskas, J. Oberle, C. Trieflinger and J. Daub, *Photochem. Photobiol. Sci.*, 2004, **3**, 939–948.
62 First, it should be noted that to avoid the notable distortion of the transient spectra observed in the range 420–450 nm at a subpicosecond time scale and mainly attributed to stimulated Raman scattering Amplification, values at wavelength below 450 nm were discarded. Second, the MCR-ALS resolution was obtained considering four components, the first component (in grey Fig. 5) is only observed at a sub-picosecond time scale, and corresponds to two percent less total variance, is not attributed. This component is nevertheless required to correctly separate the three other MCR-ALS components associated to photophysical species. The fact that this additional "species" is required to get a correct solution can be explained by that MCR-ALS provides resolution without explicit model function and, thus, the total variance as to be described. The same trick was used by Ernsting *et al.* [*J. Phys. Chem. A*, 2001, **105**, 3343–3353] for the decomposition of wave-packet femtosecond data. Our resolution was obtained under the following constraints: non-negativity and unimodality to the time-dependant concentration profiles and that non-negativity of the spectral contribution of the transient species except for band SE species that was left unconstrained (negative values are allowed but not forced).
63 M. R. Wasielewski, *Chem. Rev.*, 1992, **92**, 435–461.
64 T. Asahi, M. Ohkohchi, R. Matsusaka, N. Mataga, R. P. Zhang, A. Osuka and K. Maruyama, *J. Am. Chem. Soc.*, 1993, **115**, 5665–5674.
65 T. J. Kang, W. Jarzeba, P. F. Barbara and T. Fonseca, *Chem. Phys.*, 1990, **149**, 81–95.
66 J. A. Mondal, H. N. Ghosh, T. K. Ghanty, T. Mukherjee and D. K. Palit, *J. Phys. Chem. A*, 2006, **110**, 3432–3446.
67 J. Waluk, *Conformational analysis of molecules in excited state*, WILEY-VCH, New York, 2000.
68 M. L. Horng, J. A. Gardecki, A. Papazyan and M. Maroncelli, *J. Phys. Chem.*, 1995, **99**, 17311–17337.

Published on 09 January 2012. Downloaded by Univ Lille 1 on 31/08/2016 15:00:41.

 This journal is © the Owner Societies 2012

© 2016 Tous droits réservés. doc.univ-lille1.fr

Annexe 10.Aloïse et al, PCCP,18,15384,2016

HDR de Stéphane Aloïse, Lille 1, 2016

PCCP

PAPER

View Article Online
View Journal | View Issue

Cite this: *Phys. Chem. Chem. Phys.*, 2016, **18**, 15384

Can betaine pyridinium derivatives be used to control the photoejection of cation?†

S. Aloïse,*[a] Y. Ruan,[b] I. Hamdi,[a] A. K. Tiwari,[a] G. Buntinx,[a] C. Azarias,[cd] A. Perrier[cd] and I. Leray*[b]

Received 15th March 2016,
Accepted 9th May 2016

DOI: 10.1039/c6cp01755j

www.rsc.org/pccp

Using a combination of advanced DFT/TDDFT calculations together with ultrafast and stationary spectroscopies we have investigated the photochemistry and cationic complexation ability of 1-pyridinio-benzimidazolate (PyB) and analogs substituted by 15-aza-5-crown (PyB–Aza) or dimethyl-amino groups (PyB–DiMe). Focusing on PyB–Aza, the first aim was to assess the competitive complexation of the imidazole bridge *vs.* the macrocycle. In acetonitrile, it was found by absorption and emission that the imidazole moiety binds efficiently through lateral electrostatic interaction of high charge density cations and especially Ca^{2+} to form a 1 : 1, metal : ligand (M : L) complex. Modulation of the complexation toward *para* substitution of the phenyl ring with a donor group is reported with values ranging from $\log K$ = 3.4 to 6.8. Complexation values are properly predicted by DFT calculations. From a photochemical point of view, for the same series, the trend is parallel to the rate of the photo-release process, found to be less than 200 femtosecond (fs), the fastest photorelease characteristic time reported so far. Unlike photoinduced charge transfer molecules linked with an aza-crown group, the mechanism appears simpler with no participation of loose complexes due to the macrocavity effect. Relaxation mechanisms after cation ejection are discussed as well. Finally, even if any photoinduced translocation of cation is reported for the PyB–Aza molecule between two complexation sites, a discussion about the use of betaine pyridinium as a molecular tool for the smart manipulation of cation systems is initiated.

Published on 11 May 2016. Downloaded by Univ Lille 1 on 31/08/2016 15:03:56.

Introduction

The complexation and precise spatiotemporal release of bioactive compounds are becoming very important in the field of supramolecular chemistry, life science and nanomedicine. A particular focus has been given to the development of chemical cages for metal ions, such as calcium ions (Ca^{2+}) because of their biological importance. Ca^{2+} has been studied extensively in muscle contraction, cell signaling, gene regulation, thrombosis, wound healing, and cell death.[1]

In the race to achieve actual control of bioactive cations, the use of light is attractive because it is non-invasive and readily delivered with high spatial and temporal precision.[2] Recent examples of drug delivery systems induced by light have been successfully reported[3] even if the lack of reversibility was still a major drawback to overcome. Indeed, after photorelease, the host molecule becomes structurally different and thus unable to cage again an ion.[4] A solution consists of using photo-induced charge transfer (PCT) molecules coupled with a complexing agent, typically aza-crown, for which the cation delivery process stops with the end of illumination. Indeed, PCT leads to the positive polarization of the heteroatom of the macrocycle, resulting in Coulombic repulsion between the heteroatom and metal cation initially present in the cavity. Such a system has been proposed based on the azacrown-substituted $[(bpy)Re(CO)_3L]^+$ complex,[5] flavonol derivatives,[6] benzylhydrazone[7] and pyridyl oxadiazole.[8] Additional refinement can be obtained using fluorophores as the PCT moiety which allow tracking of the cation photo-release through stationary and time resolved spectroscopy. For example, the study of merocyanine linked to an aza-crown moiety (DCM-crown) has shown that the cation photoejection mechanism is a multi-step process occurring within hundreds of picoseconds (ps).[9] Apart from one recent novel proposition based on calixarene double cages,[10] molecular engineers dealing with the spatio-temporal control of cations are always requesting novel PCT chromophores to enlarge the possible combination of more-and-more elaborate systems.

[a] *Univ. Lille, CNRS, UMR 8516, LASIR, Laboratoire de Spectrochimie Infrarouge et Raman, F59 000 Lille, France. E-mail: stephane.aloise@univ-lille1.fr*
[b] *ENS-CACHAN PPSM-CNRS 8531, 61, av. du Président Wilson, 94235 Cachan, France. E-mail: icmleray@ppsm.ens-cachan.fr*
[c] *ITODYS, UMR CNRS 7086, Université Paris Diderot, Sorbonne Paris Cité, 15 rue Jean Antoine de Baif, 75205 Paris Cedex 13, France*
[d] *Chimie Paris Tech, PSL Research University, CNRS, Institut de Recherche de Chimie Paris (IRCP), F-75005 Paris, France*

† Electronic supplementary information (ESI) available: Additional Ca^{2+} titration using absorption and fluorescence; transient data for PyB–DiMe; scheme for $\log K$ calculations; solvatochromic and Kamlet–Taft study for PyB–Aza. See DOI: 10.1039/c6cp01755j

This journal is © the Owner Societies 2016

© 2016 Tous droits réservés.

doc.univ-lille1.fr

Published on 11 May 2016. Downloaded by Univ Lille 1 on 31/08/2016 15:03:56.

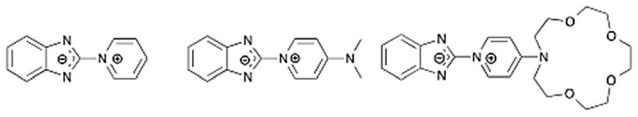

Scheme 1 Betaine pyridinium derivatives PyB–R with R = H, DiMe, aza-crown.

In this context, betaine pyridinium molecules are interesting entities because they can interact with cations. Reichardt *et al.* in 1992 reported drastic modification of UV-visible spectra of the well-known solvatochromic probe betaine-30 induced by the presence of ion, the so called halochromic effect.[11] This was rationalized in terms of electrostatic interaction between the negative phenolate oxygen and the cation. Cation selectivity has been reported using appropriate crown-ether substitution.[11,12] In the same way, focusing on neighbouring benzimidazole compounds, Kumar *et al.* reported a multiple ionophore optical probe able to screen various metal ions.[8] Apart from a few examples, the use of betaine pyridinium or analog derivatives for smart manipulation of cations is little explored in the literature.

In recent years, we have studied extensively the intramolecular charge transfer (ICT) properties of a negative solvatochromic betaine pyridinium,[13] 1-pyridinio-benzimidazolate (Scheme 1) denoted as PyB, displaying drastic dipole moment inversion induced by light.[14] In order to get a deep understanding of ICT process at the molecular level, femtosecond transient absorption spectroscopic experiments have been performed and complemented by PCM-TDDFT calculations.[13] An interesting photophysical relaxation scheme has been derived, which involves two distinct ICT excited states, S_1(CT) and S_2(CT). Excitation within the solvatochromic absorption band populates the S_2(CT) state, which leads to partial charge transfer from the betaine phenylene to the pyridinium ring. Then, the S_2(CT) state undergoes ultrafast relaxation to an emissive S_1(E) state in competition with the S_1(CT) state, with a time constant ranging from 300 fs to 20 ps depending on the solvents. The S_2(CT) → S_1(CT) transition involves a charge transfer from the imidazole bridge to the pyridinium ring and thus leads to a further increase of the ICT character. Finally, after a few picoseconds, both the S_1(CT) and S_1(E) state relaxed with distinct characteristic times. The proper localization of the ICT process on the imidazole bridge, together with the ability of the latter to attract cations, led us to undertake the cationic titration of PyB as well as to track the photorelease effect based on ultrafast spectroscopy. Furthermore, within the framework of smart systems to manipulate the cation, we synthesized a novel molecule, aza-crown linked PyB molecule, PyB–Aza (Scheme 1), with two possible complexation sites, *i.e.*, the imidazole bridge in competition with the macrocycle. To complete the series, a mono-chelating analog has been synthesized by replacing the aza crown by a dimethyl-amino substituent, PyB–DiMe (Scheme 1). We expected that cation would be complexed preferentially by the macrocycle and excitation of the S_2(CT) solvatochromic band would result in the expulsion of the cation, after efficient PCT. In the present work, we found that the imidazole bridge of such betaine pyridinium is more efficient to drive the PCT cation release effect.

Results and discussion

Synthesis of betaine pyridinium derivatives

The PyB was synthesized according to the procedure described by Abe *et al.*[14] The synthesis of PyB–DiMe and PyB–Aza are depicted in Scheme 2. PyB–DiMe was obtained directly from the coupling between 2-chlorobenzimidazole and an excess of 4-dimethylaminopyridine (DMAP) in 75% yield.[15] The synthesis of PyB–Aza was performed from the pyridinium derivative **1** (Scheme 1). **1** was achieved by palladium-catalyzed coupling of aza-15-crown-5 with 4-bromopyridine hydrochloride in toluene with a 30% yield.[16] PyB–Aza was then prepared by coupling 2-chlorobenzimidazole and **1** in *n*-butanol under argon (Ar), followed by deprotonation in concentrated ammonia (NH_3) solution with a 40% yield.[17]

Solvatochromism of PyB–Aza

As explained in the Introduction, we are interested in the study of the ICT properties of betaine pyridinium series PyB–R, PyB being our reference molecule that we have studied extensively in the past.[13] As a matter of fact, one has to ensure that original negative solvatochromic properties reported for PyB are still operative for PyB–Aza despite the crown substitution. Stationary spectra for various solvents are shown in Fig. 1a, in which one can easily recognize the same solvent effects for PyB–Aza as for PyB (see Fig. 1 of ref. 13*a*): a blue edge absorption band affected by drastic negative solvatochromism while the emission band is slightly affected by the change of the solvent polarity. In the past, absorption and emission spectra of PyB have been assigned through TDDFT calculations as an $S_0 \rightarrow S_2$(FC) transition for absorption and an S_1(opt) → S_0 transition for emission. The S_2 state arises from a HOMO−1 → LUMO electronic excitation while S_1 corresponds to a HOMO → LUMO transition. In the present work, applying the same computational strategy for PyB–Aza, we found that the same molecular orbitals (MO) are involved even if energetic inversions are observed; in brief, the absorption band is now assigned to a $S_0 \rightarrow S_1$(FC) transition for substituted PyB derivatives but involves the same MO as the electronic excitation responsible for the absorption process for PyB.

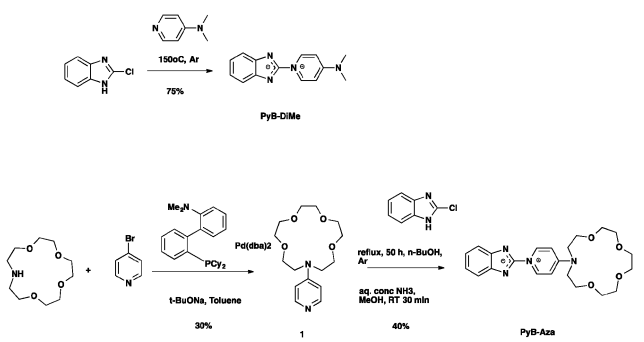

Scheme 2 Synthesis of PyB–DiMe and PyB–Aza.

© 2016 Tous droits réservés.
doc.univ-lille1.fr

Published on 11 May 2016. Downloaded by Univ Lille 1 on 31/08/2016 15:03:56.

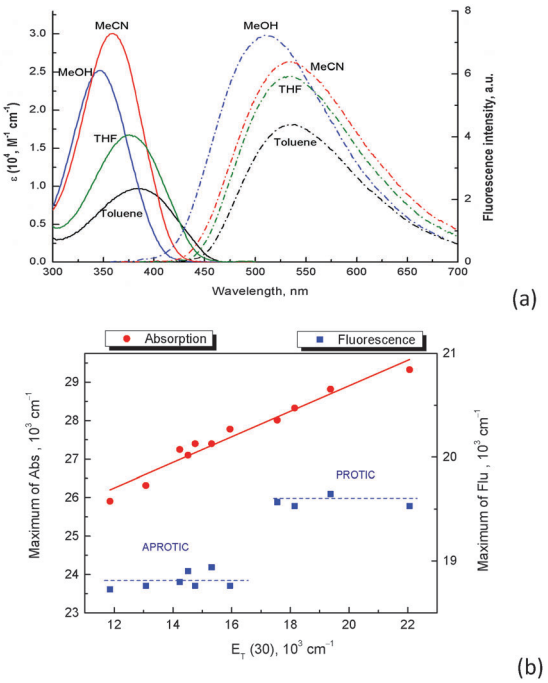

Fig. 1 (a) Solvatochromism of PyB–Aza for absorption and fluorescence spectra, the latter being recorded under excitation at maximum absorption wavelengths; direct comparison can be made with Fig. 1 of ref. 13*a*. (b) Absorption/emission solvatochromism plots for PyB–Aza as a function of the $E_T(30)$ polarity index.

Quantitatively, we have undertaken a complete solvatochromic study in 11 solvents and this is presented in Fig. 1b; results are also gathered together and shown in Table S1 (ESI†). The $E_T(30)$ plot indicates that the ground state (GS) absorption is fully influenced by the electrostatic interacting surrounding medium which contrasts with the non solvatochromic emissive S_1 state. For the latter, apart from the striking partition between protic and aprotic solvent, it is worth noticing that the dipole moment of this emissive state is probably close to zero. As presented in Table S2 (ESI†), Kamlet–Taft correlation coefficients ($\nu_{abs/fluo} = p\pi^* + a\alpha + b\beta$ with the usual meaning; see ref. 13*b*) of PyB–Aza were determined from absorption and emission solvatochromic data. In the case of absorption, the coefficient p is larger than a and b, demonstrating that electrostatic interaction dominates the solvatochromism even if the specific hydrogen bonding interaction is not negligible. In the case of emission, p is almost negligible when compared with a and b, meaning that excited state of PyB–Aza is insensitive towards solvent polarity but mainly controlled by the hydrogen bonding interaction which is easily located on the imidazole part of the molecule. Moreover, the ratio a/b are almost the same in the ground state and in the excited state, which might indicate that the same molecular groups are involved in the absorption and emission process. As we have demonstrated for PyB and this is even more pronounced for PyB–Aza, as we are dealing with two kinds of singlet state: S_1(CT) related to the strong solvatochromic absorption band and S_1(E) related to an non solvatochromic emission band.

Cation complexation of PyB–Aza

Solvatochromism being established, we are now concerned with the cation complexation abilities of PyB–Aza where, two chelating groups are in competition *i.e.*, the imidazole bridge *vs.* the crown-ether cavity. To properly undertake such a study, the compound PyB–DiMe will be helpful. In Fig. 2 and Table 1, we reported the changes observed in an acetonitrile (MeCN) solution containing the three probes upon addition of Ca^{2+} salt (perchlorate) for both absorption and emission. With the addition of Ca^{2+} in the solution of PyB–Aza, a gradual decrease in the absorption maximum at 359 nm is observed, concomitantly with the appearance of a new peak at 335 nm. A well-defined isosbestic point at 353 nm indicates the interconversion between the free ligand and the complex during titration. A blue shift is also observed for the fluorescence spectra from 533 nm to 449 nm, with a clear isoemissive point at 467 nm indicating only two emissive species in the solution. As seen in Fig. S1 (ESI†), the fluorescence spectra reach a plateau after the introduction of 1 equivalent of Ca^{2+} to the solution of PyB–Aza, demonstrating that the stoichiometry of the complex is 1 : 1. Global analysis of the whole absorption and emission spectra reveals the formation of a 1 : 1, metal : ligand (M : L) complex and the stability constant was found to be 6.8 ± 0.1.

Before going further into the discussion, questions about the cation selectivity have to be raised. In Fig. S3 (ESI†), normalized emission intensity for PyB–Aza upon addition of Li^+, Na^+, K^+, Ca^{2+}, Ba^{2+} and Sr^{2+} ions are displayed showing a preferential complexation effect for Ca^{2+} ions. Furthermore, we plot in Fig. 3 the polarity parameter $E_T(30)$ as a function of the

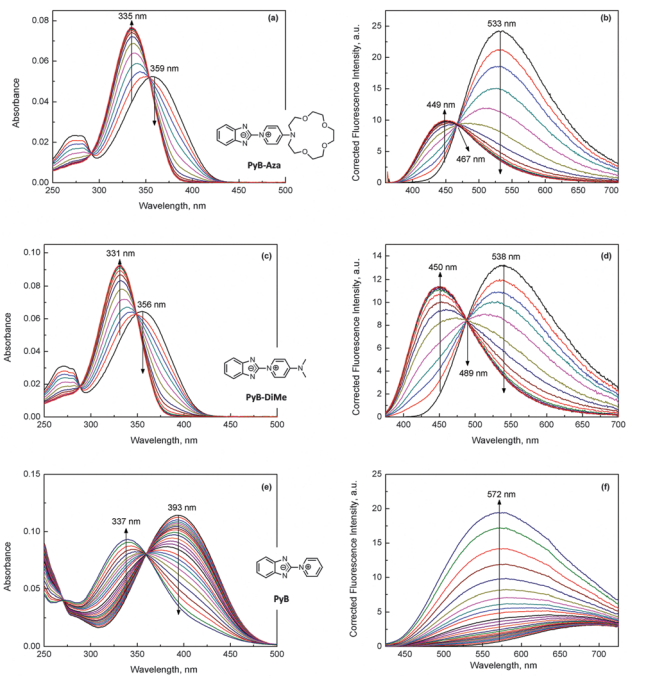

Fig. 2 Absorption (a, c and e) and fluorescence (b, d and f) spectra of PyB, PyB–DiMe and PyB–Aza in the presence of increasing concentrations of Ca^{2+} in MeCN; (a and b) [PyB–Aza] = 2.5 μM, λ_{ex} = 359 nm; (c and d) [PyB–DiMe] = 2.5 μM, λ_{ex} = 354 nm; (e and f) [PyB] = 10 μM, λ_{ex} = 393 nm.

This journal is © the Owner Societies 2016
© 2016 Tous droits réservés.
doc.univ-lille1.fr

Published on 11 May 2016. Downloaded by Univ Lille 1 on 31/08/2016 15:03:56.

Table 1 Photophysical data of PyB, PyB–DiMe and PyB–Aza and their 1 : 1 complex with Ca^{2+} and the binding constants from spectral titrations; corresponding TDDFT results are included (see text for details)

	Absorption λ_{max}/nm				Fluorescence λ_{max}/nm		Complexation constant log K	
	Ligand		Complex					
	Exp.	Calc.	Exp.	Calc.	Ligand Exp.	Complex Exp.	Exp.	Calc.
PyB	393	404	339	387	693	570	3.4 ± 0.1	3.5
PyB–DiMe	356	355	331	330	539	450	6.6 ± 0.1	4.5
PyB–Aza	359	360	335	335	534	450	6.8 ± 0.1	6.4

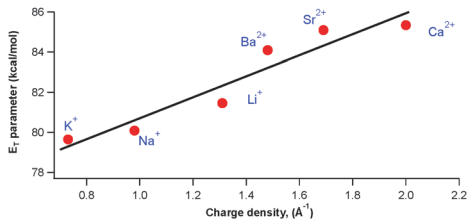

Fig. 3 $E_T(30)$ parameter deduced from absorption spectra after the addition of a metallic salt (see Fig. S2, ESI†) as a function of cationic charge density.

charge density, giving evidence for the Coulombic nature of the cation–betaine interaction.

Where is the cation located in PyB–Aza?

There are two potential binding sites for metal cations in PyB–Aza: benzimidazole moiety and aza-15-crown-5 moiety. In order to get insight into the binding process, ^{1}H NMR titration of PyB–Aza with Ca^{2+} was carried out in CD_3CN. As shown in Fig. 4, upon complexation with Ca^{2+}, proton H_c exhibits a remarkable up-field shift, while H_d shows a down-field shift. Protons of H_a and H_b also exhibit a slight down-field shift as compared with H_d. However, it is surprising to find that the addition of Ca^{2+} almost does not affect the chemical shifts of the aza-15-crown-5 moiety, which has been widely reported to bind strongly with metal ions.[18] Anyhow, in our case the ^{1}H NMR titration demonstrates that Ca^{2+} strongly binds to the imidazole moiety rather than the aza-15-crown-5 cavity.

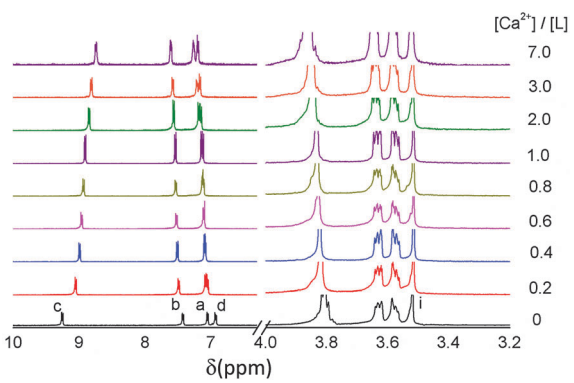

Fig. 4 ^{1}H-NMR spectra of PyB–Aza in the presence of different concentrations of $Ca(ClO_4)_2$ in CD_3CN.

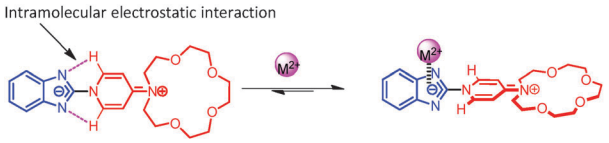

Scheme 3 PyB–Aza interacting with a metallic cation.

Indeed, the up-field shift of the proton H_c could be explained by the disappearance of the electrostatic interaction between H_c and imidazole nitrogen which probably results in a twist of the molecule as shown in Scheme 3. The slight down-field shift of protons H_a and H_b are logically affected by the presence of the interacting cation.

In order to verify the proposed binding mechanism, similar Ca^{2+} titrations were carried out on PyB–DiMe as shown in Fig. 1 and Table 1 under identical conditions. Upon addition of increasing concentrations of Ca^{2+}, blue shifts of both the absorption band from 356 nm to 331 nm and the emission band from 538 nm to 450 nm are observed. The clear isosbestic point at 348 nm and the isoemissive point at 489 nm demonstrate the equilibrium between the free ligand and complex during titration. The complexing constant was determined to be 6.63 ± 0.06. All these similarities between PyB–Aza and PyB–DiMe definitively exclude the possibility for cations to be trapped inside the aza-crown cavity. As a matter of fact, the spectral response of PyB to Ca^{2+} addition was also followed in MeCN in order to investigate the effect of an amino group appended to the pyridinium moiety on the complexation properties induced by the imidazole bridge (Fig. 1 and Table 1). The successive addition of Ca^{2+} induces one more time a similar blue shift for both the absorption band from 393 nm to 337 nm and the emission band from 693 nm to 570 nm with log K = 3.39, a much lower value as compared to PyB–Aza and PyB–DiMe. In conclusion, due to similar spectral changes upon Ca^{2+} addition for the three molecules, it seems reasonable to describe the 1 : 1 complex as a Ca^{2+} ion interacting electrostatically with the imidazole bridge of the betaine units. In addition, the several orders of magnitude between PyB and the substituted analog's complexation constant can be rationalized in term of the donating effect from the azo-dimethyl group enhancing the minus charges located on the imidazole and strengthening the attraction upon the cation.

Our computational strategy gives support to experimental findings and confirms the presence of the lateral interaction between the cation and the imidazole bridge rather than complexation inside the macrocycle. As shown in Fig. 5, for PyB–Aza, the two systems, (i) the cation inside the crown and (ii) the cation in interaction with the imidazole group, have been determined and the results are displayed for these two systems in Fig. 3 as well as an energetic MO diagram with vertical transitions determined by TDDFT. The maximum absorption wavelength calculated for the structure corresponding to Ca^{2+} inside the crown is 373 nm in MeCN whereas this wavelength reaches 335 nm for the ion in interaction with the imidazole bridge. The latter structure thus reproduces remarkably and unambiguously the experimental maximum of the absorption

© 2016 Tous droits réservés.
doc.univ-lille1.fr

Published on 11 May 2016. Downloaded by Univ Lille 1 on 31/08/2016 15:03:56.

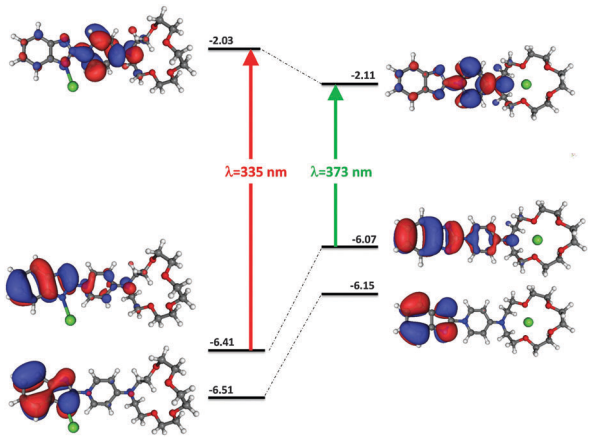

Fig. 5 TDDFT calculations of BetAza and Ca^{2+} according to lateral (left) or inside crown-ether (right) complexation.

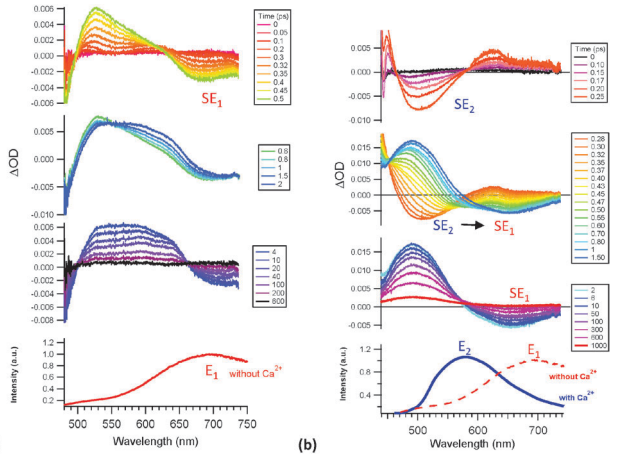

Fig. 6 (a) Femtosecond transient absorption spectra of 50 μM of PyB in MeCN following laser excitation at 320 nm, for three temporal windows; (b) similar data with an additional 40 eq. of Ca^{2+} salt in the solution. Lower panels refer to stationary emission spectra for the solution before and after addition of salt.

at 335 nm. Furthermore, as shown in Table 1, theoretical calculations of log *K* obtained for the three PyB derivatives with Ca^{2+} bound to the benzimidazole moiety reproduce remarkably well the experimental values which also confirm the cation complexation site.

Surviving complex upon light excitation: case of PyB?

At this point, for the three PyB–R molecules, we obtained strong evidences for an halochromic effect explained by the existence of a (1 : 1) M : L complex between the imidazole bridge and the cation. Analysis of emission spectra upon salt addition seems to indicate that static rather than dynamic quenching occurred. With the help of ultrafast absorption spectroscopy, we will now investigate the complex photochemistry after light excitation: will light destabilize the complex or not?

First of all, inspection of PyB transient data, with or without cation, will be the backbone of this study since we have already characterized the post-excitation mechanisms of this molecule in previous articles.[13] In short, its photophysics were discussed in terms of two distinct CT states (S_1 and S_2) and a photophysical scheme was proposed: in parallel to the ultrafast production of the emissive S_1(E) state, an ultrafast ICT process occurs from the initially populated S_2(CT) state to a new charge transfer S_1(CT) state, the reaction ranging from 300 fs to 12 ps depending on the solvent. The S_2(CT) → S_1(CT) reaction was clearly identified by transient spectroscopy with two excited state absorption (ESA) bands evolving in the opposite direction separated with a clear isosbestic point in between. We now present the transient data for PyB in Fig. 6a with new experimental conditions (320 nm laser excitation) while the effect of adding Ca^{2+} is presented in Fig. 6b according to three distinct temporal windows. Just after excitation ([0–0.5 ps] temporal window), one observes the simultaneous growth of two bands: (i) the stimulated emission (SE) negative band coming from the S_1(E) state and easily recognized as the negative mirror of the emission band of the free ligand peaking around the 690 nm band E_1 (see the red curve in the lower panel); (ii) an ESA band attributed to S_2(CT). Both states originate from the relaxation of the S_2 Franck–Condon (FC) state occurring with a characteristic time, $\tau_1 \approx 100$ fs. All characteristic times are gathered together in Table 2. Then, the ICT reaction S_2(CT) → S_1(CT) proceeds ([0.6–2 ps] temporal window) with a typical isosbestic point and a characteristic time $\tau_2 \approx 400$ fs. Finally, within the [4–600 ps] temporal window, all transient bands vanish with a bi-exponential decay; the shorter time $\tau_3 = 7$ ps is attributed to S_1(CT) decay *via* internal conversion (IC) while the longer time $\tau_4 = 140$ ps is attributed to S_1(E) decay *via* emission and IC.

The addition of Ca^{2+} changes drastically the photophysics of PyB paralleling the shift of stationary emission signals, band E_2 (with cation) and band E_1 (without cation) being separated by more than 150 nm. Indeed, between 0 and 0.25 ps one notices

Table 2 Characteristic times deduced from global fitting of transient data for PyB, PyB–DiMe and PyB–Aza

	τ_1/ps		τ_2/ps	τ_3/ps	τ_4/ps
L L:M	Solvation (FC relaxation)	Cation ejection	ICT S_2 → S_1	Decay of S_1(CT)	Decay of S_1(E)
PyB	0.10 (2)		0.40 (4)	16 (2)	140 (20)
PyB + Ca^{2+}		0.15 (1)		1.9 (4)	110 (20)
PyB–Aza	0.13 (4)			1.0 (3)	145 (20)
PyB–Aza + Ca^{2+}		0.19 (4)		0.8 (2)	85 (5)
PyB–DiMe	0.10 (2)			0.7 (1)	83 (5)
PyB–DiMe + Ca^{2+}		0.17 (1)		52 (10)	300 (90)

© 2016 Tous droits réservés. doc.univ-lille1.fr

Published on 11 May 2016. Downloaded by Univ Lille 1 on 31/08/2016 15:03:56.

the rise of a new negative SE band, *i.e.* SE_2, peaking at 500 nm concomitantly with a new ESA band near 630 nm (see Fig. 6b). Of course, one can expect the PyB–Ca^{2+} complex to emit light after laser excitation which allows to assign safely this negative band as the SE of the $S_1(E/Ca^{2+})$ states but overlapped with its own ESA. Then, during the [0.28–1.5 ps] temporal window, this SE transient band vanishes to reveal a new ESA peaking at 496 nm together with the negative SE_1 band previously reported. The overall process appears as a drastic shift of the negative transient band from the blue edge –SE_2 band, to the red edge –SE_1 band over more than 150 nm. In accordance with stationary emissions bands E_1 and E_2, we assign the SE_2 band to $S_1(E/Ca^{2+})$ due to the complex state, while the SE_1 band originates from the uncomplexed $S_1(E)$ state. In summary, we assign the transient $SE_2 \rightarrow SE_1$ shift between [0.28–1.5 ps] to the light induced release of the Ca^{2+} caused by the ICT reaction from the benzimidazole moiety to the pyridinium moiety, neutralizing the imidazole Ca^{2+} electrostatic interaction. Global fitting of both the rising SE_1 band and the vanishing SE_2 band gives a characteristic time of 150 fs which is therefore the mean duration for the photorelease process. Compare to other molecules linked with aza-crown for which the process is reported to occur within the picosecond regime,[6,9,19] the 150 fs photorelease time of this study is more than one order of magnitude faster. Indeed, due to the macrocavity effect, the photorelease mechanism of the crown linked molecules is multi-steps and occurs from the picosecond[6,9a,19c,e,f,20] to the nanosecond regime[19a,b] depending on the nature of the cation.

Finally, after photoejection, between 2 and 600 ps, the overall transient signal decreases: the SE_1 band falls to zero intensity while the transient ESA band vanishes, leading to a residual absorption near 490 nm due to a triplet state.[13] A bi-exponential decay is necessary to fit properly the data with two characteristic times τ_3 = 1.9 ps and τ_4 = 110 ps related to $S_1(CT)$ and to $S_1(E)$, respectively. It is worth noting that the final deexcitation of the singlet states do not depend drastically on the presence or absence of the cation which suggest that the Ca^{2+} is probably released into the bulk. Further analysis can be undertaken to support this statement. Indeed, it is worth considering that even after ejection of the cations out to the first solvation shell, cations are still localized inside the subsequent shells stressing Coulombic interactions for the ground and excited states of PyB. Unlike the photo-ejection process (k_1) both decays with rates k_3 and k_4 are expected to obey the well-known "energy gap law"

$$\log k \propto\sim \log\ k_0 - \frac{1}{RT}\Delta E(S_1S_0) \qquad (1)$$

where $\Delta E(S_1S_0)$ refers to the energy differences between the first excited and ground states at a given temperature T, whereas R is the gas constant. In Fig. 7, we present the logarithmic plot of the k_1 (or k_2 without Ca^{2+}), k_3 and k_4 deduced from global fitting of transient data after the addition of 0, 2, 19 and 39 equivalents of Ca^{2+} as a function of the S_1–S_0 energy gap obtained from the maximum of emission for these respective solutions. As expected, the photo-ejection case (first panel) does not depend

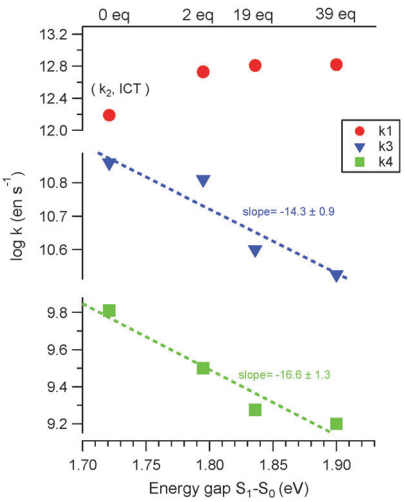

Fig. 7 Logarithmic plot of rate constants k_3 and k_4 corresponding to the biexponential decay of the red edge negative transient band (Fig. 6a and b) as a function of the energy gap S_1–S_0 deduced from stationary emission (Fig. 1b).

on calcium concentration while subsequent decays give evidence that eqn (1) is fully satisfied, the slope being close to the expected value of $-15.5\ eV^{-1}$. Closer inspection of characteristic times in Table 2 shows a higher value of τ_4 ($S_1(E)$ decay) as compared to τ_3 ($S_1(CT)$ decay) regardless of the presence of cation. This is consistent with a lack of specific interaction between PyB* and the photo-ejected Ca^{2+}, the latter having probably escaped into the bulk. As a partial conclusion, the photophysics of the PyB–Ca^{2+} M:L complex can be summarized by photorelease of the cation within 150 fs, $(PyB–Ca^{2+})^* = PyB^* + Ca^{2+}$, followed by the decay of two S_1 states ranging from 14 to 600 ps but significantly influenced by the presence of cations located in the second solvation sphere.

Photoejection of cation upon PyB–Aza light excitation?

In the continuity of PyB analysis, transient data for PyB–Aza in MeCN is presented in Fig. 8a and also divided into three temporal windows. Displayed on the first panel (up to 0.6 ps), an initial growth of the ESA band peaking at 476 nm is observed with concomitant growth of the SE_1 negative bands with a characteristic time of τ_1 = 130 fs. Following TDDFT assignments, 320 nm laser excitation falls up to the S_1 state and by analogy with the previous case, both native transient bands are straightforwardly related to the $S_1(CT)$ and $S_1(E)$ states populated after S_1 Franck–Condon state deexcitation. Inspecting the second temporal window of Fig. 8a, still in comparison with PyB (second panel of Fig. 6a), one notices the lack of $S_2 \rightarrow S_1$ IC spectral signatures which coincides logically with the fact that optically accessible state is S_1 rather than S_2 (let's say that τ_2 is missing). Finally, in the third temporal window, the ESA and SE_1 bands vanished leaving a persistent signal peaking at 470 nm attributed to the triplet state (see discussion above). As already discussed, the double exponential decay is easily assigned: $\tau_3 \sim 1$ ps is the IC $S_1(CT) \rightarrow S_0$ while $\tau_4 \sim 140$ ps represents the decay of $S_1(E)$ state. As shown in Fig. S3 (ESI†), results for PyB–DiMe are strictly similar to PyB–Aza, except for

© 2016 Tous droits réservés.
doc.univ-lille1.fr

Published on 11 May 2016. Downloaded by Univ Lille 1 on 31/08/2016 15:03:56.

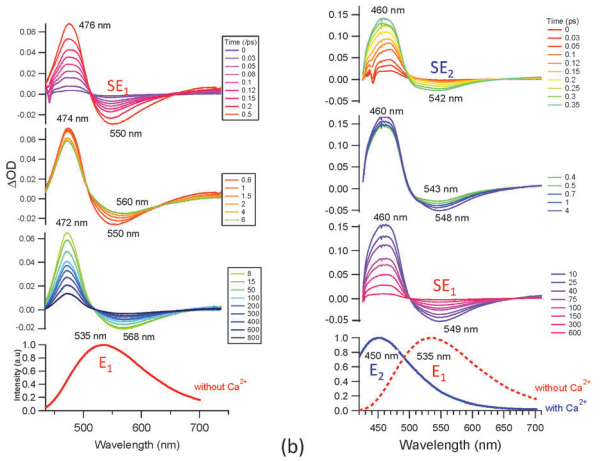

Fig. 8 (a) Femtosecond transient absorption spectra of 50 μM of PyB–Aza in MeCN following laser excitation at 320 nm, for three temporal windows; (b) similar data with an additional 100 equivalent of Ca^{2+} salt in the solution. Lower panels refer to stationary emission spectra for the solution before and after addition of salt.

the numerical values of the characteristic times τ_1, τ_3 and τ_4 as given in Table 2.

Analysis of transient data for the PyB–Aza–Ca^{2+} complex is a central result of this article because we want to assess if such stable species ($\log K \sim 7$) are still able to release their cation upon light excitation in a similar way as compared to the weakly bound analog PyB–Ca^{2+} ($\log K \sim 4$).

Unlike the previous molecule, the ultrafast photophysics of the PyB–Aza–Ca^{2+} complex are less simple to analyse because emissive states without (band E_1 at 535 nm) and with the cation (band E_2 at 450 nm) are less spaced (85 nm) than in the case of PyB (125 nm). Indeed, the ESA and SE bands strongly overlap, peaking at the same wavelength of about 460 nm. On the first two panels, compared to Fig. 6b, we cannot distinguish distinctly the drastic shift $SE_2 \rightarrow SE_1$ due to this strong spectral overlap of positive ESA bands (at 460 nm) with the expected negative SE_2 band. Anyhow, until 350 fs, we can notice a small negative band peaking at 542 nm that can be assigned to the foot of SE_2 (negative mirror of band E_2). Then, after 400 fs, the slight red shift of the negative band can be ascribed to the cation photo-release reaction since the 4 ps trace can be assigned to the free ligand SE_1 signal. As seen in Table 2, the characteristic time for such a reaction is 190 fs. Finally, after the photorelease, between 2 and 1000 ps (third panel of Fig. 8), we propose to assign the double exponential decay as the respective decays of the two singlets, *i.e.* $\tau_3 = 0.8$ ps for S_1(CT) and $\tau_4 = 85$ ps for S_1(E), previously reviewed. Similar results are obtained for the PyB–DiMe molecule (see Fig. S3, ESI†) with distinct characteristic times reported in Table 2. Note that any translocation reaction between the imidazole bridge and the macrocycle can be reported for PyB–Aza; the Ca^{2+} being probably ejected into the bulk.

Is the betaine pyridinium an efficient molecular tool for advanced photo-manipulation of cations?

Up to now, the most common approach to build cation photo-release systems was to couple an aza-crown cavity with a PCT moiety: after PCT, the heteroatom of the macrocycle is positively charged, resulting in the Coulombic repulsion between the heteroatom and the metal cation initially inside the cavity. However, as nicely evidenced by several groups, the mechanism for the photoejection process is complex, with the enrolment of at least one transient intermediate, the so-called loose complex, a kind of pre-dissociated species for which the cation still interacts weakly with the aza-crown.[9a,19d] The photorelease mechanism of this crown linked molecules is multi-step and occurs from the picosecond[6,9a,19c,e,f,20] to the nanosecond regime[19a,b] depending on the nature of the cation. Furthermore, as already emphasized by Kumar *et al.*, coordination-based open systems allow the opportunity to explore efficiently rigid sensory systems and the attraction of metal ions toward molecular receptors.[8]

Such drawbacks are bypassed with the PyB–R series. First of all, the photorelease mechanism is instantaneous, avoiding the loose complex formation reported for the aza-crown related molecules. Furthermore, to the best of our knowledge, ~200 fs is the fastest reported in the literature. The simplicity of the photo-release process is merely due to the lateral and strong Coulombic interaction engaging only one nitrogen of the imidazole moiety. Furthermore, the PyB–R can be a very efficient chelatant, $\log K \sim 6$–7, and purely stoichiometric because only the 1 : 1 M : L complex is reported. Clearly, a promising result concerns the modulation of the complexation toward *para* substitution of the phenyl ring with a donor group. Indeed, for the series R = H, DiMe, aza-crown, the complexation constants vary as $\log K = 3.4$, 6.6 and 6.8, respectively. From a photochemical point of view, for the same series, the trend is parallel to the rate of the photorelease process k_1 (Table 2) varying as 150, 170 and 190 fs. Still, focusing on the complexation constant, the state-of-the-art TDDFT strategy chosen by our group was able to reproduce quantitatively the experimental values.

Conclusions

Based on advanced spectroscopy in combination with TD-DFT calculations, the complexation and photorelease properties of PyB–Aza, PyB–DiMe and PyB on metallic cations have been investigated. In the continuity of our work undertaken in the past for PyB, it has first been found that the photophysics of PyB–Aza is characterized by one strong solvatochromic singlet excited state, S_1(CT), and one non-solvatochromic emissive state S_1(E). Upon metallic salt addition, absorption and emission spectroscopy of the three molecules has revealed clearly that the cations were not trapped on the macrocycle but strongly attracted by negative charges located on the imidazole moiety. The stoichiometry of the complex was (1 : 1).

Due to the Coulombic nature of the complexation, high charge density cations like Ca^{2+} are especially sensitive to the imidazole attraction. The possibility to tune the complexation strength upon pyridinium moiety substitution has been clearly identified with the series, PyB–R with R = H, DiMe and aza-crown; the complexation constant rising from 3.4 to 6.8, *i.e.* more than three orders of magnitude.

This journal is © the Owner Societies 2016
© 2016 Tous droits réservés.
doc.univ-lille1.fr

Published on 11 May 2016. Downloaded by Univ Lille 1 on 31/08/2016 15:03:56.

Upon light excitation, an ultrafast one-step photo-release reaction proceeds,

$$\text{PyB–R:Ca}^{2+} + h\nu \rightarrow \text{PyB–R}^{*} + \text{Ca}^{2+}$$

the remaining ligand excited state being either S_1(CT) or S_1(E). The value of the rate k_1 ($\sim 1/\tau_1$) is parallel to the ground state complexation constant. The lower the $\log K$, the lower the stability of the complex, and the higher the photorelease rate k_1. State-of-the-art TDDFT calculations were able to reproduce perfectly the experimental values of the complexation constant. Based on the same computational strategy, we initiate molecular design efforts to elaborate a smart bio-compatible system enabling light induced Ca^{2+} translocation from the imidazole moiety to a second chelating site.

Experimental

General

All commercially available reagents were used without further purification. Column chromatography was performed on silica gel 60 (40–60 μm). The solvents for column chromatography were used without purification. The reactions carried out under anhydrous conditions are performed under argon (Ar) in glassware previously dried in an oven. All commercially available reagents were used without further purification. NMR spectra were recorded on a JEOL ESC-400 spectrometer in $CDCl_3$ or in CD_3CN solvents. The chemical shift was given in units of parts per million related to TMS or solvent protons as internal reference. Mass spectrometry analyses were performed at IMAGIF/ICSN.

1-*N*-Benzimidazolyl-4-dimethylaminopyridiunium: PyB–DiMe. To a Schlenk tube, 2-chlorobenzimidiaole (0.2 g, 1.32 mmol) and dimethylpyridine (1.6 g, 13.2 mmol) were added. After the reaction mixture was stirred at 150 °C for 3 h under Ar, it was cooled down to room temperature followed by the addition of 30 mL H_2O. The precipitate was filtered off and washed with water and ethanol twice to obtain a pure product (0.27 g, 75%). ^{1}H NMR (400 MHz, CD_3OD): (d, J = 8.2 Hz, 2H), (dd, J = 6.4, 3.2 Hz, 2H), (d, J = 7.8 Hz, 2H), (dd, J = 6.4, 3.2 Hz, 2H), (s, 6H); ^{13}C NMR (100 MHz, CD_3OD): 158.3, 154.9, 146.1, 138.9, 121.3, 117.4, 108.6, 48.4 ppm; HRMS (ESI) m/z calcd for $C_{14}H_{15}N_4$ $[M + H^+]$ 239.1297, found 239.1289.

***N*-Pyridine-aza-15-crown-5: 1.** To a Schlenk tube, 4-bromopyridine hydrochloride (0.2 g, 1.0 mmol) aza-15-crown-5 (0.1 g, 0.46 mmol), *t*-BuONa (0.19 g, 2.0 mmol), $Pd(dba)_2$ (21 mg, 0.04 mmol) and 2-dicyclohexylphosphino-2′-(*N*,*N*-dimethylamino)-biphenyl (20 mg, 0.05 mmol) were added. The reaction mixture was stirred at 100 °C for 41 h under Ar. Crude product containing some triethyl amine (Et_3N) and aza-15-crown-5 was obtained by column chromatography on silica gel (elute: MeOH/DCM/Et_3N = 5 : 95 : 0.5) (40 mg, 30%). ^{1}H NMR (400 MHz, $CDCl_3$): (d, J = 5.5 Hz, 2H), (d, J = 5.0, 2H), (m, 20H).[21]

1-(1-*N*-Benzimidazolylpyridiunium)-aza-15-crown-5: PyB–Aza. Compound **1** (0.17 g, 0.57 mmol) and 2-chlorobenzimidiazole (0.13 g, 0.86 mmol) were dissolved in dry *n*-BuOH (3 mL) and stirred at 110 °C for 50 h under Ar. The solvent was evaporated and the residue was redissolved in MeOH (2 mL) followed by the addition of concentrated aqueous NH_3 (33%, 1 mL) and stirred at room temperature for 30 min. The solvent was evaporated and the crude product was separated by column chromatography (elute: MeOH/DCM/Et_3N = 2 : 95 : 1) to obtain a viscous solid which was dissolved in diluted aqueous NH_3 (10%) and extracted with $CHCl_3$. The organic layer was dried over $MgSO_4$ and evaporated to obtain the yellow solid (100 mg, 40%). ^{1}H NMR (400 MHz, $CDCl_3$): (d, J = 7.8 Hz, 2H), (dd, J = 6.0, 3.2 Hz, 2H), (dd, J = 6.0, 3.2 Hz, 2H), (d, J = 7.8 Hz, 2H), (t, J = 5.5 Hz, 4H), (m, 12H), (s, 4H); ^{13}C NMR (100 MHz, $CDCl_3$): 156.2, 154.1, 146.0, 137.8, 120.0, 117.0, 107.4, 72.3, 70.6, 70.0, 68.1, 53.8 ppm; HRMS (ESI) m/z calcd for $C_{22}H_{29}N_4O_4$ $[M + H^+]$ 413.2189, found 413.2179.

Spectroscopic techniques. All stationary absorption and fluorescence spectra were recorded using double beam CARY 5000 and FluoroMax 3 spectrometers, respectively. The spectral resolution is typically 2 nm in both experiments. Emission spectra were corrected for the lamp and detector response. Measurements were performed at ambient temperature using 1 cm quartz cells with approximately 10^{-5} M solutions, keeping the maximum absorbance less than 0.1 in order to avoid any significant reabsorption effects. Complexation constants were determined by global analysis of the evolution of all absorption and/or emission spectra by using the Specfit Global Analysis System V3.0 for 32-bit Windows system. This software uses singular value decomposition and nonlinear regression modelling by the Levenberg–Marquardt method.[22]

Transient absorption experimental set up (solution). The femtosecond transient absorption set up has already been described elsewhere.[23] Briefly, a 1 kHz Ti:sapphire laser system (coherent oscillator and a BM Industries regenerative amplifier) delivered 100 fs (0.8 mJ) pulses at 800 nm. Pump pulses were set at 350 nm by using a Palitra OPA, while probe pulses (white light continuum) were generated by focusing the fundamental beam in a CaF_2 rotating plate. The transient absorption measurements covered a 400–750 nm spectral range and a 0–3 ns temporal range. Sample solutions (about 10^{-4} M) were circulated in a flow cell equipped with 100 μm thick CaF_2 windows and characterized by a 1 mm optical path length. The pump-probe cross-correlation time was evaluated to be about 200 fs and 300 fs at 390 nm and 266 nm pump wavelength, respectively.[23] The characteristic times deduced from kinetics were obtained by fitting the GVD corrected data using a procedure proposed by Nakayama *et al.*,[24] with the result of a multi-exponential function convolved with a Gaussian pulse which approximates the pump–probe correlation function. Within this approach, global fitting was performed systematically taking into account simultaneously four or five relevant wavelengths.

Theoretical calculations. To calculate the absorption and fluorescence properties, we used density functional theory (DFT) and time-dependent density functional theory (TDDFT) formalisms according to the three-step methodology: (i) the ground state (GS) and excited states (ES) geometries of each structure were optimized without any symmetry constraint in the equilibrium limit using the linear-response (LR) polarized

© 2016 Tous droits réservés. doc.univ-lille1.fr

Published on 11 May 2016. Downloaded by Univ Lille 1 on 31/08/2016 15:03:56.

continuum model (PCM);[25] (ii) the vibrational spectra were computed at the same level of theory to check that the optimized structures correspond to true minima on the potential energy surface; (iii) the vertical transition energies to the excited states were computed with TD-DFT within the PCM scheme, relying on the state-specific (SS) approximation in its non-equilibrium limit.[26] All these calculations were performed using the Gaussian 09 package[27] at the PBE0/6-31+G(d) level, a strategy previously used for PyB.[13a,c]

To calculate the complexation energy and the complexation constant ($\log K$), we used the thermodynamic cycle presented in Fig. S4 (ESI†). The change of Gibbs free energy of reaction between the ligand and the ion ΔG°_{sol} corresponds to the sum of the gas-phase Gibbs free energy of reaction ΔG°_{gas} and the change in solvation energy, ΔG°_{solv}:

$$\Delta G^\circ_{sol} = \Delta G^\circ_{sol} + \Delta G^\circ_{solv}$$

which leads to

$$\Delta G^\circ_{sol} = \Delta G^\circ_{gas} + \Delta G^\circ_{solv}(\text{complex}) - \Delta G^\circ_{solv}(\text{ligand}) - \Delta G^\circ_{solv}(Ca^{2+})$$

with

$$\Delta G^\circ_{gas} = \Delta G^\circ_{gas}(\text{complex}) - \Delta G^\circ_{gas}(\text{ligand}) - \Delta G^\circ_{sol}(Ca^{2+})$$

The standard enthalpy and Gibbs free energy at 298.15 K in the gas phase were calculated by adding the thermal correction obtained by frequency analysis to the DFT calculation (zero-point energy corrections, ZPE, were considered). The interaction energies were corrected for the basis set superposition error (BSSE) using the counterpoise method.[28] To calculate the solvation energy, we have used the PCM model.

Acknowledgements

Chevreul institute (FR 2638), Ministère de l'Enseignement Supérieur et de la Recherche, Région Nord – Pas de Calais and FEDER are acknowledged for supporting and funding this work.

Notes and references

1 E. Carafoli, *Annu. Rev. Biochem.*, 1987, **56**, 395.
2 C. Brieke, F. Rohrbach, A. Gottschalk, G. Mayer and A. Heckel, *Angew. Chem., Int. Ed.*, 2012, **51**, 8446.
3 (*a*) G. Bort, T. Gallavardin, D. Ogden and P. I. Dalko, *Angew. Chem., Int. Ed.*, 2013, **52**, 4526; (*b*) K. A. Korzycka, P. M. Bennett, E. J. Cueto-Diaz, G. Wicks, M. Drobizhev, M. Blanchard-Desce, A. Rebane and H. L. Anderson, *Chem. Sci.*, 2015, **6**, 2419.
4 A. Momotake, N. Lindegger, E. Niggli, R. J. Barsotti and G. C. Ellis-Davies, *Nat. Methods*, 2006, **3**, 35.
5 (*a*) J. D. Lewis and J. N. Moore, *Chem. Commun.*, 2003, 2858; (*b*) J. D. Lewis, R. N. Perutz and J. N. Moore, *J. Phys. Chem. A*, 2004, **108**, 9037.
6 A. Douhal, A. D. Roshal and J. A. Organero, *Chem. Phys. Lett.*, 2003, **381**, 519.
7 G. Vantomme and J. M. Lehn, *Angew. Chem., Int. Ed.*, 2013, **52**, 3940.
8 A. Kumar, M. Chhatwal and T. Gupta, *Tetrahedron Lett.*, 2012, **53**, 5691.
9 (*a*) C. Ley, F. Lacombat, P. Plaza, M. M. Martin, I. Leray and B. Valeur, *ChemPhysChem*, 2009, **10**, 276; (*b*) P. Plaza, I. Leray, P. Changenet-Barret, M. M. Martin and B. Valeur, *ChemPhysChem*, 2002, **3**, 668.
10 (*a*) B. Valeur, I. Leray, L. Y. Zhao, V. Souchon, R. Metivier, P. Plaza, C. Ley, F. Lacombat and M. M. Martin, *ChemPhysChem*, 2010, **11**, 2416; (*b*) N. Dozova, R. Kumar, T. Pradhan, F. Lacombat, B. Valeur, J. S. Kim and P. Plaza, *Chem. Commun.*, 2015, **51**, 14859.
11 C. Reichardt, *Chem. Soc. Rev.*, 1992, **21**, 147.
12 C. Reichardt, S. Asharin Fard and G. Schäfer, *Chem. Ber.*, 1993, **126**, 143.
13 (*a*) S. Aloise, Z. Pawlowska, C. Ruckebusch, M. Sliwa, J. Dubois, O. Poizat, G. Buntinx, A. Perrier, F. Maurel, P. Jacques, J. P. Malval, L. Poisson, G. Piani and J. Abe, *Phys. Chem. Chem. Phys.*, 2012, **14**, 1945; (*b*) Z. Pawlowska, A. Lietard, S. Aloise, M. Sliwa, A. Idrissi, O. Poizat, G. Buntinx, S. Delbaere, A. Perrier, F. Maurel, P. Jacques and J. Abe, *Phys. Chem. Chem. Phys.*, 2011, **13**, 13185; (*c*) A. Perrier, S. Aloise, Z. Pawlowska, M. Sliwa, F. Maurel and J. Abe, *Chem. Phys. Lett.*, 2011, **515**, 42.
14 J. Abe, Y. Shirai, N. Nemoto, F. Miyata and Y. Nagase, *J. Phys. Chem. B*, 1997, **101**, 576.
15 E. Alcalde, I. Dinares, J. Elguero, J. P. Fayet, M. C. Vertut, C. Miravitlles and E. Molins, *J. Org. Chem.*, 1987, **52**, 5009.
16 K. W. Chi, C. Addicott and P. J. Stang, *J. Org. Chem.*, 2004, **69**, 2910.
17 N. Nemoto, J. Abe, F. Miyata, Y. Shirai and Y. Nagase, *J. Mater. Chem.*, 1998, **8**, 1193.
18 (*a*) J. D. Lewis and J. N. Moore, *Dalton Trans.*, 2004, 1376; (*b*) K. Yoshida, T. Mori, S. Watanabe, H. Kawai and T. Nagamura, *J. Chem. Soc., Perkin Trans. 2*, 1999, 393; (*c*) J. F. Letard, R. Lapouyade and W. Rettig, *Pure Appl. Chem.*, 1993, **65**, 1705.
19 (*a*) I. K. Lednev, T.-Q. Ye, R. E. Hester and J. N. Moore, *J. Phys. Chem. A*, 1997, **101**, 4966; (*b*) I. K. Lednev, R. E. Hester and J. N. Moore, *J. Phys. Chem. A*, 1997, **101**, 7371; (*c*) M. M. Martin, P. Plaza, Y. H. Meyer, F. Badaoui, J. Bourson, J. P. Lefevre and B. Valeur, *J. Phys. Chem.*, 1996, **100**, 6879; (*d*) J. F. Létard, S. Delmond, R. Lapouyade, D. Braun, W. Rettig and M. Kreissler, *Recl. Trav. Chim. Pays-Bas*, 1995, **114**, 517; (*e*) M. M. Martin, P. Plaza, Y. H. Meyer, L. Begin, J. Bourson and B. Valeur, *J. Fluoresc.*, 1994, **4**, 271; (*f*) M. M. Martin, P. Plaza, N. D. Hung, Y. H. Meyer, J. Bourson and B. Valeur, *Chem. Phys. Lett.*, 1993, **202**, 425.
20 R. Mathevet, G. Jonusauskas, C. Rulliere, J.-F. Letard and R. Lapouyade, *J. Phys. Chem.*, 1995, **99**, 15709.
21 H. Kotsuki, H. Sakai and T. Shinohara, *Synlett*, 2000, 116.
22 H. Gampp, M. Maeder, C. J. Meyer and A. D. Zuberbühler, *Talanta*, 1985, **32**, 95.

© 2016 Tous droits réservés. doc.univ-lille1.fr

23 (*a*) G. Buntinx, R. Naskrecki and O. Poizat, *J. Phys. Chem.*, 1996, **100**, 19380; (*b*) B. Moine, J. Rehault, S. Aloise, J. C. Micheau, C. Moustrou, A. Samat, O. Poizat and G. Buntinx, *J. Phys. Chem. A*, 2008, **112**, 4719.
24 T. Nakayama, Y. Amijima, K. Ibuki and K. Hamanoue, *Rev. Sci. Instrum.*, 1997, **68**, 4364.
25 J. Tomasi, B. Mennucci and R. Cammi, *Chem. Rev.*, 2005, **105**, 2999.
26 B. Mennucci, *J. Phys. Chem. Lett.*, 2010, **1**, 1666.
27 M. J. Frisch, G. W. Trucks, H. B. Schlegel, G. E. Scuseria, M. A. Robb, J. R. Cheeseman, G. Scalmani, V. Barone, B. Mennucci, G. A. Petersson, H. Nakatsuji, M. Caricato, X. Li, H. P. Hratchian, A. F. Izmaylov, J. Bloino, G. Zheng, J. L. Sonnenberg, M. Hada, M. Ehara, K. Toyota, R. Fukuda, J. Hasegawa, M. Ishida, T. Nakajima, Y. Honda, O. Kitao, H. Nakai, T. Vreven, J. A. Montgomery, Jr., J. E. Peralta, F. Ogliaro, M. Bearpark, J. J. Heyd, E. Brothers, K. N. Kudin, V. N. Staroverov, R. Kobayashi, J. Normand, K. Raghavachari, A. Rendell, J. C. Burant, S. S. Iyengar, J. Tomasi, M. Cossi, N. Rega, N. J. Millam, M. Klene, J. E. Knox, J. B. Cross, V. Bakken, C. Adamo, J. Jaramillo, R. Gomperts, R. E. Stratmann, O. Yazyev, A. J. Austin, R. Cammi, C. Pomelli, J. W. Ochterski, R. L. Martin, K. Morokuma, V. G. Zakrzewski, G. A. Voth, P. Salvador, J. J. Dannenberg, S. Dapprich, A. D. Daniels, Ö. Farkas, J. B. Foresman, J. V. Ortiz, J. Cioslowski and D. J. Fox, *Gaussian 09*, Gaussian, Inc., Wallingford, CT, 2009.
28 S. F. Boys and F. Bernardi, *Mol. Phys.*, 1970, **19**, 553.

Published on 11 May 2016. Downloaded by Univ Lille 1 on 31/08/2016 15:03:56.

© 2016 Tous droits réservés.
doc.univ-lille1.fr

© 2016 Tous droits réservés.

doc.univ-lille1.fr

Photochimie de Molécules Organiques Photofonctionnelles Etudiées par Spectroscopie d'Absorption Ultrarapide et Calculs *ab-initio*

Résumé. La photochimie de Molécules Organiques Photofonctionnelles est un thème éminemment d'actualité comme l'illustre le Prix Nobel de Chimie 2016 sur les Machines Moléculaires. Quel que soit le processus photoinduit recherché, il est toujours accompagné de processus compétitifs non désirables. Aussi, afin de pouvoir instaurer un dialogue entre photo-réactivité et structure moléculaire (synthèse), une approche multi technique peut s'avérer adéquate. Pour cela, les calculs DFT / TDDFT incluant les états excités permettent d'identifier les points topologiques importants (souvent non discernables expérimentalement) tandis que la spectroscopie résolue en temps permet d'attribuer les dynamiques de désexcitation entre ces points. De plus, le traitement des données transitoires basé sur des méthodes chimiométriques est souvent utile pour lever les ambiguïtés d'interprétation ou obtenir les signatures spectrales des différents états intermédiaires.

Deux exemples de molécules photofonctionnelles seront abordés selon le triptyque spectroscopie résolue en temps, calculs *ab inito* et traitement chimiométrique des données. Tout d'abord, nous présenterons une étude très poussée de la photophysique d'une betaine pyridinium au solvatochromisme négatif (inversion du moment dipolaire à l'état excité) et verrons que le transfert de charge photoinduit se fait en deux étapes. En guise de perspective, nous verrons comment ces molécules peuvent devenir de bons candidats pour mettre en œuvre un transfert de cation intramoléculaire photo-induit. Nous présenterons ensuite divers résultats de molécules photochromes (interrupteur moléculaire) dont une série concernant les diaryléthènes pontés, bloqués dans une conformation photoactive. Un projet d'utilisation des diaryléthènes dans des films élastomères pour obtenir des actionneurs photo-actifs (effet opto-mécanique) sera ensuite présenté.

Mots-clefs. Photochimie, Spectroscopie ultra-rapide, TDDFT, MCR-ALS, Photochromisme.

Photochemistry Of Photofunctional Organic Molecules Studied By Ultrafast Absorption Spectroscopy and *ab-initio* Calculations.

The chemistry of photofunctionnal molecules is an eminent hot topic as demonstrated by the 2016 Chemistry Nobel Prize dedicated to the 'Molecular Machine'. However, for any photoinduced process, there are always accompanying undesireable competitive processes. Consequently, in order to establish a genuine dialogue between photoreactivity and molecular structure (synthesis) a multi-field approach is required. With this aim, DFT/TDDFT calculations including excited states make it possible to identify the important topologic points (not always detectable experimentally), while time- resolved spectroscopy affords a real-time assignment of the dynamics of desexcitation between those points. And as a complement, transient data treatment based on chemometric tools can be useful to avoid ambiguities in interpretations or even to find the spectral signature of individual intermediates.

Two examples of studies of photofunctional molecules using this jointed approach (*ab initio* calculations, transient spectroscopy and chemometric data treatment) will be presented. First, we present an investigation on a pyridium betaine displaying negative solvatochromism (excited state dipole moment inversion), with the main result being a two-step intramolecular charge transfer process. In prospective, we will discuss the use of these molecules for an intramolecular cation transfer upon light excitation. Secondly, we will present various results concerning photochromic molecules (molecular switches) including a series of bridged diarylethenes blocked in suitable conformations. Finally, a project centered on the use of diaryethene injected into elastomeric films to elaborate photo-driven actuators (opto-mechanical effect) will be presented.

Keywords. Photochemistry, Ultra-fast Spectroscopy, TDDFT, MCR-ALS, Photochromism.

© 2016 Tous droits réservés.